Universitat Autònoma de Barcelona

Translation of DELOS nanovesicle formulations into new pharmaceutical candidates

Lídia Ballell i Hosa

Universitat Autònoma de Barcelona

Translation of DELOS nanovesicle formulations into new pharmaceutical candidates

Lídia Ballell i Hosa

Tesi Doctoral

Programa de Doctorat en Ciència de Materials

Directores

Dra. Lidia Priscila Ferrer Tasies

Prof. Nora Ventosa Rull

Tutora

Prof. Nora Ventosa Rull

Departament de Física i Química

Facultat de Ciències

2022

La present memòria es presenta per aspirar a Grau de Doctor per:

Lídia Ballell i Hosa

Vist i plau:

Lidia Priscila Ferrer Tasies

Nora Ventosa Rull

Bellaterra, juny 2022

LIDIA PRISCILA FERRER TASIES, Researcher of Nanomol Technologies SL and **NORA VENTOSA RULL**, Scientific Researcher of the Spanish National Research Council at the Institute of Materials Science of Barcelona (ICMAB-CSIC)

CERTIFY:

That Lídia Ballell i Hosa, Master's Degree in Drug Research, Development and Control and Bachelor's Degree in Nanoscience and Nanotechnology, has performed, under their management, the research work entitled "**Translation of DELOS nanovesicle formulations into new pharmaceutical candidates**". This work has been performed under the frame of Materials Science Ph.D program of the Physics and Chemistry Department of the Autonomous University of Barcelona.

And in witness whereof this is signed by

Directors

Dr. Lidia Priscila Ferrer Tasies

Prof. Nora Ventosa Rull

Bellaterra, June 2022

Preamble

A great part of this Ph.D. Thesis has been performed under the frame of collaborative projects. Therefore, besides the results obtained by the author, it has been decided to include some experiments obtained thanks to collaborative effort of researchers belonging to other institutions, which complete and reinforce the work presented in this Thesis.

Agraïments

“La vie sourit à qui la cherche en souriant” és una frase que ens va dir un brilliant profesor que vaig tenir durant la meva etapa escolar. I és cert, la vida somriu als qui la busquen somrient. I jo ara tancant aquesta gran etapa només puc pensar en els moments de felicitat que m’ha aportat. És per això que, tot i que em sàpiga greu que es s’acabi, vull somriure-la i donar les gràcies a tothom que l’ha fet possible (que no són pocs).

Primer de tot, vull donar les gràcies a les meves dos directores de tesi, la Prof. Nora Ventosa i la Dra. Lidia Ferrer. Nora, moltes gràcies per donar-me l’oportunitat de fer el doctorat en aquest grup tant maco. Estic molt agraïda per tot el suport, professionalitat, confiança i alhora la llibertat que transmets. Lidia, moltes gràcies per tots aquests anys. Estic molt agraïda per tot el suport i confiança. Gràcies per formar-me durant tot aquest temps i per donar-me canya quan toca, ha sigut un plaer. Considero que has estat un referent per mi durant aquests anys i he après molt de tu, rigorusitat, constància i bon rotllo. Mai oblidaré l’aventura que vam viure juntes a Cuba, és un lloc on tot ho fa especial.

Per altra banda, també vull expressar el meu agraïment a en Santi Sala. Moltes gràcies per tots aquests anys, no només per donar-me l’oportunitat de fer el doctorat en una empresa i un grup de recerca tant agradables sinó també per la teva transparència i amabilitat. Considero que la teva proximitat cap als treballadors i alhora respecte genera molt bon ambient de treball, que considero que no és fàcil de trobar. Alhora, vull agrair-te tant a tu com a la Lidia F, a la Nora i a l’Alba per donar-me l’oportunitat de participar en el projecte Nano-OligoMed i poder fer dos estades a l’estranger. Estic eternament agraïda.

També vull expressar el meu agraïment al finançament rebut a través de l’ajuda de Doctorat Industrial de l’Agaur que m’ha permès realitzar aquesta tesi doctoral. A més, vull agraïr a la Unió Europea per impulsar la recerca i innovació a través del programa Horitzó 2020, poder participar en un projecte d’aquest nivell ha estat molt enriquidor tant a nivell professional com personal. Alhora, també vull donar les gràcies en Jaume Veciana i a la Concepció Rovira per haver creat el grup Nanomol, heu creat un grup que no només és de gran qualitat sinó que alhora som una gran família i això no és fàcil de trobar.

In the frame of the rhEGF-DELOS nanovesicles pharmaceutical development, I would also like to thank all the collaborators not only from CIGB project but also from Nanonafres project. Thanks Prof. Jan Skov Pedersen’s group from Aarhus University for all the SAXS characterization. Gracias

Héctor Santana y todo el equipo del CIGB por todos los estudios realizados. Gracias Héctor por todos estos años, ha sido un placer colaborar contigo, te deseo los mejores éxitos en el futuro. També agraïr a tot l'equip de Leitat Technological Center, en especial a la Claudia Navarro, Jèssica Romero i Ramon de Leitat per tots els estudis realitzats dins el projecte Nanonafres i totes les discussions, ha sigut molt enriquidor. También agradecer al Centro de Cirugía de Mínima Invasión Jesús Usón (CCMIJU) por todos los estudios *in vivo*.

També vull agrair a tot l'equip de professionals que m'ha ajudat en totes les caracteritzacions. Gràcies al Servei de Microscòpia per a totes les caracteritzacions de cryo-TEM, confocal i SEM. En especial, vull donar les gràcies a en Martí de Cabo. Martí, ets un crack, gràcies per tot el bon rotllo que desprens i per sempre ser súper resolutiu amb mostres que semblen un mal de cap. També donar les gràcies en Salvador Bartolomé del Laboratori de Luminescència i Espectroscòpia de Biomolècules,, moltes gràcies per tot el suport en temes de fluorescència i per posar música alegre al laboratori, així dóna gust venir a treballar.

Per altra banda, també vull mostrar el meu agraïment cap als professionals de l'ICMAB que m'han ajudat en tot moment. Gràcies Neus Romà i Marta Grebolés de Sala Blanca per tota l'ajuda en les mesures de reologia. Gràcies Vega Lloberas per tot el suport en tècniques espectroscòpies, no només ensenyant les tècniques sinó també en la interpretació de resultats.

I no em vull oblidar d'agrair tot el suport tècnic durant tots aquest anys de l'Amable Bernabé i l'Arnau Jaumandreu. Gràcies als dos per facilitar-nos moltes feines del dia a dia al laboratori, sou un punt clau del grup! I com no, gràcies enormes a la Carme Gimeno. Carme, ets un sol i estic eternament agraïda per tot el teu support, professionalitat i transparència. No t'imagines tots les mals de caps que ens salvat! Gràcies de nou.

Tampoc em vull oblidar de donar les gràcies a l'Aleix, Anna i Miguel de consergeria per tota la seva amabilitat i sempre dir un "bon dia!" amb un somriure cada matí.

També vull agrair a totes les persones que han fet especial aquesta etapa de la meva vida. És per això, que vull mencionar a tota la gent que es va crear en el meu camí durant les dos estades que he realitzat a l'estranger, les qual han estat molt enriquidores a nivell personal i professional i n'estic eternament agraïda.

Cuba:

Siento que mi paso por Cuba fue una mis mejores épocas de mi vida. Me siento muy afortunada de haber vivido esta experiencia y me siento muy agradecida de haber conocido toda la gente que me rodeó en aquel momento, que llevo y llevaré en el corazón y que aún mantengo el contacto. Primero quiero agradecer a todo el equipo de UH-CIM. ¡Qué maravilla de gente!

Primero quiero agradecer a la profesora Marilyn Lanio por aceptarme en su grupo. Es usted una mujer maravillosa, con un espíritu crítico que admiro, que he disfrutado y del cual he aprendido muchísimo. Gracias por su amabilidad y por hacerme sentir en casa, estoy verdaderamente agradecida.

Gracias Claudia por nuestros ratos de diversión y pasteles sabrosos. Gracias Felipe por estar siempre alegre y con ganas de bailar y ayudar. Gracias Alexis por tus charlas en el laboratorio y por tus ganas de saber. (¡te debo un partido de básquet!). Gracias Lena (nenaaa!) por tu felicidad, tu transparencia, tus ganas de hacer cosas conmigo y tu pasión por la música. Gracias Magela por todos los cafés. Gracias Mª del Carmen por su amor y amabilidad. Gracias profesor Carlos por todas las charlas en el comedor. Gracias Pedro, Radi, Nelson, Yerandi, Anaixis, entre todos los otros components del grupo UH-CIM.

Laboratorio UH-CIM

Gracias Isbel y Felipito, gracias por hacer mi aventura cubana más intensa y enseñarme qué es lo esencial. Estoy súper agradecida de haberos conocido y de aun mantener el contacto. Muchas gracias Jorge y Lourdes, fuisteis mis padres cubanos, me disteis casa y aventura. Gracias por acogerme tan bien y gracias por la sinceridad, paciencia y amor que me disteis. Gracias sister Janette. ¡Qué suerte encontrarte! Mis días en la Habana eran mucho mejores contigo.

Carlitos, Yasminita y Javier. Gracias Javier por sacarme siempre una sonrisa, por ser paciente y por hacerme sentir. Muchas gracias por todos los lunes de Game of Thrones y por los paseos admirando las obras de la bienal, qué bien lo pasé contigo.

Strasbourg:

First of all, I would like to thank Professor Luisa De Cola for accepting me in her group. It has been a pleasure to meet you and to learn about your expertise. Thanks Ignasi, Etienne, Bianca, Alessandro, Giuseppe, Dario, Claire, Laura for being such a good labmates and friends outside of the lab. Gracias por toda la ayuda Guillermo, eres una persona increíble y que te mereces lo mejor. Gracias Mariel por tu amistad y por todo el soporte durante mi estancia. Thanks Pierre for all scientifc and personal discussions, you are such a good researcher, I hope to see you as PI in the close future. No me podría dejar a Álvaro. Álvaro, muchas gracias por todo, qué complicidad tuve contigo des el minuto 0. Gracias por hacer mi estancia tan agradable y te deseo los mejores éxitos en el futuro.

Luisa De Cola's laboratory

I evidentment també vull expressar tot el meu agraïment al grup Nanomol. Per mi, la meva estada a l'ICMAB ha sigut una etapa de creixement personal molt gran i molt intensa, on he conegut amics de veritat, amics que mare meva quina paciència tenen amb mi! Moltes gràcies David per tota la paciència i amor que rebo quan estàs a prop, ets un crack! Gràcies amigui Guillem per tots aquests anys plens d'aventures, quina sort haver-te conegut! Gràcies Josep per ser-hi sempre (encara que no ho sembli jaja). Gràcies Marta, Judit i Tere, sou un pilar fonamental de la meva etapa a l'ICMAB, sou amor pur i us trobaré molt a faltar però espero poder gaudir de moltes més experiències juntes. Gracias Adrián por ayudarme siempre. Thank you Fabiao for all the philosophical coffees. Gràcies Ramon per la complicitat.

També vull agraïr a la resta de companys que han estat en tota aquesta etapa. Formar part de la família de Nanoninos és una experiència inoblidable i motivadora. Gracies Francesc, Albert R, Albert G, Paula, Inés, Simona, Nathaly, Songbai, Ivana, Silvia, Adriana, Maria, Arnau Guasch, Marta P, Aida, Ángel, Marc M, Edu, Lamia, Sara R, Jinghai, Gong, Xavi, Sara G, Miquel C, José C, Carme M, Alejandro, Nerea, Rubén y Karla. M'encantaria escriure una frase per

cadascú però només dir-vos que moltes gràcies per tots els moments, heu fet que aquesta experiència sigui única.

També donar les gràcies a les Post-Doc del grup. Gràcies Eli, Mariana i Judit M per tots aquests anys. Ha estat un plaer treballar amb vosaltres! El grup té molta sort de tenir-vos ☺

Grup Nanomol

Nanomol Technologies

També he tingut molta sort de tenir companys de feina per part de l'empresa que són brutals. Gracies Carla, Estela, Júlia, Òscar i Alba, ha sigut un plaer treballar amb vosaltres tots aquests anys.

Finalment vull agraïr la gent que m'ha envoltat durant aquesta etapa fora del laboratori. Gràcies Alejandro Sabater per tots aquests anys vivint junts. Gràcies per tota la paciencia i amistat de debó.

Gràcies a tots els amics del poble i de la universitat (grup 120 flexions, Helena, Guillem, Esther, Queralt…) per tot el suport i per fer-me desconnectar com cal. També, agraïr al meu equip de bàsquet Unió Esportiva Cellera-Amer-Les Planes per fer-me sentir part d'un equip i estimada. En especial, moltes gràcies Imma per formar aquest magnífic equip i pel currasso en ajudar-me a muntar la tesi, gracies de debó.

I ara toca la familia. Gràcies a tota la família Ballell i Hosa per donar-me suport. Gràcies tieta Sandra per sempre preocupar-te per mi i animar-me. I com no, moltes gràcies als de casa. Moltes gràcies papa i mama per cuidar-me sempre, donar-me suport i ajudar-me a ser millor persona cada dia. Si he arribat fins aquí, en part és gràcies a vosaltres. Gràcies de debò.

També vull donar les gràcies a l'Albert, en Pol i l'Olga. Gràcies sister per la complicitat, per escoltar-me, per aguantar-me i per ajudar-me en tot moment. Sóc molt afortunada de tenir-te com a germana, no ho canviaria per res del món.

I per acabar, moltes gràcies Marc. Gràcies per la paciència, per fer-me millorar dia a dia, per fer-me veure la vida des d'un altre punt de vista i per tots els banana breads energètics per escriure la tesi. Gràcies per formar part de l'aventura, en desitjo moltes més al teu costat.

Gràcies a tots de tot cor.

Lídia Ballell

Abstract

Drug delivery systems (DDS) are constantly evolving and improving, leading to new ways to provide protection and effective delivery of active molecules at the desired site of action. Among all the DDS, in this Thesis we are interested in DELOS nanovesicles, scientifically known as Quatsomes, which are thermodynamically stable nanoscopic unilamellar vesicles, composed of ionic surfactants and sterols in an equimolar ratio.

To prepare them, a one-step eco-efficient process, named DELOS-susp (Depressurization of an Expanded Liquid Organic Solution-suspension) is used. This platform is a reproducible, scalable, and compressed fluid-based method that produces nanovesicular systems with remarkable physicochemical characteristics, in terms of homogeneity, morphology, particle size, and stability. Knowing all the potentiality that this platform presents, the aim of this Industrial Thesis between Nanomol Technologies S.L and Nanomol research unit of the Institute of Materials Science of Barcelona (ICMAB-CSIC) is to study the translation of DELOS nanovesicles into new pharmaceutical products to obtain nanomedicines in more advanced formulation states by ensuring compliance with the quality, regulatory and finished product standards required by the pharmaceutical industry.

First, this Thesis is devoted to advance on the different stages of the pharmaceutical development of a new nanomedicine based on a recombinant human epidermal growth factor and DELOS nanovesicles (rhEGF-DELOS nanovesicles) for the treatment of complex wounds, such as diabetic foot ulcers and venous leg ulcers. The research findings obtained were really promising and considered this nanoformulation as a potential nanomedicine to enter in future clinical trials for the treatment of complex wounds.

In view of the advantages of DELOS nanovesicles as topical drug delivery systems, research efforts were focused on not only designing new nanoformulations with the high skin tolerability but also on exploring the feasibility of converting these colloidal dispersions to a more suitable dosage form for topical application, such as semi-solid hydrogel pharmaceutical forms.

Finally, to further explore DELOS nanovesicles potentiality, the development of new hybrid biologic-organic and inorganic-organic nanoparticles was also studied as strategy to endow new properties to the DELOS nanovesicle platform as advanced nanocarriers for drug delivery.

In summary, the results achieved in this Thesis support that DELOS nanovesicles can be successfully used as promising pharmaceutical products for drug delivery.

List of Abbreviations

A	**AA**	Acrylamide
	Abs	Absorbance
	AEMPS	Spanish Agency of Medicines and Medical Devices
	ANOVA	Analysis of variance
	AP	Aqueous Phase
	ATR-FTIR	Attenuated Total Reflectance Fourier Transform Infrared Spectroscopy.
C	**°C**	Celsius
	CF	Compressed Fluid
	Chol	Cholesterol
	CIGB	Center for Genetic Engineering and Biotechnology
	cm	centimeter
	CMCs	Chemistry Manufacturing and Controls
	CMC	Critical Micelle Concentration
	CO_2	Carbon dioxide
	CPC	Cetylpyridinium chloride
	Cryo-TEM	Cryogenic Transmission Electron Microscopy
	CQA	Critical Quality Attribute
	CTAB	Hexadecyltrimethylammonium bromide
	CTAC	Hexadecyltrimethylammonium chloride
	Cys or C	Cysteine
D	**DDSs**	Drug Delivery Systems
	DELOS	Depressurization of an Expanded Liquid Organic Solution
	DELOS-susp	Despressurization of an Expanded Liquid Organic Solution over a suspension
	DFUs	Diabetic Foot Ulcers
	DiI	1,1'-Dioctadecyl-3,3,3',3'-tetramethylindocarbocyanine perchlorate
	DiD	1,1'-Dioctadecyl-3,3,3',3'-tetramethylindodicarbocyanine perchlorate
	DLS	Dynamic Light Scattering

E	**EDX**	Energy Dispersive X-Ray Analysis
	EE%	Encapsulation Efficiency
	e.g.	For example
	EGF	Epidermal Growth Factor
	EGFR	Epidermal Growth Factor Receptor
	ELISA	Enzyme-Linked Immunosorbent Assay
	ELS	Electrophoretic light scattering
	EMA	European Medicines Agency
	EtOH	Ethanol
F	**F**	Fluorescence
	FDA	Food and Drug Administration
	FRET	Fluorescence Resonance Energy Transfer
G	**g**	Gram
	GLP	Good Laboratory Practice
	GMP	Good Manufacturing Practices
	GSH	Glutathione
	GUVs	Giant Unilamellar Vesicles
H	**h**	Hour
	HPLC-ESI-MS	High-Performance Liquid Chromatography-Electrospray Ionization-Mass Spectrometry
I	**ICH**	International Council for Harmonisation of Technical Requirements for Pharmaceuticals for Human Use
	ICMAB	Institut de Ciència de Materials de Barcelona
	i.e.	That is
	IR	Infrared spectroscopy
K	**kDA**	kiloDalton
	kg	Kilogram
L	**LUVs**	Large unilamellar vesicles
M	**M**	Molar
	MFD	Maximum Feasible Dose

	mg	Milligram
	MIC	Minimum Inhibitory Concentration
	Min	minute
	MKC	Miristalkonium chloride
	MLVs	Multilamellar vesicles
	mM	Millimolar
	mL	Milliliter
	MSNPs	Mesoporous Silica Nanoparticles
	mV	Millivolt
	MVVs	Multivesicular vesicles
	MW	Molecular Weight
N	**N**	Number of replicates
	N_2	Nitrogen
	NASA	National Aeronautics and Space Administration
	nm	Nanometer
O	**OP**	Organic Phase
P	***p***	Statistical ***p-value***
	P	Pressure
	Pa	Pascal
	Phe	Phenylalanine
	PBS	Phosphate-buffered saline
	PDI	Polydispersity index
	PEG	Polyethylene glycol
	PFPs	Pore-forming proteins
	pH	Potential of hydrogen
	Ph.D.	Doctor of Philosophy
	pI	Isoelectric Point
Q	**QASs**	Quaternary Ammonium Surfactants
R	**rh-EGF**	Recombinant Human Epidermal Growth Factor
	RISE	Research and Innovation Staff Exchange
	RP-HPLC-ELSD	Reversed Phase – High Performance Liquid chromatography Evaporative light scattering detection

S	**SAXS**	Small-Angle X-ray Scattering
	SCDN	Silica-coated DELOS nanovesicles
	SEM	Scanning Transmission Electron Microscopy
	SD	Standard Deviation
	SGF	Simulated Gastric Fluid
	ST	Stearalkonium chloride
	STEM	Scanning Transmission Electron Microscope
	Stn (n = I, II and III)	Sticholysin I, II and III
	SUVs	Small Unilamellar Vesicles
	SV	Stern-Volmer
T	**T**	Temperature
	TEM	Transmission Electron Microscopy
	TEMOS	Tetramethyl orthosilicate
	TFF	Tangential flow filtration
	TRL	Technology readiness leve
	Trp	Tryptophan
	Tyr	Tryrosine
U	**a.u.**	Arbitrary unit
	UAB	Universitat Autònoma de Barcelona
	UHPLC	Ultra Performance Liquid Chromatography
	USP/Ph.Eur	U.S. Pharmacopeia /Pharmacopoeia Europaea
	UV-Vis	Ultraviolet-Visible spectroscopy
V	**$v \cdot v^{-1}$**	Volume per volume
	VLUs	Venous Leg Ulcers
W	**W**	Tryptophan
	wt%	Weight total
	w·v	Weight per volume

Others	**λ**	Wavelength
	℃	Celsius
	$	Dollar
	μ	micro
	3D	Three-Dimension

"No one can persuade another to change. Each of us guards a gate of change that can only be opened from inside"

– Marilyn Ferguson

1 Introduction and Objectives

1.1 Introduction

1.1.1 The revolution of nanotechnology

Which are the challenges that society is facing nowadays? Are they all possible to solve? It is well-known that humanity is gaining more knowledge and control about the matter and how to make the most benefit of it. However, humankind by itself has found some limitations to understanding nature. In this context, nanoscience can play a major role in shedding light on these borders and go beyond our intrinsic limits as humans.

Nanoscience is defined as the area of science and engineering devoted to the study of matter at the nanoscale, where the properties of materials vary from those at a larger scale with distinctive novel functional properties[1]. A nanometer (nm) is an International System of Units unit that represents a length of 10^{-9} meter. However, nanostructured materials are commonly defined as those with at least one dimension in the range of 1 to 100 nm[2,3].

Furthermore, the concept of nanotechnology also exists, and is defined as the technology that uses nanoscience in practical applications and which is one of the most promising technologies of the 21st century[3]. As defined, "Nanotechnology is the intentional design, characterization, production, and applications of materials, structures, devices, and systems by controlling their size and shape in the nanoscale range"[2,4]. Therefore, when we work in the nanoscale range, we can work with new domains that do not apply to any other scale and so reshape the world around us.

Given this scenario, nanoscience and nanotechnology represent an active field of research and a techno-economic sector that is fully expanding in many fields of application[1,2,5]. In the healthcare sector, concepts such as nanomedicine are revolutionizing not only the way we see the world, but also the future of medicine. For instance, many changes are occurring

in healthcare services mostly based on the evolution of drug delivery for therapy, imaging modalities and diagnostics[6,7]. For example, to date, surgery, chemotherapy, and radiation therapy are the most commonly used treatments for dealing with diseases such as cancer. However, it is widely known that most of the current oncological treatments face problems such as lack of specificity, cytotoxicity, short half-life, poor solubility, occurrence of multi-drug resistance, etc.[8,9].

It is noteworthy to mention that to overcome these disadvantages, the most exciting concept in nanomedical research could be the design and development of multifunctional nanoparticle complexes that can simultaneously deliver therapeutic and diagnostic agents to targeted sites[7].

In particular, nanoparticle-drug conjugates are attracting a large interest for the development of targeted drug delivery due to certain advantage that nanoparticles offer. For example, they can provide appropriate nano-size and structure similar to almost all biological systems, desired physicochemical properties, enhancement of drug hydrophobicity, ability to cross cell barriers to deliver drugs to tumor sites, drug delivery to a site-specific target, allowing to be used for diagnostics and imaging, among others[10,11]. At the same time, it is desired that they act with high specificity, efficacy and personalization, with the aim of improving the patients' quality of life[12,13].

Following this idea, there are numerous research studies on nanomedical applications in the biomedical field, from the use of novel nanobiomaterials and nanotherapeutics to improvements in diagnosis, contrast reagents, and medical devices[11,14]. Consequently, this area of knowledge is expected to address various medical concerns and challenges related to traditional medicine[15].

1.1.2. Making drugs smarter with drug delivery systems

Among all nanomedical applications, drug delivery is one of the largest research areas with the greatest interest and a very active research community, representing around 50% of all nanomedical research[14].

Drug delivery refers to the process of transporting and delivering a therapeutic agent into the body with proper pharmacokinetics, thereby achieving and/or optimizing the desired therapeutic effect while minimizing side effects if possible[16,17]. Therefore, the development of drug delivery could be used as a strategy to encapsulate or attach therapeutic drugs and deliver them to a target-site more precisely with a controlled release while reducing drug toxicity and improving patient acceptance and compliance[18,19].

Nanotechnology offers new prospects and great potentials for drug delivery, overcoming some limitations of conventional drug delivery approaches. Specifically, among the present drug delivery systems, nanoparticles as carriers have shown great potential in recent years.

As different clinical needs require different types of drug delivery systems, various designs of nanocarriers are being developed in order to meet specific requirements. In particular, nanocarriers can be categorized by different criteria, such as surface functionality, size and shape, or nanoparticle nature[20]. According to the composition, nanoparticles are classified into polymeric-based nanocarriers (e.g., polymeric nanoparticles, polymeric micelles, dendrimers, or nanogels), lipid-based nanoparticles (e.g., nanovesicles, micelles, solid-lipid nanoparticles), protein-based nanoparticles (e.g., protein-complexes, or virus-like particles), but also inorganic-based nanocarriers (e.g., metallic, magnetic, and silica nanoparticles, quantum dots, or carbon nanotubes), among other types of materials[10,16] (**Figure 1.1**).

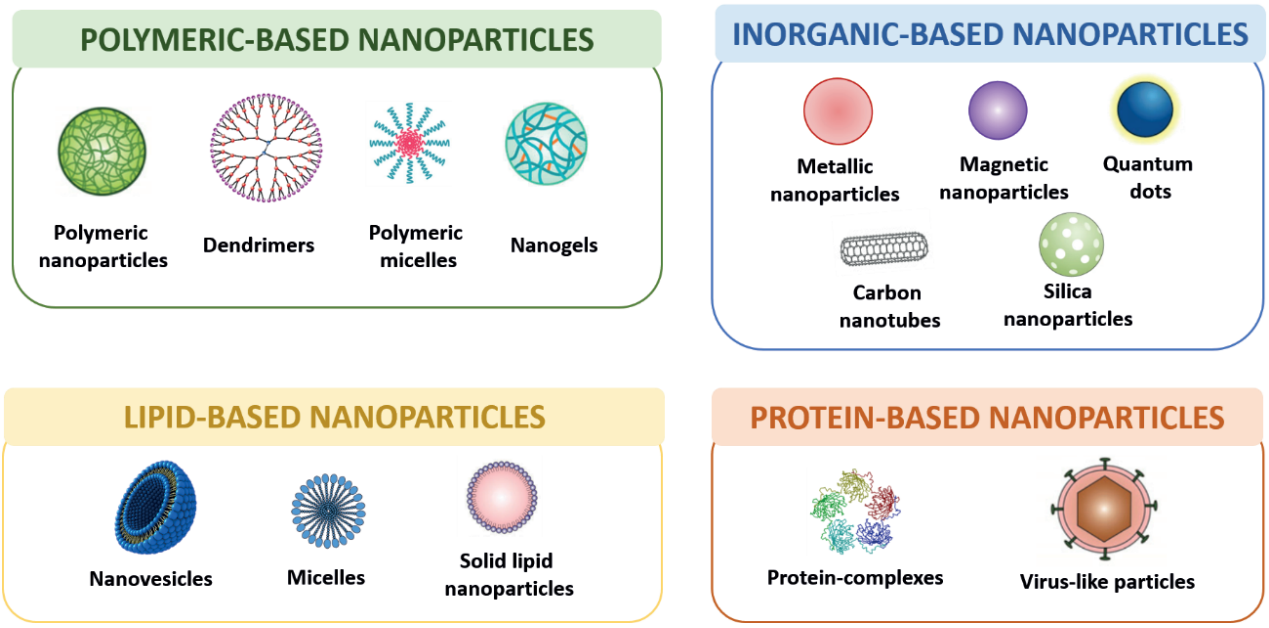

Figure 1.1: Overview of commonly used nanoparticle types, classified as polymeric-, inorganic-, lipid- and protein-based structures.

Considering all the exposed systems, the most widely used for drug delivery purposes are lipid-based nanocarriers[21] since they have been the most successful in reaching the clinical practice and arrival to the market[22]. For instance, successful lipid-based nanoparticles are the most common class of U. S. Food and Drug Administration (FDA)-approved nanomedicines[16,23,24] (**Table 1.1**).

Table 1.1: FDA-approved lipid-based nanomedicines. Adapted from[23].

Drug Company	Company	Application	Date of first approval
Doxil	Janssen	Kaposi's sarcoma, ovarian cancer, multiple myeloma	1995
DaunoXome	Galen	Kaposi's sarcoma	1996
AmBisome	Gilead Sciences	Fungal/protozoal infections	1997
Visudyne	Bausch and Lomb	Wet age-related macular degeneration, myopia, ocular histoplasmosis	2000
Marqibo	Acrotech Biopharma	Acute lymphoblastic leukaemia	2012
Onivyde	Ipsen	Metastatic pancreatic cancer	2015
Vyxeos	Jazz Pharmaceuticals	Acute myeloid leukaemia	2017
Onpattro	Alnylam Pharmaceuticals	Transthyretin-mediated amyloidosis	2018

1.1.3 Vesicles as self-assembled structures

Vesicles are a widely studied and diverse class of lipid-based nanoparticles composed of an amphiphilic membrane bilayer enclosing an aqueous core. In particular, these supramolecular structures can be formulated from a wide range of amphiphilic molecules, including lipids, polymers, and organic and inorganic small molecules. Their formation is mainly driven by thermodynamically favorable arrangement of hydrophobic moieties (e.g. nonpolar tails) while hydrophilic moieties (e.g. polar head groups) are exposed to the aqueous solution and protect the hydrophobic tails in the bilayer[22] (**Figure 1.2**). Moreover, the formed vesicles can present one or more bilayers characterized as unilamellar or multilamellar[25].

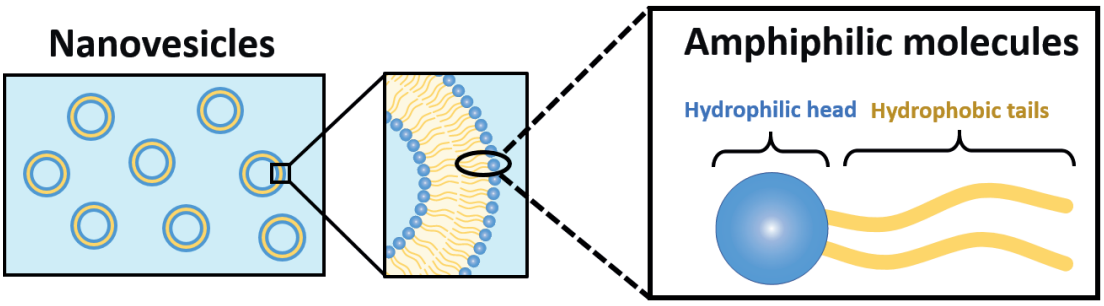

Figure 1.2: Schematic representation of the vesicles composed by the self-assembly of amphiphilic molecules.

Usually, as observed in **Figure 1.3**, they can be classified into small unilamellar vesicles/nanovesicles (SUVs, size < 200 nm and single bilayer), large unilamellar vesicles (LUVs, size ranging from 200–1000 nm and single bilayer), giant unilamellar vesicles (GUVs, size > 1000 nm and single bilayer), multilamellar vesicles (MLVs, consisting of several concentric bilayers) and multivesicular vesicles (MVVs, composed of several small vesicles entrapped into larger ones)[26,27].

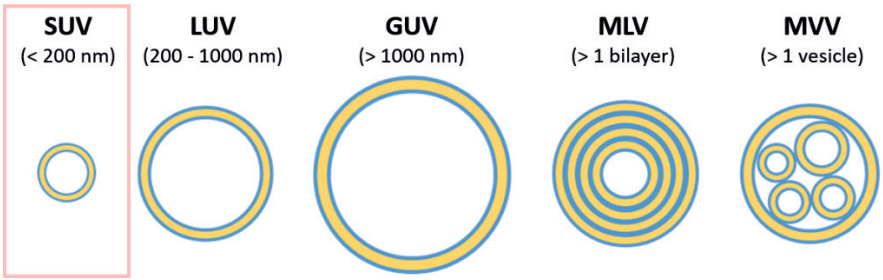

Figure 1.3: Types of vesicles depending on size and lamellarity: SUV, small unilamellar vesicle (< 200 nm); LUV, large unilamellar vesicle (200 - 1000 nm); GUV, giant unilamellar vesicle (> 1000 nm); MLV, multilamellar vesicle (> 1 bilayer); MVV multivesicular vesicle (> 1 vesicle). Adapted from[28,29].

Furthermore, vesicles are considered drug carriers since they can entrap hydrophobic compounds within the bilayers (lipidic compartment) and hydrophilic compounds in the lumen[30]. Therefore, they are potential drug delivery systems, largely employed in pharmaceutical and cosmetic fields, that can efficiently carry and protect different compounds within the body and finally deliver them at the target site[26].

In this sense, SUVs are usually requested as present as high homogeneity in size and lamellarity, which are structural parameters that need to be controlled since they can affect the vesicles' properties and performance, such as the encapsulation and release efficacy therapeutic agents[31]. Therefore, a high degree of structural homogeneity regarding size, morphology and composition is crucial for their optimum performance[32].

What is more, over the years, researchers in vesicle's drug delivery have discovered that by altering their surface functionalization by ligands (**Figure 1.4**), they can become more effective and efficient vehicles of delivering useful therapeutic substances in a targeted way. Consequently, these new smart and multifunctional systems overcome some challenges associated to conventional formulations[33,34]. For instance, the surface functionalization can provide key benefits as prolonged circulation time, enhanced cellular-uptake, higher accumulation at tumor site, and even the capacity of being stimuli-responsive to control the drug release at intended site[35,36].

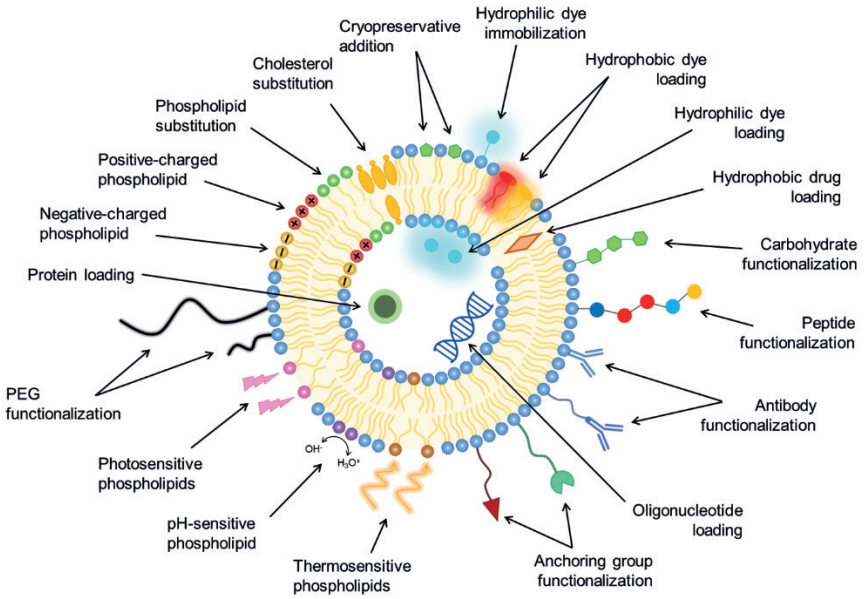

Figure 1.4: Possible modifications of a vesicle surface by the use of different ligands. Adapted from[29,36].

As shown in **Figure 1.4**, another important characteristic of vesicles is that they can integrate therapeutic substances of different nature. These actives could be small molecules and biologics, the last one defined as therapeutic products derived from biological sources and generally produced using biotechnological tools[37]. Unlike small molecular drugs (0.1- 1kDa), biologics tend to be larger (> 1 kDa) and more structurally complex, often showing potentially higher specificity, efficacy, and better targeting ability with reduced side effects[37].

Although vesicles appear to be very promising drug delivery systems, they can be prepared using a wide range of methods that can influence their characteristics such as size, lamellarity and encapsulation efficiency. Generally, the conventional methods for vesicle formation, such as thin film hydration or reverse-phase evaporation, present many shortcomings, such as poor structural homogeneity and poor stability, among others[28,38,39]. Then, to solve these drawbacks, further post-formation steps (i.e., sonication and extrusion, etc.) are required for size reduction and homogenization[40,41].

Unfortunately, these multistep procedures can damage the functionality of bioactive compounds and of oxidizing vesicle membrane components such as phospholipids[42,43]. Thus, all these weaknesses are important for the preparation of colloidal bioconjugates with expensive and/or fragile active biomolecules such as proteins, peptides, enzymes, or hormones. Then, this indicates a need to develop simple and mild processes to control of the structure at the micro-, nano-, and supramolecular levels, which are also amenable to be scalable[44].

1.1.4 DELOS-susp method to prepare nanovesicles

One of the leading alternatives to develop an efficient and environmental respectful technology for preparing nanostructured materials on an industrial scale is to use compressed fluids (CFs) technologies. In this sense, CFs take advantage of solvents such as carbon dioxide (CO_2) to replace the organic solvents, therefore serving as an alternative in synthesizing delivery systems[45]. Regarding this, CFs have proven to be very effective for the straightforward preparation of micro- and nanoparticulate materials, with reproducible supramolecular organization[46].

Indeed, a supercritical fluid (highly-compressed fluid) is defined as a substance that is above its critical pressure and temperature (P_c and T_c) and exhibits properties of both gases and liquids[47,48].

The most important feature within the supercritical region is that there is no phase boundary between the gas and liquid phases. As a results, the properties are "hybrids" of those normally associated with liquids and gases are at the same time, they are continuously adjustable from gas to liquid with small pressure and temperature variations. Thus, the viscosities and diffusivities of supercritical fluids are similar to those of the gas phase while the density is closer to that of the liquid[48].

In particular, CO_2 is the most commonly used as CFs in the pharmaceutical industry and is classified as a safe solvent by the FDA[49]. CO_2 is an inert, colorless, odorless, non-toxic, non-flammable, inexpensive, and recyclable gas. It is interesting to note that when gases such as CO_2 are compressed, they become dense phase fluids that exhibit enhanced thermodynamic properties of solvation, selection, penetration, and expansion. For example, the phase diagram of CO_2 in **Figure 1.5** clearly shows that above critical temperature and pressure CO_2 acts as a supercritical fluid (T_c = 31.1°C and P_c = 73.8 bar)[48,50,51].

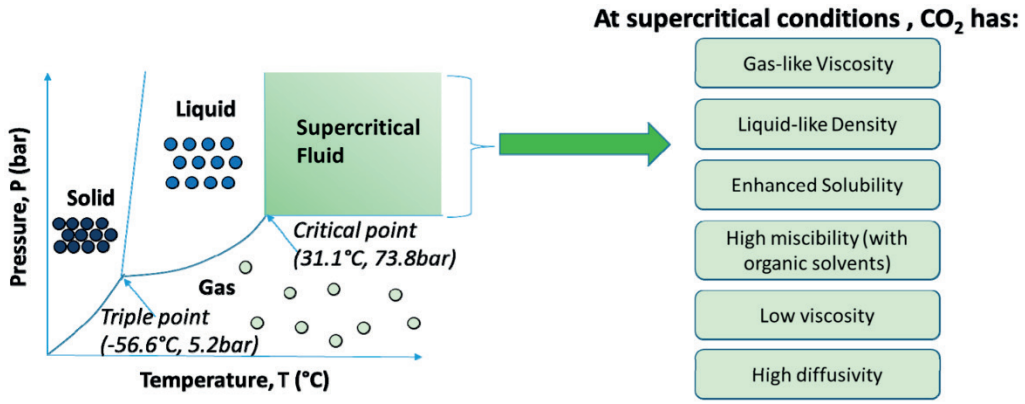

Figure 1.5: Typical phase diagram for carbon dioxide (CO_2), which exhibits three phases solid, liquid, and gas, and a supercritical region. Adapted from[49].

In connection with the thriving CFs-based technologies, the process called Depressurization of an Expanded Organic Solution (DELOS), based on compressed CO_2 was developed in Nanomol research unit of Institute of Materials Science of Barcelona (ICMAB-CSIC) and is currently owned, scaled-up and commercialized by Nanomol Technologies SL, to produce micro- and submicron-sized crystalline particles with high polymorphic purity[52,53].

In this process, CO_2 acts as a co-solvent since it is completely miscible at a given pressure and temperature with an organic solution containing the solute to be crystallized[54,55]. DELOS requires milder pressure and temperature conditions (< 10 MPa and 35 °C) than other compressed fluids-based methods[28,39], which allows the processing of heat-labile compounds while reducing the investment costs for the scale-up of the production plant[56].

Later on, a new and improved process for the production of colloidal suspensions was developed on the basis of the DELOS process. This new method, called Depressurization of an Expanded Organic Solution-Suspension (DELOS-susp) enables the one-step preparation of multifunctional cholesterol-rich nanovesicles such as liposomes (phospholipid-based vesicles) and DELOS nanovesicles, scientifically known as Quatsomes, as well as nanovesicle-(bio)active hybrids[56].

Briefly, the DELOS-susp procedure includes (**Figure 1.6**):

1. Loading the hydrophobic membrane components solution and the desired hydrophobic actives in an organic solvent (like ethanol) into a high-pressure vessel previously driven to the working temperature (T_W = 35 °C) and atmospheric pressure (**Figure 1.6a**).
2. Addition of liquid compressed CO_2 and formation of a CO_2-expanded solution with the membrane components dissolved, at T_W = 35 °C and working pressure P_w = 10 MPa (**Figure 1.6b**).
3. Finally, depressurization of the CO_2-expanded solution over an aqueous phase containing the hydrophilic membrane components and hydrophilic (bio)actives occurs. (**Figure 1.6c**). In this final step, a flow of N_2 at the working pressure P_w = 11 MPa is used to plunge the CO_2-expanded solution from the reactor, maintaining a constant pressure inside the vessel during depressurization. In this step, the expanded organic solution experiences a large, abrupt, and extremely homogenous temperature decrease produced by the CO_2 evaporation from the expanded solution. This might explain why DELOS-susp platform provides more vesicle-to-vesicle homogeneity and supramolecular organization, compared to conventional procedures[57,58].

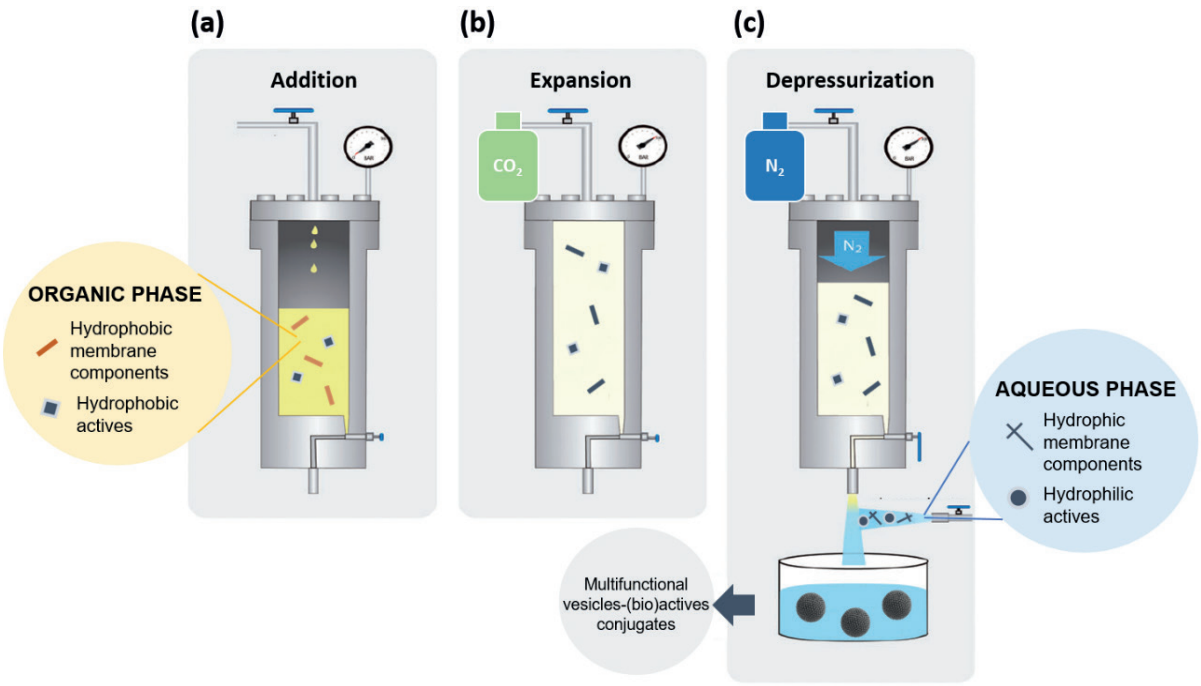

Figure 1.6: Schematic representation of the DELOS-susp method for the preparation of multifunctional nanovesicle-(bio)active hybrids incorporating actives (drugs, molecules for imaging, targeting agents etc.). The three stages of the process are described in the text.

Interestingly, this technique allows for high incorporation of cholesterol since there is not a free-solvent state[46], like in the case of conventional methods. Then, DELOS-susp platform demonstrates that it is a simple, robust, scalable and one-step process to prepare a large number of SUVs with different functionalities and high structural homogeneity, high batch-to-batch consistency and easy scalability, which are essential requirements for clinical translation[44,58].

1.1.5 Non-liposomal DELOS nanovesicles

DELOS nanovesicles, also known as Quatsomes in the scientific literature, are novel stable nonphospholipid-based nanovesicles that use aqueous mixtures of cholesterol (chol) and ionic surfactants, such as the quaternary ammonium surfactant hexadecyltrimethylammonium bromide (CTAB), in a 1:1 molar ratio, causing the formation of a synthon at the free-energy minimum state[59].

As pure species, ionic surfactants form micelles and insoluble cholesterol forms crystals in water. However, in aqueous media, the mismatch in size between the two molecules and the rigidity of the cholesterol molecule causes the polar ammonium head group of the surfactant to deform around the polar oxygen group of cholesterol. Specifically, thanks to molecular dynamic simulations, it has

been revealed that in the presence of water, CTAB and cholesterol molecules self-assemble into bimolecular amphiphiles, followed by the formation of bilayers and so the formation of DELOS nanovesicles[59,60] (**Figure 1.7**).

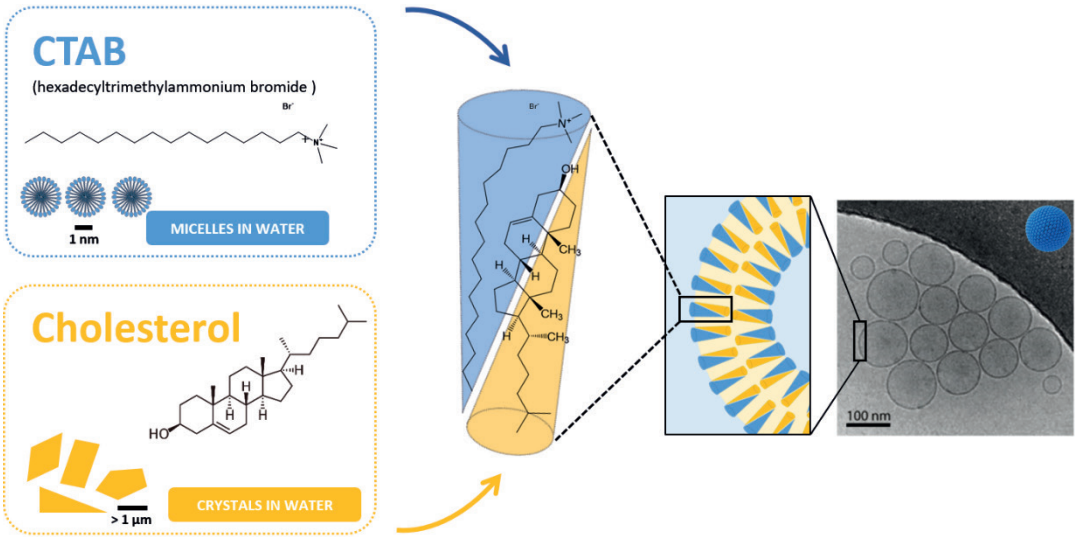

Figure 1.7: From left to right: molecular structures of CTAB and cholesterol along with a schematic representation of their structures in water. At the right: schematic representation of the organization of a CTAB-cholesterol synthon, its organization forming a membrane and a representative cryo-TEM image of these vesicles. Adapted from[59].

Due to their unilamellarity and their homogeneous morphology, DELOS nanovesicles are ideal nanoparticles for functionalizing their membranes, which is very important for a robust and efficient drug targeting[58,60]. In this sense, the hydrophilic biocompatible poly(ethylene glycol) (PEG) polymer has been efficiently anchored to the DELOS nanovesicle as strategy to avoid fast clearance of vesicles by opsonization and to increase the blood circulation time in the body[58].

More importantly, another relevant characteristic that is particular pertinent for this system is that their membrane components are not expensive and available at pharmaceutical grade. For instance, the surfactants forming the DELOS nanovesicle membrane are widely used as disinfectants, algaecides, preservatives, detergents and antistatic components, giving them antibacterial feature[26,61,62].

Knowing all this information, it can be considered that DELOS nanovesicles fulfill the structural and physicochemical requirements to be a potential encapsulation platform for site-specific delivery of both hydrophilic and lipophilic molecules with high pharmaceutical quality[58,63,64].

1.1.6 DELOS nanovesicles as a promising platform for multiple applications

It is remarkable to state that most of the current evidence found in Nanomol Group of ICMAB-CSIC and Nanomol Technologies SL, where this Industrial Ph.D. has been carried out, supports the use DELOS nanovesicles as promising platforms for different applications. In this context, different types of DELOS nanovesicles have been explored and physiochemically characterized for different purposes. For instance, as observed in **Table 1.2**, different cationic quaternary ammonium surfactants such as CTAB and myristalkonium chloride (MKC) and anionic surfactants such as sodium dodecyl sulfate (SDS) have been tested. As shown, DELOS nanovesicles constitute a promising platform not only as drug delivery systems for therapeutic applications but also as bioimaging and biosensing applications.

Table 1.2: Successful DELOS nanoformulations currently published/patented and their characteristics.

DELOS nanovesicle components	Loaded active ingredient	Application	Conclusion
Chol/CTAB	Recombinant human epidermal growth factor (rhEGF)	Drug delivery	Preliminary studies showed proper physicochemical properties and efficacy of rhEGF loaded DELOS nanovesicles for the topical treatment of complexed wounds. The importance of the nanostructuration in the efficacy of nanomedicines is confirmed[64,65].
Chol/MKC	N/A	Drug delivery	Suitability for *in vivo* dosing. Not only their structure seems to be preserved even after intravenous injection into mice but also any toxicity was observed at the administered i.v. doses in mice[66].
Chol/MKC	sRNA	Drug delivery	Stable nanovesicles with tunable pH sensitiveness that constitute an attractive platform for the efficient delivery of sRNAs (miRNA and siRNA)[67].
Chol/CTAB **Chol/MKC**	Carbocyanine dyes/Silicon nanocrystals	Optical Bio-imaging	Fluorescent-labeled DELOS nanovesicles are promising candidates for the development of fluorescent proves overcoming most of the current challenges on the design of organic dye-based systems for optical bioimaging [60,63,66,68].
Chol/MKC **Chol/SDS**	Carbocyanine dyes and Chol-DNA probe	Bio-sensing	Highly stable and bright FRET-active DELOS nanovesicles for the intracellular detection of molecular analytical targets [69].

Then, as reported, some interesting DELOS nanovesicles applications have been experimentally demonstrated, opening new challenges in the field of drug delivery, bio-imaging and bio-sensing. However, these nanoformulations are in the first stages of research and development and so in the primary Technology Readiness Levels (TRL).

Specifically, the concept of TRL scale was first introduced by the National Aeronautics and Space Administration (NASA) in the 70s as a methodology to allow more effective assessment of, and communication regarding the maturity of new technologies[70,71]. However, nowadays it is used as a tool for assessing the maturity of the development of a product and that can be applied in diverse areas of knowledge[72].

A nine-level standard scale is used in this assessment to estimate the state of technical development based on quality parameters (**Figure 1.8**). In terms of developing a nanomedicine, TRL1 is the lowest level of technology maturation, which involves the observation and reporting of basic principles, and these begin to be translated into more applied research and development[71]. Then, TRL2 focus on the experimental design, testing hypothesis and data collection, so basic research. At this step in the maturation process, active research and development is initiated and so TRL3 is achieved by the identification of preliminary candidates and preclinical studies for proof-of-concept[71].

If the efficacy of the process is demonstrated *in vivo*, the process is defined as optimized and achieves TRL4. Next, TRL5 is achieved if there is the implementation of Good Manufacturing Practices (GMP), which is realized through rigorous and precise testing in a realistic environment, and there is a high probability of the nanopharmaceutical to get into the clinical trials phase.

TRL6 involves the production of a batch according to GMP requirements to be available for Phase 1 of clinical trials, in which the pharmacokinetic and pharmacodynamic parameters will be evaluated to define the drug system model and obtain the second proof-of-concept. After entering the clinical trial phase, the model can no longer be modified. Regarding TRL7, a scale-up process is required to be structured according to GMP to be accepted in a Phase 2 of clinical trials related to safety evaluation. Finally, TRL8 refers to Phase 3 of clinical trials and marketing authorization, and TRL9 refers to post-authorization actions. Afterwards, the product is officially on the market[73,74].

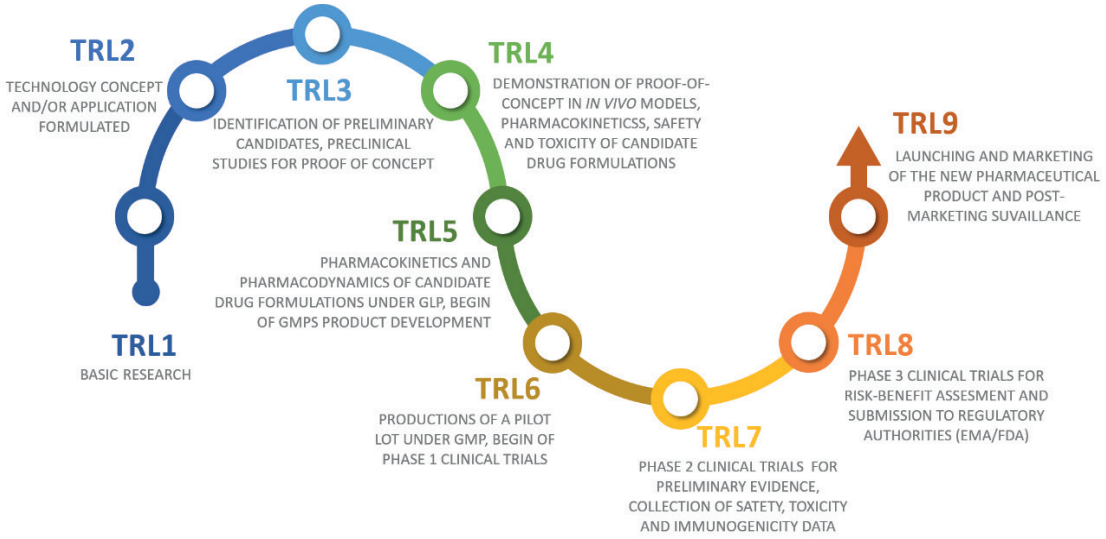

Figure 1.8: Technology Readiness Levels (TRL) and steps of research and development of a pharmaceutical product. Adapted from[73].

Then, given the potentiality of DELOS-susp technology, this Thesis is devoted to the experimental research and development of DELOS nanovesicles to a point closer to where they can merged into a new product or system[74]. To do it, it is important to highlight that this is an Industrial Ph.D thesis conducted jointly by Nanomol Technologies SL company and Nanomol Group of ICMAB-CSIC.

Essentially, Nanomol Technologies SL is a science and innovation-driven company, co-founded by researchers of Nanomol Group, that offers advanced solutions and technologies to obtain high-added-value products through particle design and nanoformulation. Therefore, this research will be in a pragmatic and applicable way to generate useful information about DELOS nanovesicles and so exploit the DELOS-susp platform, mainly for topical delivery.

Interestingly, this route of administration aims to deliver a therapeutically effective concentration of the drug directly to skin layers that are the target tissues, thus exerting a local effect[75,76].

1.1.7 Topical drug delivery

This route of administration offers several advantages, such as convenient use and easy delivery, the drug is delivered selectively at a specific site and the area of application is larger compared to other routes. In addition, it enables self-medication and offers better patient compliance compared to other routes of administration[77].

The skin is the largest organ in the human body, serving as a unique interface between the body and the external environment and providing a key barrier with immunological, sensorial and protective

capabilities[78]. In particular, the skin is a membranous, flexible, and protective cover, composed primarily of by three different tissue layers.

As shown in **Figure 1.9**, epidermis is the outermost and non-vascularized tissue layer. This tissue is based on a multi-layered structure composed of viable cells and dead keratinized cells[79]. Then, the epidermis is supported by a second layer of skin called dermis, which is an internal and vascularized tissue that contains a network of blood vessels, lymphatic vessels, hair follicles, sweat glands, among others. Finally, the hypodermis is located under the dermis, which is consists mainly of fibroblasts and adipocyte-subcutaneous fatty tissues[80].

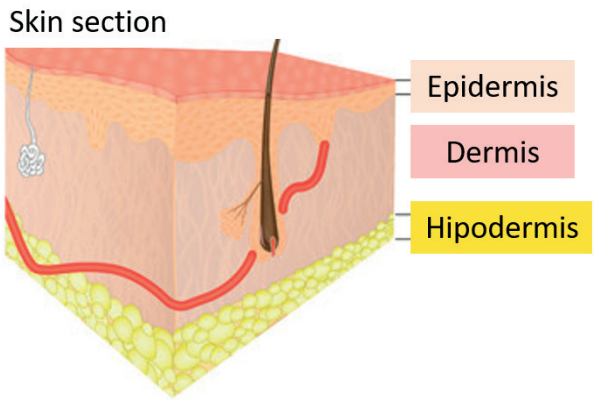

Figure 1.9: Schematic illustration of human skin layers. Adapted from[80].

However, skin can suffer disorders related to the dysfunction of the skin components or the layer's defect of human skin, affecting its integrity in different ways[78,81]. In particular, many skin-associated problems, such as complex wounds, are related especially to infectious skin disease. Therefore, they usually remain difficult to treat and so provoking a substantial economic burden to healthcare system[82,83].

Therefore, considering all these points, the delivery of nanoparticles to the skin is increasingly used to facilitate local therapies[84]. However, to become a successful topical formulation, some parameters should be considered such as:

It should be physically and chemically stable having adequate shelf life[85].

Releases drug from the formulation, if necessary, and delivers it into the skin as required for the target indication.

It is acceptable to patients, easy to apply and compatible with the desired packaging.

It can be manufactured with a process that is scalable to commercial levels.

Considering these properties and the potentiality of DELOS nanovesicles, it is hypothesized that they can offer an innovative approach to drug delivery and so be an excellent approach in the treatment of different skin diseases, such as complex wounds, acne, skin inflammation, and wound healing problems. They can provide a range of benefits including drug protection, modified pharmacokinetics and distribution, increased dose delivery to target sites, enhanced drug transport through biological membranes and prolonged or controlled drug release[58,86,87]. Finally, the antibacterial efficacy of the formulation can also help on the skin infections treatment, which might be achieved using the quaternary ammonium surfactants of the formulation, as already reported its potentiallity[88,89].

1.1.7.1 DELOS nanovesicles for the treatment of complex wounds

Complex wounds, such diabetic foot ulcers (DFUs) and venous leg ulcers (VLUs), are wounds that fails to heal and cannot heal in terms of anatomical and functional integrity not only due to severe impairment of the healing process but also due to unresolved inflammation and the presence of infection[90]. Despite significant efforts in developing strategies and commercialization of various therapeutic products, clinical success in healing chronic wounds has been limited, mainly owing to the complex nature of the healing process and our limited understanding of the processes involved in skin regeneration[90,91]. Then, new approaches, such as the use of nanomedicine, need to be introduced to overcome this problem.

In this framework, it is important to emphasize that one of the main purposes of this Thesis is the development of new pharmaceutical products based on DELOS nanovesicles for topical administration, which is a new and relatively unexplored area of Nanomol Group and Nanomol Technologies. Specifically, one of the main goals of this research was based on the reformulation of a biologic called epidermal growth factor for the treatment of complex wounds. This has attracted intense interest due to the potential applications in various facets of human healthcare, particularly to enhance the healing process. However, its functionality can be compromised if applied directly to wounds without any protection[92].

Although biologics present potentiality, the use of a nanocarrier such as DELOS nanovesicles can be an attractive platform to improve the bioavailability and efficacy of the biologic [26,58,59]. As shown in **Table 1.1**, preliminary and successful experiments were performed to try to integrate a recombinant human epidermal growth factor (rhEGF) into DELOS nanovesicles composed of cholesterol and CTAB. Interestingly, these experiments showed promising results regarding the efficacy of this new nanoformulation for the topical treatment of complex wounds.

However, this initial approach focused on TRL1 and TRL2, where basic research was conducted to obtain a proof-of-concept nanomedicine formulation named rhEGF-DELOS nanovesicles. However, the advancement of this initial nanoformulation to more mature stages such as TRL4 and TRL5 is essential to overcome its limitations and work towards future effective translation of the nanomedicine into a novel product for the topical treatment of complex wounds.

On the other hand, when developing a formulation, it is also reasonable to think that the design of a final topical drug product is a key parameter to consider to not only achieve a proper delivery of the drug but also the consumer's acceptance[93]. Therefore, choosing the proper drug dosage form, which consists of the drug substance and/or excipients, will facilitate the dosing, administration, and delivery of the content of the drug product to the patient. In this context, various formulations such as foams, sprays, hydrogels, solutions or other forms are widely used as dosage forms topical route[94].

Then, research efforts are needed on exploring the feasibility of adapting the colloidal dispersions of DELOS nanovesicles to suitable dosage forms for topical administration route. Specifically, the translation of rhEGF-DELOS nanovesicle intermediate product into new dosage forms is necessary for the treatment of complex wounds (**Figure 1.10**).

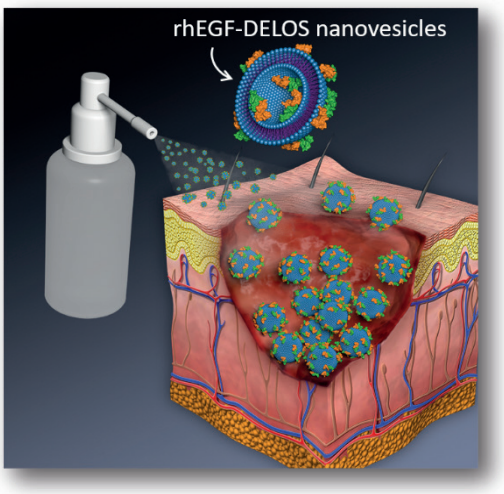

Figure 1.10: Example of a gaseous dosage form of rhEGF-DELOS nanovesicles for topical treatment of complex wounds.

From a pharmaceutical industry perspective, the innovation of DELOS nanovesicles into new final drug formulations will be a significant advance in drug delivery development, as it will lead to more differentiated DELOS nanovesicle products. This challenge motivated the present Industrial Thesis project, which is expected to boost the innovation and competitiveness of DELOS nanovesicles.

Overall, the present Thesis is devoted to deep study of the translation of DELOS nanovesicles, such as rhEGF-DELOS nanovesicles, into new pharmaceutical products for topical administration, e.g. complex wound treatment. Furthermore, the formation of hybrid structures composed of DELOS nanovesicles and biological or inorganic compounds will be also explored, to not only enhance the potential of DELOS nanovesicles but also to evaluate new routes of administration.

1.2 Objectives

Over the last years there has been intensive research activity at the Nanomol research unit of ICMAB-CSIC and at Nanomol Technologies SL, to investigate and deeply characterize highly stable and remarkably uniform DELOS nanovesicles, scientifically known as Quatsomes. Considering the high potential of these nanovesicles for the development of new nanomedicines, the main goal of this industrial thesis is to investigate the translation of DELOS nanovesicles into pharmaceutical products.

More specifically, in the present doctoral project the following five objectives are addressed:

1. Investigation and development of DELOS nanovesicles loaded with recombinant human epidermal growth factor (rhEGF), named rhEGF-DELOS nanovesicles, as an intermediate product for the preparation of pharmaceutical formulations for topical treatment of diabetic foot ulcers (DFUs) and venous leg ulcers (VLUs).
2. Translation of the rhEGF-DELOS nanovesicle intermediate product into hydrogel and gaseous dosage forms for the development of new final pharmaceutical products for the topical treatment of complex wounds and other skin diseases.
3. Study on new DELOS nanovesicles for the topical administration of synthetic and biological active ingredients with high skin tolerance and good formulatability as semi-solid hydrogel dosage forms.
4. Research and development of new hybrid biologic-organic nanoparticles based on DELOS nanovesicles integrating sticholysins proteins, which are widely used as effective pore formers on cell membrane, thus enhancing drug delivery.
5. Deep physicochemical characterization of new hybrid inorganic-organic nanoparticles composed of DELOS nanovesicles coated with a silica shell and preliminary analysis of their potential as nanocarriers for drug delivery.

1.3 References

1. S. Amir, A. Jamal, A. Elmoneim, et al. Innovations in nanoscience for the sustainable development of food and agriculture with implications on health and environment. *Sci. Total Environ.* **2021**, 768, 144990.
2. J. Jeevanandam, A. Barhoum, Y.S. Chan, A. Dufresne, M.K. Danquah. Review on nanoparticles and nanostructured materials: history, sources, toxicity and regulations. *Beilstein J. Nanotechnol.* **2018**, 9 (1), 1050–1074.
3. S. Bayda, M. Adeel, T. Tuccinardi, M. Cordani, F. Rizzolio. The history of nanoscience and nanotechnology: From chemical-physical applications to nanomedicine. *Molecules* **2020**, 25 (1), 112.
4. K. Riehemann, S.W. Schneider, T.A. Luger, et al. Nanomedicine—challenge and perspectives. *Angew. Chemie Int. Ed.* **2009**, 48 (5), 872–897.
5. A. Huguet-Casquero, E. Gainza, J.L. Pedraz. Towards Green Nanoscience: From extraction to nanoformulation. *Biotechnol. Adv.* **2021**, 46, 107657.
6. B. Jamil, M. Rai. Nanotheranostics: An emerging nanoscience. In *Nanotheranostics: Applications and Limitations*; Rai, M., Jamil, B., Eds.; Springer International Publishing, **2019**; pp 1–18.
7. C. Lee Ventola. The Nanomedicine Revolution: Part 1: Emerging Concepts. *Pharm. Ther.* **2012**, 37 (9), 512.
8. Z. Cheng, M. Li, R. Dey, Y. Chen. Nanomaterials for cancer therapy: current progress and perspectives. *J. Hematol. Oncol.* **2021**, 14 (1), 1–27.
9. M. Chamundeeswari, J. Jeslin, M.L. Verma. Nanocarriers for drug delivery applications. *Environ. Chem. Lett.* **2019**, 17 (2), 849–865.
10. P. Taneja, S. Sharma, V.B. Sinha, A.K. Yadav. Advancement of nanoscience in development of conjugated drugs for enhanced disease prevention. *Life Sci.* **2021**, 268, 118859.
11. C. Fornaguera, M.J. García-Celma. Personalized nanomedicine: A revolution at the nanoscale. *J. Pers. Med.* **2017**, 7 (4), 12.
12. H. Boulaiz, P.J. Alvarez, A. Ramirez, et al. Nanomedicine: Application Areas and Development Prospects. *Int. J. Mol. Sci.* **2011**, 12 (5), 3303–3321.
13. B. Pelaz, C. Alexiou, R.A. Alvarez-Puebla, et al. Diverse Applications of Nanomedicine. *ACS Nano* **2017**, 11 (3), 2313–2381.

14. C. Zhang, L. Yan, X. Wang, et al. Progress, challenges, and future of nanomedicine. *Nano Today* **2020**, 35, 101008.

15. H. Hao, Y. Chen, M. Wu. Biomimetic nanomedicine toward personalized disease theranostics. *Nano Res.* **2021**, 14 (8), 2491–2511.

16. C. Li, J. Wang, Y.Y. Wang, et al. Recent progress in drug delivery. *Acta Pharm. Sin. B* **2019**, 9 (6), 1145–1162.

17. H. Wen, H. Jung, X. Li. Drug Delivery Approaches in Addressing Clinical Pharmacology-Related Issues: Opportunities and Challenges. *AAPS J.* **2015**, 17 (6), 1327–1340.

18. A.M. Vargason, A.C. Anselmo, S. Mitragotri. The evolution of commercial drug delivery technologies. *Nat. Biomed. Eng. 2021 59* **2021**, 5 (9), 951–967.

19. J.K. Patra, G. Das, L.F. Fraceto, et al. Nano based drug delivery systems: recent developments and future prospects. *J. Nanobiotechnology* **2018**, 16 (1), 1–33.

20. Y. Deng, X. Zhang, H. Shen, et al. Application of the Nano-Drug Delivery System in Treatment of Cardiovascular Diseases. *Front. Bioeng. Biotechnol.* **2020**, 7, 489.

21. M. Germain, F. Caputo, S. Metcalfe, et al. Delivering the power of nanomedicine to patients today. *J. Control. Release* **2020**, 326, 164–171.

22. U. Kauscher, M.N. Holme, M. Björnmalm, M.M. Stevens. Physical stimuli-responsive vesicles in drug delivery: Beyond liposomes and polymersomes. *Adv. Drug Deliv. Rev.* **2019**, 138, 259–275.

23. M.J. Mitchell, M.M. Billingsley, R.M. Haley, et al. Engineering precision nanoparticles for drug delivery. *Nat. Rev. Drug Discov.* **2021**, 20 (2), 101–124.

24. J.P. Martins, J. das Neves, M. de la Fuente, et al. The solid progress of nanomedicine. *Drug Deliv. Transl. Res.* **2020**, 10 (3), 726–729.

25. C.J. Camilo, D.O.D. Leite, A.R.A.E. Silva, et al. Lipid vesicles: applications, principal components and methods used in their formulations. A review. *Acta Biológica Colomb.* **2020**, 25 (2), 339–352.

26. N. Grimaldi, F. Andrade, N. Segovia, et al. Lipid-based nanovesicles for nanomedicine. *Chem. Soc. Rev.* **2016**, 45 (23), 6520–6545.

27. . Akbarzadeh, R. Rezaei-Sadabady, S. Davaran, et al. Liposome: classification, preparation, and applications. *Nanoscale Res. Lett.* **2013**, 8 (1), 1–9.

28. L. Maja, K. Željko, P. Mateja. Sustainable technologies for liposome preparation. *J. Supercrit. Fluids* **2020**, 165, 104984.

29. G. Vargas-Nadal. Novel Quatsome nanovesicles, prepared using compressed CO2, for the development of advanced nanomedicines "Doctoral dissertation," Universitat de Barcelona, **2020**.

30. P. Trucillo, R. Campardelli, E. Reverchon. Liposomes: From bangham to supercritical fluids. *Processes* **2020**, 8 (9), 1022.

31. V. Nele, M.N. Holme, U. Kauscher, et al. Effect of Formulation Method, Lipid Composition, and PEGylation on Vesicle Lamellarity: A Small-Angle Neutron Scattering Study. *Langmuir* **2019**, 35 (18), 6064–6074.

32. B. Flühmann, I. Ntai, G. Borchard, S. Simoens, S. Mühlebach. Nanomedicines: The magic bullets reaching their target? *Eur. J. Pharm. Sci.* **2019**, 128, 73–80.

33. N.T.T. Le, V. Du Cao, T.N.Q. Nguyen, et al. Soy lecithin-derived liposomal delivery systems: Surface modification and current applications. *Int. J. Mol. Sci.* **2019**, 20 (19), 4706.

34. A.A. Khan, K.S. Allemailem, S.A. Almatroodi, A. Almatroudi, A.H. Rahmani. Recent strategies towards the surface modification of liposomes: an innovative approach for different clinical applications. *3 Biotech* **2020**, 10 (4), 1–15.

35. M.K. Riaz, M.A. Riaz, X. Zhang, et al. Surface functionalization and targeting strategies of liposomes in solid tumor therapy: A review. *Int. J. Mol. Sci.* **2018**, 19 (1), 195.

36. H. Wang, Y. Huang. Combination therapy based on nano codelivery for overcoming cancer drug resistance. *Med. Drug Discov.* **2020**, 6, 100024.

37. F.D. Makurvet. Biologics vs. small molecules: Drug costs and patient access. In *Medicine in Drug Discovery*; **2021**; Vol. 9, p 100075.

38. G. Bozzuto, A. Molinari. Liposomes as nanomedical devices. *Int. J. Nanomedicine Dovepress* **2015**, 10, 975–999.

39. B.S. Pattni, V. V. Chupin, V.P. Torchilin. New Developments in Liposomal Drug Delivery. *Chem. Rev.* **2015**, 115 (19), 10938–10966.

40. S. Verma, S.K. Singh, G. Jambheshwar, P. Mathur. Nanoparticle vesicular systems: A versatile tool for drug delivery. *J. Chem. Pharm. Res.* **2010**, 2 (2), 496–509.

41. M. Çagdas, A.D. Sezer, S. Bucak. Liposomes as Potential Drug Carrier Systems for Drug Delivery. In *Application of Nanotechnology in Drug Delivery*; Sezer, A. D., Ed.; IntechOpen, **2014**; pp 1--50.

42. A.M. Seddon, P. Curnow, P.J. Booth. Membrane proteins, lipids and detergents: Not just a soap opera. *Biochim. Biophys. Acta - Biomembr.* **2004**, 1666 (1–2), 105–117.

43. L. Maja, K. Željko, P. Mateja. Sustainable technologies for liposome preparation. *J. Supercrit. Fluids* **2020**, 165, 104984.

44. M.A.W. Eaton. Improving the translation in Europe of nanomedicines (a.k.a. drug delivery) from academia to industry. *J. Control. Release* **2012**, 164 (3), 370–371.

45. R.K. Kankala, Y.S. Zhang, S. Wang, C. Lee, A. Chen. Supercritical Fluid Technology : An Emphasis on Drug Delivery and Related Biomedical Applications. *Adv. Healthc. Mater.* **2017**, 6 (16), 1700433.

46. E. Elizondo, J. Larsen, N.S. Hatzakis, et al. Influence of the Preparation Route on the Supramolecular Organization of Lipids in a Vesicular System. *J. Am. Chem.Soc* **2012**, 134 (4), 1918–1921.

47. I. Pasquali, R. Bettini. Are pharmaceutics really going supercritical? *Int. J. Pharm.* **2008**, 364 (2), 176–187.

48. B. Topuz, G. Günal, S. Guler, H.M. Aydin. Use of supercritical CO2 in soft tissue decellularization. In *Methods in Cell Biology*; Caballero, D., Kundu, S. C., Reis, R. L., Eds.; Academic Press, **2020**; Vol. 157, pp 49–79.

49. S.H. Soh, L.Y. Lee. Microencapsulation and Nanoencapsulation Using Supercritical Fluid (SCF) Techniques. *Pharmaceutics* **2019**, 11 (1), 21.

50. P. Chakravarty, A. Famili, K. Nagapudi, M.A. Al-Sayah. Using Supercritical Fluid Technology as a Green Alternative During the Preparation of Drug Delivery Systems. *Pharmaceutics* **2019**, 11 (12), 629.

51. T. Castor. Phospholipid Nanosomes. *Curr. Drug Deliv.* **2005**, 2 (4), 329–340.

52. S. Sala, A. Córdoba, E. Moreno-Calvo, et al. Crystallization of Microparticulate Pure Polymorphs of Active Pharmaceutical Ingredients Using CO2-Expanded Solvents. *Cryst. Growth Des.* **2012**, 12 (4), 1717–1726.

53. S. Sala, E. Elizondo, E. Moreno, et al. Kinetically driven crystallization of a pure polymorphic phase of stearic acid from CO2-expanded solutions. *Cryst. Growth Des.* **2010**, 10 (3), 1226–1232.

54. N. Ventosa, S. Sala, J. Veciana, J. Torres, J. Llibre. Depressurization of an Expanded Liquid Organic Solution (DELOS): A New Procedure for Obtaining Submicron-or Micron-Sized Crystalline Particles. *Cryst. Growth Des.* **2001**, 1 (4), 299–303.

55. N. Ventosa, S. Sala, J. Veciana. DELOS process: A crystallization technique using compressed fluids: 1. Comparison to the GAS crystallization method. *J. Supercrit. Fluids* **2003**, 26 (1), 33–45.

56. M. Cano-Sarabia, N. Ventosa, S. Sala, et al. Preparation of uniform rich cholesterol unilamellar nanovesicles using CO2-expanded solvents. *Langmuir* **2008**, 24 (6), 2433–2437.

57. E. Elizondo, J. Veciana, N. Ventosa. Nanostructuring molecular materials as particles and vesicles for drug delivery, using compressed and supercritical fluids. *Nanomedicine* **2012**, 7 (9), 1391–1408.

58. I. Cabrera, E. Elizondo, O. Esteban, et al. Multifunctional Nanovesicle-Bioactive Conjugates Prepared by a One-Step Scalable Method Using CO2-Expanded Solvents. *Nano Lett.* **2013**, 13 (8), 3766–3774.

59. L. Ferrer-Tasies, E. Moreno-Calvo, M. Cano-Sarabia, et al. Quatsomes: Vesicles Formed by Self-Assembly of Sterols and Quaternary Ammonium Surfactants. *Langmuir* **2013**, 29 (22), 6519–6528.

60. J. Morla-Folch, G. Vargas-Nadal, T. Zhao, et al. Dye-Loaded Quatsomes Exhibiting FRET as Nanoprobes for Bioimaging. *ACS Appl. Mater. Interfaces* **2020**, 12 (18), 20253–20262.

61. S.T. Larsen, H. Verder, G.D. Nielsen. Airway Effects of Inhaled Quaternary Ammonium Compounds in Mice. *Basic Clin. Pharmacol. Toxicol.* **2012**, 110 (6), 537–543.

62. M.C. Jennings, K.P.C. Minbiole, W.M. Wuest. Quaternary Ammonium Compounds: An Antimicrobial Mainstay and Platform for Innovation to Address Bacterial Resistance. *ACS Infect. Dis.* **2016**, 1 (7), 288–303.

63. A. Ardizzone, S. Kurhuzenkau, S. Illa-Tuset, et al. Nanostructuring Lipophilic Dyes in Water Using Stable Vesicles, Quatsomes, as Scaffolds and Their Use as Probes for Bioimaging. *Small* **2018**, 14 (16), 1703851.

64. M.H.J. Santana, R.L. Ventosa, D.E. Martinez, et al. Vesicles which include epidermal growth factor and compositions that contain same. WO2014019555 A1, 2012.

65. I. Cabrera. Nanovesicle-bioactive conjugates to be used as nanomedicines , prepared by a one-step scalable method using CO2-expanded solvents "Doctoral dissertation," Universtitat Autònoma de Barcelona, **2013**.

66. G. Vargas-Nadal, M. Muñoz-Ubeda, P. Alamo, et al. MKC-Quatsomes: a stable nanovesicle platform for bio-imaging and drug-delivery applications. *Nanomedicine Nanotechnology, Biol. Med.* **2020**, 24, 102136.

67. A. Boloix, N. Feiner-Gracia, M. Köber, et al. Engineering pH-Sensitive Stable Nanovesicles for Delivery of MicroRNA Therapeutics. *Small* **2021**, 18 (3), 2101959.

68. D.A. Silbaugh, L. Ferrer-Tasies, J. Faraudo, et al. Highly Fluorescent Silicon Nanocrystals Stabilized in Water Using Quatsomes. *Langmuir* **2017**, 33 (50), 14366–14377.

69. M. Rossetti, L. Stella, J. Morlà-Folch, et al. Engineering DNA-Grafted Quatsomes as Stable Nucleic Acid-Responsive Fluorescent Nanovesicles. *Adv. Funct. Mater.* **2021**, 31 (46), 2103511.

70. G. Salazar, M.N. Russi-Vigoya. Technology Readiness Level (TRL) as the foundation of Human Readiness Level (HRL) Understanding the TRLs as the foundation of Human Readiness Level (HRL). *Sage Journals Ergon. Des. Q. Hum. Factors Appl.* **2021**.

71. J.C. Mankins. Technology readiness assessments: A retrospective. *Acta Astronaut.* **2009**, 65 (9–10), 1216–1223.

72. A. Olechowski, S.D. Eppinger, N. Joglekar. Technology readiness levels at 40: A study of state-of-the-art use, challenges, and opportunities. *Portl. Int. Conf. Manag. Eng. Technol.* **2015**, 2084–2094.

73. E.B. Souto, G.F. Silva, J. Dias-ferreira, et al. Nanopharmaceutics: Part II—production scales and clinically compliant production methods. *Nanomaterials* **2020**, 10 (3), 455.

74. A.L. Olechowski, S.D. Eppinger, N. Joglekar, K. Tomaschek. Technology readiness levels: Shortcomings and improvement opportunities. *Syst. Eng.* **2020**, 23 (4), 395–408.

75. I.K. Tadwee, S. Gore, P. Giradkar. Advances in Topical Drug Delivery System: A Review. *Int. J. Pharm. Res. Allied Sci.* **2011**, 1 (1), 14–23.

76. M. Cui, C. Wiraja, S.W.T. Chew, C. Xu. Nanodelivery Systems for Topical Management of Skin Disorders. *Mol. Pharm.* **2021**, 18 (2), 491–505.

77. M. Sharadha, D. V. Gowda, N. Vishal Gupta, A.R. Akhila. An overview on topical drug delivery system – updated review. *Int. J. Res. Pharm. Sci.* **2020**, 11 (1), 368–385.

78. W. Wang, K. Lu, C. Yu, Q. Huang, Y.-Z. Du. Nano-drug delivery systems in wound treatment and skin regeneration. *J. Nanobiotechnology* **2019**, 17 (1), 1–15.

79. J.A. Bouwstra, P.L. Honeywell-Nguyen. Skin structure and mode of action of vesicles. *Adv. Drug Deliv. Rev.* **2002**, 54, S41–S55.

80. K.V. Krishna, A. Pandit, Y. Rochev. Biomimetic Lipid-Based Nanosystems for Enhanced Dermal Delivery of Drugs and Bioactive Agents. *ACS Biomater. Sci. Eng.* **2017**, 3 (7), 1262–1272.

81. S. Kasolang, W.A. Adlina, N.A. Rahman, N.R. Nik. Common skin disorders : A review. *J. Tribol.* **2020**, 25, 59–82.

82. M. Gupta, U. Agrawal, S.P. Vyas. Nanocarrier-based topical drug delivery for the treatment of skin diseases. *Expert Opin. Drug Deliv.* **2012**, 9 (7), 783–804.

83. K. Järbrink, G. Ni, H. Sönnergren, et al. The humanistic and economic burden of chronic wounds: a protocol for a systematic review. *Syst. Rev.* **2017**, 6 (1), 1–7.

84. T.W. Prow, J.E. Grice, L.L. Lin, et al. Nanoparticles and microparticles for skin drug delivery. *Adv. Drug Deliv. Rev.* **2011**, 63 (6), 470–491.

85. B. Du, V.R. Daniels, Z. Vaksman, et al. Evaluation of Physical and Chemical Changes in Pharmaceuticals Flown on Space Missions. *AAPS J.* **2011**, 13 (2), 299–308.

86. P. Severino, J.F. Fangueiro, S. V. Ferreira, et al. Nanoemulsions and nanoparticles for non-melanoma skin cancer: Effects of lipid materials. *Clin. Transl. Oncol.* **2013**, 15 (6), 417–424.

87. F. Lai, C. Caddeo, M.L. Manca, et al. What's new in the field of phospholipid vesicular nanocarriers for skin drug delivery. *Int. J. Pharm.* **2020**, 583, 119398.

88. A.S. Inácio, A. Nunes, C. Milho, et al. In vitro activity of quaternary ammonium surfactants against streptococcal, chlamydial, and gonococcal infective agents. *Antimicrob. Agents Chemother.* **2016**, 60 (6), 3323–3332.

89. Â.S. Inácio, N.S. Domingues, A. Nunes, et al. Quaternary ammonium surfactant structure determines selective toxicity towards bacteria: Mechanisms of action and clinical implications in antibacterial prophylaxis. *J. Antimicrob. Chemother.* **2016**, 71 (3), 641–654.

90. S. Sharifi, M.J. Hajipour, L. Gould, M. Mahmoudi. Nanomedicine in Healing Chronic Wounds: Opportunities and Challenges. *Mol. Pharm.* **2021**, 18 (2), 550–575.

91. H. Park, C. Copeland, S. Henry, A. Barbul. Complex Wounds and Their Management. *Surg. Clin. North Am.* **2010**, 90 (6), 1181–1194.

92. L. Ferrer-Tasies, H. Santana, I. Cabrera-Puig, et al. Recombinant Human Epidermal Growth Factor/Quatsome Nanoconjugates: A Robust Topical Delivery System for Complex Wound Healing. *Adv. Ther.* **2021**, 4 (6), 2000260.

93. R.K. Chang, A. Raw, R. Lionberger, L. Yu. Generic Development of Topical Dermatologic Products: Formulation Development, Process Development, and Testing of Topical Dermatologic Products. *AAPS J.* **2013**, 15 (1), 41–52.

94. T. Garg, G. Rath, A.K. Goyal. Comprehensive review on additives of topical dosage forms for drug delivery. *Drug Deliv.* **2015**, 22 (8), 969–987.

"Danger for most of us is not that our aim is too high and we miss it, but that it is too low and we reach it"

– Michelangelo

2

rhEGF-DELOS nanovesicles: a re(nano)formulation of the recombinant human epidermal growth factor towards topical complex wound healing treatment

2.1 Introduction

As mentioned in the Introduction of the present dissertation, Nanomol Technologies SL is a science and innovation-driven company that offers advanced solutions and technologies to obtain high-added-value products through particle design and nanoformulation. To this end, the company's Research and Development area department is dedicated to generating new knowledge through the introduction of new offerings or the improvement of existing offerings that allow a company to remain competitive and generate profits[1].

Specifically, Nanomol Technologies SL is devoted to a very important topic, namely the development of new drug nanoformulations by the reformulation of pre-existing active molecules using the DELOS-susp technology as innovative platform to produce new nanomedicines with outstanding properties.

This Chapter will focus specifically on the study and further development of a novel nanomedicine based on the reformulation of a protein called recombinant human Epidermal Growth Factor (rhEGF), which has therapeutic activity for complex wound healing, to enable the topical administration of this protein and promote more efficient wound healing treatments. This reformulation has been attempted using highly stable nanovesicles, prepared by the DELOS-susp one-step and green methodology.

2.1.1 Complex wounds and their treatment: special focus on diabetic foot, venous and leg ulcers

Wound healing is a complex biological process that leads to the restoration of tissue integrity[2]. However, some wounds fail to heal in a timely and orderly manner, resulting in chronic and non-

healing wounds that require continued care. In clinical practice, there are several different types of wound healing, primary healing, which occurs when the wounds can be closed immediately with sutures and heal quickly, and secondary healing, which occurs when the wound has undergone extensive tissue loss and the repair process is prolonged[3].

In this Chapter, we will focus on those wounds that present a major challenge to surgeons and consume substantial health care resources, which are chronic wounds. Complex wounds are the term used to group together the well-known challenging wounds that do not heal primarily, that can be either chronic or acute and demand specialized care[4]. In this context, chronic wounds are a public health problem that needs to be addressed, with an estimated prevalence of 2% in the general population, imposing a significant economic burden on healthcare systems with estimated annual costs of more than US$50 billion and an expense expected to increase in the coming years[5–7].

These types of wounds include wounds that require special care, such as diabetic foot ulcers (DFUs), venous leg ulcers (VLUs), pressure ulcers (PUs), and open surgical wounds, which share a common risk of infection and slow healing since they can remain open for months to years[8–10]. To understand them better, it is important to know their underlying cause. DFUs occur primarily in patients with diabetes which is a systemic disease that causes neuropathy and arterial damage and affects many tissues and organs, such as the occurrence of chronic wounds on the feet. On the other hand, VLUs are mainly caused due to damage to the superficial and/or deep venous systems of the leg, consequently causing venous hypertension, and reduced blood flow which results in even minor wounds not healing due to the poor fluid in the lower extremities. Lastly, PUs are commonly seen in hospitals and in residential care homes for the elderly and frail and/or immobile, or individuals with spinal cord injuries[11] (**Figure 2.1**).

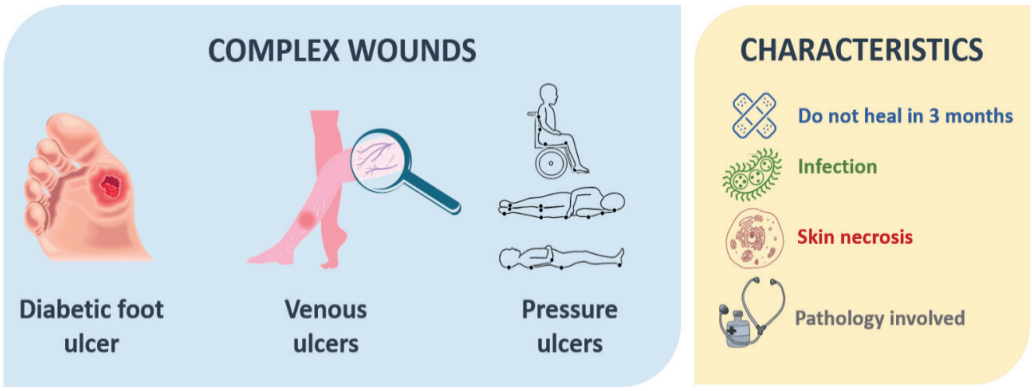

Figure 2.1: Complex wounds classification and its challenging characteristics involved.

Although presenting different origins, these wounds are considered to be classified as complex wounds since they can encompass similar conditions, such as[4]:

1. Extensive skin loss. Traditionally, chronic wounds are defined as wounds that have not spontaneously healed within 3 months.
2. The presence of elevated proinflammatory cytokines, high protease levels, excessive neutrophils, and senescent cells that fail to respond to reparative stimuli[12].
3. The presence of infections, which are a common complication of chronic wounds and may themselves be the cause of the tissue loss problem. For example, open wounds leave the wound bed at risk for colonization by opportunistic pathogens, aggravating the patient's condition. Bacterial colonization of wounds is often facilitated by the production of a slimy extracellular matrix known as biofilm, which is thought to affect up to 80% of chronic wounds. Thus, this is a well-known community concern as almost half of all DFUs are classified as infected, which is strongly correlated with amputations and increased mortality[13].
4. Reduced viability of superficial tissues- clear necrosis, or signs of circulation impairment.
5. Association with systemic pathologies affecting normal healing, leading wounds to not heal with simple care and requiring special attention. Feet ulcers in diabetic patients and many forms of vasculitis are common examples.

Knowing that wound healing is a complex regulated process in which chronic ulcers are the result of a multicausal and complex physiopathological process that is not yet fully understood[11], specific treatments should be found to accelerate and enhance the wound healing process. Even though wound healing is a challenging health issue, exciting therapeutic opportunities have emerged, such as biomaterial-based treatments that have shown benefits in improving small-sized and uncomplicated neuropathic ulcers[14]. For instance, basic treatment for proper wound care in DFUs includes strict metabolic control, debridement, offloading (i.e., relieving pressure from the wound area), dressings and antimicrobials[15]. However, finding effective therapies that could reduce amputations in ischemic and complicated forms of neuropathic wounds remains a challenge.

Biologics represent a new category of drugs that have rapidly gained prominence in the last decade due to their high selectivity and strong therapeutic efficacy along with limited side effects[14]. Since their discovery by Cohen in 1962, biological molecules termed epidermal growth factors (EGFs) have attracted considerable interest due to their potential applications in various facets of human health care, particularly in enhancing the healing process. The deficiency of EGF is thought to be one of the pathophysiologic fundamentals in complex wounds[16].

2.1.2 Epidermal Growth Factor (EGF)

Epidermal Growth Factor or EGF is a small protein that plays an important role in regulating cell growth, epidermal cell proliferation and differentiation, which may be useful in enhancing wound healing[15]. This protein is a single-chain polypeptide of 53 amino acids (**Figure 2.2**) with a molecular weight (Mw) of 6216 g·mol^{-1} and an isoelectric point of 4.6, which is the pH in solution at which the net surface charge of the protein is zero[17]. Hence, this protein presents a negative charge under physiological conditions and also has shown its maximum stability at pH values between 5.5 and 8.0, with an optimum close to pH 7.0[18].

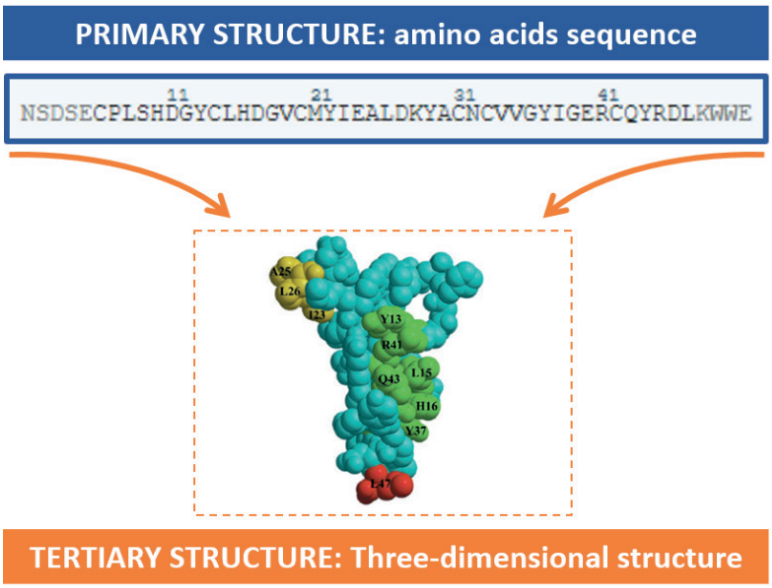

Figure 2.2: Schematic representation of the primary and tertiary structure of EGF. Adapted from[19].

Research data characterizing EGF have shown that it facilitates wound healing when delivered directly to the wound site because it can promote angiogenesis and regulate many aspects of cellular activity, including cell migration, proliferation and extracellular matrix metabolism[20]. Its mechanism of action relies on the binding of EGF protein to the EGF receptor (EGFR), a transmembrane tyrosine kinase protein expressed on most human cell types, including those that play a critical role in wound healing such as fibroblasts, endothelial cells and keratinocytes (**Figure 2.3**)[21,22]. Clinical studies have shown evidence of the beneficial effect of topical application of EGF in low-grade neuropathic ulcers, but not in high-grade wounds due to protease-driven cleavage associated with the rich proteolytic environment found in these wounds and therefore compromising bioavailability and efficacy of EGF in plain EGF-based treatments[15,21,23].

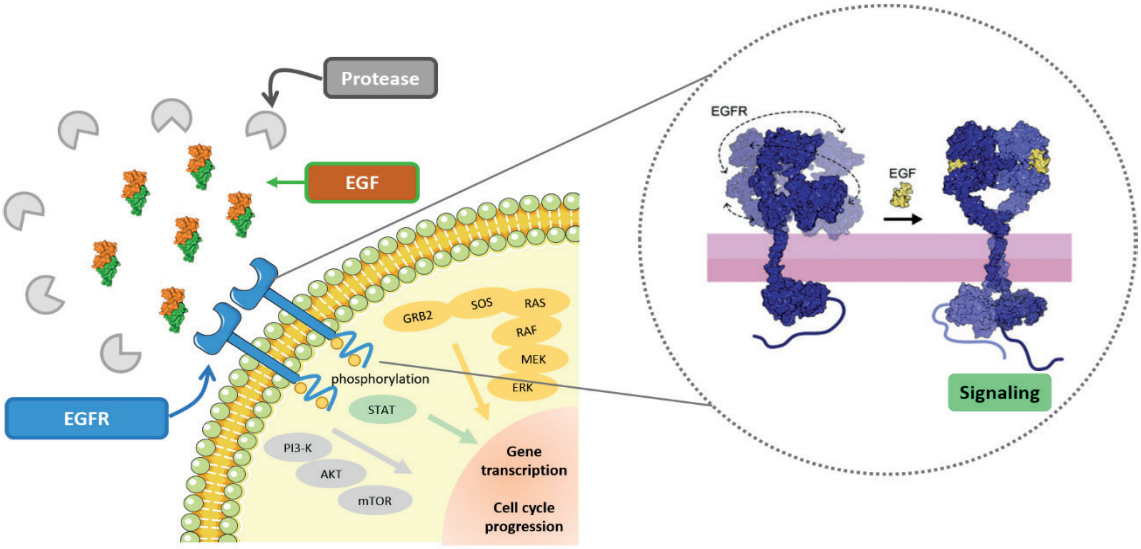

Figure 2.3: Simplified mechanism of the Epidermal Growth Factor Receptor (EGFR) activation by EGF interaction in the cell membrane. Adapted from[24].

Aware of these data, the Center for Genetic Engineering and Biotechnology (CIGB) in Cuba had developed and commercialized novel therapeutic products using recombinant human epidermal growth factor (rhEGF), known as Heberprot-P®. This product is devoted to treating complex wounds such as DFUs, as it has been demonstrated that the impaired wound healing in diabetic patients is partly due to a relative lack of growth factors (including EGF) at the wound site[21,25,26]. At the same time, it should be highlighted that this EGF-based formulation is administered by direct intralesional infiltration, what can overcome the limitations described before of EGF bioavailability and efficacy[27].

In terms of treatment quality, this approach has been shown to accelerate healing of deep and complex DFUs, reduce the risk of amputation, shorten healing time and hence future complications, and help improve patients' quality of life[21], however it can be extremely painful during the last stages of wound closure.

Although this treatment has opened up new challenges in the field of complex wound management, other innovative methods of administering rhEGF are being explored to further improve its bioavailability, efficacy and patient's compliance.

2.1.3 DELOS nanovesicles as an attractive platform to improve current EGF-based formulations

As already stated in **Chapter 1**, the development of new drug nanoformulations by reformulating already existing active molecules, such as rhEGF, can be done by using the

DELOS-susp technology as an innovative platform for the production of new nanomedicines with outstanding properties. In this regard, it should be emphasized that recent findings have shown that research into drug reformulation using various promising delivery systems improves the physicochemical and therapeutic properties of the drug and offers new advantages not only in terms of targeting and therapeutic efficacy, but also in offering safety compared to the existing formulations[28–30].

Therefore, in this case, the development of a new nanoformulation based on the use of DELOS nanovesicles integrating rhEGF protein (rhEGF-DELOS nanovesicles) will overcome the obstacles associated with the topical route, i.e., EGF's clearance from the application site, probably by protease driven cleavage and receptor-mediated endocytosis within hours. At the same time, these new nanoformulations might offer an alternative route of drug delivery compared to current EGF-based treatments by moving from intralesional to topical administration, which is a non-invasive route.

As explained in the Introduction of the present dissertation (**Chapter 1**), DELOS nanovesicles are commonly based on the mixture of sterols and quaternary ammonium surfactants (QASs). It is remarkable to say that cationic lipid-based vesicles have been the subject of various cosmetic and epicutaneous drug delivery studies over the past decades due to their effective drug delivery of biologically active molecules into and through the skin, as the incorporation of polar amphiphiles increases the likelihood of skin penetration[31]. Then, quaternary ammonium surfactants such as CTAB, the most studied cationic surfactant in Nanomol group for the preparation of DELOS nanovesicles, would be of great interest to be used in this nanoformulation.

Furthermore, the presence of CTAB confers several interesting properties on the DELOS nanovesicles and hence on the formulation of the new nanomedicine based on rhEGF-DELOS nanovesicles. First, its positive charge is ideal for electrostatic interaction with negatively charged proteins such as rhEGF (**Figure 2.4**), and second, QASs such as CTAB are widely used as disinfectants, algaecides, detergents, and antistatic components as well as an antimicrobial preservative used in cosmetic and pharmaceutical formulations. Therapeutically, CTAB is used at concentrations between 0.1–1.0% $w \cdot v^{-1}$ in aqueous solutions, creams or sprays as a topical antiseptic for skin, burns and wounds[32,33]. In particular, some studies have shown that the use of the CTAB cationic surfactant can act as an antibacterial agent and thus contribute to the inhibition of bacterial adhesion and biofilm formation without antimicrobial resistance, which could be an appropriate approach to tailor the specifics of biofilms commonly found in chronic wounds[34,35].

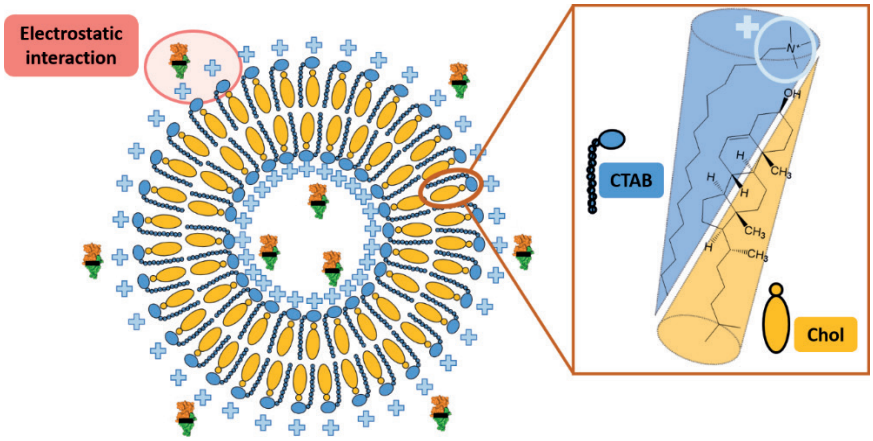

Figure 2.4: Schematic representation of a DELOS nanovesicle composed of equimolar ratio of cholesterol and the cationic CTAB surfactant interacting electrostatically with the negatively charged rhEGF protein.

2.1.4 Origin of the rhEGF-DELOS nanovesicles drug product development

The knowledge previously described led to the hypothesis that a more efficient treatment could be developed for complex wounds. Historically, the work presented here stems from a collaborative research project between the Nanomol group of ICMAB-CSIC and CIGB in Cuba, which began in 2010 with the goal of developing new topical formulations based on rhEGF loaded in DELOS nanovesicles with controlled physicochemical and pharmacological properties to treat DFUs.

After the initial proof-of-concept for integrating rhEGF into DELOS nanovesicles, excellent results were obtained under the framework of the PhD Thesis of Dr. Ingrid Cabrera of the Nanomol group, in terms of protein entrapment efficiency and nanoformulation stability, which led to a technological development platform protected under the patent "**Vesicles comprising epidermal growth factor and composition thereof - wo2014 / 019555**" in 2012[36].

On the basis of the promising results achieved with this new nanoformulation, in 2016 Nanomol Technologies SL and Heber Biotec, the commercializing company of CIGB, jointly started a new project for the development and preclinical research of rhEGF-DELOS nanovesicle conjugates as a new pharmaceutical product for the treatment of DFUs. The promising results obtained in the DFU project quickly broadened the project vision, and the rhEGF-DELOS nanovesicle conjugates were explored for their therapeutic application on other types of complex wounds such as VLUs. In this case, a project called Nanonafres was launched with the financial support of RIS3CAT program of the Generalitat of Catalonia, aligned with the European Commission (EC) National/Regional Research and Innovation Strategies for Smart Specialization (RIS3 strategies) (15/10/2016-15/04/2020).

Nanonafres project was the result of a multidisciplinary consortium of seven Spanish partners to develop a novel pharmaceutical formulation of rhEGF to promote wound healing in patients with VLUs topically. This consortium included the two institutions collaborating in this Industrial PhD project, ICMAB-CSIC and Nanomol Technologies SL. Both institutions were relevant for the evolution of the Nanonafres project since their main objective and contribution was the scientific development of the nanoformulation.

In more detail, Nanomol Technologies SL acted not only as a project leader but also as an R&D+I and technology promoter, and the public scientific research center ICMAB-CSIC was the institution also engaged in research and development in drug nanoformulation. Besides, Leitat Technological Center-Biomed with expertise in preclinical studies was also involved in the project. And finally, other institutions such as primary care centers and public hospitals as EAP Osona Sur-Alt Congost SLP, El EAP Vallcarca-Sant Gervasi, Consorci Sanitari de Terrassa, and Fundació Salut-Consorci Sanitari del Maresme were also involved to design the clinical development.

The Nanonafres project was expected to last 42 months with the objective to obtain a preliminary proof of concept in the use of rhEGF-DELOS nanovesicle conjugates to treat VLUs topically. In this regard, it is really important to understand that the development of a new drug product involves many stages before being commercialized. **Figure 2.5** shows a scheme including all these stages, such as drug discovery and development, preclinical research, research development, regulatory agencies review and approval and post-marked drug safety and monitoring[37].

Figure 2.5: Scheme of the stages involved in the drug discovery and development process of **rhEGF-DELOS nanovesicles as a drug product to treat both DFUs (CIGB project) and VLUs (Nanonafres project)**.

In this context, this Chapter focuses on the contribution of this doctoral project in the early phases of the drug product development process (**Figure 2.5**), mainly on the optimization and preclinical research of the new nanoformulation based on rhEGF-DELOS nanovesicles as a drug product to treat both DFUs (CIGB project) and VLUs (Nanonafres project). To do this, the main idea is to jointly develop an intermediate nanoformulation based on rhEGF-DELOS nanovesicles and then adapt it to a final formulation suitable for each wound type.

It is important to note that one of the key characteristics to consider on the wound type is wound exudate. Wound exudate is a general term given to liquid produced from wounds when hemostasis is achieved and helps keep the wound moist, provides nutrients, and provides the medium for epithelial cell migration and mitosis and is therefore crucial to the wound healing process[38]. It is worth recalling that patients with VLUs generally have increased wound exudate compared to patients with other forms of chronic skin ulcers such as DFUs. Then, these high levels of exudate in VLUs contain proteases and inflammatory cytokines that may damage the surrounding healthy skin, making them challenging to be treated[39]. Therefore, the current recommendations for managing this excess of wound exudate are to use wound dressings that manage this wound exudate while maintaining a moist wound[40,41]. Then, considering the exudate, different dosage forms will be designed to better treat DFUs and VLUs.

So, in the frame of drug development, we will first perform the rhEGF-DELOS nanovesicle nanoformulation optimization to obtain an appropriate intermediate drug product. This new drug delivery system was studied in detail to understand the associated Critical Quality Attributes (CQA), which are the physical, chemical, biological properties or characteristics that should be within an appropriate range to ensure the desired product quality[42]. With these factors in mind, we are then on the right track towards an efficient and clinically applicable drug product[43].

As shown in **Figure 2.5**, after optimizing the rhEGF-DELOS nanoformulation, the next challenging stage, also explained in this Chapter, was the preclinical evaluation phase for quality, safety, and efficacy assessment. This stage includes studies to evaluate the *in vitro* and *in vivo* efficacy and toxicology of the optimized rhEGF-DELOS nanovesicle nanoformulation, noting in our case that these studies carried out in the preclinical setting were performed in collaboration with CIGB and one of the collaborators of Nanonafres project, which is Leitat Technological Center-Biomed.

Towards this end, the development of the nanoformulation based on rhEGF-DELOS nanovesicles for the treatment of DFUs and VLUs will focus on concrete technological readiness levels, as already explained in ***Chapter 1****. In this case, the nanoformulation will move from different stage of maturity to facilitate the translation of the product into the clinic. On this basis and starting with TRL3, a preliminary candidate will be defined and preclinical studies for proof-of-concept will be carried on. Afterwards, the nanoformulation development will continue until TRL5, in which the efficacy and safety of the nanoformulation in vivo is determined*[44].

2.2 Optimization of rhEGF-DELOS nanovesicles as intermediate drug product

Becoming a potential drug product to treat DFUs and VLUs requires a thorough understanding of the nanomedicine candidate in order to optimize it properly and achieve the required quality attributes for the intended indication and route of administration.

2.2.1 Nanoformulation background

In order to optimize the new nanoconjugates based on rhEGF-DELOS nanovesicles, it is first important to know the preliminary initial approaches carried out in the frame of Doctoral Thesis by Dr. Ingrid Cabrera as part of the research collaborative project with the CIGB Institute[27]. In this study, highly stable DELOS nanovesicles integrating rhEGF were successfully prepared by the one-step DELOS-sup methodology, described in detail in **Section 6.2.1 of Chapter 7**) using rhEGF manufactured and provided by CIGB. This protein was stored in lyophilized form prior to use, which was a convenient form to allow for a longer shelf life of the protein.

In particular, the preparation methodology was based on first preparing a solution of ethanol containing cholesterol (68 mM) and loading it into the reactor and pressurizing it with compressed CO_2. Thereafter, depressurization of the volumetrically expanded organic phase was performed over an aqueous solution of water containing CTAB (7.8 mM) and the rhEGF protein in the desired concentrations. The starting lyophilized protein was first reconstituted into a liquid suspension with phosphate buffer (10 mM, pH 7.0), a widely used buffer in protein formulations that has been reported to help rhEGF exhibit maximum stability[18] (**Figure 2.6**).

Then, in all preparations, the final theoretical concentration of cholesterol and CTAB was 7.3 mM of each component, respectively, and the optimal rhEGF concentration found ranged between 25 to 125 $\mu g \cdot mL^{-1}$, which corresponds to rhEGF:CTAB (mmol:mol) ratio of 0.6:1 to 2.9:1. So, if we consider this rhEGF concentration range, the final concentration of phosphate buffer in the dispersant medium ranges from 0.013 to 0.063 mM, respectively.

It should be noted that no additional steps were required to achieve the desired structural properties of the conjugates or to increase the loading and, that homogeneous, opalescent colloidal dispersions of rhEGF-DELOS nanovesicles were obtained with this method.

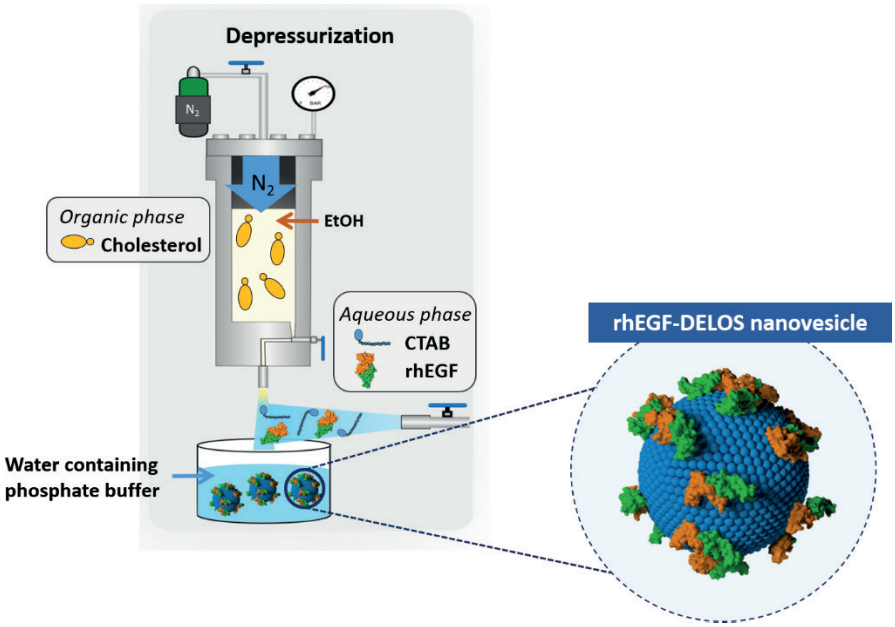

Figure 2.6: Schematic illustration of the DELOS-susp method for the preparation of rhEGF-DELOS nanovesicle formulation optimized under the framework of the Doctoral Thesis by Dr. Ingrid Cabrera[27].

Mean particle sizes, particle size distributions (or polydispersity index (PDI)), and apparent zeta potentials of the rhEGF-DELOS nanovesicles prepared at bench scale were determined using a Zetasizer Nano ZS as described in the **Section 6.3.1** of **Chapter 6**. These are important critical quality attributes of colloidal systems that play an important role in determining their stability, drug loading, drug release, biodistribution, and targeting ability[45].

Mean vesicle size of rhEGF-DELOS nanovesicles with 25 and 125 $\mu g \cdot mL^{-1}$ of protein and Blank-DELOS nanovesicles (same formulation but without rhEGF) was below 200 nm and increased, as well as PDI, with increasing the amount of protein used in the preparation whereas no differences in zeta potential were observed when the protein concentration was in the range of 25 to 125 $\mu g \cdot mL^{-1}$ (**Table 2.1**). Additionally, the zeta potential values were very high in accordance with the great stability of these nanoconjugates. It should be highlighted that 200 $\mu g \cdot mL^{-1}$ of rhEGF was also tested but it presented macroscopical instability of the sample. Regarding the morphology of the nanovesicles, cryo-TEM images of the rhEGF-DELOS nanovesicles prepared with protein concentration of 25, 75 and 125 $\mu g \cdot mL^{-1}$ were taken, showing homogeneous, unilamelar and spherical vesicles (**Figure 2.7**)[27].

In addition, entrapment efficiency percentages (EE%) were determined using 30 KDa centrifugal filter devices, which were used to separate the non-integrated rhEGF from the loaded rhEGF-DELOS nanovesicles, and then an enzyme-linked immunosorbent assay (ELISA) was used to quantify the

rhEGF[27]. The EE% remained very high (≥ 97%) for all obtained conjugates regardless of protein loadings, showing that there is favorable interaction between the DELOS nanovesicles and rhEGF (**Table 2.1**).

Then, the results of this study of the development of rhEGF-DELOS nanovesicle in the frame of the Doctoral Thesis by Dr. Ingrid Cabrera in 2013 showed good results in terms of physicochemical properties, in colloidal stability and in terms of high entrapment efficiency of the protein when the formulation was prepared by DELOS-susp methodology.

Table 2.1 Physicochemical characteristics of rhEGF-DELOS nanovesicles obtained by DELOS-susp method obtained in the frame of the Doctoral Thesis by Dr. Ingrid Cabrera in 2013[27].

rhEGF concentration in rhEGF-DELOS nanovesicles ($\mu g \cdot mL^{-1}$)	**Ratio rhEGF:CTAB (mmol:mol)**	**Mean particle size (nm)**	**PDI**	**Zeta Potential (mV)**	**EE (%)**
0	0	121 ± 7	0.23 ± 0.01	74 ± 5	N/A
25	0.6	98 ± 4	0.30 ± 0.01	73 ± 5	98.0 ± 1.3
75	1.8	131 ± 9	0.34 ± 0.02	74 ± 3	99.0 ± 1.0
125	2.9	146 ± 14	0.45 ± 0.01	78 ± 4	99.3 ± 0.5

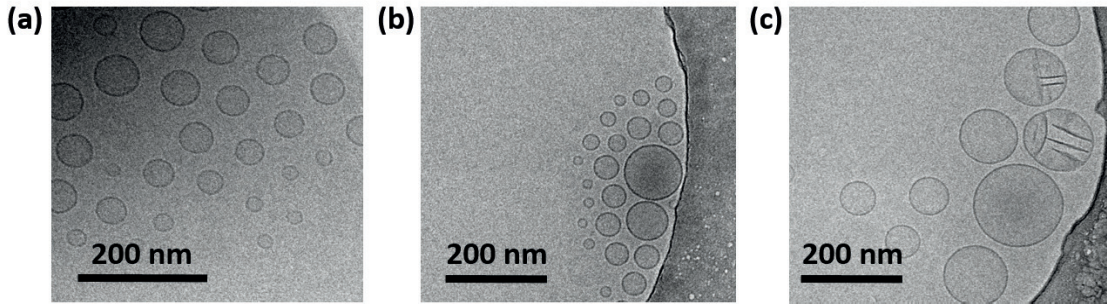

Figure 2.7: Cryo-TEM images of rhEGF-DELOS nanovesicles prepared by the DELOS-susp methodology integrating a theoretical initial rhEGF concentration of (a) 25, (b) 75 and (c) 125 µg·mL-1 and obtained in the frame of the Doctoral Thesis by Dr. Ingrid Cabrera in 2013[27].

Considering that this section serves as an introduction to the background of work undertaken on formulating rhEGF-DELOS nanovesicles for the treatment of DFUs in the frame of the Doctoral

Thesis by Dr. Ingrid Cabrera in 2013[27], these promising nanoformulations were also evaluated biologically, obtaining that:

1. The specific enzymatic activity of rhEGF integrated into DELOS nanovesicles was at least two times higher than that for the free protein, confirming that rhEGF does not lose its function at the site of action when integrated into DELOS nanovesicles.
2. The protein integrated into the DELOS nanovesicles showed an antimicrobial activity and showed eight times higher resistance to degradation by proteases compared to free rhEGF. These are important factors to consider when treating chronic wounds like DFUs, which present proteolytic environment that may affect the bioavailability of the protein-based drugs used during a treatment.
3. The rhEGF-DELOS nanovesicles were used for the compassionate treatment of 12 patients and showed outstanding results in the cicatrization of the treated complex wounds. As can be ascertained from **Figure 2.8**, complete re-epithelialization of the wound was observed by the 12th week of treatment, indicating a significant clinical improvement in the patients' quality of life.

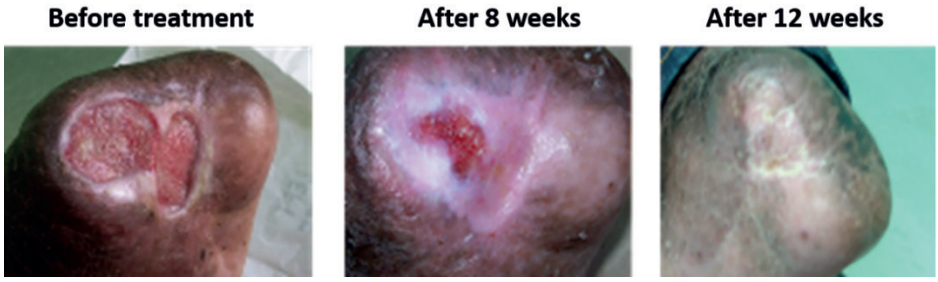

Figure 2.8: Images showing the evolution of wound healing in compassionate patients before the treatment and after 8 and 12 weeks they received the rhEGF-DELOS nanovesicle treatment[27].

Although a large body of evidence suggested that rhEGF-DELOS nanovesicles could be considered as a potential nanomedicine for the topical treatment of complex wounds, this preliminary study received limited attention for formulation optimization. To develop an optimized nanoformulation, the initial parameters used in the frame of the Doctoral Thesis by Dr. Ingrid Cabrera in 2013 were genuinely considered and various experiments were appropriately selected to develop a robust nanomedicine, more efficient, with more control over CQAs and more stable and that can progress to the clinical stage.

2.2.2 Identification of the Critical Quality Attributes (CQAs) and specifications of the rhEGF-DELOS nanovesicles product

As already mentioned, for pharmaceutical products, quality is regarded as a mandatory topic and must be assured for all. To ensure pharmaceuticals product's quality to get therapeutic benefit, it is important the identification and relevant characterization of CQA. Therefore, identifying the CQA values will highlight the characteristics that can impact the overall quality of the nanomedicine, thus helping to define strategies that can enable faster, more efficient and controlled drug product development[43,46–48].

In our case, the identification of CQAs and specifications of the new drug product have been defined to ensure adequate quality of the nanomedicine. These parameters were proposed as part of the Nanonafres project, in a consultation with the Spanish Agency of Medicines and Medical Devices (AEMPS) in July 2018, to find support in developing the new nanomedicine and to design the clinical trials. It is worth remarking here that the selected CQAs were also considered in the ICH Q8 recommendations as well as in relevant Chemistry Manufacturing and Controls (CMC) guidelines of FDA and EMA [49–51], which were the following:

Macroscopic appearance: rhEGF-DELOS nanovesicle samples should be a homogeneous and translucent liquid suspension with no sedimentation.

Mean vesicle size: Particle size distribution is a key parameter for effective biomedical applications as it can affect the drug product quality attributes such as biodistribution and kinetics of drug release[48]. Based on our prior knowledge, it is desirable that the mean particle size of rhEGF-DELOS nanovesicle formulations should be between 40-100 nm. A particle size of less than 200 nm is also beneficial for the sterility of the nanovesicle product, as this size allows sterile filtration of the final product using a 0.22 µm pore size filter[52].

Polydispersity index (PDI): This physical parameter defines the degree of non-uniformity of a particle size distribution. This index is dimensionless and aims reduced values indicating good homogeneity of the dispersion. Although PDI values below 0.5 are generally reported as acceptable, in this case a PDI between 0.01 to 0.35 is desirable[48].

Zeta potential: it indicates the net electrostatic load on the particle surface and is an important parameter when evaluating the stability of colloidal systems. For instance, particles with a high negative or positive zeta potential value will repel each other, indicating that the colloidal system is stable[52]. In contrast, reducing the zeta potential value to nearly neutral results in particle aggregation. In addition, the charge of the nanovesicles can effect on drug loading as well as systemic circulation time and interactions with the target tissues[45]. In our case, we have defined a zeta potential value in the range of +40 to +150 mV as the acceptance limit.

Particle morphology and lamellarity: Vesicles must be spheroidal and, mostly, unilamellar. Lamellarity can affect the entrapment efficiency and release, thus impacting the protein delivery[53].

rhEGF Entrapment Efficiency (EE%) and loading capacity: EE% is the amount of protein integrated into the vesicles compared to the total amount of protein, while drug loading is the amount of protein contained relative to the amount of membrane components used. High EE% is very important as it could reduce manufacturing costs and increase drug concentration in the final formulation, allowing greater flexibility in dosing. In this nanoformulation, it was desired an EE% above 90%.

Inactive ingredients and rhEGF degradation products: The assessment of the purity of the nanomedicine, which may be composed of the desired product and multiple product-related substances, is a relevant factor that needs to be considered. If impurities can arise, these materials should be characterized to the extent possible[54].

Specific biological activity of rhEGF: Investigating the biological activity of rhEGF, which is its ability to achieve its defined biological effect, is a necessary and important part of the overall product characterization testing. This analysis helps ensure the stability of the protein when incorporated into the DELOS nanovesicle formulation, thus confirming not only its preserved activity but also its protein potency in the final nanoformulation, ensuring adequate clinical efficacy[54].

pH: The measurement of pH is important for assessing the drug product function as it is known that the role of the solution environment in rhEGF protein is a relevant parameter for chemical and physical protein degradation[18,55]. Knowing that the maximum stability of rhEGF is found at pH values between 5.5 and 8.0, with an optimum near pH 7.0[18], the optimum pH range for the nanoformulations was defined between 5.5 and 7.0.

Sterility and absence of pyrogens or bacterial endotoxins: Removing potential harmful germs or microorganisms prior to the application of the nanomedicine is a crucial quality criterion for medical products, not only for the intended marked product but also for healthcare.

Leakage rate and *in vitro* drug release kinetics: Understanding the kinetics of drug release can be a crucial parameter for the success of the nanoformulation such as its therapeutic efficacy and toxicology[56].

Then, the defined specifications for quality control and the corresponding acceptance limits are summarized in **Table 2.2**.

Table 2.2: Quality specifications of the product to be developed determined in consultation with AEMPS.

Attributes/Test performed	Method/Reference	Criteria/ Limits of acceptance
Macroscopic appearance	Visual observation USP/Ph. Eur.	Homogeneous liquid and translucent appearance macroscopically
Mean vesicle size	DLS/Z-sizer	50- 100 nm
Polydispersity index	DLS/Z-sizer	0.01- 0.35
Zeta Potential	DLS/Z-sizer	+40- +150 mV
Particle morphology	SAXS/Cryo-TEM	Spherical and unilamellar
rhEGF entrapment efficiency	Centrifugal filter devices/ ELISA: Need for further development	> 90%
Total Ethanol content	GC with FID detector	To be defined
Total and free CTAB content	RP-HPLC-ELSD	To be defined
Total cholesterol content	RP-HPLC-ELSD	To be defined
Total rh-EGF content	RP-HPLC-ELSD	To be defined
Degradation products related to inactive ingredients	To be defined	To be determined
Degradation products related to rh-EGF	SDS-PAGE	> 95,0% of the main peak
	RP-HPLC-UV	> 95,0% of the main species
Specific biological activity	Cellular proliferation assay	> 4.000.000 IU·mg^{-1}
pH	USP/Ph. Eur.	5.5 – 7.0
Sterility	USP/Ph. Eur.	Sterile
Absence of pyrogens or bacterial endotoxins	USP/Ph. Eur.	Pyrogen-free
Leakage rate	RP-HPLC-ELSD/ ELISA	To be defined
***In vitro* drug release kinetics**	Ultracentrifugation/ELISA	To be defined

Regarding **Table 2.2**, it can be established that there are several issues that need to be addressed in order to transform the initial rhEGF-DELOS nanovesicle formulation obtained in Doctoral Thesis of Dr. Ingrid Cabrera into a pharmacological product. Despite the significance of all designated quality

specifications, some of them were not considered a priority in the present development stage and will be deemed in further stages.

Summarizing, the CQA of the rhEGF-DELOS nanovesicles were identified in detail. However, in the present Thesis, the most strategic and key parameters to be evaluated were: the control of pH in the nanoformulation, the configuration of the DELOS-susp methodology for the preparation of rhEGF-DELOS nanovesicles and the development of a robust analytical method to control the protein entrapment efficiency.

2.2.3 Control of pH in the nanoformulation

One of the main parameters that should be considered when optimizing a nanoformulation is its composition. The analysis of each component of the preliminary rhEGF-DELOS nanovesicle formulation described above was based on the use of cholesterol and CTAB as membrane components, rhEGF as active pharmaceutical ingredient, and water and EtOH as the dispersant medium. Besides, as stated before, the starting lyophilized rhEGF should be reconstituted. For that, in the Doctoral Thesis of Dr. Ingrid Cabrera (**Section 2.2.1**) a phosphate buffer (10 mM, pH 7) was used.

Considering for example the production of rhEGF-DELOS nanovesicles with a final rhEGF concentration of 100 $\mu g \cdot mL^{-1}$ (ratio rhEGF:CTAB (mmol:mol) of 2,2), the final amount of phosphate buffer present in the final nanoformulation is approximately 0.05 mM (**Figure 2.6**). If we characterize this nanoformulation with the presence of phosphate buffer (0.05 mM, pH 7.0) as dispersant medium and without the presence of rhEGF, as a reference Blank-DELOS nanovesicles sample (**Figure 2.9a**), it can be observed that it presents proper physicochemical properties in terms of particle size distribution, which remained constant over time with a mean particle size around 80 nm and also presents a suitable polydispersity value around 0.3. Furthermore, the morphology of these Blank-DELOS nanovesicles observed by cryo-TEM images (**Figure 2.9b**) revealed a high density of unilamellar nanovesicles with good homogeneity in terms of size, lamellarity, and supramolecular membrane organization, which plays an important role in the functionalization of their membranes, making them competent drug targeters[57].

However, a close examination of the pH of the nanoformulation over time (see **Section 6.3.2**), which is a crucial parameter in this project, shows that the use of phosphate buffer (0.05 mM, pH 7.0) in the Blank-DELOS nanovesicle formulation does not stabilize the pH value over time (**Figure 2.9c**). The pH of this nanoformulation is destabilized over time and varies from an acidic pH of 4.0 after production to 6.5 after 12 weeks of production, mainly caused by the presence of CO_2 present in the DELOS-susp process.

Using this method described in **Section 6.2.1** of **Chapter**, CO_2 is depressurized from high pressure to ambient conditions to form DELOS nanovesicles, which can result in CO_2 remaining solubilized in the aqueous phase, thereby acidifying the pH of the nanoformulation[58]. Then, although the presence of phosphate buffer (0.05 mM, pH 7.0) as dispersant medium in Blank-DELOS nanovesicles presents good physicochemical properties in terms of morphology, size and zeta potential, it does not have enough buffering capacity to reach a stable pH of the nanoformulation close to 5.5-7.0 over time, the acceptance limit pH range established for the proper stability of rhEGF[18] (**Table 2.2**).

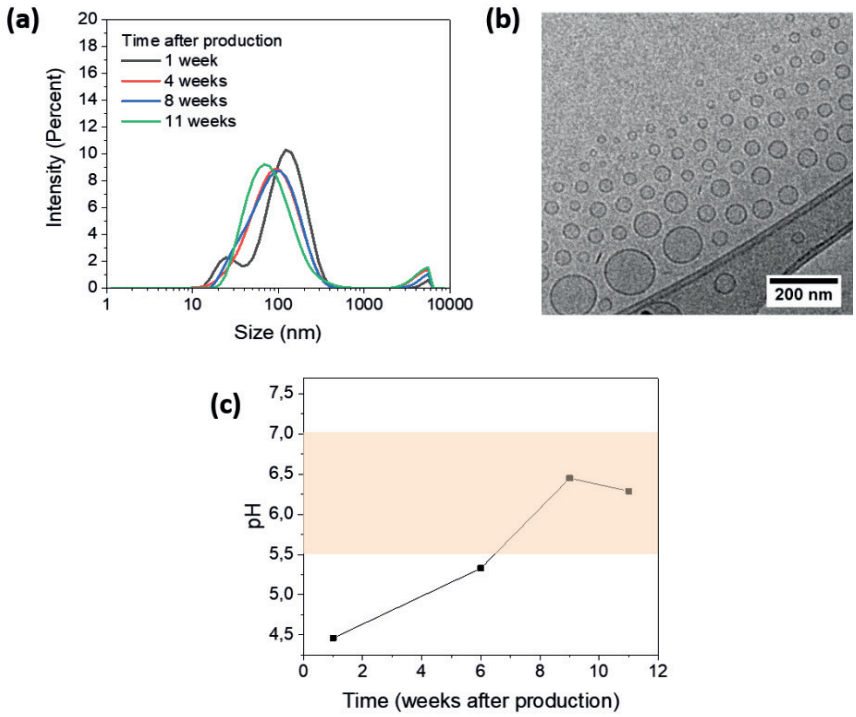

Figure 2.9: (a) Particle size distribution over time, (b) morphology 14 weeks after preparation with the DELOS methodology, and (c) pH evolution over time of reference Blank-DELOS nanovesicles in phosphate buffer (0.05 mM pH 7.0). Samples were stored until use at 5 ± 3 °C.

Regarding the pH, this issue has been reported in the literature, suggesting that the environment in which rhEGF is found is a relevant parameter for chemical and physical protein degradation. Knowing then that the maximum stability of rhEGF is at pH 5.5 to 8.0, with an optimum near pH 7.0[18], it can be assumed that when the rhEGF is placed in phosphate buffer (0.05 mM, pH 7.0), its stability is affected because its pH is unstable over time between 4.5 to 6.5. In addition, it is reported that chemical and physical protein degradation and aggregation can occur when the pH is close to 4 and 5[18]. To control the degradation of the rhEGF in rhEGF-DELOS nanovesicles in the presence of phosphate buffer (0.05 mM, pH 7.0) as dispersant medium, the chemical stability of rhEGF was

determined by measuring its molecular weight by High-Performance Liquid Chromatography-Electrospray Ionization-Mass Spectrometry (HPLC-ESI-MS) (see **Section 6.3.5**).

In our case, it is known that rhEGF produced by CIGB consists of a mixture of 51 and 52 amino acids whose theoretical masses of $rhEGF_{1-51}$ and $rhEGF_{1-52}$ are 5946.66 and 6059.82 $g \cdot mol^{-1}$, respectively. As the mass is a very specific property of a molecule, the determination of the molecular weight by HPLC-ESI-MS can enable the analysis of the stability of the rhEGF during the preparation of rhEGF-DELOS nanovesicles by the DELOS-susp methodology[59].

Table 2.3 contains the molecular weight of rhEGF studied through HPLC-ESI-MS. As shown, it was discovered that rhEGF suffered a mass reduction of both types of rhEGF protein present in the mixture, $rhEGF_{1-51}$ and $rhEGF_{1-52}$, in the presence of phosphate buffer (0.05 mM, pH 7.0) as dispersant medium in the rhEGF-DELOS nanovesicles compared to when it is free in phosphate buffer (10 mM, pH 7.0), which is our reference of stability maximum stability. Thus, it was confirmed that phosphate buffer (0.05 mM, pH 7.0) is not a suitable dispersant medium for the preparation of rhEGF-DELOS nanovesicles and thus it was evident that this was a key point that needed to be optimized.

Table 2.3: Molecular weight of rhEGF studied through High-Performance Liquid Chromatography-Electrospray Ionization-Mass Spectrometry (HPLC-ESI-MS).

Sample	Dispersant medium	pH	Tr (min)	M1/z	M2/z	Molecular weight ($g \cdot mol^{-1}$)	Comments
Original rhEGF	Phosphate buffer (10 mM, pH 7.0)	7.0	3.5	1190.2 (+5)	1487.8 (+4)	5946	Minority peak
			3.8	1213.0 (+5)	1516.0 (+4)	6060	
rhEGF integrated in DELOS nanovesicles	Phosphate buffer (0.05 mM, pH 7.0)	4.5	3.5	1167.4 (+5)	1459.0 (+4)	5832	Minority peak
			3.8	1190.1 (+5)	1487.3 (+4)	5945	

For this reason, there was a desire to use a more appropriate dispersant medium that would help achieve adequate pH control of the rhEGF-DELOS nanoformulation. It should be emphasized that Blank-DELOS nanovesicle formulations, after being prepared using the DELOS-susp methodology, were not subjected to any manipulation that could affect the spontaneous pH evolution, only opening and closing the vial for its analysis.

Summary in relation to chemical composition and pH of the dispersant media used in the rhEGF-DELOS nanovesicle formulation, they are important factors that can affect the stability of the rhEGF protein, and so have an impact on its functionality.

2.2.3.1 Influence of the aqueous medium on the physicochemical properties of DELOS nanovesicles without rhEGF: looking for a suitable pH value of the nanoformulation

The use of different dispersant medium that ensure a pH close to pH 7.0 for the stability and non-degradability of rhEGF is a well-known problem that requires a proper approach. To this end, several new dispersant media have been proposed to improve the pH performance of the rhEGF-DELOS nanovesicle formulation, which is described below.

This issue was explored by preparing Blank-DELOS nanovesicles (without rhEGF) using the same process previously described in the Doctoral Thesis of Dr. Ingrid Cabrera and schematized in **Figure 2.10** (see **Section 6.2.1**). In all cases, Blank-DELOS nanovesicles were prepared using theoretical equimolar ratio between cholesterol and CTAB with a concentration 7.3 mM of each component, respectively, and by screening dispersant media at pH 7.0 using buffers of different nature, which are described in the next section. In this case, the protein rhEGF was not integrated into the DELOS nanovesicle production to assess the impact of the dispersant medium in the DELOS nanovesicles formation. Deep physicochemical characterization was performed, in terms of mean particle size, PDI and zeta potential over time, as well as morphological analysis by cryo-TEM (**see 6.3.3 section**).

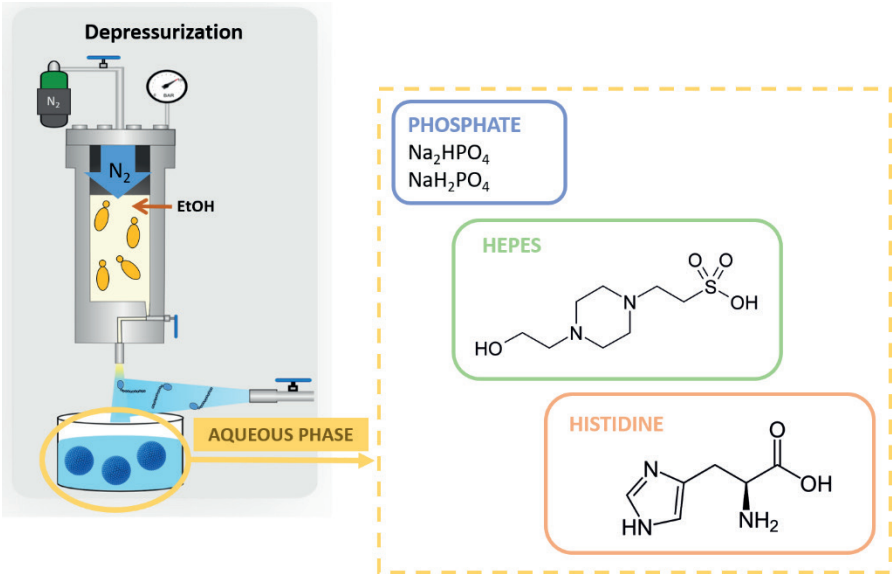

Figure 2.10: Schematic representation of the depressurization step of the DELOS-susp process to obtain Blank-DELOS nanovesicles composed of cholesterol and CTAB using different dispersant media at pH 7.0 as the aqueous phase.

Production of Blank-DELOS nanovesicles in phosphate buffer (10 mM, pH 7.0)

Since rhEGF is produced by CIGB in phosphate buffer (10 mM, pH 7.0), it seemed interesting to use this dispersant medium in the synthesis of the DELOS nanovesicle as a strategy to have an appropriate pH of the nanoformulations close to pH 7.0 and at the same time, ensure the correct stability of the protein. This buffer is based on the mixture of 5.8 mM of Na_2HPO_4 and 4.2 mM of $NaH_2PO_4 \cdot H_2O$, which at pH 7.0, the species in **Equation 2.1(2)** are the most prevalent, as the pH is close to the equilibrium constant K_2, which is 7.21.

$$(1)\ H_2PO_4 \xleftrightarrow{pKa_1=2,12} H^+ + H_2PO_4^-$$

$$(2)\ H_2PO_4^- \xleftrightarrow{pKa_2=7,21} H^+ + HPO_4^{2-}$$

$$(3)\ HPO_4^{2-} \xleftrightarrow{pKa_3=12,44} H^+ + PO_4^{3-}$$

Equation 2.1: Equilibrium equations of the phosphate buffer and their corresponding equilibrium constants.

This option was either not reasonable for our purposes because the sample, while showing the desired pH over time, pH between 6.5 and 7.0, they showed macroscopic changes over time as compared to Blank-DELOS nanovesicles in phosphate buffer (0.05 mM, pH 7.0), evolving from a transparent appearance to a whitish opal as observed in **Figure 2.11a**. This evolution of the macroscopic appearance was also observed by DLS analysis (**Figure 2.11b**), which showed that the particle size distribution changed significantly becoming unstable over time, probably due to the interaction between the salts and the membrane components. As shown in **Figure 2.11c**, this instability was also confirmed by cryo-TEM, which also showed unfavorable changes in the morphology of the Blank-DELOS nanovesicles, which did not show homogeneous structures. Importantly, the salt concentration used in the phosphate buffer media (10 mM) is in the same range as the concentration of the membrane components (≈ 7.3 mM).

It is noteworthy to point out under this buffer condition, the pH of the nanoformulation is near 6.5 after its production and slightly increasing up to pH 7.0 after 20 weeks of its production. This slight increase is due to the possible release of CO_2 coming from the DELOS-sup process that has remained dissolved in the formulation and removed over time and so increasing the pH (**Figure 2.11d**). Consequently, increasing the concentration of phosphate buffer from 0.05 mM as described previously to 10 mM as dispersant media for the nanoformulation has demonstrated the ability to maintain stable the pH around 5.5-7, which is the desired limit of acceptance of this attribute for this nanoformulation.

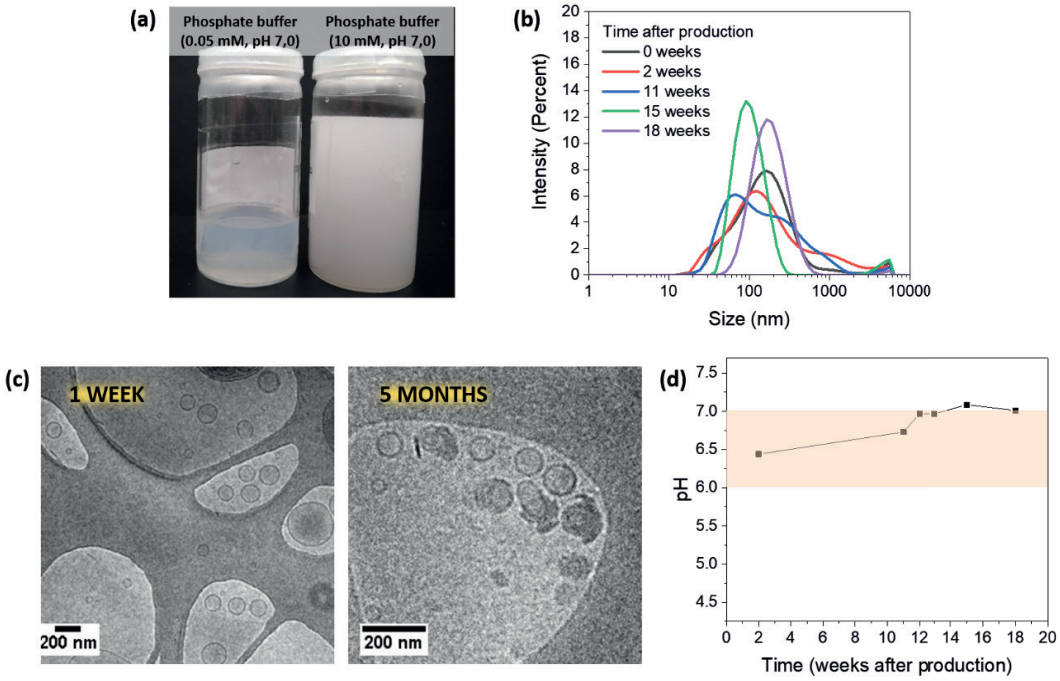

Figure 2.11: (a) Macroscopic appearance of Blank-DELOS nanovesicles in phosphate buffer (0.05 mM, pH 7.0) and (10 mM, pH 7.0) 4 months after production, (b) particle size distribution over time, (c) morphology at 1 week and 5 months after production (d) pH evolution of Blank-DELOS nanovesicles in phosphate buffer (10 mM, pH 7.0). Samples were stored until use at 5 ± 3 °C.

Production of Blank-DELOS nanovesicles in phosphate buffer (5 mM, pH 7.0)

Given the inappropriate behavior of the physicochemical properties such as the instability of the particle size distribution and morphology of Blank-DELOS nanovesicles using phosphate buffer (10 mM, pH 7.0) as dispersant medium, it was proposed to handle the buffer research through another approach. At this stage, it was decided to try the use of a less concentrated phosphate buffer, specifically phosphate buffer (5 mM, pH 7.0).

Regarding this formulation, it showed a stable particle size distribution over the period studied (14 weeks), but also exhibits a significant population of particles near 1 µm (**Figure 2.12a**). These results were also confirmed by cryo-TEM, which showed a high structural homogeneity of the prepared nanoformulations (**Figure 2.12b**). As for pH, the value obtained was in the range of pH 5.5-7, which was the acceptance limit for this CQA (**Figure 2.12c**).

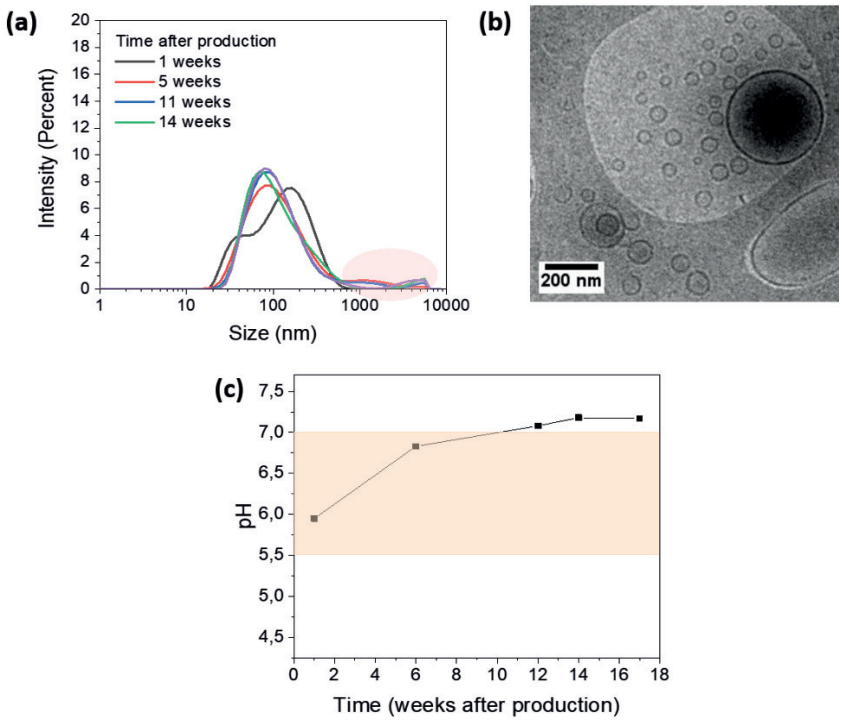

Figure 2.12: (a) Particle size distribution over time and (b) morphology 5 months after production and (c) pH evolution over time of Blank-DELOS nanovesicles in phosphate buffer (5 mM pH 7.0). Samples were stored until use at 5 ± 3 °C.

Production of Blank-DELOS nanovesicles in Hepes buffer (5 mM, pH 7.0)

Following the same strategy as previously described, Hepes buffer solution (5 mM, pH 7.0) was also considered for being studied since rhEGF was found to be thermodynamically stable in this buffer[60]. The Hepes molecule also called 4-(2-hydroxyethyl)-1-piperazineethanesulfonic acid, is a zwitterionic (positive and negative charge on different atoms within the molecule) organic chemical that can act as a biological buffering agent with pKa of 7.55 (**Figure 2.13**). Hepes buffer has an optimal pH range of 6.8-8.2, which can help maintain the physiological pH in cell cultures regardless of fluctuations in carbon dioxide concentration generated by cellular respiration[61].

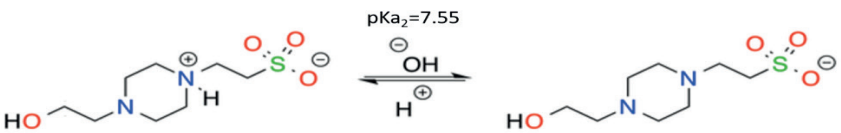

Figure 2.13: Dissociation step and pKa value of Hepes at 20 °C. Reproduction from[62].

One of the main disadvantages of this approach is that the Hepes molecule has adverse effects if not protected from light, as it forms hydrogen peroxide due to exposure to light[63]. Thus, Blank-DELOS nanovesicles containing this buffer must be protected from light.

After the production and examination of the Blank-DELOS nanovesicles using this buffer, it was revealed proper physicochemical properties such as stability over time in both particle size distribution and zeta potential (**Figure 2.14a**). Upon examining its morphology, homogeneous small unilamellar DELOS nanovesicles were observed (**Figure 2.14b**), which is an important factor for a robust system that maintains excellent stability over time, especially when used in medical applications. In terms of pH, this buffer presents enough buffering capacity to reach a stable pH of the nanoformulation between 5.5-7.0, which is the acceptance limit pH range established for the proper stability of rhEGF[18], from the beginning of the Blank-DELOS nanovesicles production up to the evaluated time (10 weeks). (**Figure 2.14c**). Naturally, this type of buffer can be useful for enhancing the physicochemical properties of the rhEGF-DELOS nanovesicles formulation.

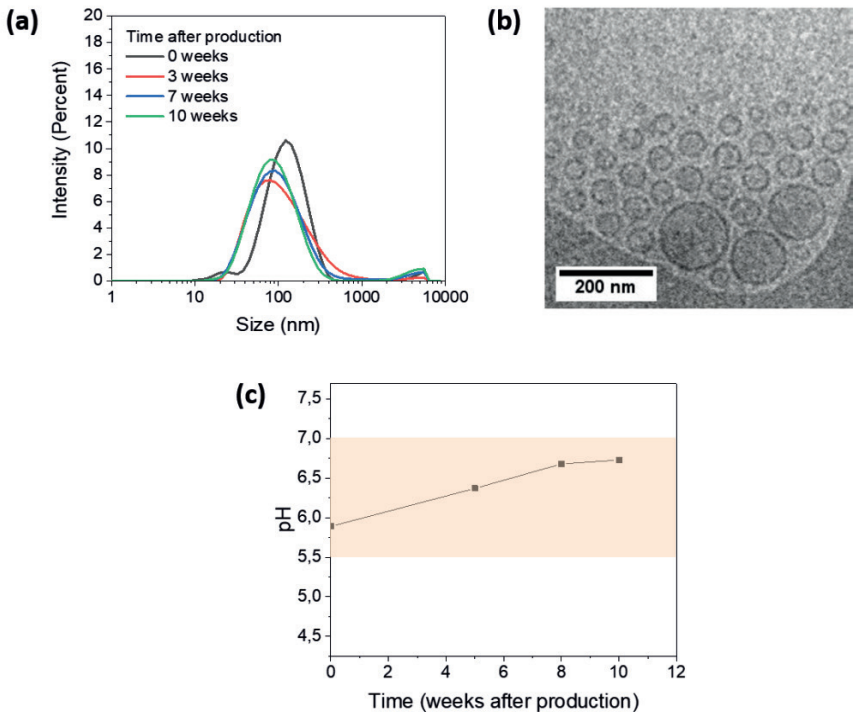

Figure 2.14 (a) Particle size distribution over time and (b) morphology 5 months after production and (c) pH evolution over time of Blank-DELOS nanovesicles in Hepes buffer (5 mM pH 7.0). Samples were stored until use at 5 ± 3 °C.

Production of Blank-DELOS nanovesicles in histidine buffer (5 mM, pH 7.0)

Finally, another approach based on the use of histidine buffer (5 mM, pH 7.0) as dispersant medium for the formation of Blank-DELOS nanovesicles is presented. Histidine is one of the codified amino acids used in the biosynthesis of proteins, which has an effective pH range of 5.5-7.4[64](**Figure 2.15**), and some studies support its positive correlation between its use in rhEGF and a low degradation reaction rate constant of the protein[18]. In addition, histidine buffer has also been described as the most common buffer for commercially available protein therapeutics, like antibody formulations, with histidine concentrations ranging from 3 mM to 50 mM and pH = 5.5–6.5[65–67]. Consequently, histidine was considered a promising approach for being evaluated.

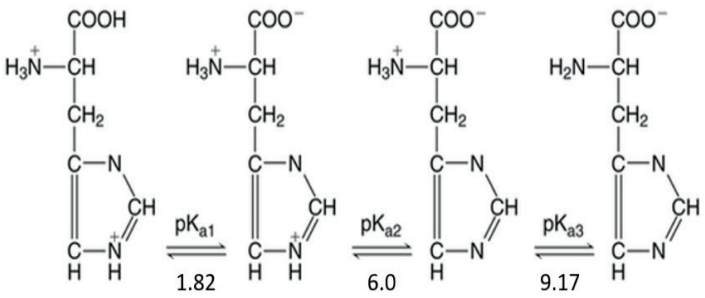

Figure 2.15: Chemical structure of L-histidine. Adapted from[68].

After preparing the Blank-DELOS nanovesicles with histidine buffer (5 mM, pH 7.0), the data were carefully examined. From the preliminary data, it was found that the histidine buffer seemed very promising. Not only was long-term stability observed over time but also proper vesicle morphology was detected (**Figure 2.16a,b**). Interestingly, this buffer also presents enough buffering capacity to achieve a stable pH of the nanoformulation between 5.5-7.0, which corresponds to the pH range of the acceptance limit set for the proper stability of rhEGF[18], from the beginning of the Blank-DELOS nanovesicles production up the evaluated time (28 weeks) (**Figure 2.16c**).

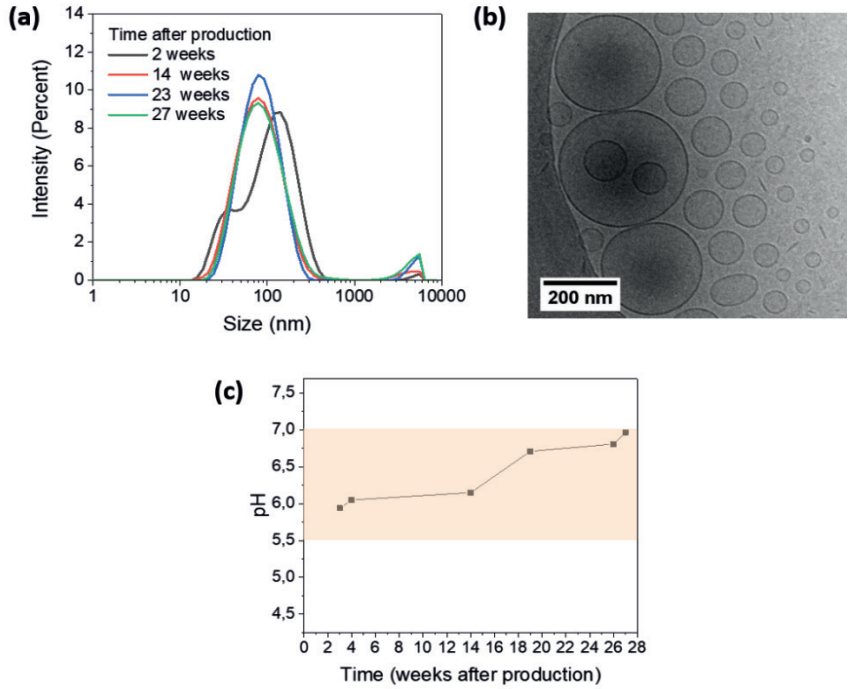

Figure 2.16: Particle size distribution over time and (b) morphology 5 months after production and (c) pH evolution over time of the Blank-DELOS nanovesicles in histidine buffer (5 mM pH 7.0). Samples were stored until use at 5 ± 3 °C.

Then, in the light of the reported results on the buffer screening for the production of Blank-DELOS nanovesicles, it was conceivable that histidine buffer (5 mM, pH 7.0) was the most promising dispersant medium for improving the nanoformulation compared to the previous nanoformulation using phosphate buffer (0.05 mM, pH 7.0). The results obtained here using the other described dispersant media for the preparation of Blank-DELOS nanovesicles may have had some implications. Undoubtedly, phosphate buffer (10 mM, pH 7.0) showed some destabilization of the nanoformulation over time, and so it was discarded from the study. At the same time, phosphate buffer (5 mM, pH 7.0) was also rejected as a precaution against it evolved similarly as phosphate buffer (10 mM, pH 7.0). Finally, Hepes buffer (5 mM, pH 7.0) was also refused from the study due to its possible cytotoxic effects if light-exposed.

Consequently, this optimization of the nanoformulation can be considered to be a significant step forward for achieving better results of the rhEGF-DELOS nanovesicles formulation. From this point, histidine buffer (5 mM, pH 7.0) was used for resuspending rhEGF from its lyophilized form and as a dispersant medium for the production of rhEGF-DELOS nanovesicles.

Summarizing, it was demonstrated that the use of different aqueous medium strongly influences on the physicochemical properties of DELOS nanovesicles (particle size, pH and stability). In this case,

the most appropriate dispersant medium was histidine buffer (5 mM, pH 7.0), which will be used in further studies of rhEGF-DELOS nanovesicles pharmaceutical development.

2.2.3.2 Preparation of rhEGF-DELOS nanovesicles in histidine buffer (5 mM, pH 7.0) as dispersant medium

To confirm the suitability of histidine buffer (5 mM, pH 7.0) in the preparation of rhEGF-DELOS nanovesicles, they were synthesized using the DELOS-susp methodology, the same described in the previous **Section 2.2.3.1** and **Figure 2.17**. In this case, the volumetric expanded organic solution of cholesterol, ethanol, and compressed CO_2 was depressurized over an aqueous phase of histidine buffer (5 mM, pH 7.0), containing CTAB and the rhEGF protein at the chosen concentrations 25 and 100 $\mu g \cdot mL^{-1}$, which corresponds to the equivalent of 0.6 and 2.2 (ratio rhEGF:CTAB (mmol:mol)) respectively (see **Section 6.2.1**).

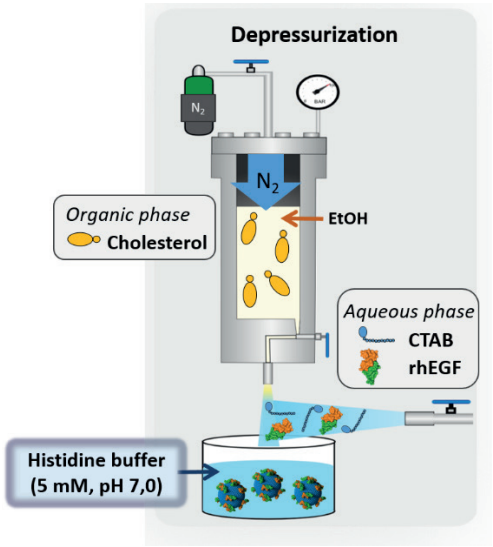

Figure 2.17: Schematic representation of rhEGF-DELOS nanovesicles preparation by DELOS-susp methodology using histidine buffer (5 mM, pH 7.0) as dispersant medium.

As observed in **Figure 2.18a,** rhEGF-DELOS nanovesicles with 25 and 100 $\mu g \cdot mL^{-1}$ exhibit stable particle size distributions over time, with mean hydrodynamic diameter of around 100 nm for rhEGF-DELOS nanovesicles with 25 $\mu g \cdot mL^{-1}$, and a somewhat smaller diameter of around 85 nm in the case of rhEGF-DELOS nanovesicles with 100 $\mu g \cdot mL^{-1}$. In addition, samples were homogenous with a stable PDI and no larger than 0.4. In addition, cryo-TEM images show unilamellar and spherical shaped vesicles, confirming that the incorporation of rhEGF protein in the nanoformulation containing histidine buffer (5 mM, pH 7.0) maintains the morphology of the nanovesicles (**Figure 2.18b,c**).

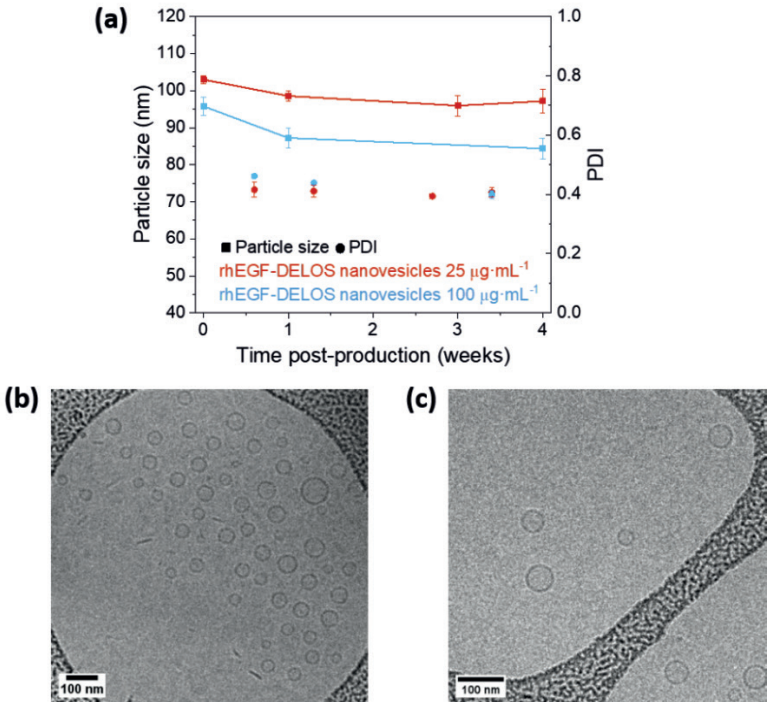

Figure 2.18: (a) Stability of hydrodynamic diameter distribution and PDI of rhEGF-DELOS nanovesicles with 25 and 100 μg·mL^{-1} over time using histidine buffer (5 mM, pH 7.0) as dispersant medium, (b) and (c) cryo-TEM images of the rhEGF-DELOS nanovesicles with 25 and 100 μg·mL^{-1} respectively, using histidine buffer (5 mM, pH 7.0) as dispersant medium.

Furthermore, thanks to HPLC-ESI-MS (see **Section 6.3.5**) it was confirmed that the use of histidine buffer (5 mM, pH 7.0) is an appropriate strategy to protect rhEGF from degradation when it is integrated into the DELOS nanovesicles in suspension, achieving similar results of the molecular mass of rhEGF compared to the original free rhEGF stored in phosphate buffer (10 mM, pH 7.0), which was our reference of stability (**Table 2.4**).

Table 2.4: Molecular weight of rhEGF studied through High-Performance Liquid Chromatography-Electrospray Ionization-Mass Spectrometry (HPLC-ESI-MS).

Sample	Dispersant medium	pH	Tr (min)	M1/z	M2/z	Molecular weight ($g \cdot mol^{-1}$)	Comments
Original rhEGF	Phosphate buffer (10 mM, pH 7.0)	7.0	3.5	1190.2 (+5)	1487.8 (+4)	5946	Minority peak
			3.8	1213.0 (+5)	1516.0 (+4)	6060	
rhEGF integrated in DELOS nanovesicles	Histidine buffer (5 mM, pH 7.0)	6	3.5	1190.2 (+5)	1487.6 (+4)	5946	Minority peak
			3.8	1213.0 (+5)	1515.9 (+4)	6060	

In conclusion, it has been shown that histidine buffer (5 mM, pH 7.0) is a suitable dispersant medium for the preparation of the rhEGF-DELOS nanovesicles as it can avoid the degradation of the rhEGF in suspension. Then, the benefits of using this buffer in the rhEGF-DELOS nanovesicles prototype were reconfirmed.

2.2.4 Configuration of the DELOS-sup methodology for the preparation of rhEGF-DELOS nanovesicles

As the goal of this project is to reach the clinical phase, one of the key parameters to achieve it is to ensure the scalability of the process from laboratory to pilot production to prepare large batches for the clinical trials. For this reason, it should be noted that in our case it is necessary to understand in detail each part of the manufacturing process of nanovesicles to consider what factors can affect the effectiveness of the process. The DELOS-susp methodology to produce rhEGF-DELOS nanovesicles is a straightforward process, however, some process parameters can be optimized to increase the yield. For example, the position of the surfactant can have an impact on making the performance of the method easier.

Previously, rhEGF-DELOS nanovesicle nanoformulations were prepared according to the procedure schematically represented in **Figure 2.19a**. As previously mentioned, the methodology briefly consisted of loading a solution of cholesterol in an ethanol organic solution into a high-pressure reactor with pressurized and compressed CO_2. Finally, this volumetrically expanded organic solution was depressurized over the histidine buffer (5 mM, pH 7.0) containing CTAB and the rhEGF protein at the chosen concentration.

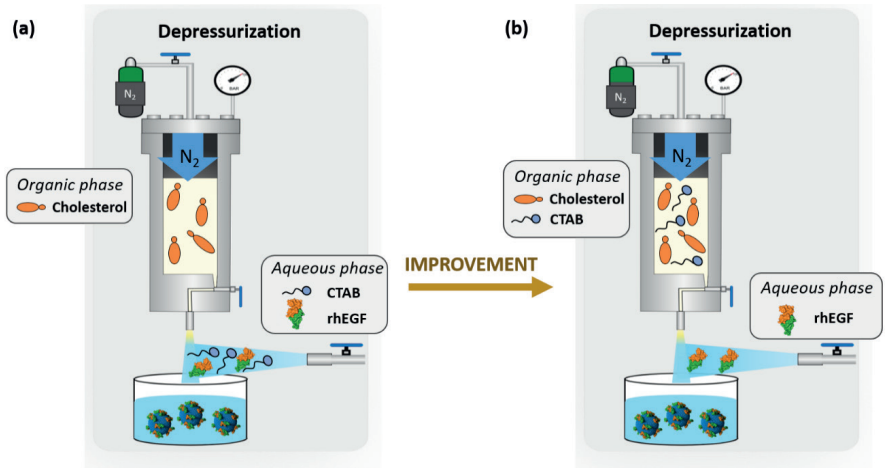

Figure 2.19: Schematic representation of the DELOS-sup methodology (a) adding cholesterol to the organic phase and CTAB and rhEGF to the aqueous phase and (b) adding cholesterol and CTAB to the organic phase and rhEGF in the aqueous phase.

One strategy was to modify the localization of the membrane components during the DELOS-sup process by placing them together in just one step, e.g., adding both to the organic phase. As stated before, CTAB was always added in the aqueous phase based on histidine buffer (5 mM, pH 7.0) together with the rhEGF. However, it is important to emphasize that when CTAB and rhEGF were mixed, a temporal aggregation was initially observed followed by disaggregation upon mixing after a few minutes. Then, the introduction of CTAB into the organic phase along with the cholesterol is expected to help streamline and simplify the methodology to prepare rhEGF-DELOS nanovesicles.

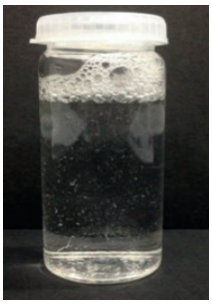

Figure 2.20: Temporal aggregate formation when mixing CTAB and rhEGF in the aqueous phase to prepare rhEGF-DELOS nanovesicles, rhEGF:CTAB ratio (mmol:mol) = 0.6.

To evaluate the impact of changing the rhEGF-DELOS nanovesicle preparation method by DELOS-susp in the CQAs, rhEGF-DELOS nanovesicles containing 25 and 100 $\mu g \cdot mL^{-1}$ of rhEGF were produced by DELOS-susp and then characterized. Briefly, the usual procedure previously described based on preparing rhEGF-DELOS nanovesicles with cholesterol and CTAB at a final theoretical concentration of 7.3 mM of each component was followed. In this case, as observed in **Figure 2.19b**, both

membrane components were dissolved together in ethanol organic solution and then placed in a high-pressure reactor with pressurized and compressed CO_2. Then, it was depressurized over an aqueous phase of histidine buffer (5 mM, pH 7.0), also containing the rhEGF protein at the chosen concentrations, 25 and 100 µg·mL^{-1}, equivalent of 0.6 and 2.2 (ratio rhEGF:CTAB (mmol:mol)) respectively, were the promising nanoconjugates prototypes that had previously presented excellent physicochemical properties[69] (see **Section 6.3.1** and **6.3.3** for more information) (Error: Reference source not found **2.18**).

Thus, a correct evaluation of the physicochemical properties of the rhEGF-DELOS nanovesicles depending on the position of the CTAB (organic phase (OP) or aqueous phase (AP)) was performed. Based on the results observed in **Figure 2.21** of the physicochemical properties of the prepared batches, we make the following observations. On the one hand, it was found that both approaches presented good quality results in terms of the stability of the particle size distribution over time (**Figure 2.21a**). However, changing the position of the CTAB to the organic phase in the production process yielded surprisingly good results, since the vesicular systems obtained not only had slightly smaller particle size but also lower PDI and lower zeta potential values than the rhEGF-DELOS nanovesicles prepared with the CTAB in the aqueous phase (**Figure 2.21a,b,c**).

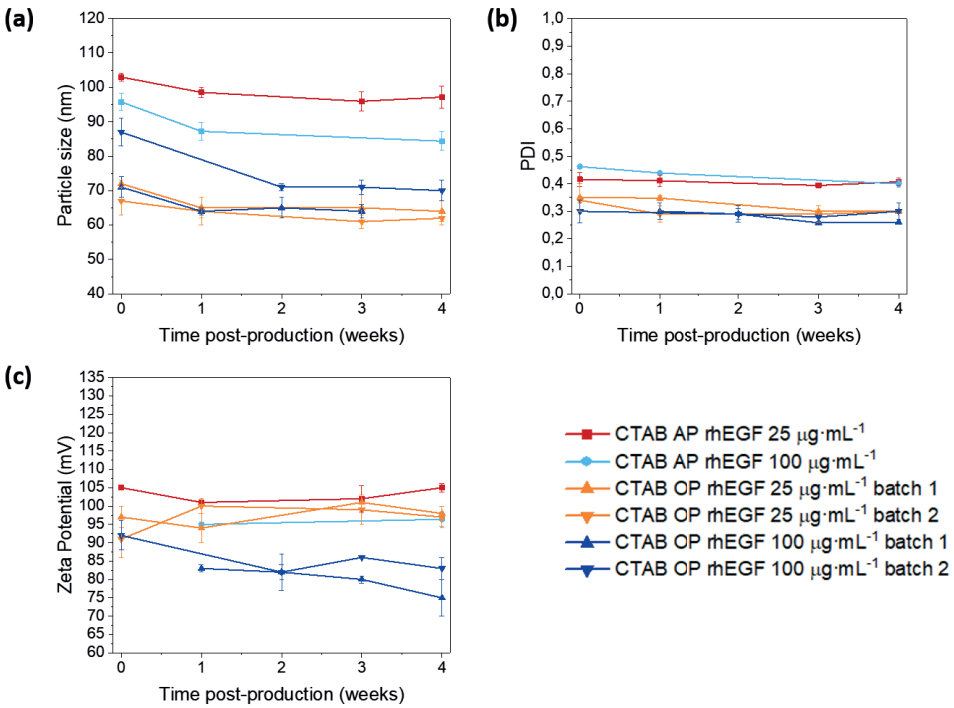

Figure 2.21: (a) Particle size, (b) PDI and (c) zeta potential evolution over time of rhEGF-DELOS nanovesicles with 25 and 100 µg·mL-1 of rhEGF comparing the CTAB addition in the aqueous phase (AP) or in the organic phase (OP) in the DELOS-susp process.

Furthermore, as shown in **Figure 2.22a,b**, cryo-TEM images of these optimized rhEGF-DELOS nanovesicles containing 25 and 100 $\mu g \cdot mL^{-1}$ of rhEGF confirmed the presence of spherical, homogeneous and unilamellar vesicles.

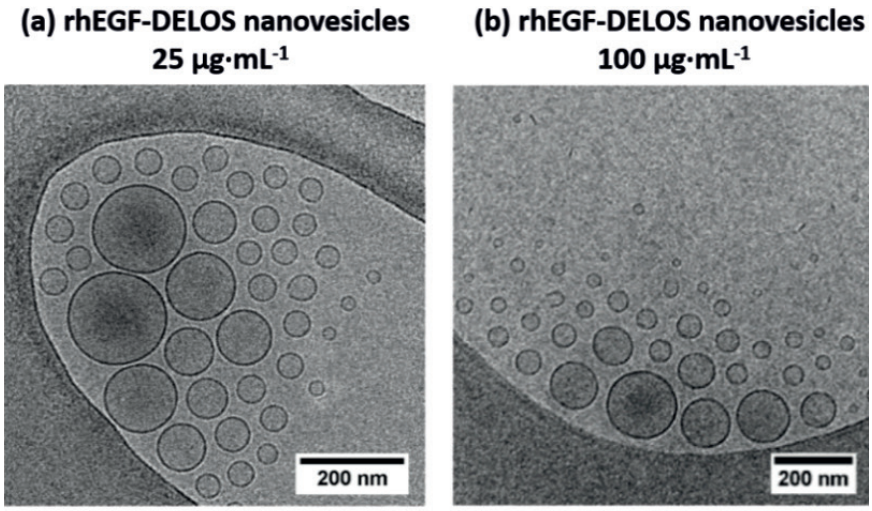

Figure 2.22: Cryo-TEM images of the rhEGF-DELOS nanovesicle formulation adding CTAB in the organic phase. (a) rhEGF-DELOS nanovesicles with a final rhEGF concentration of 25 $\mu g \cdot mL^{-1}$ and (b) rhEGF-DELOS nanovesicles with a final rhEGF concentration of 100 $\mu g \cdot mL^{-1}$.

Consequently, changing the CTAB position during the preparation of rhEGF-DELOS nanovesicles in the DELOS-sup method allows the preparation of nanoconjugates with a more homogeneous size, meeting the quality requirements of the nanoformulations. Based on these results, it was decided that CTAB should be added to the organic phase instead of the aqueous phase for the preparation of the prototype nanomedicine using the DELOS-susp process. As a result, vesicles with better physicochemical properties can be obtained and the production process is also simplified.

As a summary, the results presented so far in this chapter defined all the components that constitute the rhEGF-DELOS nanovesicle and its preparation methodology for obtaining an optimized nanoformulation as pharmaceutical product intermediate, which are described in ***Table 2.5*** *and their role in the nanoformulation.*

Table 2.5: rhEGF-DELOS nanovesicles optimized nanoformulation: components and process parameters for obtaining the intermediate pharmaceutical product.

Component	Quantity per mL	Function	Position during the preparation of the nanoformulation by DELOS-susp	Specification
rhEGF	25 to 100 µg	Active pharmaceutical ingredient	Aqueous phase	Depending on the manufacturer
Cholesterol	2.83 mg	Membrane component	Organic phase	USP/Ph. Eur.
CTAB	2.70 mg	Membrane component	Organic phase	USP/Ph. Eur.
Histidine	0.60 mg	pH regulator buffer	Aqueous phase	USP/Ph. Eur.
EtOH	0.10 mL	Solubilizer of membrane components	Organic phase	USP/Ph. Eur.
Water for injection	q.s. 1 mL	Dispersant médium	Aqueous phase	USP/Ph. Eur.

2.2.5 Development of a robust analytical method to control protein entrapment efficiency

Another important quality attribute to be defined in the rhEGF-DELOS formulation is the entrapment efficiency (EE%) as previously described as a CQA (**Table 2.2**). The protein EE% is the ratio of the integrated drug to the initial drug feed during the preparation of the nanovesicles. From an economic point of view, high encapsulation efficiency is important as it leads to cost-effective production of nanoparticles, while in the context of therapeutic efficacy, high drug loading is an important feature of nanoparticles[43].

It is important to note that to control the rhEGF entrapment efficiency, an analytical and robust method had to be defined that could accurately quantify the amount of rhEGF integrated into the DELOS nanovesicle membrane and the free rhEGF in the dispersant medium. With this aim in mind, the methodology used was based on rhEGF-DELOS nanovesicles ultracentrifugation, to separate the rhEGF integrated into the rhEGF-DELOS nanovesicles from the free one in the medium. Then, the EE% is calculated by fluorescence spectroscopy thanks to the intrinsic fluorescence of the rhEGF tryptophans.

Briefly, ultracentrifugation is a process that uses centrifugal force to separate and purify mixtures of particles in a liquid medium using the principle of sedimentation. Its main principle is to simply sediment or pellet rhEGF-DELOS nanovesicle samples from the dispersant medium in which free rhEGF stands (supernatant) by high-speed ultracentrifugation, as shown in **Figure 2.23**.

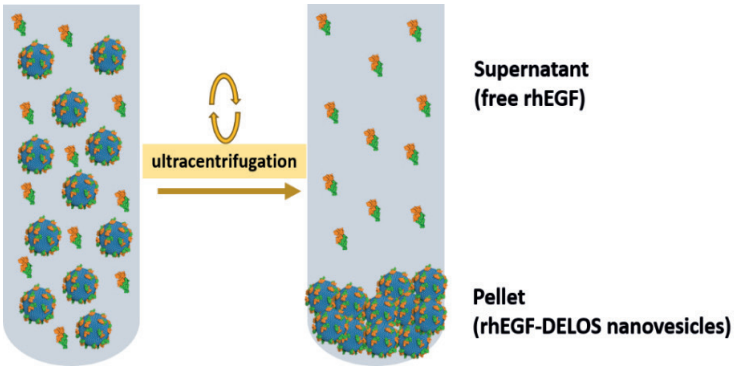

Figure 2.23: Ultracentrifugation methodology to separate the non-integrated rhEGF in rhEGF-DELOS nanovesicles.

To do it, 1 mL of rhEGF-DELOS nanovesicle optimized formulation was prepared and subjected to ultracentrifugation (see **Section 6.3.8**). A first approach of ultracentrifugation at 90.000 g, at 5 °C for 8 hours and 24 hours was performed, however, the nanovesicle formulation did not generate any sediment producing a pellet. It should be emphasized that the sedimentation rate dependents not only on the centrifugal field applied, but also on the type of particle, such as its density and its hydrodynamic radius[70].

Considering that we were dealing with small nanovesicles that require higher expenditure of energy and time, it was crucial to carefully adjust the experimental parameters for the complete pelleting of rhEGF-DELOS nanovesicles. For this reason, different conditions of ultracentrifugation such as temperature, time and centrifugal force were studied. Setting the time at 6 hours, which is a suitable analysis time, four different ultracentrifugation conditions were analyzed: 200.000 g at 10 °C, 400.000 g at 10 °C, 400.000 g at 4 °C and 600.000 g at 4 °C. Then, for all the studied conditions, the encapsulation efficiencies were calculated using the optimized parameters of the rhEGF fluorescence intensity as follows in **Table 2.6**.

Table 2.6: Fluorescence measurement conditions of rhEGF-DELOS nanovesicles with a final rhEGF concentration of 25 and 100 μg·mL^{-1}.

Measurement conditions	rhEGF-DELOS nanovesicles 25 μg·mL^{-1}	rhEGF-DELOS nanovesicles 100 μg·mL^{-1}
Excitation wavelength	295 nm	295 nm
Excitation slit	5 nm	5 nm
Emission wavelength	300-450 nm	300-450 nm
Emission slit	10 nm	5 nm
Maximum intensity wavelength	345 nm	345 nm

So, when free rhEGF and rhEGF-DELOS nanovesicles were separated by ultracentrifugation, the encapsulation efficiency of rhEGF was determined by measuring the fluorescence intensity of rhEGF from the pellet and comparing it to the fluorescence intensity of the original sample, using the following **Equation 2.2**:

$$EE_{pellet}(\%) = \frac{I_{pellet\ 345\ nm}}{I_{initial\ sample\ 345\ nm}} \cdot 100\%$$

Equation 2.2: Formula to calculate the rhEGF encapsulation efficiency from the measured fluorescence intensity in the pellet of rhEGF integrated into the DELOS nanovesicles.

Based on these calculations, different values of the rhEGF encapsulation efficiency in rhEGF-DELOS nanovesicles were calculated from all ultracentrifugation conditions. As shown in **Figure 2.24a**, it can be clearly seen that in all cases the EE% of rhEGF in the rhEGF-DELOS nanovesicles exceeds 90%, which is the minimum value defined in the product's CQAs list. In addition, it was also confirmed that at the maximum ultracentrifugation conditions tested (600000 g, 4 °C for 6 hours), the rhEGF did not sediment and remained in suspension, confirming again that the ultracentrifugation method achieves a proper separation of free and integrated rhEGF in DELOS nanovesicles.

However, to distinguish which condition was most appropriate, fluorescence measurements of each supernatant fraction were then performed at 302 nm. By measuring the intensity at this wavelength, we look for the contribution of Rayleigh scattering due to elastic scattering of photons by particles whose size is smaller than the wavelength of the scattered photons (DELOS nanovesicle size is around 60 nm, so smaller than the wavelength of 302 nm). In addition, either absorption nor emission fluorescence from rhEGF or other components is detected at 302 nm. Consequently, the intensity at 302 nm would be proportional to the concentration of particles such as DELOS nanovesicles remaining in the supernatant after centrifugation.

Results illustrated in **Figure 2.24b** show that a decrease in the fluorescence intensity of the rhEGF-DELOS nanovesicles can be observed with increasing centrifugal force. These results could be related to less scattering from the nanovesicles, meaning that with increasing centrifugal force, more rhEGF-DELOS nanovesicles sediment in the pellet, effectively separating the unintegrated rhEGF from the rhEGF-integrated one in rhEGF-DELOS nanovesicles.

Then, regarding the maximum tested ultracentrifugation condition, which was 600.000 g at 4 °C for 6 hours, it presents a similar supernatant fluorescence intensity between rhEGF-DELOS nanovesicles, free rhEGF and the dispersant medium (histidine buffer (5 mM, pH 7.0)), meaning that almost no DELOS nanovesicles were present in the supernatant. Consequently, this condition of ultracentrifugation confirms an optimal separation of rhEGF-DELOS nanovesicles from free rhEGF and so a proper determination of rhEGF entrapment efficiency in rhEGF-DELOS nanovesicles.

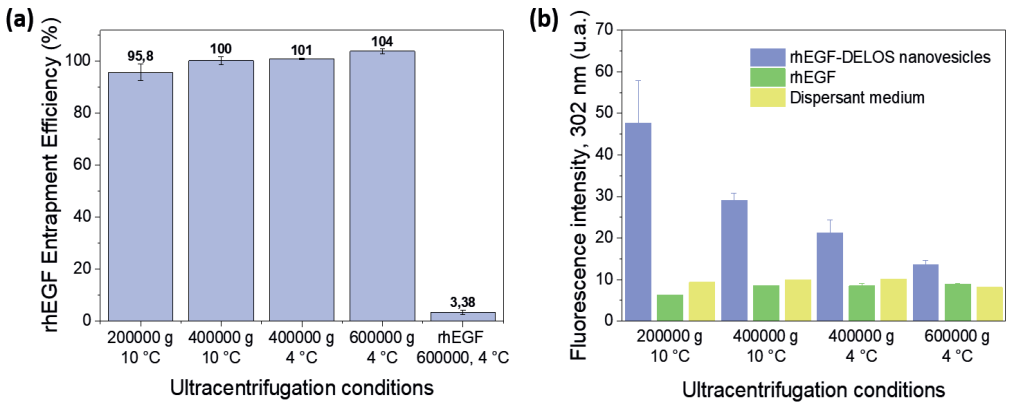

Figure 2.24: (a) Evaluation of the rhEGF encapsulation efficiency from the measured fluorescence intensity in the pellet of rhEGF integrated into the DELOS nanovesicles by using different ultracentrifugation conditions and (b) Fluorescence intensity at 302 nm of the supernatants of the rhEGF-DELOS nanovesicles, rhEGF and dispersant medium (histidine buffer (5 mM, pH 7.0)) from the use of different ultracentrifugation conditions. All ultracentrifugation conditions lasted 6 hours.

To validate this ultracentrifugation process, the integrity of the rhEGF-DELOS nanovesicles upon formation of a pellet was examined by cryo-TEM. **Figure 2.25** shows that the morphology of rhEGF-DELOS nanovesicles maintained the original structure after ultracentrifugation, confirming that this procedure is non-destructive for this nanoformulation.

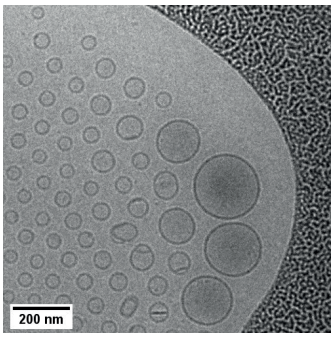

Figure 2.25: Representative cryo-TEM image of the rhEGF-DELOS nanovesicles present in the pellet obtained after the ultracentrifugation process under the condition of 600.000 g at 4 °C for 6 hours.

Therefore, based on these results, it was decided that the calculation of the rhEGF encapsulation efficiency in DELOS nanovesicles has to be performed using an ultracentrifugation method at 600.000 g of 4 °C for 6 hours, followed by fluorescence measurements at 345 nm.

Consequently, the rhEGF entrapment efficiency (EE%) in the optimized rhEGF-DELOS nanoformulations containing 25 and 100 $\mu g \cdot mL^{-1}$ of rhEGF was determined. Overall, the results presented in **Table 2.7** show that the EE% of both systems remained very high (≥97%) regardless of the protein loadings.

Table 2.7: Entrapment efficiency of rhEGF in the optimized rhEGF-DELOS nanovesicle formulations loaded with different rhEGF concentrations and measured after one week (N = 2).

Optimized rhEGF-DELOS nanovesicles	EE (%)
rhEGF-DELOS nanovesicles with 25 $\mu g \cdot mL^{-1}$ of rhEGF	97 ± 3
rhEGF-DELOS nanovesicles with 100 $\mu g \cdot mL^{-1}$ of rhEGF	98 ± 1

To conclude, we have successfully develop a robust and suitable method to accurately evaluate the encapsulation efficiency of rhEGF in our optimized nanoformulations. By using ultracentrifugation method at 600.000 g of 4 °C for 6 hours, followed by fluorescence measurements at 345 nm, both nanoformulations exhibited high encapsulation efficiencies at approximately 98%. These are promising and relevant results as encapsulation efficiency is critical quality attribute that must be carefully controlled for the nanoformulation efficacy.

2.2.6 Further physicochemical characterization of the optimized rhEGF-DELOS nanoformulation considering defined CQAs and scalability

Previous studies have shown that an optimization in the rhEGF-DELOS nanovesicle formulation can be achieved for the treatment of DFUs and VLUs using the compressed CO_2-based DELOS-susp platform towards the preclinical development stage, including the establishment of the critical quality attributes. Then, henceforth, this new optimized rhEGF-DELOS nanoformulations, now referred to as the intermediate formulation will always be related to the one prepared using DELOS-susp and the composition defined in **Table 2.5**. Therefore, here we provide further experimental evaluations of this new intermediate product considering the CQAs and specifications defined in **Section 2.2.2** to verify in detail its potential in terms of physicochemical characterization.

First, thanks to the collaboration with the group of Prof. Jan Skov Pedersen from the Department of Chemistry and Interdisciplinary Nanoscience Center (iNANO, Aarhus, Denmark), small-angle X-ray scattering (SAXS) measurements were performed on Blank-DELOS nanovesicles and rhEGF-DELOS nanovesicles (rhEGF 100 $\mu g \cdot mL^{-1}$) that were sent to study their homogeneity and thus gain a further understanding of the DELOS nanovesicles morphology (see **Section 6.3.4** for more details). This technique can provide unique structural information with the advantage of measuring the average properties of the bulk samples that can be otherwise obviated by using only microscopic techniques such as cryo-TEM or confocal microscopy.

As shown in **Figure 2.26**, SAXS data for Blank-DELOS nanovesicles and rhEGF-DELOS nanovesicles have a broad maximum at large scattering vector moduli q, which originates from the shell-core-shell cross-section structure of the vesicles, where the electron density of the hydrocarbon core is lower than that of the buffer and the electron density of the shells is higher than the buffer[71]. The rhEGF-DELOS nanovesicles samples display additional extensive high-frequency ripples, which originates from the overall size of the vesicles and a very low size polydispersity. The corresponding data for Blank-DELOS nanovesicles do not show these oscillations, which means that this sample is somewhat more polydisperse. However, an aged sample (20 months) has also been measured and the data (not shown) display the same high-frequency ripples as the rhEGF-DELOS nanovesicles.

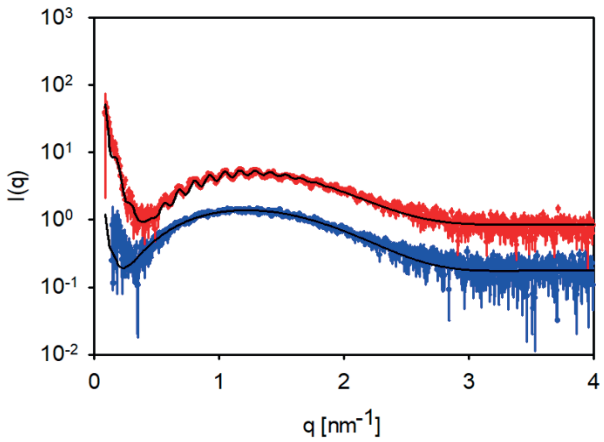

Figure 2.26: Experimental SAXS profiles at room temperature of Blank-DELOS nanovesicles in blue, and rhEGF-DELOS nanovesicles loaded dispersions, in red.

Additionally, exposing the Blank-DELOS nanovesicles sample to ultra-sound also results in SAXS with ripples, and this together with the behavior of the aged sample shows that the equilibrium structure of the Blank-DELOS nanovesicles sample is also that of very monodisperse vesicles. Since the fresh rhEGF-DELOS nanovesicles sample already is very monodisperse, it is reasonable to conclude that the association of the rhEGF enhances molecular exchange, which brings the system faster into equilibrium.

The SAXS data were fitted with a model of spherical vesicles with a Gaussian number size distribution, where the cross-section of the vesicles is a shell-core-shell structure. The model fits the data very well and reproduces the high-frequency ripples for the rhEGF-DELOS nanovesicles confirming a vesicular structure, as observed by cryo-TEM (**Figure 2.23**). According to the modeling, the outer radius for the Blank-DELOS nanovesicles and the rhEGF-DELOS nanovesicles was 31 ± 8 and 27.22 ± 0.03 nm, respectively, whereas the membrane thickness for both samples was 4.4 nm. The polydispersity for the Blank-DELOS nanovesicles is estimated to be >10%, whereas it is only 2.6%

for rhEGF-DELOS nanovesicles. These results are in agreement with the cryo-TEM images and DLS results (**Table 2.5** and **Figure 2.21** and **Figure 2.22**), when considering that the polydispersities of DLS are usually overestimated.

Moreover, the release profile of rhEGF from the rhEGF-DELOS nanovesicles with 100 μg·mL^{-1} of rhEGF in the dispersant medium conditions of water/10% EtOH (v·v^{-1}), histidine buffer (5 mM, pH 7.0) was also investigated through the shaking incubation of the conjugates at 32 and 37 °C and after storage times of 0.5, 1, 2 and 3 days (see **Section 6.4.2**). The released rhEGF was determined by ultracentrifugation followed by ELISA (**Figure 2.27**). No burst release of loaded rhEGF was clearly observed at the beginning of the study at both pH values; neither any rhEGF release was observed for the sample maintained during 3 days at pH 5.5 after incubation at temperatures 32 and 37 °C. However, at pH 7.0 a small rhEGF release was observed that tends to increase with time but remains below 5% after the 3 days at 32 °C. A higher amount of rhEGF (from 10 to 15%) was released at the same pH after storage at 37 °C. Then, thanks to this experiment, it was illustrated the importance of pH and temperature in the release of rhEGF from rhEGF-DELOS nanovesicles.

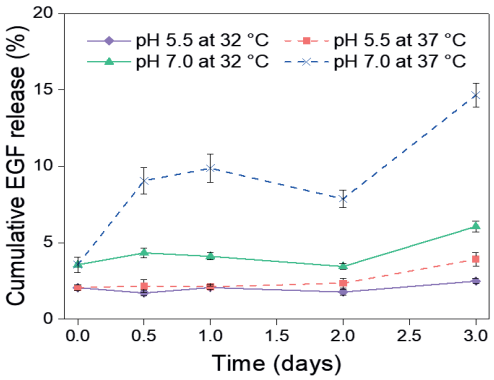

Figure 2.27: The time-release profile of rhEGF-DELOS nanovesicles (rhEGF 100 μg·mL^{-1}) at pH 5.5 (32 °C, lilac line, and 37 °C, red dashed line) and pH 7.0 (32 °C, green line, and 37 °C, blue dashed line). Data is plotted as mean ± SD (N = 3 per group).

On the other hand, we are interested in developing a robust nanomedicine that can progress to the clinical stage. For this reason, it is essential to attain a complete reproducibility of their physicochemical characteristics, morphology and drug substance loading among different batch productions, which is called batch-to-batch consistency.

Besides, it is very important the use of methodologies that allow nanomedicine production at an industrial scale with suitable and reproducible characteristics, involving a minimum number of steps and equipment and meeting the requirements of the pharmaceutical guidelines and the good manufacturing practices (GMP).

In this regard, the reproducibility under a 40-fold scale-up has been checked to evaluate the potentiality of the DELOS-susp as a robust manufacturing platform for the production of rhEGF-DELOS nanovesicles (rhEGF 100 μg·mL^{-1}) from bench-scale (obtaining 25 mL of nanoformulation) to pilot-scale (delivering 1 L of nanoformulation). Robustness and reproducibility of the rhEGF-DELOS nanovesicles production by DELOS-susp methodology were evaluated by measuring the mean particle size, PDI, apparent zeta potential, and EE% values of different batches produced at the different scales, by high-pressure vessels with different volumes (**Figure 2.28a**).

From the obtained data average shown in **Figure 2.28b**, one can see that the standard deviations of the mean particle sizes, apparent zeta potentials and EE% values are small with a coefficient of variation (CV) of 2.6-11.6% in all cases, indicating a high degree of reproducibility during scale-up of the DELOS-susp method for the rhEGF-DELOS nanovesicles.

(a)

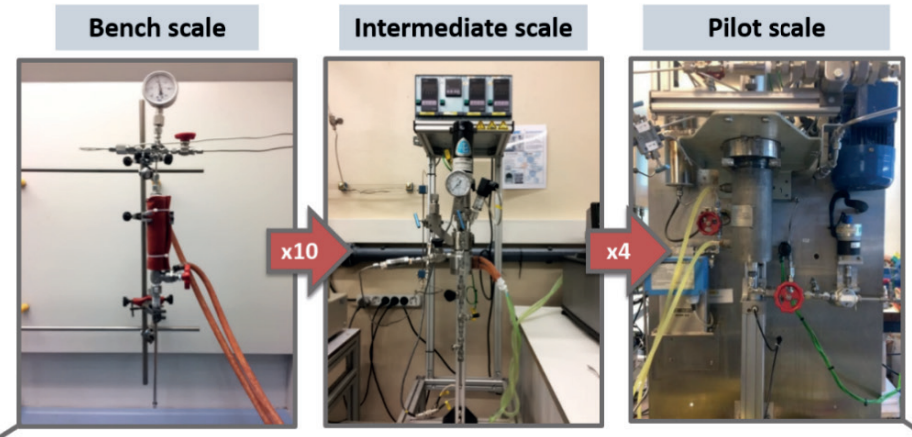

(b)

High-pressure vessel	Particle mean size (nm)	PDI	Apparent Zeta potential (mV)	EE (%)
Bench scale P6 mL (batch size 25 mL)	68 ± 5	0.29 ± 0.00	82 ± 0	98 ± 1
Intermediate scale P50 mL (batch size 250 mL)	60 ± 4	0.27 ± 0.01	90 ± 7	95 ± 1
Pilot scale P300 mL (batch size 1 L)	59 ± 3	0.23 ± 0.02	84 ± 1	93 ± 1
Mean	62.3	0.26	85.3	95.3
SD	4.9	0.03	4.2	2.5
CV (%)	7.9	11.6	4.9	2.6

Figure 2.28: (a) Reactors used for scale-up studies using DELOS-susp method. From left to right: P6, P50 and P300 mL and (b) Physicochemical characteristics of rhEGF-DELOS nanovesicles (rhEGF 100 μg·mL^{-1}) prepared with different high-pressure vessels from bench-scale to pilot-scale (t = 1 week and N = 2).

In summary, rhEGF-DELOS nanovesicles were further characterized in terms their physicochemical properties. The aforementioned results confirmed that not only is this nanoformulation highly monodisperse, but also that pH and temperature can be relevant factors for the release of rhEGF from rhEGF-DELOS nanovesicles. Furthermore, high reproducibility was observed when scale-up of the DELOS-susp method for this nanoformulation preparation.

2.2.7 Summary of the section

In this work, it can be concluded that an optimized drug product of rhEGF-DELOS nanovesicles for the treatment of DFUs and VLUs has been obtained, henceforth referred to as an intermediate product. Overall, the aligned efforts to optimize the nanoformulation have not only enabled to gain immense knowledge about the critical parameters that can impact on the performance of our drug product, but also to optimize them to improve the quality and safety of the nanoformulations.

On the basis of the obtained results, it can be concluded that a better drug product with higher stability can be obtained when histidine buffer (5 mM, pH 7.0) is used as dispersant medium and the position of the CTAB surfactant is changed to the organic phase in the DELOS-susp configuration to produce the rhEGF-DELOS nanovesicles.

Furthermore, the two intermediate products with rhEGF protein concentration of 25 and 100 $\mu g \cdot mL^{-1}$ showed appropriate physicochemical properties in relation to the defined CQAs and specifications of the nanoformulation. On the other hand, not only a robust analytical method to control the protein entrapment efficiency was developed, showing high rhEGF EE% (≥ 97%) of the intermediate product. This is a very important since it not only minimizes the protein loss during the fabrication process but also impacts on the cost of the process. Moreover, it should be highlighted that a complete reproducibility of the physicochemical characteristics of the intermediate product from bench-scale to pilot-scale was observed.

Generally, rhEGF-DELOS nanovesicles intermediate product is a promising nanoformulation that has the right properties for successful nanomedicine development, preclinical studies are necessary as a next step to demonstrate the drug product's safety and efficacy before its clinical validation.

2.3 Preclinical evaluation phase for quality, safety, and efficacy assessment of rhEGF-DELOS nanovesicles intermediate product

After selecting the intermediate nanoformulation (**Table 2.5**), this system was further investigated to evaluate its safety and efficacy and to verify its potential. Within this framework, it is worth highlighting the importance of well-known institutions such as the Nanotechnology Characterization Laboratory, established by the National Cancer Institute with the Food and Drug Administration and the National Institute of Standards and Technology, as it has established a preclinical characterization cascade of nanomedicines to provide pharmaceutical guidance for researchers[72].

This guideline not only performs the physicochemical characterization but also preclinical tests such as the immunological, pharmacological and toxicological properties of nanoparticles and devices by providing an overview of the parameters that should be well-thought-out in the development of novel nanomedicines to obtain the approval from the regulatory authorities. For instance, some nanomedicine performance characteristics need to be guaranteed such as the product reproducibility and the compliance with of quality, safety, and efficacy[73].

The motivation of this section is based on studying the safety and efficacy of our promising nanoformulation based on rhEGF-DELOS nanovesicles. Assuming the topical administration of the nanovesicles developed as carriers for rhEGF, various non-clinical activities have been proposed to demonstrate its potentiality. Subsequently, accurate preclinical studies were conducted to evaluate the efficacy and toxicology of the intermediate product. To do this, some *in vitro* preclinical exploratory quality assessment studies were first carried out and then, after observing it potential *in vitro,* some *in vivo* efficacy and toxicity tests were performed to substantiate the safety of the nanoformulation and to understand the behavior of the nanoformulation in more detail[74].

It is important to emphasize that the approach of the pharmaceutical Heberprot-P® (Heber Biotec)[15] was used as our reference model, whose clinical trial was based on intralesional administration of 75 µg of EGF in patients suffering type 2 diabetes mellitus presenting a mean ulcer size of 16.3 cm^2. Taking these values into account, the administered dose was then 5 $\mu g \cdot cm^{-2}$, which will be our reference value for the efficacy and toxicological studies of the intermediate product of rhEGF-DELOS nanovesicles.

Furthermore, for the present work, which describes all the efficacy and safety studies, all the *in vitro* biological assays were performed by members of the different specialized laboratories of the CIGB Institute and Leitat Technological Center-Biomed. It is sufficient to point out that within the framework of this Thesis, all the nanoformulations were prepared and fully characterized for a correct development of the experiments and at the same time, we actively participated in the design of the experiments and the discussion of the results.

2.3.1 In vitro preclinical evaluation of the intermediate product of rhEGF-DELOS nanovesicles for quality efficacy and toxicity assessment

2.3.1.1 In Vitro Protein-Specific Bioactivity

One of the first questions that arises is whether the manufacturing process used to prepare the nanoconjugates impairs the bioactivity of the protein and thus loses its function at the site of action. Therefore, thanks to the CIGB laboratory collaboration, the bioactivity of the rhEGF-DELOS nanovesicles intermediate product (**Table 2.5**) was determined by the ability of the samples to induce cell proliferation in 3T3 A31 mouse fibroblast cells, since this cell line shows overexpression of EGF receptor[75] (see **Section 6.4.3**).

To determine the cytotoxicity and cell biocompatibility of the DELOS nanovesicles, a dose–response curve was first investigated with the same cell line as for the cell proliferation test. The viability test after 24 h of incubation time revealed that cationic nanoconjugates exhibited a dose-dependent toxicity.

When cells were exposed to rhEGF-DELOS nanovesicles with 25 $\mu g \cdot mL^{-1}$ and Blank-DELOS nanovesicles with a CTAB surfactant concentration higher than 6.7 $\mu g \cdot mL^{-1}$, cell viability was reduced to about 40%. However, since the DELOS nanovesicles were diluted and the cells were exposed to surfactant concentrations ranging from 3.35 to 0.8375 $\mu g \cdot mL^{-1}$, Blank-DELOS nanovesicles showed no cytotoxic effect. Furthermore, rhEGF-DELOS nanovesicles exhibited a statistically significant increased cell proliferation activity (about 50% increased) as compared to the Blank-DELOS nanovesicles group (**Figure 2.29a,b**).

(a)

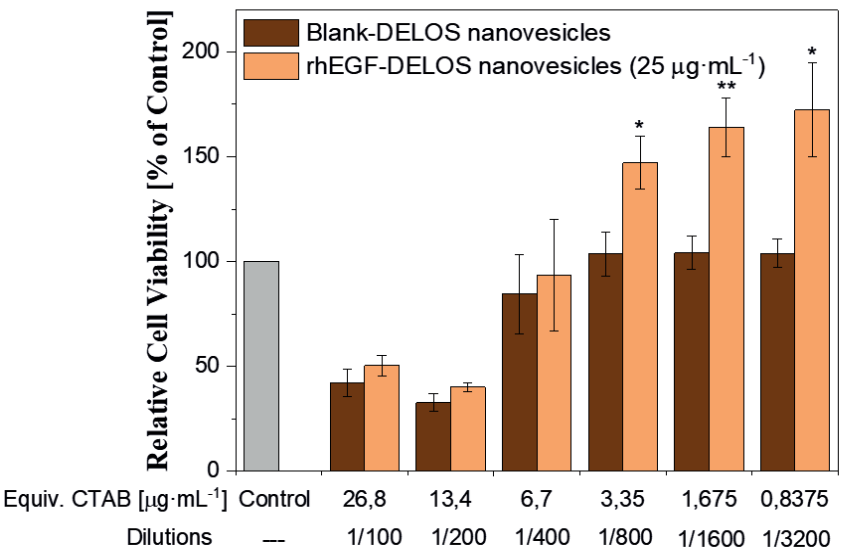

(b)

Dilutions	1/100	1/200	1/400	1/800	1/1600	1/3200
Equiv. CTAB Concentration ($\mu g \cdot mL^{-1}$)	26.8	13.4	6.7	3.35	1.675	0.8375
Equiv. EGF Concentration ($\mu g \cdot mL^{-1}$)	250.0	125.0	62.5	31.25	15.625	7.8125
P-value	0.126	0.098	0.588	0.022*	0.003**	0.010*

Figure 2.29: (a) Graph of cytocompatibility of Blank-DELOS nanovesicles (brown) and rhEGF-DELOS nanovesicles (rhEGF 25 $\mu g \cdot mL^{-1}$) (orange) as a function of surfactant concentration. Proliferation of 3T3 clone A431 murine fibroblast cells was determined by crystal violet assay following 24 h samples exposure and is expressed as a fraction of the control (untreated) cells. Data are plotted as mean ± SD, N = 4. Statistical significance determined via pairwise t-test between cells exposed to Blank-DELOS nanovesicles and rhEGF-DELOS nanovesicles (rhEGF 25 $\mu g \cdot mL^{-1}$) and (b) Table of the P-Value determined via pairwise t-test between cells exposed to Blank-DELOS nanovesicles and rhEGF-DELOS nanovesicles (rhEGF 25 $\mu g \cdot mL^{-1}$) in the proliferation of 3T3 A431 murine fibroblast cells as a function of surfactant concentration to determine the cytocompatibility of DELOS nanovesicles (N = 4 per group). *$p < 0.05$ and **$p < 0.01$.

Taking this result into account, the minimum dilution of DELOS nanovesicles valid for performing a cell proliferation assay and studying their bioactivity must be 1/400-fold since at this dilution DELOS nanovesicles contains a CTAB concentration of 6.7 $\mu g \cdot mL^{-1}$ (the maximal non-cytotoxic concentration).

To compare the specific bioactivity of the protein at different rhEGF-DELOS nanovesicles formulations, the specific activity of the samples was calculated by dividing the absolute biological activity by the protein concentration of each sample. Blank-DELOS nanovesicles were also included as a control in these assays and no cell proliferation increase was observed. From **Figure 2.30**, a point worth noticing of these experiments was that the rhEGF bioactivity was not only preserved after rhEGF-DELOS nanovesicles preparation by DELOS-susp methodology but also increased. The half-maximal effective dose (ED50) of rhEGF-DELOS nanovesicles and free rhEGF towards fibroblast cell line lines were in the ranges 1.27–1.40 and 2.70–3.06 $ng \cdot mL^{-1}$, respectively.

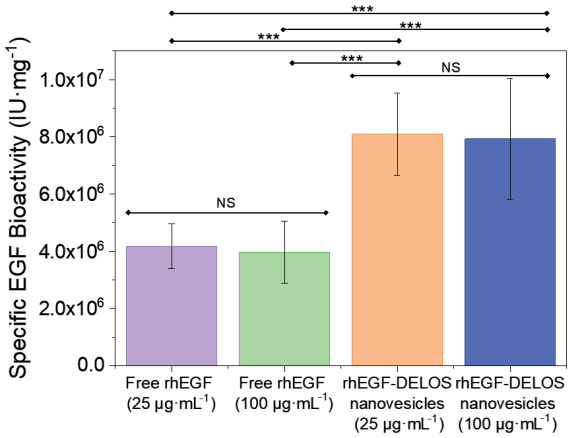

Sample	ED50 (ng·mL⁻¹) Mean (95% CI)
Free rhEGF 25 µg·mL⁻¹	2.70 (2.30-3.10)
Free rhEGF 100 µg·mL⁻¹	3.06 (2.66-3.46)
rhEGF-DELOS nanovesicles 25 µg·mL⁻¹	1.27 (0.87-1.67)
rhEGF-DELOS nanovesicles 100 µg·mL⁻¹	1.40 (1.00-1.80)

Figure 2.30: Specific biological activity of rhEGF and rhEGF-DELOS nanovesicles in cell proliferation assay in 3T3 A431 murine fibroblast cell line. The inset Table shows a mean half-maximal effective dose (ED50) and 95% confidence interval (CI) for the same groups. Data plotted as mean ± SD (N = 8 per group).

This increase was at least twice the potency for rhEGF-DELOS nanovesicles, compared to the free biomolecule at the same bulk concentration. As expected, and shown in **Figure 2.31**, cell proliferation shows dose–response within the range of tested concentrations for both free rhEGF and rhEGF-DELOS nanovesicles. At low rhEGF concentrations, (0.625–5.0 ng·mL^{-1}), rhEGF-DELOS nanovesicles also have statistically significantly higher cell proliferation activity than free rhEGF at the same bulk concentration.

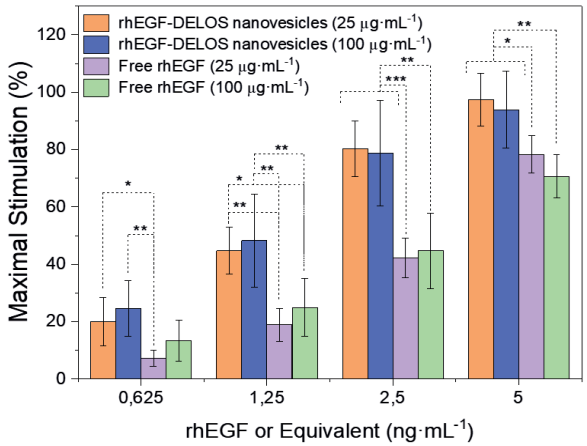

Figure 2.31: Cell proliferation assay in 3T3 clone A431 murine fibroblast cell line for 24 h (rhEGF-DELOS nanovesicles (rhEGF 25 µg·mL^{-1}) (orange), rhEGF-DELOS nanovesicles (rhEGF 100 µg·mL^{-1}) (blue), free rhEGF 25 µg·mL^{-1} (purple), free rhEGF 100 µg·mL^{-1} (green)). Data are plotted as mean ± SD (N = 6). The Percentage of Maximal Stimulation was calculated as described in Methods (in vitro biological activity by cell proliferation assay). Note: the concentration of free rhEGF is equal to the nanocarrier concentration of rhEGF in loaded formulations (rhEGF-DELOS nanovesicles) in each corresponding group. P-values, *p < 0.05, **p < 0.01 and ***p < 0.001 in one-way ANOVA followed by Tukey test.

As discussed in a previous section, the activity increase could be related to the immobilization of the protein in the vesicle membrane with probably a "site-specific" orientation of the active protein region towards the surrounding media, which is favorable for interaction with the EGFR. It is well-known that the EGFR is organized in small clusters of 150 nm average diameter on the cells' plasma membrane[76]. This surface matched well with that of the rhEGF-DELOS nanovesicles with an average diameter of 50–70 nm (**Figure 2.21 and Figure 2.22**). Additionally, the presentation of the immobilized ligands attached to the DELOS nanovesicles membrane would induce a nanometer-scale clustering of the ligand. This would favor the multimerization of the receptor; since two receptors that bind to ligands immobilized on the same DELOS nanovesicles would be nearby, favoring dimerization-dependent signaling (**Figure 2.32**).

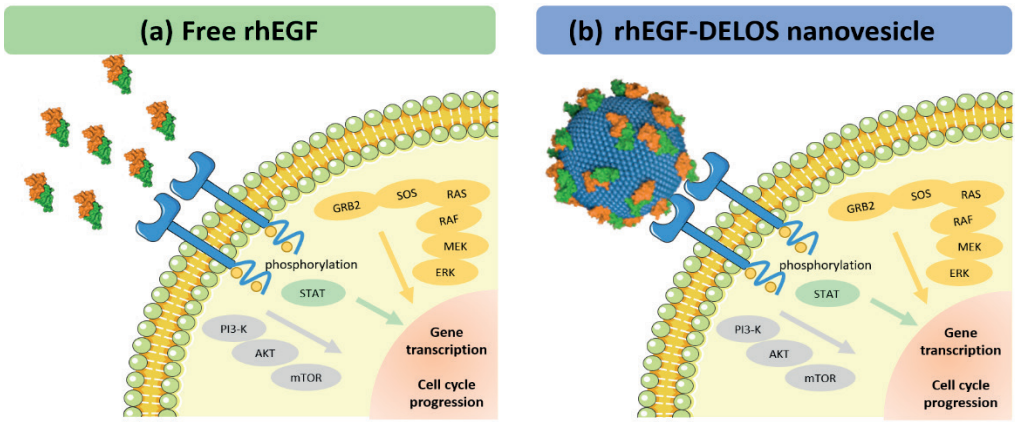

Figure 2.32: Idealized scheme illustrating the potential mechanism of interaction of (a) free rhEGF and (b) rhEGF-DELOS nanovesicles with the EGF receptor at the cell surface, which seems more favorable for rhEGF-DELOS nanovesicles.

2.3.1.2 In Vitro Resistance to Proteases Chronic

Chronic wounds, such as DFUs, present a proteolytic environment that can affect the bioavailability of protein-based drugs used during treatments. Therefore, the protective properties of the intermediate product were evaluated through their ability to preserve the stability and bioactivity of rhEGF in the presence of proteases. In this study performed by CIGB laboratory, chymotrypsin was selected as a protease model because it has many cutting sites in the rhEGF sequence, and its rhEGF proteolysis was sensitive to the ELISA assay (see **Section 6.4.4**). The results in **Figure 2.33** show that at the same rhEGF bulk concentration, the intermediate product of rhEGF-DELOS nanovesicles with 25 and 100 $\mu g \cdot mL^{-1}$ of rhEGF (**Table 2.5**) presented increased stability against chymotrypsin compared to the free protein. As expected, for the same kind of sample, with higher rhEGF concentration, higher proteolysis was observed, probably because saturation conditions

were not reached. Thus, the amount of protein decreases during the first 3 h in all cases, however, or the rhEGF-DELOS nanovesicles formulations, the decrease was much smaller. Between 3 and 24 h of incubation, the protein contents remained practically constant near to 20% for free rhEGF at 25 μg·mL^{-1} and below 5% for free rhEGF at 100 μg·mL^{-1}.

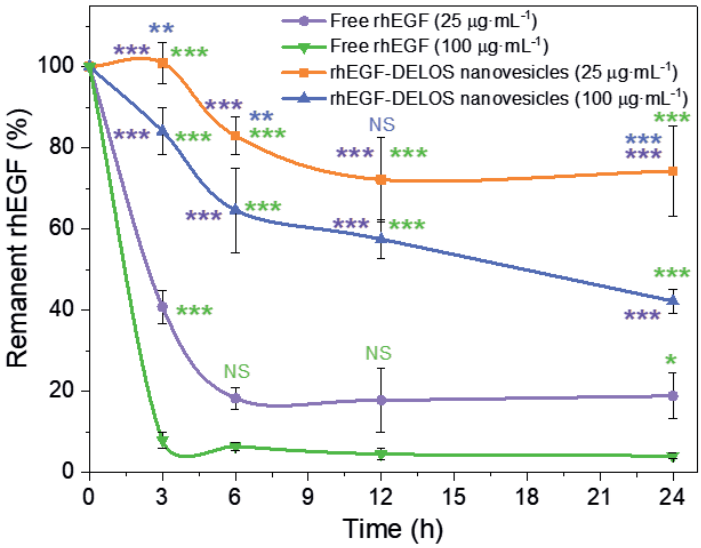

Figure 2.33: Assessment of time-course proteolytic stability of free rhEGF at 25 and 100 μg·mL^{-1} (purple and green lines, respectively) and rhEGF-DELOS nanovesicles at 25 and 100 μg·mL^{-1} (orange and blue lines, respectively) against chymotrypsin at 32 °C in the dispersant medium (histidine buffer (5 mM, pH 7.0)/10% EtOH (v·v^{-1})). Purple, green and blue asterisks represent statistical significance for free rhEGF at 25 μg·mL^{-1}, free rhEGF at 100 μg·mL^{-1}, rhEGF-DELOS nanovesicles at 25 μg·mL^{-1}, and rhEGF-DELOS nanovesicles at 100 μg·mL^{-1} experimental groups, respectively, at the indicated time point. *p < 0.05, **p < 0.01, ***p < 0.001 and NS: non-significant differences. All statistical analyses were conducted by one-way ANOVA followed by Tukey pairwise comparison.

On the other hand, for rhEGF-DELOS nanovesicles incubated between 6 and 24 h, the amounts of protein remained practically constant near to 70% for rhEGF-DELOS nanovesicles at 25 μg·mL^{-1} and near to 40% at 100 μg·mL^{-1}. At the same rhEGF bulk concentration, the overall percentage of undamaged protein was about 35-50%; higher when it is nanoformulated in DELOS nanovesicles than free. It is likely that the free rhEGF degrades much quicker than the rhEGF grafted on DELOS nanovesicles because the free protein will exhibit multiple degradation sites exposed to the solvent (**Figure 2.34**). Solvent exposed active sites of the protein may be recognized by a broader array of degradative enzymes like proteases. Since the ultimate purpose of this work was the use of the rhEGF-DELOS nanovesicles as a topical formulation, a high resistance to proteases might be translated to better bioavailability and a longer and more effective action of the rhEGF in the wound's areas.

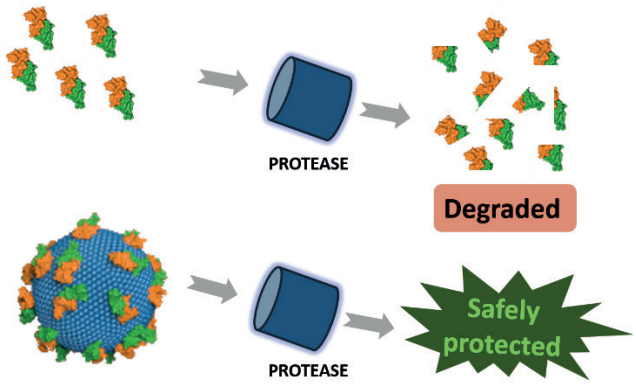

Figure 2.34: Idealized scheme illustrating the potential protection of rhEGF from wound environment proteolytic degradation by its incorporation to DELOS nanovesicles as compared to free protein.

2.3.1.3 Biocidal Activity

As already mentioned, wound infection is one of the most contributing important factors to wound chronicity and, thereby, efficient control of infection is an appropriate quality attribute for a drug topical delivered intended for the treatment of chronic wounds. Samples of the intermediate product containing rhEGF concentrations of 25 and 100 $\mu g \cdot mL^{-1}$ and Blank-DELOS nanovesicles were tested *in vitro* to evaluate their biocidal activity (see **Section 6.4.5**). The effectiveness of the different colloidal systems was assayed against bacteria, yeast, and fungus.

As shown in **Figures 2.35a,b**, the intermediate formulation with and without the presence of rhEGF (Blank-DELOS nanovesicles) presented antimicrobial activity against Gram-positive bacteria, yeast and fungi. Remarkable is the fact that some microorganisms sensitive to rhEGF-DELOS nanovesicles (e.g., *Staphylococcus aureus*) are among the main microorganisms known to contribute to serious complications in wound infection and microbial flora of chronic wound biofilms and burns[75]. The encountered antimicrobial properties of rhEGF-DELOS nanovesicles demonstrated the great potential of the preparations based on DELOS nanovesicles as topical formulations. The antimicrobial activity of QASs has been generally attributed to their ability to destroy cell membrane structure[77]. Indeed, QASs exerts antimicrobial activity through its positive charge at physiological pH, which destabilizes bacterial cell walls and alters bacterial osmotic equilibrium[20]. These events result in the precipitation of cytoplasmic contents and trigger microbial cell death[78]. By their antiseptic activity, rhEGF-DELOS nanovesicles may also act as a prophylactic agent that prevents microbial infections, hindering the formation of biofilms. In fact, it has already been reported that Blank-DELOS nanovesicles have antibiofilm activity against *Staphylococcus aureus* and *Pseudomonas aeruginosa* biofilms[77].

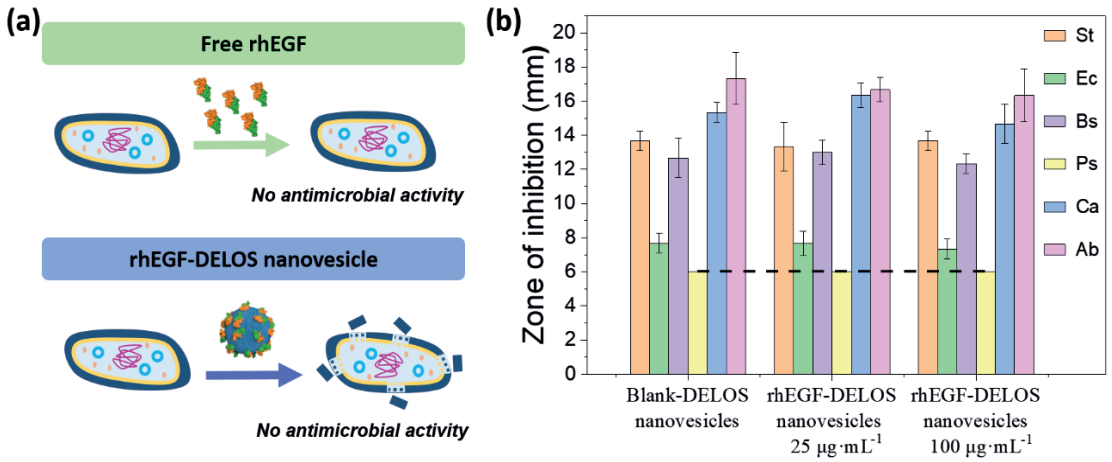

Figure 2.35: Antimicrobial activity of assayed DELOS nanovesicles (a) Scheme illustrating the rhEGF-DELOS nanovesicles antimicrobial activity against potential wound environment microorganism. (b) Antimicrobial activity assessed by zone of inhibition during the agar well diffusion assays: Blank-DELOS nanovesicles and rhEGF-DELOS nanovesicles with rhEGF at 25 and 100 µg·mL^{-1} bulk concentration against different microorganisms (N = 3; error bar = SD). St: Staphylococcus aurous, Ec: Escherichia coli, Bs: Bacillus subtilis, Ps: Pseudomonas aeruginosa, Ca: Candida albicans, Ab: Aspergillus brasiliensis. Discontinuous line represents the well diameter.

According to these findings, the anchoring of rhEGF to nanovesicles could favor dimerization-dependent EGF-EGF receptor signaling while shielding the protein from other degradation pathways, permitting optimization of their pharmacological properties. Then, this antiseptic activity of the intermediate product formulation may act as a prophylactic agent preventing microbial infections hindering the formation of biofilms being therefore attractive for topical treatments.

2.3.1.4 Ex vivo permeation in human skin

Another interesting parameter to evaluate the therapeutic efficacy of new nanomedicines for topical administration is the study of their permeation and diffusion. In this context, the use of *in vitro* static diffusion cells to assess skin permeability has become a preferred research approach, creating greater awareness of the relationships between the skin and the drug formulation[79].

In our case, to assess the kinetics and absorption profile of the rhEGF contained in the intermediate product formulation (**Table 2.5**) through the skin, *ex vivo* skin permeation assays in Franz-type diffusion cells were used thanks to the Leitat Technological Center-Biomed partner of the Nanonafres' project. Franz diffusion studies help to evaluate the skin penetration and diffusion of an active pharmaceutical ingredient through the skin[80]. To simulate human skin conditions,

damaged human skin with impaired barrier function due to tape stripping was used to better mimic the permeation behavior in wounds.

Using this method, described in **Section 6.4.6**, our approach was to study and compare the absorption profile of free rhEGF and rhEGF integrated into DELOS nanovesicles, both in a concentration of 100 $\mu g \cdot mL^{-1}$. As a reference, a 100 µL of free rhEGF sample using the same medium and with an equivalent amount of total rhEGF as contained in DELOS nanovesicles was applied on 1 cm^2 of epidermal side of the skin, achieving an applied dose of 10 $\mu g \cdot cm^{-2}$. This applied dose is considered to be an infinite dose, compared to the expected 5 $\mu g \cdot cm^{-2}$ in Heberprot-P® product. It is important to considerer that infinite dose gives data on pharmacokinetic parameters, since when it is necessary to know the amount absorbed in the different layers of the skin, the real quantities of finite doses are chosen, but in order to compare penetration of various active ingredients through the skin, infinite dosage is required to assess the enough amount in the receptor fluid[81].

Then, following this procedure, aliquots were collected from the receptor side to evaluate the non-trespassed, the absorbed and permeated rhEGF by ELISA methodology. Based on these results evaluating the permeation of rhEGF, it was observed that rhEGF was significantly reduced when encapsulated in DELOS nanovesicles (**Figure 2.36a**), suggesting that rhEGF integrated into DELOS nanovesicles might be more strongly absorbed through the skin over time than the free rhEGF.

Focusing on the permeation kinetics, the results revealed significant differences between the permeation of free rhEGF and rhEGF integrated into DELOS nanovesicles. As shown in **Figure 2.36a**, the rhEGF flux in the linear part of the curve showed that the permeation in rhEGF-DELOS nanovesicles was 2.7 times slower than in the free rhEGF solution, at 123 and 330 $ng \cdot cm^{-2} \cdot h^{-1}$, respectively. Careful examination of the data revealed that after 24 h, rhEGF contained in the free rhEGF solution completely permeated (103% ± 28%), while only half of the dose of the encapsulated rhEGF in rhEGF-DELOS nanovesicles passed to the skin (50% ± 10%) as observed in **Figure 2.36b**. This is the most relevant finding and perhaps the most significant, as the encapsulation of rhEGF in DELOS nanovesicles allows for better retention of the protein in the skin, achieving a more localized and long-lasting effect and, consequently, a more effective and efficient treatment.

Additionally, another way to test the effectiveness of rhEGF-DELOS nanovesicles not trespassing skin, CTAB was quantified by Ultra-High Performance Liquid Chromatography tandem Mass Spectrometry (UPLC-MS/MS) after 24 h and showed that only 5% of the applied dose permeated, minimizing the safety concerns when using this cationic surfactant (**Figure 2.36**c).

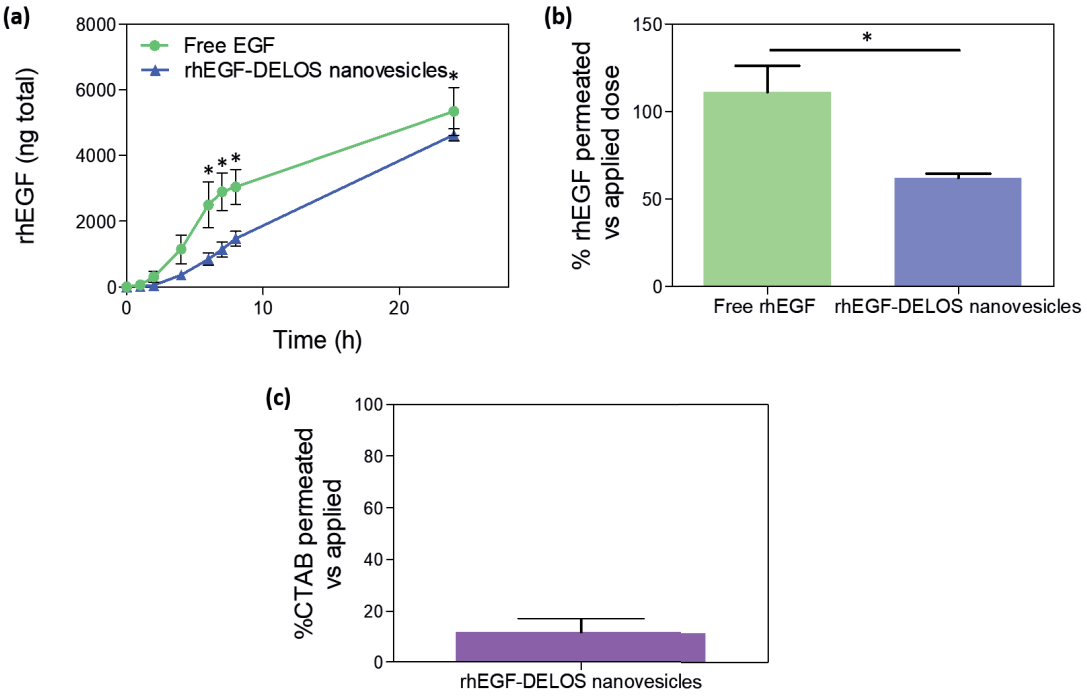

Figure 2.36: ***Ex vivo*** permeation of free rhEGF and rhEGF-DELOS nanovesicles through damaged skin. (a) rhEGF permeated (quantified in the receptor fluid) during 24 h. (b) rhEGF permeated (%) after 24 h relative to the applied dose. (c) CTAB permeated (%) after 24 h relative to the applied dose. The mean of 4 experimental replicates ± SD is shown. *p < 0.05 determined via two-way ANOVA with Sidak post hoc test.

Therefore, thanks to the results obtained in this *ex vivo* permeation test, it can be concluded that clearly the free rhEGF permeates more in the skin compared to the rhEGF integrated into the DELOS nanovesicles, which did not show an effective permeation of rhEGF through the skin suggesting its inability to reach the circulation system when topically administered and favoring a local effect and a not systemic absorption. Then, it seems reasonable to assume that this intermediate formulation has a huge potential for being successfully applied topically, especially to complex wounds.

2.3.1.5 Irritation on a 3D *in vitro* skin model by EpiSkin ™

Furthermore, one of the pharmacological tests to validate the safety of the nanoformulation prototype for topical administration is the skin irritation test. To do it, in the frame of Nanonafres project, recommendations were adopted from test guideline 404 published by the Organization for Economic Co-operation and Development (OECD), which is a reference to ensure the best

available science for chemical testing. This guidance recommends several strategies involving the performance of validated and recognized *in vitro* and *ex vivo* tests for corrosion and irritation to avoid unnecessary testing on laboratory animals and offers some alternatives to follow the 3R fundamental principles: Replacement, Reduction and Refinement to study more efficiently and ethically both chemical and biological products[82].

In our case, special attention was paid to *in vitro* human skin models, specifically 3D models of human skin that are commercially available for skin corrosion and irritation. In particular, the reconstructed human epidermis EpiSkin™ test has been used as a recognized method for testing skin irritation (*OECD (2015), Test Nº. 439: In Vitro Skin Irritation: Reconstructed Human Epidermis Test Method, OECD Publishing, Paris)* and also validated by the European Center for the Validation of Alternative Methods (ECVAM) in 2003 for skin corrosion analysis[83].

This reconstructed human epidermis model is obtained from human keratocytes derived from the skin and cultured in specialized structures such as collagen or polycarbonate structures until all the different epidermal layers are fully formed due to cell differentiation[84]. These non-transformed epidermal keratinocytes closely mimic the histological, morphological, biochemical and physiological characteristics of the upper parts of human skin such as the epidermis[85]. Then, thanks to this model, it stands as a biologically and metabolically active barrier that mimics the route of human topical exposure. Thus, any irreversible damage to the skin can be assessed as visible necrosis through the epidermis to the dermis.

Episkin™ Skin Irritation Test methodology

Following the indications of OCDE Guideline Test No.439: In Vitro Skin Irritation: Reconstructed Human Epidermis Test Method (28 July 2015), with a refinement of the protocol to adapt it for a proper evaluation of the DELOS nanovesicles, the test was carried out in collaboration with Leitat Technological Center partner of Nanonafres project. To do it, the systems of interest were applied to the skin of 0.5 cm^2 of surface, in a volume of 20 ± 0.5 µL (40 ± 1 $\mu L \cdot cm^{-2}$) (see **Section 6.4.7**). The samples tested for the study were as follows, using the same formulations described in **Table 2.5** as reference:

1. Positive control: an irritant agent like SDS 5% $w \cdot v^{-1}$.
2. Negative control: phosphate buffer saline (pH 7.4).
3. Dispersant media: histidine buffer (5 mM, pH 7.0)/10% EtOH ($v \cdot v^{-1}$).
4. Blank-DELOS nanovesicles: intermediate formulation without rhEGF.
5. Intermedia formulation with rhEGF 25 $\mu g \cdot mL^{-1}$.

6. Intermedia formulation with rhEGF 100 $\mu g \cdot mL^{-1}$.
7. CTAB in dispersant medium: same CTAB concentration as the intermediate formulation (**Table 2.5**). So, 7.3 mM of CTAB was dissolved in histidine buffer (5 mM, pH 7.0)/10% EtOH ($v \cdot v^{-1}$).

These 7 groups were applied for 24 h and 48 h on the reconstructed skin and the resulting cytotoxicity as measured by two variables. First, cell viability was measured by mitochondrial activity using MTT assay, which linearly relates the number of viable cells to mitochondrial activity since its activity is reflected by the conversion of the tetrazolium salt MTT into formazan crystals. Thus, a variation in viable cell number can be identified by measuring the formazan concentration revealed in optical density[86].

Additionally, interleukin-1α (IL-1α), which was also considered as a marker to assess skin irritation, was quantified by ELISA technique (see **Section 6.4.1**). This molecule is the principal cytokine released by keratinocytes in irritation the process and initiator of secondary inflammation pathways[87], so, it was of great interest to be evaluated.

Episkin™ Skin Irritation Test Results

Based on the results summarized in **Figure 2.37**, we make the following observations. The results achieved for the dispersant media used in DELOS nanoformulations present proper cell viability after 24 and 48 hours of exposure, since the feasible values are close to 100%, similar to the negative control (PBS).

Comparatively, when focusing on empty DELOS nanovesicles and the rhEGF-DELOS nanovesicles with 25 and 100 $\mu g \cdot mL^{-1}$ of rhEGF, although there is a slight decrease of the feasibility compared to the negative control, this value is close to 80% and it was considered not to be a proper tolerability of the nanoformulations by the skin and so, DELOS nanovesicles could be classified as non-irritant.

Conversely, free CTAB in dispersant media induced an irritant response in both exposure times, 24 and 48 h, since the cell viability was less than 50%. All these findings cause great concern regarding how CTAB surfactant is structured, since it has potentiality to cause skin irritation when it is in free solution but improving its tolerability when it is nanostructured in DELOS nanovesicles, which is a relevant factor to be considered.

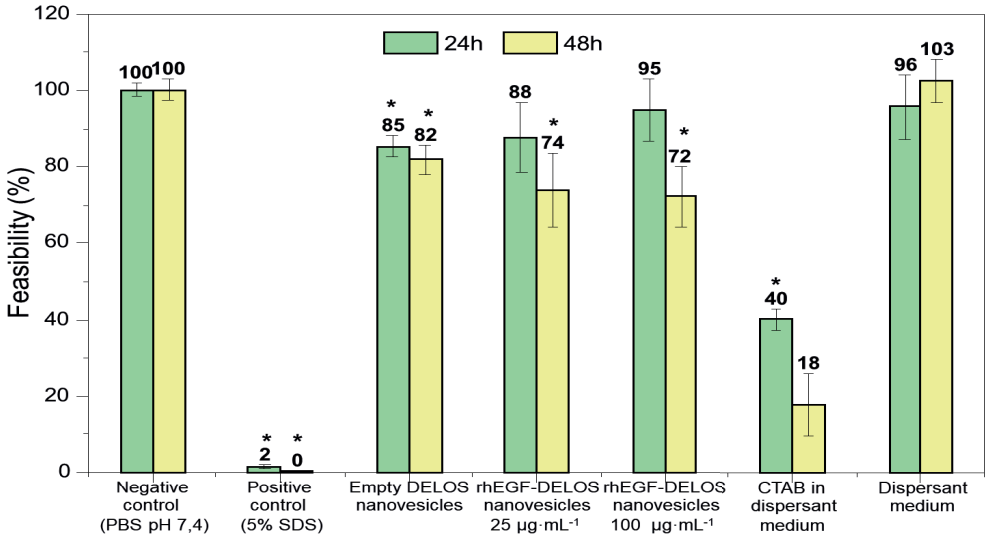

Figure 2.37: In vitro skin irritation of empty DELOS nanovesicles, rhEGF-DELOS nanovesicles and corresponding controls in the reconstructed human epidermal model Episkin™. Results obtained of cell viability after 24 h (green) and 48 h (yellow) of exposure. The mean of 3 experimental replicates ± SD is shown. *$p < 0.05$ with respect to negative control (PBS), determined via two-way ANOVA with Dunnett post hoc test.

Regarding the levels of the released inflammatory interleukin-1α cytokine, they were evaluated by the ELISA (Enzyme-Linked Immunosorbent Assay) technique, which allows for a more detailed approach to the experiment. As shown in **Figure 2.38**, levels of the IL-1α from empty DELOS nanovesicles induced a slight irritant response after 24 h of exposure but this was not sustained after 48 h. Conversely, compared to the negative control (PBS) tested, the rhEGF-DELOS nanovesicles groups did not show a significant statistical irritant response compared to the tested negative control (PBS), the rhEGF-DELOS nanovesicles groups did not show a significant statistical irritant response, again indicating the suitability of the rhEGF-DELOS nanovesicles nanoformulations for topical administration.

Finally, by examining the data, significant changes were detected in the IL-1α levels for free CTAB in dispersant medium since it presented values more than 40 $pg \cdot mL^{-1}$ in both exposure times, 24 and 48 h, which corresponded to values similar to those one observed from the negative control of the experiment (solution of 5% SDS in PBS). Therefore, this is one of the most relevant results of this experiment as it shows that the irritability of CTAB can change depending on how it is nanostructured. The irritation induced by this surfactant is largely reduced when nanostructured into DELOS nanovesicles, suggesting that rhEGF-DELOS nanovesicles might be well-tolerated by a topical route.

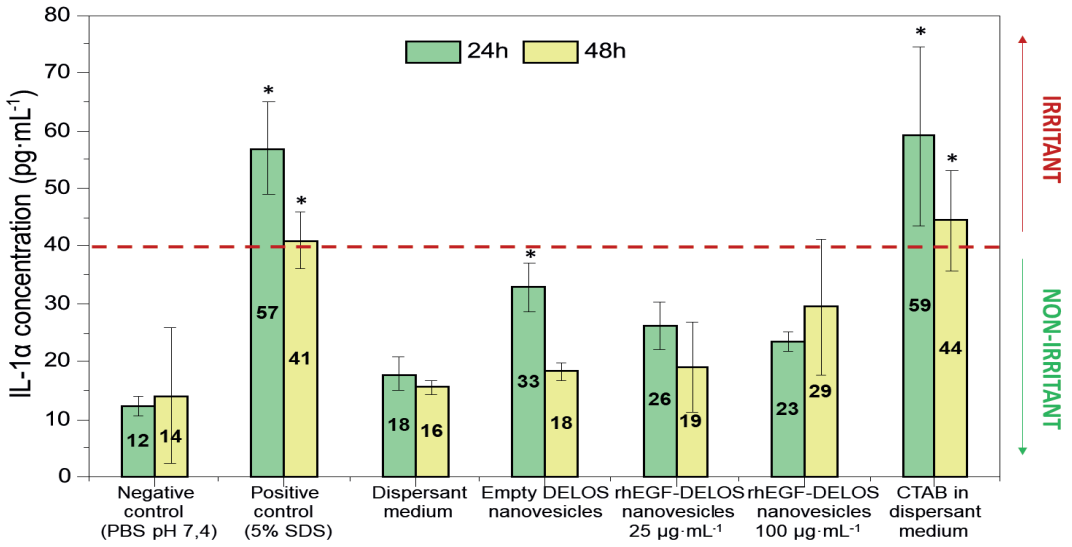

Figure 2.38: ***In vitro*** skin irritation of empty DELOS nanovesicles, rhEGF-DELOS nanovesicles and corresponding controls in the Episkin™ reconstructed human epidermal model. Results obtained of interleukin-1α release, after 24 h (green) and 48 h (yellow) of exposure. The mean of 3 experimental replicates ± SD is shown. *$p < 0.05$ concerning the negative control (PBS).

To summarize, in vitro cellular and tissue assays have been performed presenting promising results in terms of quality, efficacy and toxicity properties. With these results in mind and following the assay cascade to evaluate a new nanomedicine implemented by the National Institute of Health - Nanotechnology Characterization Laboratory (NIH-NCL), further characterization of the nanoformulation was considered. In particular, we were interested in understanding the nanoformulations not only in terms of compatibility, efficacy and safety but also in identifying risks and optimizing the drug formulation through in vivo studies prior to its clinical use[72].

2.3.2 *In vivo* preclinical evaluation of the intermediate product of rhEGF-DELOS nanovesicles for quality efficacy and toxicity assessment

2.3.2.1 In vivo wound healing efficacy in a diabetic mouse model by topical administration

The *in vivo* preclinical efficacy studies of the nanoformulations are crucial to simulate the clinical environment, therefore another important property to evaluate is the wound healing capacity (ulcer reduction) of rhEGF-DELOS nanovesicles. In this case, experiments in animal models were desirable to allow reasonable comparisons to human beings and were therefore performed with db/db mice, the most widely used mouse model for Type 2 diabetes mellitus. Specifically, excisional

wound in db/db mice has been validated as a relevant model to stimulate the chronic wounds of type II diabetes[88].

Then, thanks to the collaboration with Jesús Usón Minimally Invasive Surgery Centre (CCMIJU), the study was conducted comparing the intermediate formulation of rhEGF-DELOS nanovesicles (**Table 2.5**) with and without rhEGF (Blank-DELOS nanovesicles), free rhEGF in the equivalent concentration of the intermediate formulation, which was 100 $\mu g \cdot mL^{-1}$ and the dispersant medium was used as a control. Indeed, during a treatment applied (see **Section 6.5.1**) three times a week for 14 days with a dose of 6 $\mu g \cdot cm^{-2}$, an increase in wound closure rate was observed in the mice group treated with rhEGF-DELOS nanovesicles (rhEGF 100 $\mu g \cdot mL^{-1}$) and free rhEGF 100 $\mu g \cdot mL^{-1}$ in the dispersant media compared to those groups treated with Blank-DELOS nanovesicles and only the dispersant media (**Figure 2.39**).

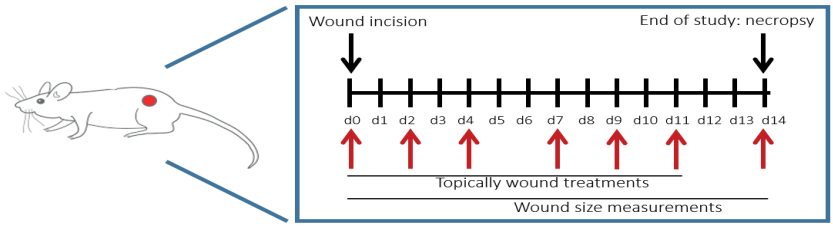

Figure 2.39: Overview of the study design of the in vivo wound healing efficacy and toxicity study of rhEGF-DELOS nanovesicles in cutaneous wound model in db/db mice.

Actually, comparing with Blank-DELOS nanovesicles statistically significant differences in percent wound closure were observed in favor of the rhEGF-DELOS nanovesicles since day 2 onwards of treatment while for free rhEGF, the differences start from day 7 onwards of treatment. Furthermore, comparing with dispersant media statistically significant differences in percent wound closure were observed in favor of the rhEGF-DELOS nanovesicles at days 4 and 11 of treatment while for free rhEGF the differences were only at day 11 of treatment (**Figure 2.40**).

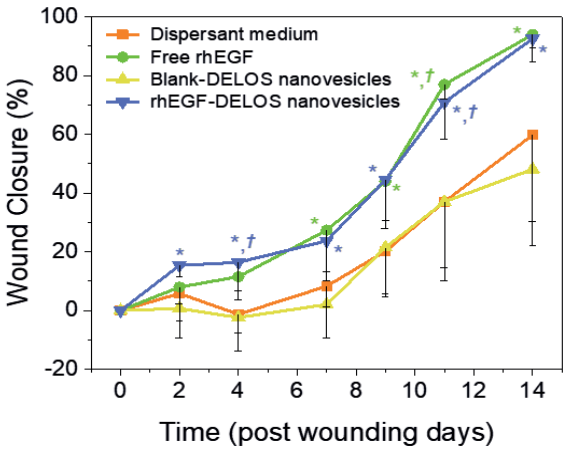

Figure 2.40: Closing speed of rhEGF-DELOS nanovesicles (rhEGF 100 µg·mL^{-1}) (blue triangles ▼), Blank-DELOS nanovesicles (yellow triangles ▲), dispersant media (orange squares ■) and free rhEGF 100 µg·mL^{-1} (green dots ●). The number of animals were N = 3 (two wound per animal) except for the free rhEGF group with N = 2. $^{*,\dagger}p < 0.05$ (*,†rhEGF-DELOS nanovesicles group and *,†free rhEGF group), statistical analyses were by one-way ANOVA followed by Tukey pairwise comparison. *Significant differences with respect to the Blank-DELOS nanovesicles group, and †significant differences with respect to the dispersant media group.

On the other hand, compared to the baseline area of the wound at day 0, statistically significant differences were observed from day 7 onwards of treatment for the rhEGF-DELOS nanovesicles group and from day 9 onwards of treatment with free rhEGF, while for Blank-DELOS nanovesicles and dispersant media groups the differences start from day 11 onwards. So, earlier statistical differences in percent wound closure compared to control groups and of wound area compared to the baseline at day 0 were observed for rhEGF-DELOS nanovesicles in comparison to free rhEGF. Moreover, baseline wound area at day 0 was statistically significant larger for the group treated with rhEGF-DELOS nanovesicles compared to the group treated with free rhEGF in the dispersant media ($p = 0.013$).

Interestingly, the closing speed of the wound with the first doses of rhEGF-DELOS nanovesicles was somewhat superior to the free rhEGF although this difference was equilibrated at later dosing probably because of the high concentration of rhEGF used in this assay, which may compensate for the higher efficacy of rhEGF-DELOS nanovesicles. Representative photography images of wound evolution at days 0, 9, 11 and 14 of treatment clearly show the faster speed of closing wound in the rhEGF-DELOS nanovesicles group with respect to the controls (**Figure 2.41a**). Because the current clinical practice demands a complete closure of the wound and not the partial reduction of the wound area, the percentage of closed wounds in the different groups was also evaluated,

considering that a wound healing occurs only when the closure was greater than 95%. Under this criterion, after 11 days of treatment, any group showed all wounds healed. However, the percentage of wound closure was 67% at 14 days of study for the rhEGF-DELOS nanovesicles group, while for the control Blank-DELOS nanovesicles, dispersant medium, and free rhEGF control groups was 0%, 17%, and 50%, respectively (**Figure 2.41b**).

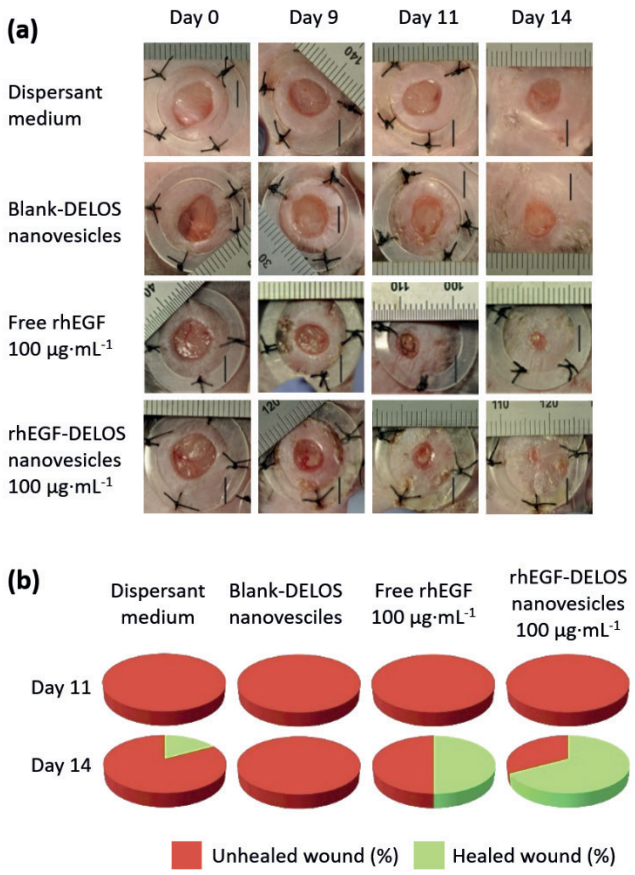

Figure 2.41: (a) Representative photograph during the topical treatment following of the wound healing process in the groups, bar represent 5 mm. (b) Evolution of healed wounds of different groups after 11 and 14 days of treatment. Wounds were considered healed only when more than 95% of wound closure is achieved.

After the wound healing study, the most relevant clinical symptomatology for all mice was evaluated. All animal groups show high levels of glucose (hyperglycemia) during the treatment (about 600 $mg \cdot dL^{-1}$), compared to normal levels of the specie (about 200 $mg \cdot dL^{-1}$), in agreement with the pathology of the animals, i.e., their diabetic condition, and no statistically significant difference (ANOVA p-value = 0.289) were observed among groups (**Figure 2.42).**

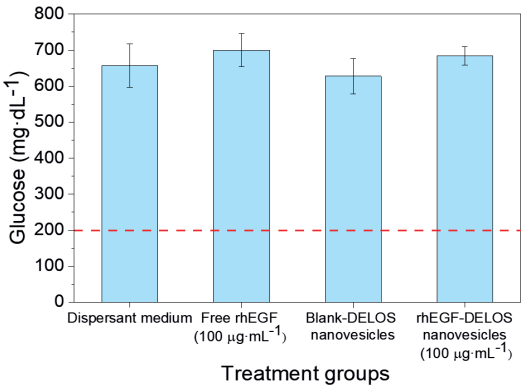

Figure 2.42: Concentration of glucose at the end of the study, demonstrating similar values among groups and hyperglycemia levels. Red discontinuous line indicates the normal level of glucose in mice. Data plotted as mean ± SD. The number of animals were N = 3 (two wound per animal) except for the free rhEGF group with N = 2. None statistical differences for concentration of glucose at the end of the study among treated animal groups by one-way ANOVA followed by Tukey pairwise comparison.

Because bodyweight change is considered critical for safety evaluation, this was monitored during the study. As shown in **Figure 2.43**, in all treatment groups, a decrease of body weight was observed during the study, but no statistical differences were observed among the four groups at any time measured during the 14 days' treatment period. The decrease in body weight was supposed to be associated with the conditions of animals, hyperglycemic and obese mice with large wounds, and not causally related to the rhEGF-DELOS nanovesicles treatment. Furthermore, no further toxicity signs were associated with the rhEGF-DELOS nanovesicles treatment considering clinical symptoms, hematological and biochemical evaluations with no statistically significant differences among the study groups in none of the parameters.

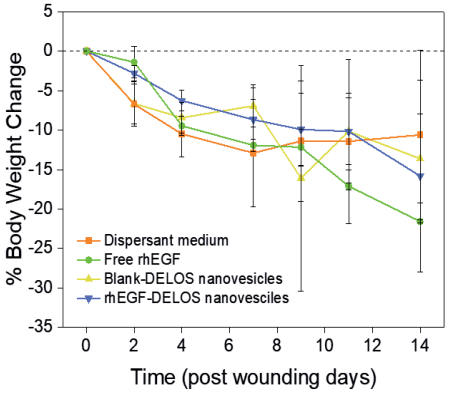

Figure 2.43: Evolution of body weight of all animals was recorded during each treatment with rhEGF-DELOS nanovesicles (blue triangles▼) Blank-DELOS nanovesicles (yellow triangles ▲), dispersant media (orange squares ■) and free rhEGF (green dots ●). All animals spearing healthy throughout the study based on eating and behavior under their condition of hyperglycemic. The number of animals were N = 3 (two wound per animal) except for the free rhEGF group with N = 2.

In conclusion, promising results have been obtained during the *in vitro* preclinical evaluation of the intermediate product of rhEGF-DELOS nanovesicles to assess the quality, efficacy and toxicity. Therefore, these results prompted us to continue the preclinical development and testing of the nanoformulation by evaluating its toxicology *in vivo* through some of the different assays required to start human clinical trials.

2.3.2.2 *In vivo* toxicity preclinical studies

In the course of the toxicological study experimental design, the required dose to be applied played an important role. For the purpose of the optimized rhEGF-DELOS nanovesicles safety evaluation, the inclusion criterion of ulcerative areas is between 2 and 15 cm^2. In addition, for both DFUs and VLUs treatments, it is intended to support the safety use of rhEGF in the planned exploratory clinical trial with the toxicological information generated as part of lyophilized rhEGF product used for the indication of DFUs by CIGB.

This toxicology information currently covers a therapeutic dose of up to 75 $\mu g \cdot patient \cdot day^{-1}$ following the intralesional route, and as previously discussed, the administered dose was of 5 $\mu g \cdot cm^{-2}$, which will be our reference value for the efficacy and toxicological studies of rhEGF-DELOS nanovesicles. At the same time, it is known that lower extremity ulcers of venous etiology are very exudative, so modulating the volume of nanoformulation to be applied and concentrating the rhEGF-DELOS nanovesicles formulation, the desired rhEGF administered dose of rhEGF proposed to use it in clinical trials could be achieved.

To make the dose reasonable for the toxicity studies and finally for the clinical studies on patients, it was necessary to develop a methodology that allows a higher rhEGF concentration of the nanoformulation. By modulating the concentration of the nanoformulation, the final suspension volume is influenced and consequently it adapts perfectly to the required doses for each analysis.

Development of a prototype suitable for preclinical toxicology testing

To modulate the volume and concentration of the intermediate formulation (**Table 2.5**) to achieve an adequate administration dose, a tangential flow filtration (TFF) was used as the method of concentration as explained in **Section 6.2.2**.

TFF is a fast and efficient way to separate and purify different types of particles and is also used to concentrate solutions. The basics of this technique are really simple, where the feed stream, based on the sample of interest, flows as one part parallel to the membrane surface, while a portion passes through the membrane (permeate) while the remainder (retentate) is recirculated back to

the feed reservoir (**Figure 2.44**). An important note must be made here on the pore sizes of the membrane, as these are typically between 0.1 and 10 µm and then, the separation of the different components of the sample can be modulated depending on the pore size chosen. In addition, special attention was paid to the possibility that this technique can be scaled-up, thus offering the possibility of being applied in pilot-scale trials if required[89].

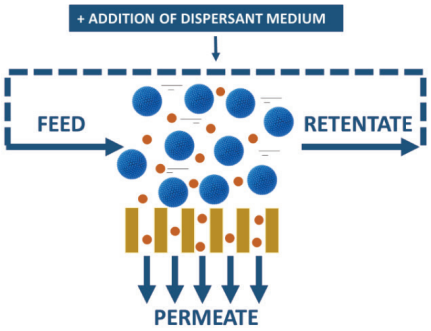

Figure 2.44: Schematic diagram of the tangential flow filtration (TFF) mechanism.

As well as being a simple technique, this method is also practical and is therefore also useful for concentrating samples by simply removing the dispersant medium from a solution while retaining the solute molecules. As a result, the concentration of the molecules of interest increases equivalent to the decrease in solution volume. In this study, we evaluated the ability of the nanoformulation to concentrate 2-, 4-, 8-, and 10-fold the membrane components and rhEGF protein concentration (**Table 2.8**) using a TFF system designed with a 100 kDa molecular weight cutoff membrane was fitted. This limit perfectly retains the nanoformulation as the membrane is up to 6 times lower than the molecular weight of the system, which is recommended[89].

Table 2.8: Final theoretical concentration of each compound of the intermediate product prototype when concentrating using TFF.

	Concentration				
Concentration by TFF (times)	**rhEGF (µg·mL^{-1})**	**CTAB (mg·mL^{-1})**	**Cholesterol (mg·mL^{-1})**	**Histidine (mg·mL^{-1})**	**Ethanol (mg·mL^{-1})**
0 (original sample)	100	2.70	2.83	0.60	0.107
2	200	5.40	5.66	0.60	0.107
4	400	10.8	11.3	0.60	0.107
8	800	21.6	22.6	0.60	0.107
10	1000	27.0	28.3	0.60	0.107

From the short review above, we now provide the main findings and contribution of the experimental procedures carried out during this investigation. First, as shown in **Figure 2.45**, the macroscopical appearance of all the concentrated rhEGF-DELOS nanovesicle samples was excellent since none of them present neither sedimentation nor precipitation.

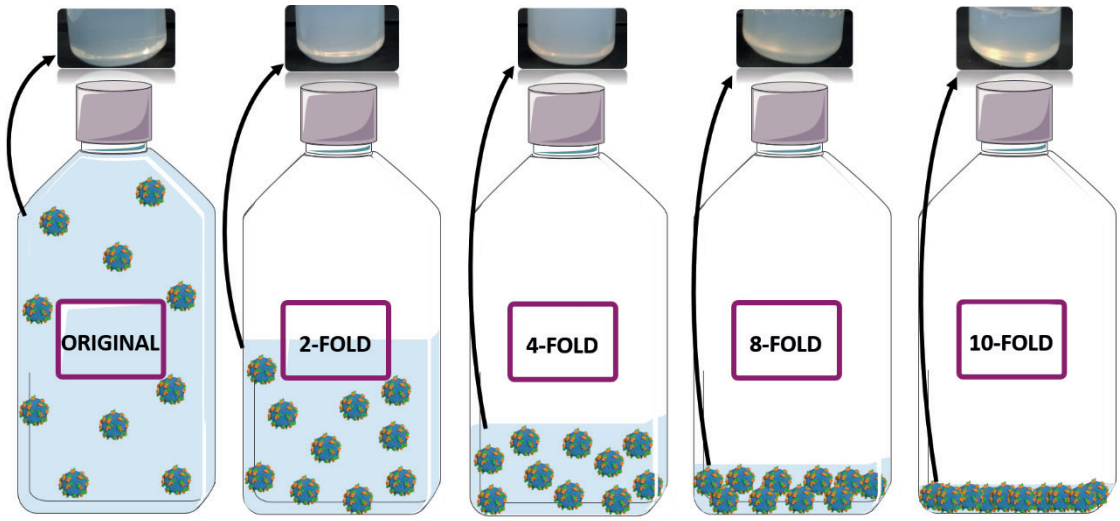

Figure 2.45: Macroscopical appearance and schematic illustration of rhEGF-DELOS nanovesicles formulations: original and concentrated 2-, 4-, 8-, and 10-fold by TFF technique.

To confirm that the concentration step did not produce precipitate, these samples were also evaluated through an optical microscope (see **Section 6.3.9**). As can be seen in **Figure 2.46b**, all the different samples present, the original and the concentrated ones, showed a minimal number of precipitates. These results are interesting and help to justify the stability of the samples since cholesterol would be the membrane compound observed microscopically if they had a tendency to precipitate as it is the only hydrophobic and insoluble compound.

Alternatively, to confirm the absence of cholesterol precipitation, control samples were prepared. These controls were based on dispersing the equivalent amount of cholesterol used in each rhEGF-DELOS nanovesicle sample (**Table 2.8**) in the same dispersant medium, namely buffer histidine (5 mM, pH 7.0) with 10% EtOH ($v \cdot v^{-1}$), to estimate the cholesterol precipitates in the suspension.

By carefully examining the samples observed in **Figure 2.46**, this experiment illustrated that the presence of cholesterol precipitates is proportional to its concentration. Then, when the images of the cholesterol control group were compared to the rhEGF-DELOS nanovesicles, the results suggested that the concentration step, performed by the TFF method, did not alter the macro- and micro-stability of the nanoformulation, thereby avoiding the presence of precipitates.

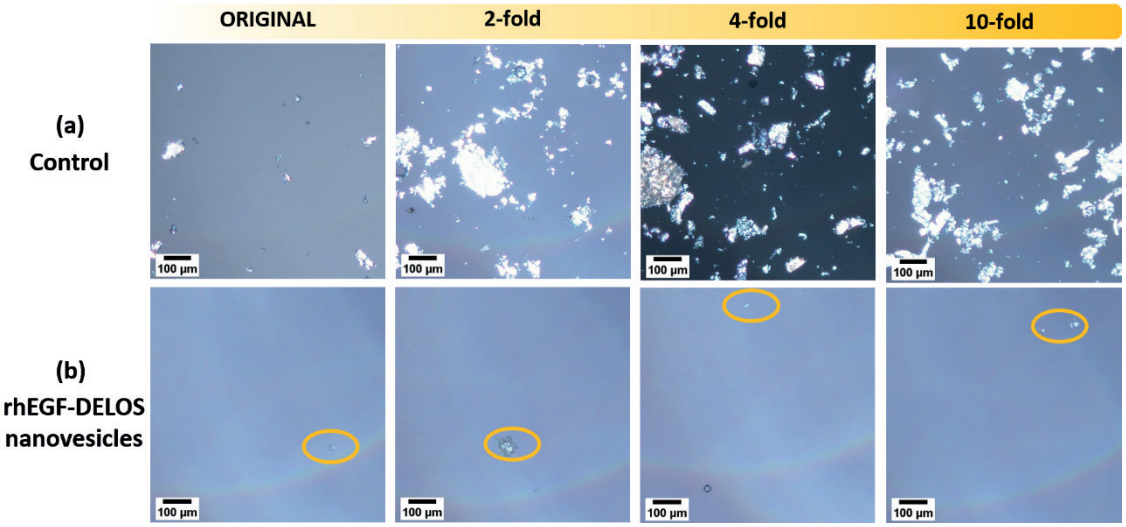

Figure 2.46: Microscopic appearance of (a) cholesterol as control group in the same concentration as rhEGF-DELOS nanovesicles and (b) rhEGF-DELOS nanovesicle formulations: original and concentrated 2-, 4-, 8- and 10-fold by TFF technique. Yellow circles represent the small amount of cholesterol aggregates found in the samples.

Following this study, the particle size distribution and zeta potential of the samples were evaluated by DLS showing maintenance of the of particle size distribution and zeta potential values at all the concentrations tested (see **Section 6.3.1** and **Table 2.9**). At the same time, it was confirmed again by cryo-TEM images that concentration TFF method was a good approach to obtain high-quality results in terms of vesicle morphology, as well as all concentrations maintaining spherical and unilamellar morphology (**Figure 2.47**). It is noteworthy that, as expected, a large number of vesicles were observed when concentration cycles were increased.

Table 2.9: Physicochemical characteristics of the rhEGF-DELOS nanovesicles after TFF concentration

Concentration by TFF (times)	Particle size (nm)	PDI	Zeta Potential (mV)
0 (original sample)	54 ± 1	0.24 ± 0.00	89 ± 2
2	63 ± 1	0.25 ± 0.01	92 ± 3
4	64 ± 1	0.25 ± 0.01	87 ± 1
8	64 ± 1	0.27 ± 0.00	94 ± 5
10	58 ± 2	0.23 ± 0.01	95 ± 4

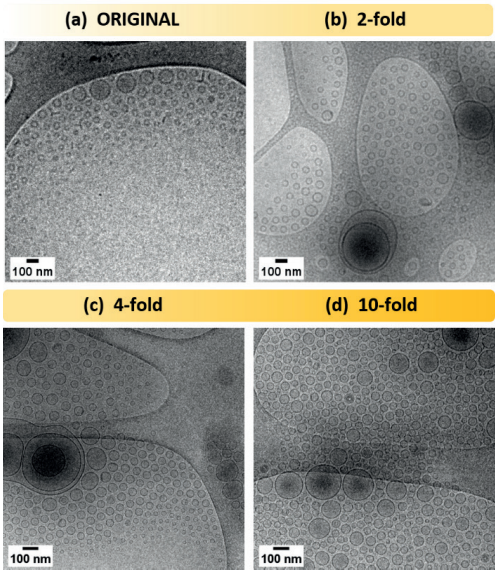

Figure 2.47: Cryo-TEM image of rhEGF-DELOS nanovesicles formulations (a) original and concentrated (b) 2-, (c) 4-, and (d) 10-fold by TFF technique.

Finally, one of the main outcomes of this task was to evaluate the trend of rhEGF encapsulation efficiency in the nanovesicles when the nanoformulations is concentrated. EE% values were calculated experimentally using the robust methodology developed in **Section 2.2.5** based on ultracentrifugation and fluorescence and described in **Section 6.3.8**. The results of the procedure appeared to be in line with our expectations as more pellet was observed with increasing concentration of the nanoformulation (**Figure 2.48a**). At the same time, when evaluating the encapsulation efficiency value of the samples by fluorescence, an EE% of over 97% is observed in all cases (**Figure 2.48b**).

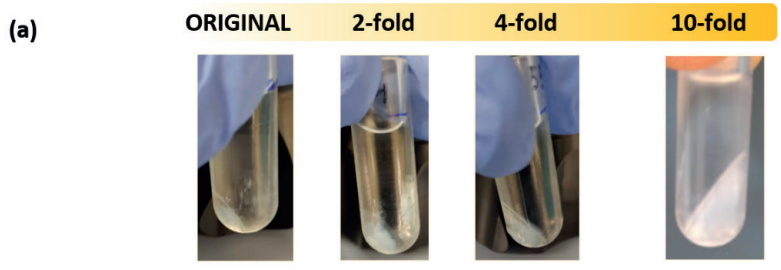

Figure 2.48: (a) Macroscopic appearance of the pellet and (b) encapsulation efficiency of rhEGF in rhEGF-DELOS nanovesicles of the original and concentrated 2-, 4-, and 10-fold by TFF technique.

Therefore, all results indicate that our TFF approach with the Repligen KrosFlo® KR2i system is a promising strategy to achieve the right physicochemical properties of concentrated rhEGF-DELOS nanovesicles. Thus, through all the physicochemical characterization carried out, TFF is a validated strategy to perfectly modulate the concentration of the rhEGF-DELOS nanovesicles formulation by up to 10-fold concentration, in case it is necessary to reduce the volume of the nanoformulation and thereby to achieve the appropriate required dose for both preclinical and clinical *in vivo* assays.

In vivo toxicity study in rats by subcutaneous administration

Assessing the safety of new pharmaceutical products requires regulatory studies on animals to protect human health and the environment[90]. In this context, the risk assessment can be evaluated by various sources. In our case, toxicological screening is very important for the development of new drugs and expanding the therapeutic potential of existing molecules, and very useful to study the associated side effects that they can cause[91].

Before performing a regulatory toxicology on animals, which is necessary before administering the nanoformulation to humans with a range of safety precautions, in the frame of Nanonafres project a previous discussion was held with the Spanish Agency of Medicines and Medical Devices (AEMPS) in July 2018. Thanks to this meeting, AEMPS supported us in the preclinical studies, not only in terms of experimental design but also in the results obtained. In order to administer the nanoformulation in humans with a safety margin, it is previously required to carry out a regulatory toxicology study with a duration equal to the clinical trial (8 weeks). However, prior to this regulatory study, the AEMPS suggested conducting a non-GLP pilot dose-finding study, also called 1-week dose range study in rat, with the aim to assess the tolerability of the initially selected doses of intermediate formulation of rhEGF-DELOS nanovesicles.

The doses identified as tolerated (according to the criteria of a toxicologist), from the initial study, will form part of the main study (GLP) of 8-week duration that allows defining a safety margin for the drug product before its administration in humans. This pilot study should make it possible to determine the tolerated dose associated with the two potentially toxic components of the product: CTAB and rhEGF. However, the main objective will be to establish the tolerability of CTAB, since the tolerability profile of rhEGF has already been described during the development of Heberprot-P® (Heber Biotec) as the Nanonafres consortium has access to all the toxicological documentation of Heberprot-P® product.

Therefore, thanks to these recommendations, the toxicological study was conducted by the Leitat Technological Center with the aim of evaluating the toxicity associated with the administration of the nanoformulations and also providing information on their side effects. In this case, this study was designed as a 1-week dose-ranging study in rats, as summarized in **Table 2.10** and described

in detail in **Section 6.5.2**, with the assessment of biochemical, haematological, and histological parameters. For this purpose, 30 Sprague-Dawley rats, half male and half female, were given a subcutaneous injection of 1.4 $mL \cdot kg^{-1}$ of volume of each treatment group every day for one week. It should be highlighted that choosing subcutaneous administration route instead of topical one was justified as an estimation of a worst-case exposure of the nanoformulation, such as systemic absorption.

Table 2.10: Summary of the non-GLP assay looking for the dose.

Animal model	Sprague-Dawley rat				
Administration route	Subcutaneous				
Study duration	5 days				
Frequency of administration	Once per day				
Groups	1	2	3	4	5
Treatment	Dispersant medium	DELOS nanovesicles (Higher dose)	rhEGF-DELOS nanovesicles (Lower dose)	rhEGF-DELOS nanovesicles(original)	rhEGF-DELOS nanovesicles (Higher dose)
	histidine buffer (5 mM, pH 7) with 10% EtOH ($v \cdot v^{-1}$)	DELOS nanovesicles without rhEGF concentrated 10-fold	rhEGF-DELOS nanovesicles diluted 1/18	rhEGF-DELOS nanovesicles (original)	rhEGF-DELOS nanovesicles concentrated 10-fold
Administration volumes	1,4 $mL \cdot kg^{-1}$	1,4 $mL \cdot kg^{-1}$ (37,8 $mg \cdot kg^{-1}$CTAB)	1,4 $mL \cdot kg^{-1}$ (7,75 $\mu g \cdot kg^{-1}$EGF; 0,21 $mg \cdot kg^{-1}$B)	1,4 $mL \cdot kg^{-1}$ (140 $\mu g \cdot kg^{-1}$ rhEGF; 3,78 $mg \cdot kg^{-1}$)	1,4 $mL \cdot kg^{-1}$ (1400 $\mu g \cdot kg^{-1}$ rhEGF; 37,8 $mg \cdot kg^{-1}$)
Animals	3M + 3F	3M + 3F	3M + 3F	3M + 3F	3M + 3F

The toxicological evaluation of the animals then consisted of the assessment of various clinical signs such as local tolerance, weight control, haemogram and macroscopic examination of post-mortem tissues and organs (brain, lungs, heart, liver, spleen, pancreas and kidney). In addition, this

study also included the quantification of rhEGF by ELISA and CTAB technique by Ultra Performance Liquid Chromatography (UHPLC) in plasma and in the mentioned organs, which coincided with the last day of the study.

In this toxicological study, three dose levels of rhEGF-DELOS nanovesicles were evaluated and the dispersant medium (Group 1) and the Blank-DELOS nanovesicles (Group 2) at the equivalent highest dose were used as controls to assess the effect of the dispersant medium and the nanovehicle alone, respectively. Regarding the dose levels of rhEGF-DELOS nanovesicles, these can be justified as follows:

1. **Lowest dose** (Group 3)**.** The lowest dose was chosen because it is the equivalent clinical dose in the rat. As previously described, our reference model was the administered dose in Heberprot-P® in humans, which was 75 µg of rhEGF in a mean ulcer size of 16.3 cm^2 equivalent to 5 $\mu g \cdot cm^{-2}$. However, if we calculate the dose in reference to the weight of the patient, assuming 60 kg of weight per patient, the rhEGF equivalent dose was 1.25 $\mu g \cdot kg^{-1}$. Then, to calculate the equivalent clinical dose in rats for subcutaneous administration, the topical human clinical dose multiplied by a factor of 6.2 ($1.25 \mu g \cdot kg^{-1} \cdot 6.2 = 7.75 \mu g \cdot kg^{-1}$) was taken into account[92]. To achieve this dose, the rhEGF-DELOS nanovesicle formulation will be diluted 18 times.

2. **Intermediate dose** (Group 4)**.** This dose was selected based on the results of a study conducted as part of the Flucelvax®/Optaflu® influenza vaccine registration process, which showed that a CTAB exposure of 17.2 $mg \cdot kg^{-1}$ was tolerated by intramuscular administration in rabbits[93] (repeated dose GLP study in which two CTAB administrations were made in 1 week (day 1 and day 8)). In our case, with the intermediate dose of rhEGF-DELOS nanovesicles, we would achieve slightly higher exposure levels (18.9 $mg \cdot kg^{-1}$ of CTAB) after 5 days of daily treatment. Particular attention was paid to the clinical dose of CTAB allowed in 0.225 $\mu g \cdot kg^{-1}$ of CTAB in the Flucelvax®/Optaflu® influenza vaccine administered intramuscularly. In this case, the rhEGF-DELOS nanoformulation will be applied directly without any modification.

3. **Higher dose** (Group 5)**.** The higher dose corresponds to the maximum feasible dose of rhEGF-DELOS nanovesicles that can be obtained from the concentrating the intermediate product 10-fold as explained previously, which might approximate to the Maximum Feasible Dose (MFD), a dose that attempts to maximize exposure in toxicity studies[94].

4. So, these 5 groups of samples were fully prepared and characterized in the framework of this Thesis, and the observations from the results of these experiments seem to indicate that all batches retain similar properties to each other (**Table 2.11**). It is worth noting that the lower dose of rhEGF-DELOS nanovesicles (Group 3), although diluted 1/18 $v \cdot v^{-1}$ in dispersant media, this dilution does not affect the physicochemical parameters of the nanoformulation. At the same time, it should be noted that all other groups: 2, 4 and 5 also have appropriate physicochemical properties.

Table 2.11: Physicochemical properties of the administrated batches in the pilot assay "1-week dose range study in rat"

Batch	Mean size (nm)	PDI	Zeta Potential (mV)
GROUP 2**: Blank-DELOS nanovesicles (Higher dose)**	62 ± 1	0.43 ± 0.02	84 ± 1
GROUP 3**: rhEGF-DELOS nanovesicles (Lower dose)**	55 ± 1	0.22 ± 0.01	60 ± 7
GROUP 4: **rhEGF-DELOS nanovesicles (original)**	56 ± 1	0.26 ± 0.00	88 ± 3
GRUP 5**: rhEGF-DELOS nanovesicles (Higher dose)**	60 ± 1	0.44 ± 0.00	83 ± 0

The results of this study are well documented in the report "Anexo_5_toxicological_Leitat from the COMRDI15_MT-Justif_Final_vfinal_v11", which describes the most relevant conclusions obtained in this study which are the following:

1. There are no significant differences in behavior, weight, or other conditions in either male or female treated animals compared to their control, which was the own dispersant media. Weight loss would be expected if the nanoformulations had a significant toxic effect.
2. Assessment of clinical grades such as macroscopic alterations of the organs and tissues did not reveal any evidence of side effects that could be attributed to the administration of the nanoformulation throughout the study.
3. Since the administration of nanoformulation did not lead to detectable changes in the parameters evaluated previously explained, it is conceivable showed that the highest administered dose of the nanoformulation, 1400 $\mu g \cdot kg^{-1}$ of DELOS nanovesicles with and without rhEGF, cannot be considered as an MTD, although it is 180 times higher than the therapeutic dose calculated for rats.
4. Blood analysis showed that plasma rhEGF levels were not significant 4 hours after the last administration of the nanoformulations.
5. After the 5 days of the study (i.e., 5 administrations), no accumulation of rhEGF was detected in any tissue since the protein concentrations found were minimal (less than 250 $pg \cdot mL^{-1}$).
6. There were no effects or alterations in hematological parameters in any of the samples analyzed, cholesterol level or significant levels of CTAB.

The outcome of the different toxicological analysis led to the conclusion that no maximum tolerable dose for topical administration was found after repeated administration. Therefore, although the objective of finding the Maximum Tolerant Dose has not been achieved, considering all the positive results, we contemplate that the next step is to perform the central study (GLP) of 8 weeks' duration that allows defining a safety margin for the drug product before its administration in humans. This study will be done using the same doses as the explained non-GLP "1-week dose range study in rat", and probably this 8-week study will better define the MTD.

In this regard, it is important to note that AEMPS recommends that this study should be conducted with the final formulation to be translated into the clinic or with a very close version. Therefore, the definition of the final pharmaceutical form of the rhEGF-DELOS nanovesicles is required prior to toxicology testing.

Importantly, thanks to this project, Nanomol Technologies SL was able to achieve an adequate scale-up of the DELOS-susp technology and produce up to 1-2 liters of the nanoformulation. Looking forward, a pilot plant for the production of the clinical batches of rhEGF-DELOS nanovesicles under the current Good Manufacturing Practices (GMP) requirements will be available by the end of 2022.

Summarizing, in vivo preclinical assessment on quality and toxicity of the intermediate rhEGF-DELOS nanovesicles nanoformulation was correctly performed, showing promising results. Although future studies are needed, this evaluation has had a great relevance for understanding the behaviour of the nanoformulation, which is a key point in the field of nanomedicine.

2.3.3 Summary of the section and Perspectives

This first Chapter deals with the translation of rhEGF-DELOS nanovesicles towards new pharmaceutical formulation for the treatment of complex wounds.

Once obtained the optimized intermediate product of rhEGF-DELOS nanovesicles, its efficacy and toxicology have been examined in detail. In terms of efficacy, it presented promising results such as two times more of *in vitro* protein-specific bioactivity of the rhEGF when integrated in rhEGF-DELOS nanovesicles respect to the free rhEGF. At the same time, it presents biocidal activity, against Gram-positive bacteria, yeast, and fungus, preventing microbial infections hindering the formation of biofilms being therefore attractive for topical treatments.

Moreover, this intermediate product can be classified as a skin non-irritant system according to the human epidermal EpiSkin™ model as any signs of cytotoxicity were detected when exposed to a 3D human reconstructed model EpiSkin™ model for 24 and 48 hours, the exposure time recommended for clinical trials. In addition, e*x vivo* permeation testing of rhEGF-DELOS nanovesicles using

damaged human skin and a Franz-type cell showed no an effective permeation of rhEGF through the skin, suggesting that when administered topically it is unable to reach the circulatory system.

Regarding the evaluation of wound healing capacity, through ulcer reduction assessment, rhEGF-DELOS nanovesicles indicated that when applied by topical route on excisional wounds artificially produced in genetically diabetic mice a 67% of mice presented a complete wound closure after 14 days without any sign of toxicity while assays with proper controls only showed 0–50% wound closures. Furthermore, the closing speed of the wound with the first doses of rhEGF-DELOS nanovesicles was clearly superior to the control free rhEGF.

Lastly, the 1-week dose range study in rats to evaluate the tolerability of rhEGF-DELOS nanovesicles did not allow the determination of the tolerated dose, but no significant toxicological alterations were observed, indicating the correct tolerability of the nanoformulations at the tested dose in rats.

In summary, effective translation of the product into the clinic has been correctly achieved, advancing from TRL3, where a preliminary candidate was defined, to TRL5, in which preclinical proof-of-concept studies were conducted. Undoubtedly, this novel rhEGF-DELOS nanovesicle intermediate formulation can be considered as an innovative product with high added value as it meets the basic requirements of production, storage stability, patient compliance and high efficacy with minimal side effects. Consequently, it is considered as a potential nanomedicine to enter in future clinical trials for the treatment of DFUs and VLUs.

Part of the above reported results have been published in:

1. "Ferrer-Tasies, L., Santana, H., Cabrera-Puig, I., González-Mira, E., Ballell-Hosa, L., Castellar-Álvarez, C.,... & Ventosa, N. (2021). Recombinant human epidermal growth factor/quatsome nanoconjugates: a robust topical delivery system for complex wound healing. *Advanced Therapeutics*, *4*(6), 2000260"[69].

2.4 References

1. S. James. What Is R&D? Research And Development In Business https://forrestbrown.co.uk/news/what-is-r-and-d/ (accessed Dec 17, 2021).

2. S. Singh, A. Young, C.E. McNaught. The physiology of wound healing. *Surg.* **2017**, 35 (9), 473–477.

3. S. Enoch, D.J. Leaper. Basic science of wound healing. *Surgery* **2007**, 26 (2), 31–37.

4. M.C. Ferreira, P.T. Júnior, V. Fernandes Carvalho, F. Kamamoto. Complex wounds. *Clinics* **2006**, 61 (6), 571–578.

5. C.K. Sen, G.M. Gordillo, S. Roy, et al. Human skin wounds: A major and snowballing threat to public health and the economy. *Wound Repair Regen.* **2009**, 17 (6), 763–771.

6. R. Diegelmann. Wound healing: an overview of acute, fibrotic and delayed healing. *Front. Biosci.* **2004**, 9 (1), 283–289.

7. D.G. Armstrong, J. Wrobel, J.M. Robbins. Guest Editorial: are diabetes-related wounds and amputations worse than cancer? *Int. Wound J.* **2007**, 4 (4), 286–287.

8. G. Norman, C. Shi, M.J. Westby, et al. Bacteria and bioburden and healing in complex wounds: A prognostic systematic review. *Wound Repair Regen.* **2021**, 29 (3), 466–477.

9. D.F. Bandyk. The diabetic foot: Pathophysiology, evaluation, and treatment. *Semin. Vasc. Surg.* **2018**, 31 (2–4), 43–48.

10. G.C. Gurtner, S. Werner, Y. Barrandon, M.T. Longaker. Wound repair and regeneration. *Nature* **2008**, 453 (7193), 314–321.

11. R. Nunan, K.G. Harding, P. Martin. Clinical challenges of chronic wounds: searching for an optimal animal model to recapitulate their complexity. *Dis. Model. Mech.* **2014**, 7 (11), 1205–1213.

12. N.X. Landén, D. Li, M. Ståhle. Transition from inflammation to proliferation: a critical step during wound healing. *Cell. Mol. Life Sci. 2016 7320* **2016**, 73 (20), 3861–3885.

13. A.J. Boulton, D.G. Armstrong, M.J. Hardman, et al. Diagnosis and Management of Diabetic Foot Infections. In *Diagnosis and Management of Diabetic Foot Infections*; American Diabetes Association Inc., Arlington (VA), **2020**.

14. N. Škalko-Basnet. Biologics: the role of delivery systems in improved therapy. *Biologics* **2014**, 8, 107.

15. J.I. Fernández-Montequín, B.Y. Betancourt, G. Leyva-Gonzalez, et al. Intralesional administration of epidermal growth factor-based formulation (Heberprot-P) in chronic diabetic foot ulcer: treatment up to complete wound closure. *Int. Wound J.* **2009**, 6 (1), 67–72.

16. V.W. Wong, G.C. Gurtner. Tissue engineering for the management of chronic wounds: current concepts and future perspectives. *Exp. Dermatol.* **2012**, 21 (10), 729–734.

17. P.G. Righetti. Determination of the isoelectric point of proteins by capillary isoelectric focusing. *J. Chromatogr. A* **2004**, 1037 (1–2), 491–499.

18. H. Santana, Y. González, P.T. Campana, et al. Screening for stability and compatibility conditions of recombinant human epidermal growth factor for parenteral formulation: Effect of pH, buffers, and excipients. *Int. J. Pharm.* **2013**, 452 (1–2), 52–62.

19. S. Lu, J.-J. Chai, M. Li, et al. Crystal Structure of Human Epidermal Growth Factor and Its Dimerization. *J. Biol. Chem.* **2001**, 276 (37), 34913–34917.

20. S. Barrientos, O. Stojadinovic, M.S. Golinko, H. Brem, M. Tomic-Canic. Growth factors and cytokines in wound healing. *Wound Repair Regen.* **2008**, 16 (5), 585–601.

21. P.A. López-Saura, J. Berlanga-Acosta, J.I. Fernández-Montequín, et al. Intralesional Human Recombinant Epidermal Growth Factor for the Treatment of Advanced Diabetic Foot Ulcer: From Proof of Concept to Confirmation of the Efficacy and Safety of the Procedure. In *Global Perspective on Diabetic Foot Ulcerations*; Dinh, T., Ed.; IntechOpen, London, UK, **2011**; pp 217–238.

22. M.M. Santoro, G. Gaudino. Cellular and molecular facets of keratinocyte reepithelization during wound healing. *Exp. Cell Res.* **2005**, 304 (1), 274–286.

23. P.A. Prats, J. Duconge, C. Valenzuela, et al. Disposition and receptor-site binding of 125I-EGF after topical administration to skin wounds. *Biopharm. Drug Dispos.* **2002**, 23 (2), 67–76.

24. M. Kaplan, S. Narasimhan, C. de Heus, et al. EGFR Dynamics Change during Activation in Native Membranes as Revealed by NMR. *Cell* **2016**, 167 (5), 1241-1251.e11.

25. J. Berlanga, J.I. Fernandez, E. López, et al. Heberprot-P: a novel product for treating advanced diabetic foot ulcer. *MEDICC Rev.* **2013**, 15, 11–15.

26. J.I. Fernández-Montequín, B.Y. Betancourt, G. Leyva-Gonzalez, et al. Intralesional administration of epidermal growth factor-based formulation (Heberprot-P) in chronic diabetic foot ulcer: treatment up to complete wound closure. *Int. Wound J.* **2009**, 6 (1), 67–72.

27. I. Cabrera. Nanovesicle-bioactive conjugates to be used as nanomedicines , prepared by a one-step scalable method using CO2-expanded solvents “Doctoral dissertation,” Universtitat Autònoma de Barcelona, **2013**.

28. A. Sharma, U.S. Sharma. Liposomes in drug delivery: Progress and limitations. *Int. J. Pharm.* **1997**, 154 (2), 123–140.

29. G.A. Hughes. Nanostructure-mediated drug delivery. *Nanomedicine Nanotechnology, Biol. Med.* **2005**, 1 (1), 22–30.

30. P. Goyal, K. Goyal, S. V Kumar, et al. Liposomal drug delivery systems – Clinical applications. *Acta Pharm* **2005**, 55 (1), 1–25.

31. D.R. Nogueira, M. Carmen Morán, M. Mitjans, et al. New cationic nanovesicular systems containing lysine-based surfactants for topical administration: Toxicity assessment using representative skin cell lines. *Eur. J. Pharm. Biopharm.* **2013**, 83 (1), 33–43.

32. S. Quirce, P. Barranco. Cleaning Agents and Asthma. *J Investig Allergol Clin Immunol* **2010**, 20 (7), 542–550.

33. R.C. Rowe, M.Q. Paul Sheskey. Handbook of pharmaceutical excipients; London, UK and Washington, DC, USA, **2009**.

34. C. Attinger, R. Wolcott. Clinically Addressing Biofilm in Chronic Wounds. *Adv. Wound Care* **2012**, 1 (3), 127–132.

35. X. Ye, J. Feng, J. Zhang, et al. Controlled release and long-term antibacterial activity of reduced graphene oxide/quaternary ammonium salt nanocomposites prepared by non-covalent modification. *Colloids Surfaces B Biointerfaces* **2017**, 149, 322–329.

36. M.H.J. Santana, R.L. Ventosa, D.E. Martinez, et al. Vesicles which include epidermal growth factor and compositions that contain same. WO2014019555 A1, 2012.

37. R.C. Mohs, N.H. Greig. Drug discovery and development: Role of basic biological research. *Transl. Res. Clin. Interv.* **2017**, 3 (4), 651–657.

38. G. Stansfield. Managing wound exudate in the diabetic foot ulcer. *Diabet. Foot* **2000**, 3 (3), 93–99.

39. World Union of Wound Healing Societies (WUWHS), Consensus Document. *Wound exudate: effective assessment and management*, Wounds International; **2019**.

40. G. Dabiri, E. Damstetter, T. Phillips. Choosing a Wound Dressing Based on Common Wound Characteristics. *Adv. Wound Care* **2016**, 5 (1), 32.

41. T.F. O'Donell Jr, M.A. Passman, W.A. Marston, et al. Management of venous leg ulcers: Clinical practice guidelines of the Society for Vascular Surgery® and the American Venous Forum. *J. Vasc. Surg.* **2014**, 60 (2), 3S-59S.

42. T. Bastogne. Quality-by-design of nanopharmaceuticals – a state of the art. *Nanomedicine Nanotechnology, Biol. Med.* **2017**, 13 (7), 2151–2157.

43. M.S. Taha, S. Padmakumar, A. Singh, M.M. Amiji. Critical quality attributes in the development of therapeutic nanomedicines toward clinical translation. *Drug Deliv. Transl. Res.* **2020**, 10 (3), 766–790.

44. E.B. Souto, G.F. Silva, J. Dias-ferreira, et al. Nanopharmaceutics: Part II—production scales and clinically compliant production methods. *Nanomaterials* **2020**, 10 (3), 455.

45. A. Porfire, M. Achim, C. Barbalata, et al. Pharmaceutical Development of Liposomes Using the QbD Approach. In *Liposomes: Advances and Perspectives*; Catala, A., Ed.; IntechOpen, **2019**; pp 1–20.

46. M. Kapoor, S.L. Lee, K.M. Tyner. Liposomal Drug Product Development and Quality: Current US Experience and Perspective. *AAPS J.* **2017**, 19 (3), 632–641.

47. E.M.A. Committee for Human Medicinal Products. ICH guideline Q8 (R2) on pharmaceutical development; **2017**.

48. A. Porfire, M. Achim, C. Barbalata, et al. Pharmaceutical Development of Liposomes Using the QbD Approach. *Liposomes - Adv. Perspect.* **2019**.

49. E. Medicines Agency. ICH guideline Q10 on pharmaceutical quality system; **2015**.

50. CDER-FDA. Liposome Drug Products: Chemistry, Manufacturing, and Controls; Human Pharmacokinetics and Bioavailability; and Labeling Documentation https://www.fda.gov/regulatory-information/search-fda-guidance-documents/liposome-drug-products-chemistry-manufacturing-and-controls-human-pharmacokinetics-and (accessed Apr 3, 2022).

51. J. Tomsen-Melero. Study of New Liposomes for the Delivery of Enzymes through Biological Membranes "Doctoral dissertation," Universitat Autònoma de Barcelona, **2021**.

52. G. Amasya, U. Badilli, B. Aksu, N. Tarimci. Quality by design case study 1: Design of 5-fluorouracil loaded lipid nanoparticles by the W/O/W double emulsion- Solvent evaporation method. *Eur. J. Pharm. Sci.* **2016**, 84, 92–102.

53. J. Merlo-Mas, J. Tomsen-Melero, J.L. Corchero, et al. Application of Quality by Design to the robust preparation of a liposomal GLA formulation by DELOS-susp method. *J. Supercrit. Fluids* **2021**, 173, 105204.

54. CDER-FDA. Guidance for Industry Q6B Specifications: Test Procedures and Acceptance Criteria for Biotechnological/Biological Products; **1999**.

55. European Medicines Agency. ICH Topic Q 6 B Specifications: Test Procedures and Acceptance Criteria for Biotechnological/Biological Products; **1999**.

56. M. Sethi, R. Sukumar, S. Karve, et al. Effect of Drug Release Kinetics on Nanoparticle Therapeutic Efficacy and Toxicity. *Nanoscale* **2014**, 6 (4), 2321–2327.

57. N. Grimaldi, F. Andrade, N. Segovia, et al. Lipid-based nanovesicles for nanomedicine. *Chem. Soc. Rev.* **2016**, 45 (23), 6520–6545.

58. L. Maja, K. Željko, P. Mateja. Sustainable technologies for liposome preparation. *J. Supercrit. Fluids* **2020**, 165, 104984.

59. C.S. Ho, C.W.K. Lam, M.H.M. Chan, et al. Electrospray Ionisation Mass Spectrometry: Principles and Clinical Applications. *Clin. Biochem. Rev.* **2003**, 24 (1), 3.

60. N.A. Kim, D.G. Lim, J.Y. Lim, K.H. Kim, S.H. Jeong. Fundamental analysis of recombinant human epidermal growth factor in solution with biophysical methods. *Drug Dev. Ind. Pharm.* **2015**, 41 (2), 300–306.

61. J. Michl, K.C. Park, P. Swietach. Evidence-based guidelines for controlling pH in mammalian live-cell culture systems. *Commun. Biol.* **2019**, 2 (1), 1–12.

62. M. Häring, M.M. Pérez-Madrigal, D. Kühbeck, et al. DNA-Catalyzed Henry Reaction in Pure Water and the Striking Influence of Organic Buffer Systems. *Molecules* **2015**, 20 (3), 4136–4147.

63. J.L. Lepe-Zuniga, J.S. Zigler, I. Gery. Toxicity of light-exposed Hepes media. *J. Immunol. Methods* **1987**, 103 (1), 145.

64. U. of S. and T. of China. Important Biological Buffers http://staff.ustc.edu.cn/~liuyz/methods/buffer.htm (accessed Jan 27, 2022).

65. H. Holmegaard Sorensen, L. Skriver, A. Rassing Hoelgaard. A stabilized pharmaceutical formulation comprising growth hormone and histidine. DK Patent EP1197222A2, 2002.

66. D. Sek. Breaking old habits: Moving away from commonly used buffers in pharmaceuticals https://www.europeanpharmaceuticalreview.com/article/13699/breaking-old-habits-moving-away-from-commonly-used-buffers-in-pharmaceuticals/ (accessed Nov 15, 2021).

67. R.G. Strickley, W.J. Lambert. A review of Formulations of Commercially Available Antibodies. *J. Pharm. Sci.* **2021**, 110 (7), 2590–2608.

68. M.H. Stipanuk, M. Caudill. Structure, Nomenclature, and Properties of Proteins and Amino Acids. In *Biochemical, Physiological and Molecular Aspects of Human Nutrition*; Elsevier Inc, St Louis, MO, **2013**; pp 69–90.

69. L. Ferrer-Tasies, H. Santana, I. Cabrera-Puig, et al. Recombinant Human Epidermal Growth Factor/Quatsome Nanoconjugates: A Robust Topical Delivery System for Complex Wound Healing. *Adv. Ther.* **2021**, 4 (6), 2000260.

70. K. Ohlendieck, S. E. Harding. Centrifugation and Ultracentrifugation. In *Wilson and Walker's Principles and Techniques of Biochemistry and Molecular Biology*; **2018**; pp 424–453.

71. T. Narayanan, J. Gummel, M. Gradzielski. Probing the Self-Assembly of Unilamellar Vesicles Using Time-Resolved SAXS. In *Advances in Planar Lipid Bilayers and Liposomes*; Iglic, A., Kulkarni, C. ., Eds.; Elsevier, **2014**; Vol. 20, pp 171–196.

72. Nanotechnology Characterization Laboratory. Assay Cascade Protocols https://ncl.cancer.gov/resources/assay-cascade-protocols (accessed Dec 1, 2021).

73. C. Fornaguera, M.Á. Lázaro, P. Brugada-Vilà, et al. Application of an assay Cascade methodology for a deep preclinical characterization of polymeric nanoparticles as a treatment for gliomas. *Drug Deliv.* **2018**, 25 (1), 472–483.

74. S. Soares, J. Sousa, A. Pais, C. Vitorino. Nanomedicine: Principles, properties, and regulatory issues. *Front. Chem.* **2018**, 6, 360.

75. B.A. Lipsky, C. Hoey. Topical antimicrobial therapy for treating chronic wounds. *Clin. Infect. Dis.* **2009**, 49 (10), 1541–1549.

76. A. Abulrob, Z. Lu, E. Baumann, et al. Nanoscale imaging of epidermal growth factor receptor clustering: Effects of inhibitors. *J. Biol. Chem.* **2010**, 285 (5), 3145–3156.

77. Y. Jiao, L. na Niu, S. Ma, et al. Quaternary ammonium-based biomedical materials: State-of-the-art, toxicological aspects and antimicrobial resistance. *Prog. Polym. Sci.* **2017**, 71, 53–90.

78. B.A. Mast, G.S. Schultz. Interactions of cytokines, growth factors, and proteases in acute and chronic wounds. *Wound Repair Regen.* **1996**, 4 (4), 411–420.

79. S.F. Ng, J.J. Rouse, F.D. Sanderson, V. Meidan, G.M. Eccleston. Validation of a static Franz diffusion cell system for in vitro permeation studies. *AAPS PharmSciTech* **2010**, 11 (3), 1432–1441.

80. S. Zsikó, K. Cutcher, A. Kovács, et al. Nanostructured Lipid Carrier Gel for the Dermal Application of Lidocaine: Comparison of Skin Penetration Testing Methods. *Pharmaceutics* **2019**, 11 (7), 310.

81. L. Coderch, I. Collini, V. Carrer, C. Barba, C. Alonso. Assessment of Finite and Infinite Dose In Vitro Experiments in Transdermal Drug Delivery. *Pharmaceutics* **2021**, 13 (3), 364.

82. A.D. Irritation/Corrosion. OECD Guideline for Testing of Chemicals; **2015**.

83. Métodos de reemplazo a las pruebas con animales https://nomasviviseccion.cl/experimentacion-en-animales/metodos-de-reemplazo-a-las-pruebas-con-animales/ (accessed Jul 4, 2018).

84. Verónica Martínez Ocaña. Marcadores de irritación en modelos celulares y organotípicos como alternativa a los ensayos in vivo aplicado al estudio de tensioactivos de tipo lipoaminoácido. "Doctoral dissertation," Universitat de Barcelona, **2007**.

85. J. Choi, H. Kim, J. Choi, et al. Skin corrosion and irritation test of sunscreen nanoparticles using reconstructed 3D human skin model. *Environ. Health Toxicol.* **2014**, 29, e2014004.

86. J. van Meerloo, G.J.L. Kaspers, J. Cloos. Cell Sensitivity Assays: The MTT Assay. In *Cancer cell culture*; Humana Press, **2011**; pp 237–245.

87. J. Cotovio, M. Grandidier, P. Portes, R. Roguet, A.S. Bois. The in vitro acute skin irritation of chemicals: Optimisation of the EPISKIN prediction model within the framework of the ECVAM validation process. *Altern. to Lab. Anim.* **2005**, 33 (4), 329–349.

88. X.T. Wang, C.C. McKeever, P. Vonu, C. Patterson, P.Y. Liu. Dynamic Histological Events and Molecular Changes in Excisional Wound Healing of Diabetic DB/DB Mice. *J. Surg. Res.* **2019**, 238, 186–197.

89. L. Schwartz, K. Seeley. Introduction to tangential flow filtration for laboratory and process development applications; **2014**.

90. K.L. Chapman, H. Holzgrefe, L.E. Black, et al. Pharmaceutical toxicology: Designing studies to reduce animal use, while maximizing human translation. *Regul. Toxicol. Pharmacol.* **2013**, 66 (1), 88–103.

91. S. Parasuraman. Toxicological screening. *J. Pharmacol. Pharmacother.* **2011**, 2 (2), 74.

92. U.S. Food and Drug Administration. Guidance for Industry: Estimating the Maximum Safe Starting Dose in Initial Clinical Trials for Therapeutics in Adult Healthy Volunteers; Rockville, Maryland, **2005**.

93. T. Goods Administration. Australian Public Assessment Report for inactivated influenza virus vaccine (containing 15 µg haemagglutinin of virus Types A H1N1+ A H3N2 + B) About the Therapeutic Goods Administration (TGA); **2015**.

94. European Medicines Agency. Committee for medicinal products for human use (CHMP) ICH guideline M3 (R2)-questions and answers; **2012**.

"Yesterday is history, tomorrow is a mystery, but today is a gift, that is why it's called the present"

– Master Oogway"

3

Advances in DELOS nanovesicles for topical drug delivery by converting them into suitable final dosage forms

3.1 Introduction

In the previous Chapter, promising results were obtained in the pharmaceutical development of an intermediate product candidate based on liquid suspension of rhEGF-DELOS nanovesicles for epidermal regeneration of complex wounds. However, the definition of a final drug product and thus a marketable final dosage form was still missing. At this point, the translation of this nanoformulation into a final drug product was also pursued to open new perspectives of the system[1].

As already explained in **Chapter 2**, the feasibility study of the preclinical phase of the development of the rhEGF-DELOS nanovesicles formulation, although successful, it still requires an 8-week GLP toxicological study, which allows to define a safety margin for the drug product before the administration to humans. In this regard, it is important to note that AEMPS recommended us that this study should be conducted using the final drug product formulation intended to reach the clinic, or with a very close version. Therefore, the definition of the final pharmaceutical form of the rhEGF-DELOS nanovesicles is required prior to toxicological testing. Then, one of the aims of the present research work was to translate the intermediate nanoformulation of rhEGF-DELOS nanovesicles developed and optimized in **Chapter 2** into a final dosage form.

To understand this section, it is necessary to clarify why the development of a final dosage form is necessary. Generally, in drug delivery, the active pharmaceutical ingredient (API) is delivered to the patient through diverse methods and forms named pharmaceutical dosage. Thus, APIs are usually not supplied as pure chemical compounds to prevent or treat diseases. Then, the development of a dosage form involves combining the API with other components, widely known as excipients or pharmaceutical inactive ingredients and converting it into a final valuable medicinal compound[2,3].

The pharmaceutical dosage form is important in drug delivery not only because it makes an active pharmaceutical ingredient administrable, but also because it can influence on compliance,

pharmacokinetics, manufacturing, shelf life, efficacy of therapy and many other parameters affecting the outcome of drug therapy[2].

Among the dosage forms commonly administered, they can be classified depending on the physical form of the final pharmaceutical product such as solid (tablets, capsules, powders, etc.), semi-solid (creams, gel, ointment and paste), liquid form (emulsion, injection, lotion, suspension, etc.) and gaseous dosage form (gas and aerodispersion)[3,4] (**Figure 3.1**). In view of this, in this research, the development of two different dosage forms for rhEGF-DELOS nanovesicles was considered, such as a gaseous form administered via a device such a spray (aerodispersion), and also a semi-solid form, by converting the formulation into a hydrogel, which had never been studied before.

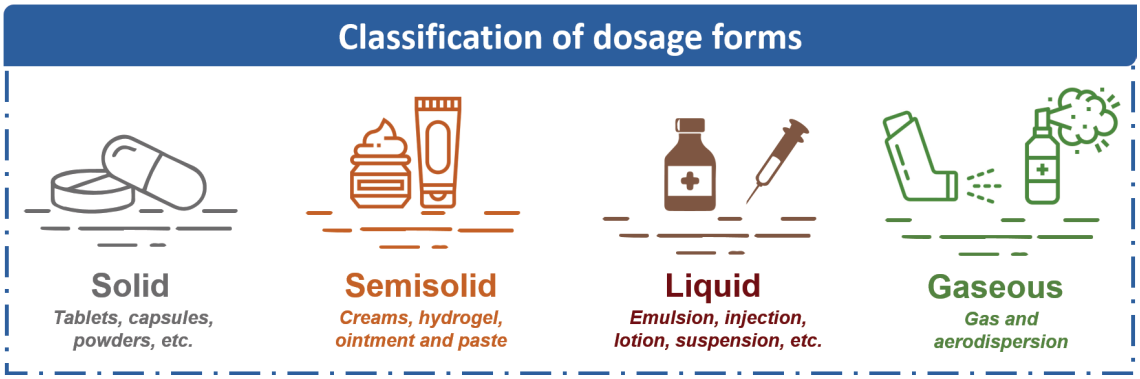

Figure 3.1: Schematic representation of the classification of the different existing types of dosage forms based on the physical form.

Furthermore, the specific development of the final dosage form of rhEGF-DELOS nanovesicle formulation was an inspiration and starting point for the company and the research group. In this way, it was considered to further improve the DELOS platform and have a broader range of potential DELOS nanovesicle formulations suitable for topical administration.

As explained in the Introduction of this dissertation (**Chapter 1**), one of the main goals of Nanomol Technologies SL and the Nanomol Group is research and development to provide powerful knowledge. In particular, we are interested in expanding the frontiers of the DELOS-susp platform to generate a wealth of research and understanding. Subsequently, our aim will be also to broaden and rethink the existing research on the nanoformulation developed for topical administration and to generate new ones with equally excellent properties.

Therefore, in this **Chapter 3**, we will work in early stages like TRL2 in terms of Technology Readiness Level of the research and development of a pharmaceutical product, specifically on technology formulation.

To do this, within the scope of this work, we will evaluate for the first time the translation of the rhEGF-DELOS nanovesicles intermediate product into a final dosage form suitable for topical administration, e.g., a liquid dispersion administered with a spray in a gaseous dosage form, or in semi-solid form such as hydrogels. Then, from these studies, we investigated the possibility of generating new DELOS nanoformulations through the DELOS-susp methodology by evaluating the use of components of different nature. Afterwards, the most suitable generated nanoformulations were converted into hydrogels with several hydrogelling agents with innovative properties.

Overall, it should be noted that our approach here would assume several guideline recommendations. For instance, as mentioned in ICH Q5E, "it is important to evaluate the relevant quality attributes of the product to demonstrate that the manufacturing process changes will not have an adverse impact on the quality, safety and efficacy of the drug product"[5]. Therefore, extensive characterization of the rhEGF-DELOS nanovesicles drug product will be performed in the following stage of drug development.

3.2 Moving from intermediate product to final dosage form of rhEGF-DELOS nanovesicles

To develop a final drug product, some quality target product profile considerations can be included as recommended in the ICH Guideline Q8 (R2) Pharmaceutical Development. Among them, we can find the intended use in clinical setting, the route of administration, the dosage form, the dosage strengths, the container closure system, the quality criteria of the drug product (sterility, purity, drug release) appropriate to the intended marketed product, among others[6].

It was already explained in the previous Chapter that a distinction was made between the treatments of DFUs and VLUs in the development of the rhEGF-DELOS nanovesicles. The most important point to note is that each treatment should have a different final dosage form, as the underlying pathologies involved in complex wounds vary by wound type, and consequently, different dosage forms approaches can be applied to achieve successful treatments[7].

As mentioned in **Chapter 2**, it is well known that one of the challenges in managing complex wounds is to consider wound exudate, mainly in patients with VLUs who generally have increased wound exudate compared to patients with other forms of chronic skin ulcers such as DFUs. Therefore, according to current recommendations for managing this excess of wound exudate, this issue can be addressed through the use of wound dressings that manage this wound exudate while maintaining a moist wound[8,9].

Literature on the subject is abundant and easy to find, with pharmaceutical dosage forms such as liquid dispersions administered by spray, creams, ointments and gels being commonly used for topical administration[10]. Then, after careful consideration, it was suggested that potential dosage

forms to treat DFUs and VLUs would consist of a packaged product that could be directly applied topically to patients in hydrogel form to treat DFUs (**Figure 3.2a**), which is considered a viable option to absorb wound exudate and keep the wound moist for faster healing[11]. In contrast, the use of a gaseous dosage form has been considered as a possible viable option for treating VLUs due to its highly exudative nature (**Figure 3.2b**). It has been reported that using a hydrogel on wounds with excess exudate and applying it to an already moist wound results in even higher fluid levels[12]. Thus, to address this challenge, we investigated for the first-time possible approaches to develop new dosage forms of rhEGF-DELOS nanovesicles as a final drug product.

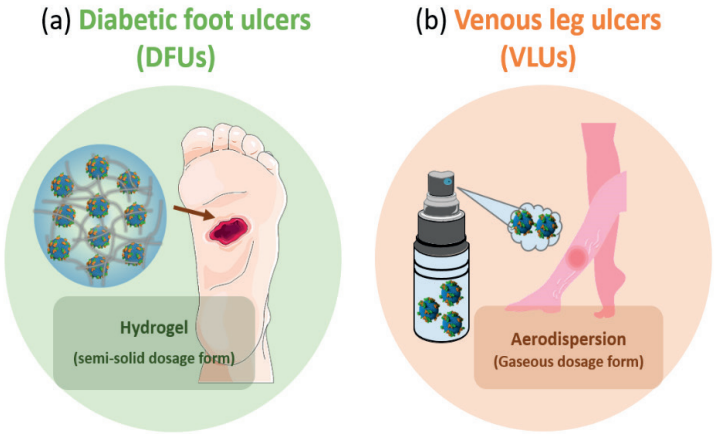

Figure 3.2: Representation of the strategic dosage forms approaches of rhEGF-DELOS nanovesicles to treat complex wounds such as (a) diabetic foot and (b) venous leg ulcers.

3.2.1 Sprayed rhEGF-DELOS nanovesicles suspension as an attractive pharmaceutical dosage form

To date, skin sprays are a potential therapeutic strategy for wound healing applications due to their versatility to deliver different types of materials[13] such as suspensions of solid or liquid particles. When these suspensions are sprayed and so-called aerodispersions, they can be applied to the skin simply by gently pressing the spray container against the skin and initiating the spraying[14].

In particular, sprays received special attention in this work since spraying a topical formulation into a wound can provide certain benefits such as the formation of a film directly on the wound when applied. This film can then offer physical protection and prevent entry of microorganisms from the external environment. Importantly, film formation allows control over air and moisture permeability, thereby maintaining a favorable environment for wound healing and avoiding maceration due to excessive moisture accumulation[15]. Furthermore, topical sprays present the ability to treat large wounds or spray over areas with unfavorable topography, to reduce the application time, and the homogeneous distribution of the sprayed suspensions[13].

Another benefit in our case is that rhEGF-DELOS nanovesicle intermediate formulation can be sprayed in liquid suspension directly onto the skin without any prior sample-processing step, making it a very motivating approach. Therefore, this study provides an exciting opportunity to advance our knowledge on the development of a final drug product.

Thanks to some collaborating companies, we could define the most suitable type of spray device for administering rhEGF-DELOS nanovesicles in gaseous dosage form. In particular, Aptar Pharma Company suggested that the most appropriate was the *Airless Dispensing Solution* device with an Advanced Preservative Free pump (**Figure 3.3**). This spray device allowed the sterile administration of the product, as already described as an essential CQA for the drug product (**Table 2.2** of **Chapter 2**), and without the addition of preservatives to ensure the sterility of the nanoformulation solution over time. In addition, to achieve sample sterility, it would also be possible to use sterile membrane filtration and then add the sample to the device, thereby maintaining the sterility.

Figure 3.3: Selected Aptar Pharma device for the administration of the final product of rhEGF-DELOS nanovesicles as sprayed dosage form.

It is therefore important to evaluate the performance of this spray device to ensure its applicability for administering our optimized nanoformulation. To achieve this, we estimated in preliminary experiments that the critical parameters that needed to be evaluated in the current stage of the project were the position of the spray device, the physicochemical properties of the nanoformulation before and after spraying, and the coverage area of the sprayed liquid dispersion.

3.2.1.1 Evaluation of the spray device position for improving topical drug delivery

One of the most important points when spraying is to ensure that the suspension is well dispensed regardless of the position of the bottle (face-down, face-up, lateral…). Special attention should be paid to the fact that complex wounds, such as venous ulcers, can have different orientations in the patient and can thus complicate the product administration.

For this reason, in order to ensure reproducible dispensing, we evaluated different spray orientations.

First, as they were preliminary studies, the spray devices were manually filled. Then, the spray device was fixed in a metal structure at various positions, as shown in **Figure 3.4** and finally, the head of the spray device was pressed, and the sprayed liquid suspension was poured directly into a vial (see **Section 6.2.3**).

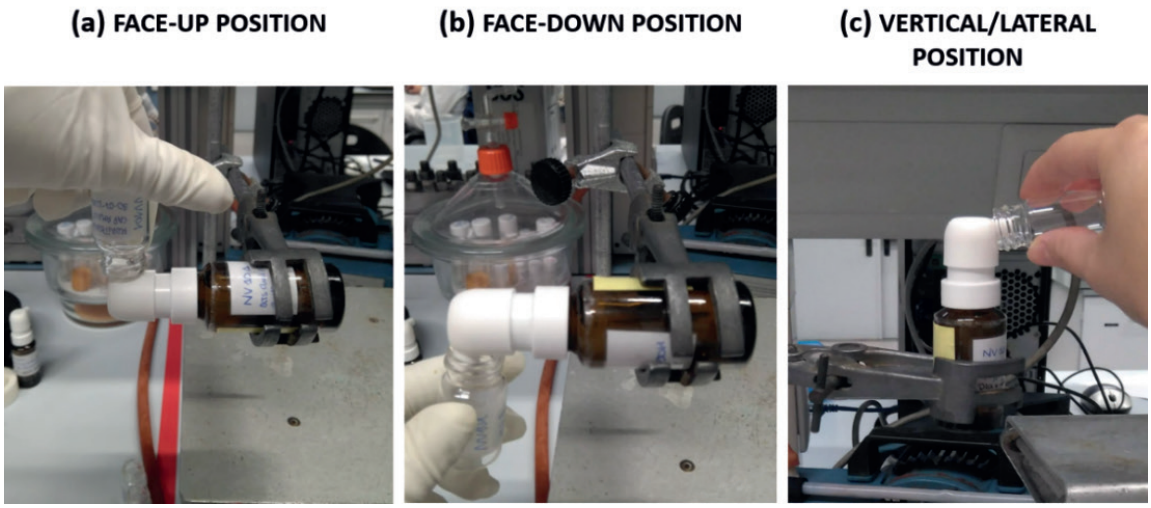

Figure 3.4: Image of the three evaluated positions, (a) face-up, (b) face-down and (c) vertical/lateral for spraying rhEGF-DELOS nanovesicles with the Aptar Pharma device.

With the purpose of studying the relationship between spray device position and the dispensing efficiency, first the intermediate formulations with and without 100 $\mu g \cdot mL^{-1}$ of rhEGF, henceforth referred to as rhEGF-DELOS nanovesicles and Blank-DELOS nanovesicles respectively, were produced by DELOS-susp. Specifically, these formulations were prepared using the composition described in **Table 2.5** in **Chapter 2** and then, they were placed in the spray device. Afterwards, 3 positions were evaluated: face-up, face-down and vertical/lateral.

Planned comparisons provided clear support that face-up and face-down positions are critical positions as it is impossible to spray at a given point because the spray tube itself could not hold enough sample. Conversely, the results illustrated in **Table 3.1** show that the vertical/lateral position is the most suitable one for spraying Blank-DELOS and rhEGF-DELOS nanovesicles due to its high recovery fraction value. This value was determined by dividing the experimental volume recovered by a theoretical volume of 150 µL. A recovery fraction value greater than 98% was obtained for both sprayed samples, indicating proper spray performance. Furthermore, good repeatability after 10 dispenses was achieved in both cases, as a low relative standard deviation (RSD) was obtained, which means that the measurement data is precise.

Table 3.1: Mean recovered volume, RSD and recovery fraction of Blank-DELOS and rhEGF-DELOS nanovesicles after 10 dispenses with spray device in vertical/lateral position (N = 10).

	Mean recovered volume (µL)	RSD (%)	Recovery fraction (%)[1]
Blank-DELOS nanovesicles	148	0.41	99
rhEGF-DELOS nanovesicles	150	0.39	100

[1]Obtained from dividing the experimental recovered volume to the theoretical one (150 µL).

Summarizing, the present study confirmed that the vertical/lateral position was the most appropriate spray orientation strategy for the administration of both Blank-DELOS nanovesicles and rhEGF-DELOS nanovesicles. Therefore, the spray device position is an important parameter to be taken into account in future clinical trials.

3.2.1.2 Spray device distance and area of covering

It is worth noting that another important factor to consider for the success of the nanoformulation treatment using a gaseous dosage form is the application distance, since depending on the application distance, the amount of treatment applied to a unit of area can change.

To assess the correlation between the sprayed area and the distance, three different distances were evaluated: 2, 5 and 10 cm, and the corresponding sprayed areas were measured. As can be seen from the data in **Table 3.2**, the 2 cm distance behaves differently than the 5 and 10 cm distances. What is interesting about this data is that a spray distance of 2 cm produces a circumferential-like surface and therefore an even distribution of the applied suspension, resulting in a final sprayed area of approximately 4.6 cm^2 with an RSD of 23% (N = 10).

Conversely, a spray distance of 5 and 10 cm distributes the suspension in an elliptical geometry and thus non-uniformly, which means that there is a diffusion of the dose, moving from an intense spray in the center to a less intense one at the extremes. Because of this, these approaches are not recommended, as they seem inefficient.

Another notable observation is that there is a direct correlation between spray device distance and area sprayed, as distance increases the area behaves the same, reaching 43.5 cm^2 of sprayed area at 10 cm sprayed distance.

Table 3.2: Characteristics of the correlation between the distances of spray device application and sprayed area after 10 dispensing (N = 10).

	Distance of spray application		
	2 cm	**5 cm**	**10 cm**
Type of area	Circumference ($A = \pi \cdot r^2$)	Ellipse ($A = \pi \cdot r_1 \cdot r_2$)	Ellipse ($A = \pi \cdot r_1 \cdot r_2$)
Sprayed area (cm^2)	4.6	22.0	43.5
RSD (%)	23	6.5	9.8

In conclusion, the results presented so far in this section indicates that there is a dependency between the spray distance and the type of produced area. It should be highlighted that these distances are just first approximation values, so it would be reasonable to further study other distances such as between 2 and 5 cm since they are the ones that produce a sprayed area consistent with the inclusion criteria in the ulcer clinical trials, which were defined as ulcers between 5-15 cm^2.

3.2.1.3 Physicochemical properties of the sprayed nanoformulation

Another important research question when using this spray device was whether the physicochemical properties of the intermediate formulation of rhEGF-DELOS nanovesicles with and without 100 $\mu g \cdot mL^{-1}$ rhEGF were changed upon spraying. To confirm that spraying was an appropriate administration strategy for our nanoformulation, the same procedure as in **Section 3.2.1.2** was followed, using rhEGF-DELOS nanovesicles and Blank-DELOS nanovesicles (**Table 2.5**). In this case, the spray device was placed in vertical/lateral position and then, the sprayed solution was evaluated by DLS (see **Section 6.3.1** for more details). The results of the analysis are presented in **Table 3.3** showing no differences in terms of mean particle size, polydispersity, and zeta potential values between the two groups before and after spraying.

Table 3.3: Comparison of physicochemical properties of Blank-DELOS and rhEGF-DELOS nanovesicles before and after spraying.

		Particle size distribution		Zeta Potential
		Mean (nm)	**PDI**	**(mV)**
Blank-DELOS nanovesicles	Before spraying	67 ± 1	0.24 ± 0.01	89 ± 1
	After spraying	67 ± 1	0.23 ± 0.01	93 ± 2
rhEGF-DELOS nanovesicles	Before spraying	59 ± 1	0.22 ± 0.01	94 ± 4
	After spraying	59 ± 1	0.22 ± 0.01	93 ± 10

Once confirmed that some of the critical quality attributes, such as the particle size distribution, PDI and zeta potential are not altered, another important parameter to monitor is whether the entrapment efficiency of rhEGF into DELOS nanovesicles is affected when the rhEGF-DELOS nanoformulation suspension is sprayed. To determine it, the entrapment efficiency of rhEGF in the sprayed and non-sprayed rhEGF-DELOS nanovesicles was analyzed by the optimized methodology described in **Section 2.2.5** and in **Section 6.3.8**. By carefully examining the data, it was determined that no significant differences were observed between the two groups, since the rhEGF incorporation efficiency of rhEGF-DELOS nanovesicles was 98 and 100%, before and after spraying respectively. Thus, the results indicate that the entrapment efficiency of rhEGF is not altered when the rhEGF-DELOS nanovesicle suspension is sprayed with the Aptar Company's *Airless Dispensing Solution* device with an Advanced Preservative Free pump, which is an important parameter to ensure the effectiveness of the nanoformulation.

In summary, the use of the selected Aptar Pharma device for administering rhEGF-DELOS nanovesicles as a gaseous dosage form indicates strong potential for its topical application, e.g., for the treatment of complex wounds. Not only does it demonstrate ease of preparation, which is important when working at industrial scale, but the nanoformulation also exhibits suitable and unaltered physicochemical properties when aerodispersed.

3.2.2 Hydrogel as a final pharmaceutical dosage form of rhEGF-DELOS nanovesicles

Despite the wide use of conventional spray dosage form due to their acceptability and ease of use, research and development of other new rhEGF-DELOS nanovesicle dosage forms for the topical route of administration remained unexplored. For this reason, there was also the aim to further explore the possibility of adopting other promising approaches for skin delivery of the rhEGF-DELOS nanovesicles, such as hydrogels.

3.2.2.1 Hydrogel definition and classification

A hydrogel is a soft, three-dimensional, cross-linked polymeric material that contains at least two components, one of which is a liquid that is present in large quantities, and the other is a hydrogelling agent that can be liquid or solid. Interestingly, the hydrogelling agent is able to retain a large amount of water in its swollen state while maintaining the structure due to the cross-linking of the individual polymer chains[16–18].

Hydrogels can be classified in many ways due to the different properties. The most common classification is by the type of cross-linking network such as physical-based or self-assembled (non-

covalent bonds and dependent on environmental reactions), chemical-based (covalent bonds), or through biochemical polymers (depending on biological agents). Furthermore, depending on the source, they can be classified as natural or synthetic polymers, which can have different physicochemical properties that can affect the final product[17]. In addition, they can be also categorized according to their polymer composition, their network morphology/configuration, their sensitivity to the environment (response) and their electrical charge depending on the ionic charges of the bound groups[17–19] (**Figure 3.5**).

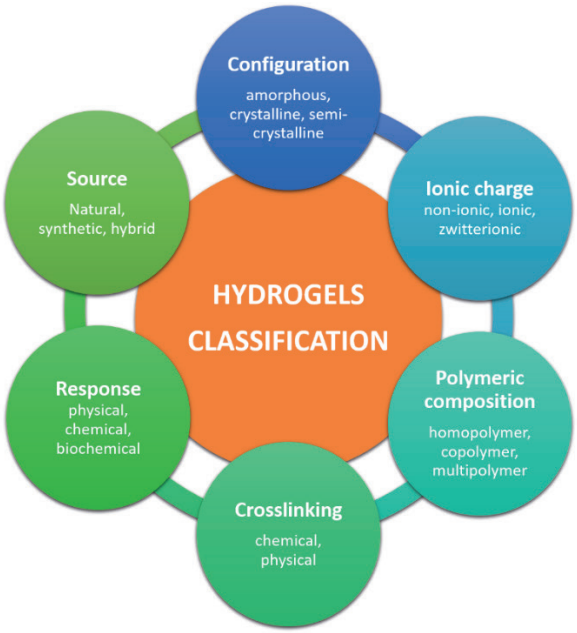

Figure 3.5: Schematic representation of the classification of different types of hydrogels. Adapted from[19].

Then, depending on the type of hydrogelling agent used, different properties can be achieved. For instance, depending on the mucoadhesive characteristics, the hydrogel can provide prolonged contact at the site of administration compared to an aqueous solution, thereby improving the therapeutic outcome[17,20]. Equally important is the consideration of the combination of hydrogelling agent properties such as consistency, concentration used and degree of solubility for the optimization of the topical formulation as these can influence the final product viscosity, which is a critical parameter for the final product[21,22].

Furthermore, to develop a semi-solid formulation as a hydrogel for topical application, some essential parameters must be considered to ensure a good quality of the product. It should be smooth, inert, physically and chemically stable and compatible not only with the skin but also with the active ingredient to be incorporated. In addition, it should have a consistency that allows for adequate spreading and softness upon application, without sensitizing the skin or delaying wound healing[23].

Moreover, the ideal treatment of open wounds should include maintaining moisture at the wound site, removal of excess exudate, freedom from particles and toxic contaminants, ability to remove without further trauma, impermeability to bacteria, comfort and the possibility of gas exchange and infrequent changes[24,25].

With all these factors in mind and for the first time, a polymer called Methocel™ K4M was selected for the development of a rhEGF-DELOS nanovesicle-based hydrogel for the treatment of complex wounds. Importantly, this polymer was chosen for its non-ionic charge, which is an important parameter to avoid electrostatic interactions with the vesicles and hence possible aggregation. This instability phenomenon was previously observed in preliminary studies performed by Nanomol Group when ionic commercial polymers were used to gellify DELOS nanovesicles, i.e., using sodium carboxymethyl cellulose (CMC) and Sepineo™ P600 polymers[26–28]. For this reason, non-ionic charged polymers have been intensively considered as a viable option for the development of rhEGF-DELOS nanovesicle-based hydrogels.

3.2.2.2 Methocel™ K4M as a promising polymer for the preparation of rhEGF-DELOS nanovesicle-based hydrogels

Methocel™ K4M, also known as hydroxypropyl methylcellulose, is a water-soluble cellulose ether biopolymer derived from cellulose, the most abundant polymer in nature, and a characteristic product of The Dow Chemical Company[29]. It is a polymeric backbone of cellulose, a natural carbohydrate, containing a repeating backbone of anhydroglucose (**Figure 3.6**). This type of polymer is a renewable raw material derived primarily from wood pulp, that offers exceptional flexibility and a combination of properties not typically found in other water-soluble polymers[29].

In addition, being a natural polymer can offer several advantages as biomaterials tend to present inherent soft-tissue like properties, low toxicity, stable cross-linked three-dimensional intact mesh network and large surface area for cellular contact. Therefore, these properties are really interesting for their application in both regenerative and reparative processes, such as the treatment of complex wounds[30].

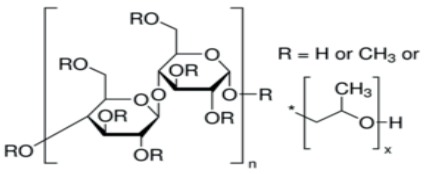

Figure 3.6: Molecular structure of Methocel™ K4M. Reproduction from[31].

The reason for the name Methocel™ K4M is that there exist several types of Methocel classified according to different rules. The first letter categorizes the type of cellulose ether, i.e., its "chemistry". For instance, the letter "A" designates methylcellulose (MC) products and "E," "F" and "K" different hydroxypropyl methylcellulose (HPMC) products. Then, the number after the chemistry designation indicates the viscosity of the product in millipascal seconds (mPa·s), measured at a concentration of 2 wt% in water at 20 °C. When denoting viscosity, the letter "M" is used to represent a multiplier of 1000[32].

Methocel pharmaceutical grade products meet United States Pharmacopoeia (USP XXIII), European Pharmacopoeia (EP) and Japanese Pharmacopoeia (JP) specifications. In addition, methylcellulose (METHOCEL™ A products) is Generally Recognized As Safe (GRAS) by the U.S. Food and Drug Administration (FDA)[33]. Furthermore, this polymer is extensively used in pharmaceutical applications as it fulfils two essential requirements: biocompatibility and biodegradability, being also used in injectable formulations and transdermal films or gels, giving the DELOS nanovesicles a wider range of applications[34–36].

For all these reasons, this polymer represents an attractive option to be tested for transforming rhEGF-DELOS nanovesicles liquid suspension to a new dosage form such as a hydrogel.

3.2.2.3 Preparation and physicochemical characterization of Methocel™ K4M-DELOS nanovesicle-based hydrogels

In this work, we first investigated the effect of Methocel™ K4M concentration on hydrogel formation. To this end, different compositions of hydrogels were prepared, as mentioned in **Table 3.4**, using 3 concentrations of Methocel™ K4M: 1, 2 and 4 wt%, which are concentrations commonly used to prepare topical formulations[37].

To determine whether these concentrations were suitable for the formulation of rhEGF-DELOS nanovesicles, three different hydrogel-based samples were prepared. These hydrogels were based on the dispersing medium used for the intermediate rhEGF-DELOS nanovesicle formulation (buffer histidine (5 mM, pH 7.0)/10% EtOH ($v \cdot v^{-1}$)), as a control group and the intermediate DELOS nanovesicles formulation with and without 100 $\mu g \cdot mL^{-1}$ of rhEGF, named rhEGF-DELOS nanovesicles and Blank-DELOS nanovesicles, respectively (**Table 2.5**). Thus, to prepare the hydrogels, Methocel™ K4M was added to the aqueous dispersion to have the desired final concentration of the hydrogelling agent. To ensure proper polymer dissolution, the total amount of Methocel™ K4M was added and left hydrating for a complete swelling at room temperature for 2 h. Then, the dispersion was gently stirred until the hydrogelling agent was completely dissolved, and a semi-solid form was achieved (see **Section 6.2.4**).

Table 3.4: Screening of the conditions of the prepared Methocel™ K4M-based hydrogels.

	Dispersant medium	Blank-DELOS nanovesicles	rhEGF-DELOS nanovesicles
Methocel™ K4M concentration	1 wt%	2 wt%	2 wt%
	2 wt%	4 wt%	4 wt%
	4 wt%		

Macroscopic appearance of Methocel™ K4M-DELOS nanovesicle-based hydrogels

Once the hydrogels were prepared following the procedure described previously, they were examined macroscopically (**Figure 3.7**). Colorless and homogeneous semi-solid formulations were obtained with the appropriate consistency, thus showing excellent organoleptic properties at any concentration, and using dispersant medium, Blank-DELOS nanovesicle and rhEGF-DELOS nanovesicles. Such data should be of great interest for this project as Methocel™ K4M showed no macroscopic disadvantage.

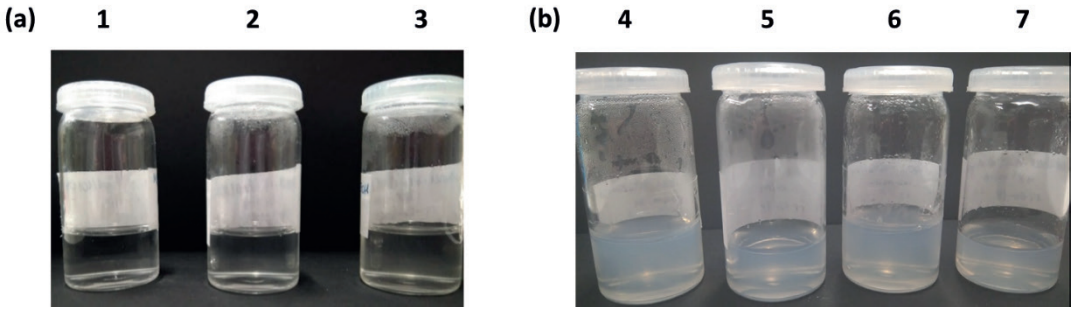

Figure 3.7: Macroscopic appearance of Methocel™ K4M-based hydrogels using a) dispersant medium, buffer histidine (5 mM, pH 7.0)/10% EtOH ($v \cdot v^{-1}$). From 1 to 3 the concentration of 1, 2 and 4 wt% of Methocel™ K4M is represented. b) 4 and 5 represent hydrogels with 2 wt% of Methocel™ K4M with Blank- and rhEGF-DELOS nanovesicles respectively, 6 and 7 hydrogels with 4 wt% of Methocel™ K4M with Blank- and rhEGF-DELOS nanovesicles, respectively.

Study of the viscosity and rheology behavior of the Methocel™ K4M-DELOS nanovesicles-based hydrogels

As mentioned above, this study aimed to formulate a hydrogel based on rhEGF-DELOS nanovesicle-based hydrogel for being applied to complex wounds. Aside from ensuring that the macroscopic appearance corresponds to the correct properties, not only the viscosity but also the rheological properties of dermal drug delivery systems are important when developing new formulations.

These parameters are relevant as they relate to spreadability and skin feel and can also affect the skin penetration of the incorporated active ingredients[38].

To provide all the desired properties of a hydrogel dressing for complex wounds, hydrogels should be easy to apply and cover the entire wound without dripping, improving quality of care and patient compliance. Therefore, to better understand the importance of rheology testing of a material, rheological concepts are described, and a discussion of the related results follows.

The term "rheology" comes from the Greek word "rheos", which means "everything flows upon time interval". In view of this, rheology is the science concerned with the deformation and flow of materials induced by applied shear forces[39]. Thanks to the multiple possibilities offered by this study, the measurement of rheological properties can have a tremendous impact on the development of formulations, since it can affect their acceptability, physical stability and even bioavailability[40].

Concerning the rheological characterization of hydrogels, it provides insight into the internal structure complexity of the hydrogel and thus helps to elucidate its behavior[41]. To study deformation and flow properties, a force is applied to a material and then the response is evaluated. At this point, the degree of the fluid's ability to resist an applied shear force is referred to as internal friction or viscosity. Therefore, for a given area, a constant force called shear stress is applied to the top plate, causing it to move at static velocity. As a result of this force, the fluid adjacent to the top plate flows at the top plate velocity while the fluid adjacent to the stationary bottom plate flows at zero velocity. This creates a velocity gradient between the plates from top to bottom, which is called the shear rate (**Figure 3.8**)[42].

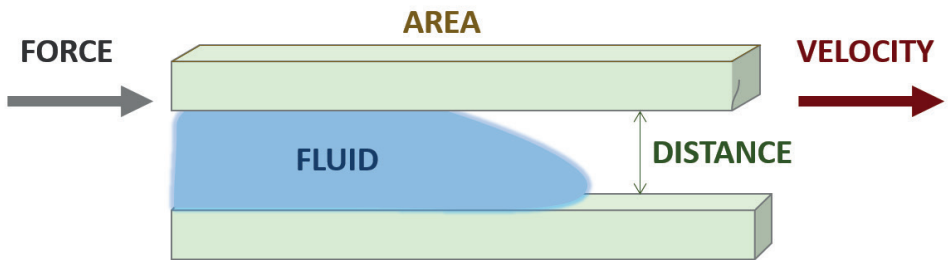

Figure 3.8: Representative image of the parameters used in the viscosity measurement. Adapted from[42].

Then, by combining the shear stress values with the shear rate, the viscosity value (η) for each substance can be determined (**Equation 3.1**).

(3.1)

$$viscosity\ (\eta) = \frac{shear\ stress}{shear\ rate}$$

In our case, to evaluate the viscosity and rheological behavior of the prepared hydrogels (**Table 3.4**), a methodology that simulates the shearing conditions experienced by the hydrogels in *in vivo* application was applied, as described in **Section 6.3.10**. The viscosity results seen from **Table 3.5** show that there is a clear tendency to increase the viscosity value of the hydrogels as the concentration of Methocel™ K4M polymer is increased. In addition, the viscosity performs equally in the different situations of hydrogels with and without the presence of DELOS nanovesicles. Based on this current work, it was sufficient to indicate that these results could show that this hydrogelling agent is not altered upon changing the aqueous medium and incorporating nanovesicles such as DELOS nanovesicles.

Furthermore, it was found that such an approach also provides high-quality results on rhEGF-DELOS nanovesicles, which present similar viscosity values to the Blank-DELOS nanovesicle formulation. By carefully examining the value of the apparent viscosity of the hydrogels in the zone where the shear rate is constant, we can conclude that all have a value in agreement with the appropriate consistency for topical application and the viscosities reported in the literature for topical formulation products[43].

Table 3.5: Viscosity values of the different Methocel™ K4M-based hydrogels examined.

Aqueous phase used	Methocel™ K4M content (wt%)	Viscosity (Pa·s)
Dispersant medium	1	0.15
	2	1.23
	4	8.66
Blank-DELOS nanovesicles	2	1.40
	4	7.84
rhEGF-DELOS nanovesicles	2	1.32
	4	9.27

Besides, this study examined the rheological parameters of the Methocel™ K4M-based hydrogels with different polymer concentrations. One of the main parameters to be described is the type of flow and deformation that our hydrogel can exhibit. For classification, materials can be divided into 2 categories depending on whether the flow properties follow the Newton's law or not (**Figure 3.9**):

- Newtonian system. In this case, the shear rate is directly proportional to the shear stress, the higher the viscosity, the greater the force per unit area (shear stress) required to generate a shear rate[44].
- Non-Newtonian system. It does not follow Newton's law of flow and thus, their viscosity is not constant and depends on the shear rate. Depending on the type of fluid, they can be classified as plastic, pseudoplastic and dilatant[45].

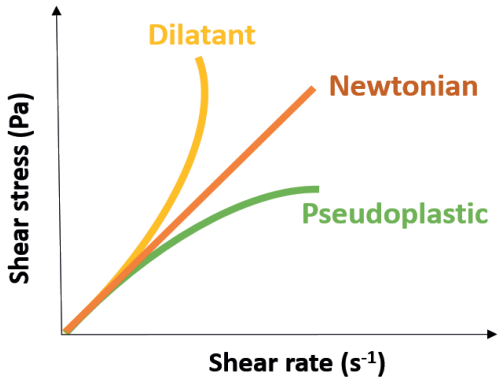

Figure 3.9: Typical flow curves of shear stress and deformation rate relationship of different fluids.

One of the main topics to be explored in this project is the ability to produce pseudoplastic hydrogels, which are hydrogels that lie between elastic and viscous behavior, i.e., have the ability to recover their original shape when external force is removed[46]. This pseudoplastic flow concept is applicable to polymers in solution whose consistency curve starts at the origin and the flow curve is non-linear (**Figure 3.9**). Consequently, the viscosity cannot be expressed by a single value since the viscosity of a pseudoplastic substance decreases with increasing shear rate (rate at which deformation is applied)[47].

Therefore, it makes sense to assess the flow behavior of the semi-solid systems when evaluating the developed hydrogels formulations based on DELOS nanovesicles. The flow curves of the Methocel™ K4M-DELOS nanovesicles-based hydrogels were recorded according to the methodology described in **Section 5.3.10**. It is shown in **Figure 3.10** that increasing the shear rate increased the shear stress of all Methocel™ K4M-based hydrogels containing dispersing medium, Blank-DELOS nanovesicles and also rhEGF-DELOS nanovesicles. This result is explained by the non-Newtonian model of pseudoplastic flow behavior, which is due to the reversible deformation of the hydrogel together with increasing force velocity in terms of shear rate[48]. This is a desirable property for topical products as it indicates that the product can be spread easily under mild forces, allowing film formation on the skin's surface.

This shear-induced thinning is a very useful feature for products intended to be applied to ulcers or damaged skin. However, once the shear stress is removed, it is desirable that the viscosity of the formulation increases rapidly to avoid leakage[49]. Within this framework, another important issue that can arise when characterizing hydrogels is their thixotropic behavior. The return of the hydrogel to its original structure is termed thixotropy and is assessed by monitoring the change in viscosity during the post-shear recovery process[50]. In our case, it can be clearly seen that little or no thixotropy was observed for Methocel™ K4M-based hydrogel samples at 2 wt% (**Figure 3.10a**), while those at 4 wt% exhibited a larger hysteresis area and hence higher thixotropy as did the 2

wt% hydrogels (**Figure 3.10b**). This behavior can be understood as a breakdown of the structure that does not immediately recover when the stress is removed or reduced.

This property can define the therapeutic efficacy of the product, such as retention time at the site of administration and bioavailability[50]. Consequently, thixotropy is a desirable property for pharmaceutical products such as complex wounds because they should have high consistency in the container, spread easily, remain at the desired site of application when dispensed and regain consistency over time[47].

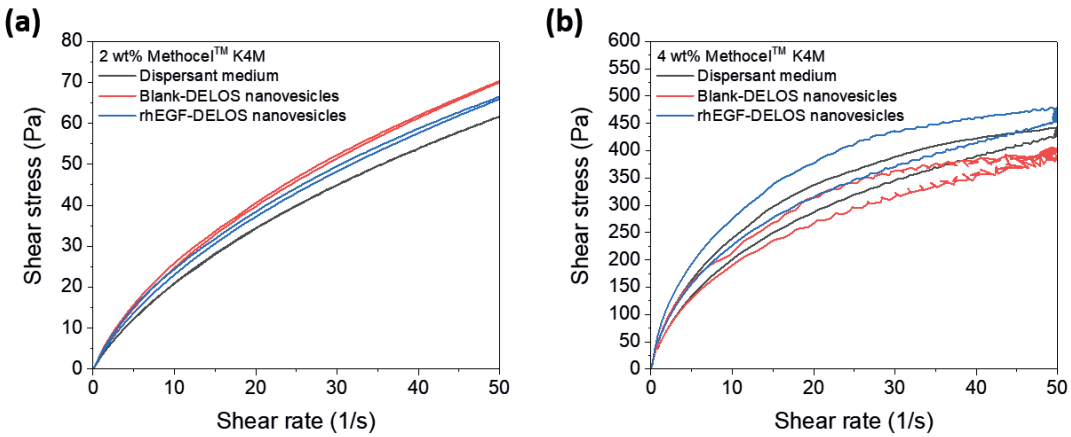

Figure 3.10: Shear stress as a function of shear rate, (a) 2 wt% and (b) 4 wt% Methocel™-based hydrogels containing dispersant medium (black), Blank-DELOS nanovesicles (red) and rhEGF-DELOS nanovesicles (blue).

In conclusion, 2 wt% Methocel™K4M seems to be a suitable choice for producing rhEGF-DELOS nanovesicle hydrogels for future topical administration, not only because of its good pseudoplasticity and thixotropic behavior but also because of its ease of preparation. For these reasons, 2 wt% Methocel™ K4M-based hydrogels were selected as promising final dosage forms to be studied in more detail.

3.2.2.4 Integrity of DELOS nanovesicles when gellified with Methocel™ K4M

It is worth noting that the process of gellification changes the properties of the nanovesicle medium (i.e., viscosity), which could compromise the integrity of the vesicles during the process. To investigate whether the properties of the nanovesicles are preserved in the hydrogel, mainly their integrity as a nanostructure, we used fluorescence spectroscopy techniques. In particular, we integrated fluorophores into DELOS nanovesicles prepared by DELOS-susp composed of CTAB and cholesterol in an equimolar ratio (7.3 mM each) and using water/10% EtOH ($v \cdot v^{-1}$) as dispersant medium.

Specifically, these DELOS nanovesicles containing the fluorophores 1,1'-Dioctadecyl-3,3,3',3'-tetramethyl-indocarbocyanine perchlorate (DiI) and 1,1'-Dioctadecyl-3,3,3',3'-tetramethyl-indodicarbocyanine perchlorate (DiD) (**Figure 3.11**)[51] have been extensively studied in the Nanomol Group[52] and referred to as DiI/DiD-DELOS nanovesicles in the following sections of this work.

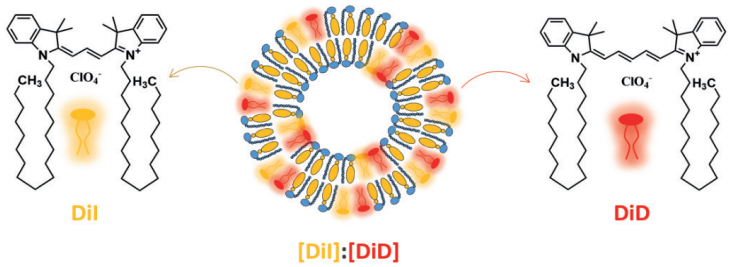

Figure 3.11: Representative picture of the molecular structure of DiI and DiD and their integration into the membrane of DELOS nanovesicles (DiI/DiD-DELOS nanovesicles).

We are particularly interested in these dyes as they are classified as a well-known Fluorescence Resonance Energy Transfer (FRET) pair[53–55]. FRET is a phenomenon that occurs between two fluorescent molecules by a non-radioactive mechanism. This mechanism is based on a resonant transfer of electronic excitation energy from an excited-state donor fluorophore to a ground-state acceptor molecule[56]. Subsequently, this acceptor molecule will then emit fluorescent light. To ensure that the FRET phenomenon occurs between two molecules, two requirements must be fulfilled:

1. The emission spectrum of the donor molecule must completely or partially overlap with the fluorescence absorption spectrum of the acceptor molecule in order to generate enough energy for dipole-dipole coupling. The extension of the overlap area between these two spectra is related to the efficiency of the phenomenon, a higher overlap leads to a more efficient FRET (**Figure 3.12a**)[56].

1. The distance range between the donor and acceptor fluorophores should typically be between 1 and 10 nm to observe the energy transfer from donor to acceptor, making FRET a highly spatially-responsive optical technique. In most cases, when the distance is greater than about 10 nm, the FRET signal disappears, reading only the emission of the excited molecule (**Figure 3.12b**). Thus, the FRET efficiency is strongly dependent on the spacing of the fluorphores[57].

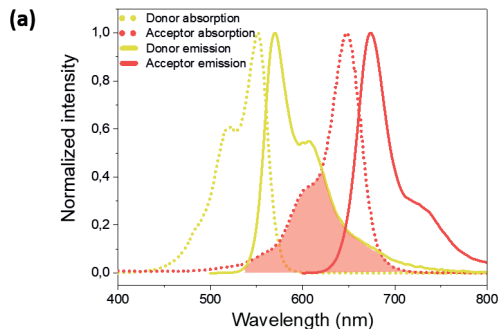

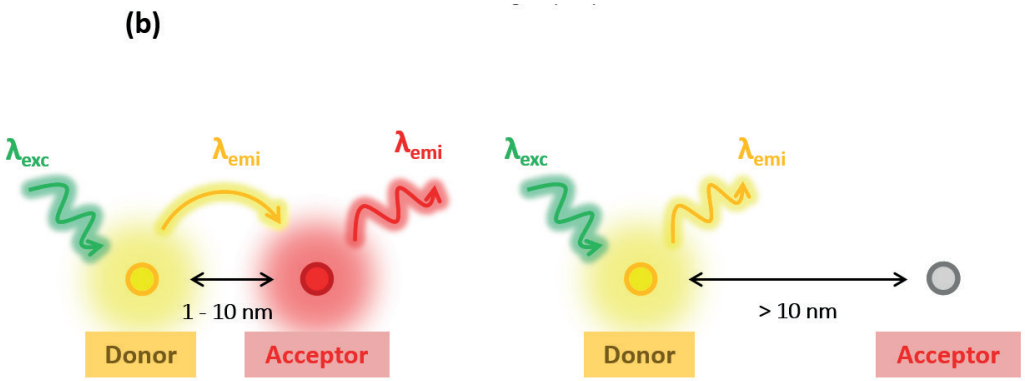

Figure 3.12: **(a) Absorption and emission bands of DiI and DiD in ethanol, with the spectral overlap highlighted in a red region, and (b) Diagram illustrating the relationship between the distance of the dyes and the FRET signal. When the distance between dyes is in the range of 1-10 nm, there is FRET emission, while when the distance increases and becomes greater than 10 nm, the FRET signal vanishes**[58].

Therefore, this spectroscopic tool, also known as a spectroscopic ruler, is very useful to monitor the donor-acceptor FRET pair integrated into the nanovesicle membrane, thus probing the stability and integrity of the nanovesicles. If the FRET emission fluorescence then vanishes, this is an indication of the disruption of the nanovesicles and thus of a spatial separation of DiI and DiD[57,59] (see **Figure 3.13**). Hence, DELOS fluorescent nanovesicles exhibiting FRET offer interesting properties that can be applied in studying their integrity when they are converted into a hydrogel dosage form.

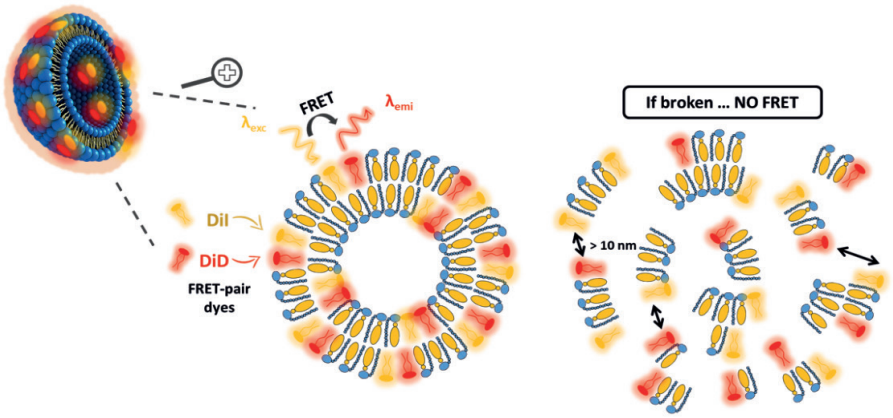

Figure 3.13: Representative scheme of the presence or absence of FRET phenomena in the whole vs dissociate DiI/DiD-DELOS nanovesicles, respectively.

Importantly, DiI and DiD are amphiphilic molecules whose incorporation into the DELOS nanovesicle membrane is driven by hydrophobic interactions and whose leakage, once entrapped at the membrane, is negligible[52,60]. On this basis, to investigate the integrity of DELOS nanovesicles in

the gelled state, DiI/DiD-DELOS nanovesicles were first prepared in water by the DELOS-susp methodology (**see Section 6.2.1**). For this purpose, DiI (50 µM) and DiD (50 µM) were dissolved in ethanol together with the membrane components cholesterol (7.3 mM) and CTAB (7.3 mM) and added to the reactor. Then, the compressed solution was depressurized onto water.

This DiI/DiD-DELOS nanovesicles formulation, as already reported[51], exhibited no differences in the vesicle size and morphology compared to the control sample, which is based on the same nanovesicle formulation but without fluorophores (**Figure 3.14a,b**). Therefore, after preparing the nanoformulations, DiI/DiD-DELOS nanovesicles by DELOS-susp methodology, they were gellified with 2 wt% of Methocel™ K4M (see **Section 6.2.4**) to assess the stability and integrity of the nanovesicles by the fluorescence emission of the dye pair (**Figure 3.14c**).

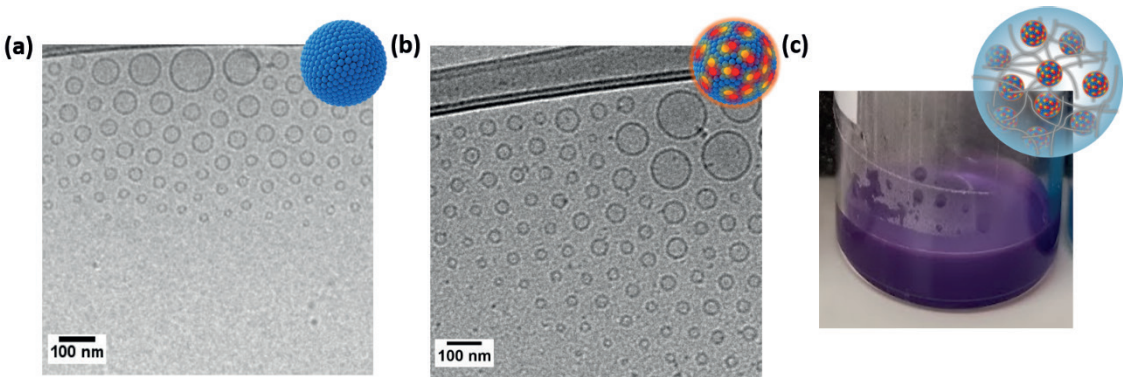

Figure 3.14: Cryo-TEM images of (a) Control sample of DELOS nanovesicles without fluorophores and (b) DiI/DiD-DELOS nanovesicles, in water; (c) Macroscopic image of the DiI/DiD-DELOS nanovesicles-based Methocel™ K4M hydrogel.

Thus, to study the integrity of the DELOS nanovesicles when gellified, absorption spectra of nanovesicles loaded simultaneously with DiI and DiD were first recorded under both conditions, in liquid dispersion and in gel (**Figure 3.15a** and **Section 6.3.6**). Absorption spectra reveal that nanovesicles either in liquid dispersion or in gel maintain DiI and DiD molecules in the nanovesicle nanostructure since no change in the main absorption bands (Abs_{DiI} = 551 nm and Abs_{DiD} = 650 nm) is observed. It is worth noting that DiD is prone to form aggregates like H-dimers, which is generally reported by an increase in the absorption shoulder at 600 nm[51,61]. However, the spectra shown in **Figure 3.15a** points out the absence of these aggregates or other non-monomeric forms of DiD. From this information, we first concluded that nanovesicles appear to maintain their membrane stability when transferred to the gel.

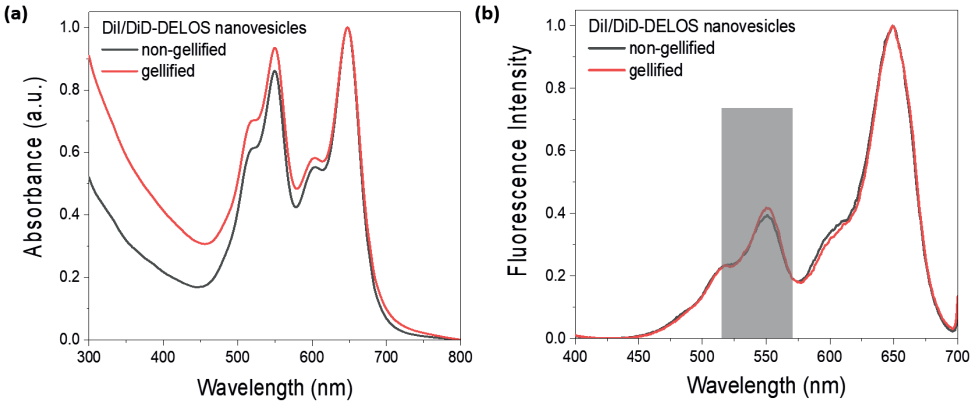

Figure 3.15: (a) Absorption and (b) excitation spectra of gellified (red) and non-gellified (black) DiI/DiD-DELOS nanovesicles.

Secondly, FRET efficiency between DiI and DiD, as a donor and acceptor respectively, was interrogated through excitation and emission fluorescence spectroscopy (see **Section 6.3.7**). Planned comparisons of the gellified and non-gellified groups revealed that the excitation spectra of the dyes are similar among the groups (**Figure 3.15b**). More importantly, excitation spectra also indicated the presence of FRET phenomena since DiI (donor) is excited when probing the DiD (acceptor) emission at λ_{em} = 710 nm (**Figure 3.15b**), highlighted excitation band in grey). Indeed, the FRET efficiency was estimated through the ratiometric approach from emission spectra upon excitation at 490 nm using the following **Equation 3.2**[62]:

$$Efficiency\ FRET\ (E_{FRET},\%) = \frac{Intensity\ DiD}{Intensity\ DiI + Intensity\ DiD} \qquad \textbf{(3.2)}$$

Two emission bands appeared at ~569 and ~673 nm corresponding to the DiI and DiD emission, indicating again that both dyes are stably entrapped at the nanovesicle membrane indistinctly of its medium. The estimation of FRET efficiency in the non-gellified and gellified DiI/DiD-DELOS nanovesicles resulted in similar values of practically 70% (**Figure 3.16**).

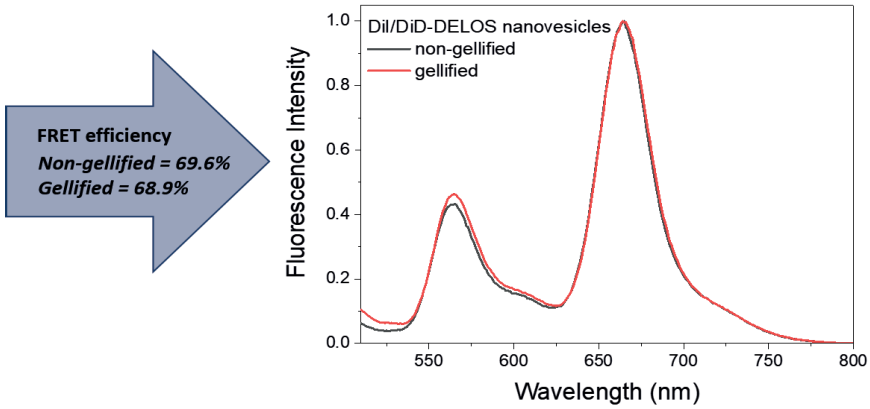

Figure 3.16*:* Emission spectra of gellified (red) and non-gellified (black) DiI/DiD-DELOS nanovesicles with their FRET efficiency value.

Finally, the morphology of DiI/DiD-DELOS nanovesicles-based hydrogel was observed by the cryo-TEM technique. As observed in **Figure 3.17**, this analysis indicated that the morphology of these DELOS nanovesicles was not altered when being gellified with Methocel™ K4M at 2 wt%, suggesting again their stability in the hydrogel.

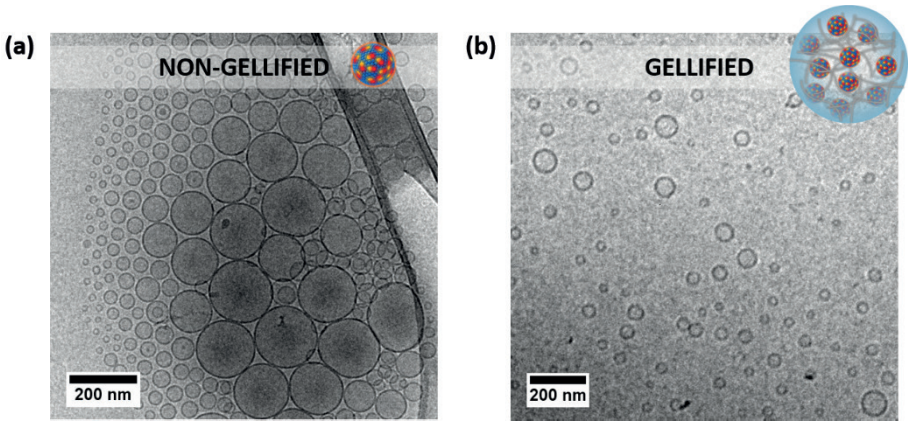

Figure 3.17: Cryo-TEM images of (a) non-gellified and (b) gellified DiI/DiD-DELOS nanovesicles. DiI/DiD-DELOS nanovesicles were prepared using water as the dispersant medium. Gellified nanovesicles were previously diluted 1:100 in water to ensure adequate fixation and preservation of the hydrogel sample in the grid.

Taking all these results together, it becomes clear from the spectroscopic data, but also from the cryo-TEM observation, that the Methocel™ K4M gelling agent does not affect the structure of the DELOS nanovesicles. Thus, we can affirm that spectroscopic measurements of DiI and DiD in nanovesicle-based hydrogels demonstrating the preservation of FRET emission are indicative of membrane integrity.

Finally, DiI/DiD-DELOS nanovesicle-based hydrogels were examined by confocal fluorescence microscopy to assess the distribution of the two dyes in the hydrogel (described in **Section 5.3.11**). During the analysis, DiI and DiD emission signals were recorded showing colocalization of the two dyes, meaning an overlap of them in the final image due to their close position in the structure. As shown in **Figure 3.18,** there is a significant presence of yellow dots representing the colocalization of the two dyes used, DiI (in green) and DiD (in red), in the same region. This phenomenon emphasizes that the two dyes associate with the same vesicle structure, again representing the integrity of the vesicles when gellified with 2 wt% Methocel™ K4M. Furthermore, the magnification of the confocal image reveals the abundance of dispersed particles with a particle size smaller than 1 µm, suggesting that DELOS nanovesicles are mostly not aggregated in the hydrogel.

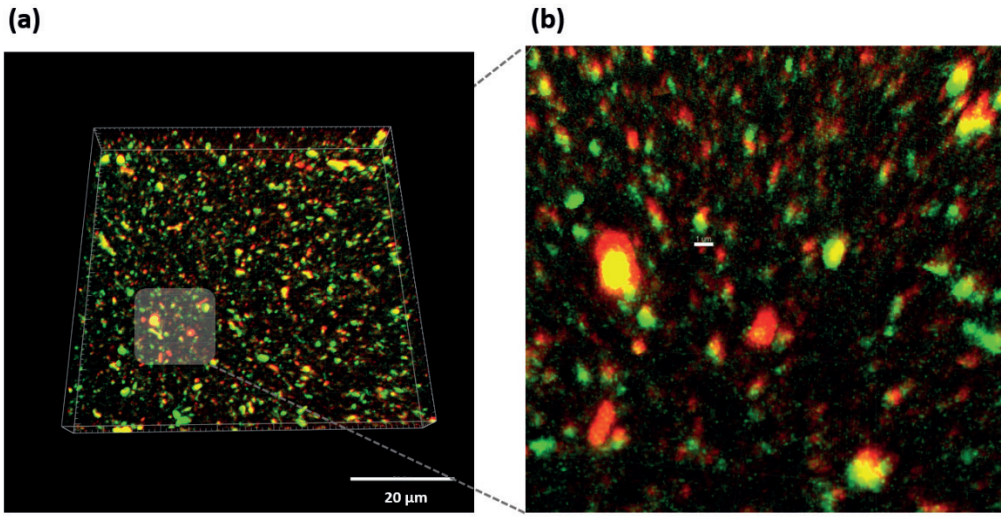

Figure 3.18: Colocalization analysis of DiI and DiD in DiI/DiD-DELOS nanovesicle-based Methocel™ K4M hydrogel by confocal imaging, DiI/DiD-DELOS nanovesicles were prepared using water as dispersant medium. (a) General view of the overlay images of excited DiI with 488 nm light (in green) and DiD with 633 nm light (in red). The yellow color represents the colocalization of the two dyes, indicating the presence of the two dyes in an unaltered vesicle; (b) Magnification of the grey box revealing the abundance of particles smaller than 1 µm, indicating the homogeneous dispersion of DELOS nanovesicles in the hydrogel.

Overall, it is worth noting that all of these experimental results go beyond the extensive literature and demonstrate the integrity of the DELOS nanovesicle formulations when being gellified, which is an important finding for understanding their behavior.

3.2.2.5 Evaluation of the *in vitro* protein-specific bioactivity to evaluate the potentiality of rhEGF-DELOS nanovesicles as a semi-solid dosage form

Once confirmed the integrity of the DELOS nanovesicles when gellified with 2 wt% of Methocel™ K4M, the most promising hydrogelling agent concentration for preparing Methocel™ K4M DELOS nanovesicles-based hydrogels, we further evaluated its use in gellifying rhEGF-DELOS nanovesicles. Once the hydrogel was prepared by mixing the rhEGF-DELOS nanovesicles suspension (**Table 2.5**) with 2 wt% of Methocel™ K4M (see **Section 6.2.4**) and presenting proper macroscopical appearance (**Figure 3.19a**), the rhEGF-DELOS nanovesicle integrity was also characterized by cryo-TEM. As observed in **Figure 3.19b,c**, it was confirmed that the morphology of rhEGF-DELOS nanovesicles was not altered when being gellified using this formulation. Therefore, it suggests the stability and integrity of rhEGF-DELOS nanovesicles in the hydrogel, which is an important finding in understanding their behavior.

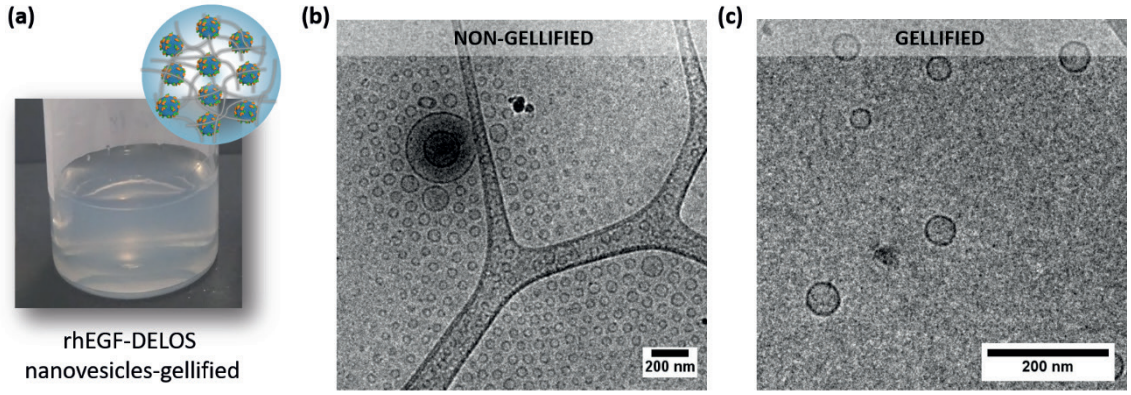

Figure 3.19: (a) Macroscopic image of rhEGF-DELOS nanovesicle-based hydrogel using buffer histidine (5 mM, pH 7.0)/10% EtOH ($v \cdot v^{-1}$) as dispersant medium, and cryo-TEM images of (b) non-gellified and (b) gellified rhEGF-DELOS nanovesicles with 2 wt% of Methocel™ K4M. Gellified nanovesicles were previously diluted 1:100 in water for an adequate fixation and preservation of the hydrogel sample in the grid.

After confirming the integrity of rhEGF-DELOS nanovesicles upon hydrogelation with 2 wt% Methocel™ K4M, another step towards a semi-solid dosage form as a new pharmaceutical product with proper performances was the evaluation of the rhEGF-specific bioactivity in gellified rhEGF-DELOS nanovesicles.

For this purpose and thanks to the collaborators of CIGB in Cuba, *in vitro* measurements were performed to compare free and integrated rhEGF in DELOS nanovesicles both in liquid dispersion and in gel form. However, prior to the experiment, it was evaluated whether the hydrogelling agent Methocel™ K4M could interfere with the rhEGF colorimetric assay for determining the biological activity of the rhEGF. A placebo hydrogel (without both free rhEGF

and nanovesicles) and a hydrogel containing Blank-DELOS nanovesicles (**Table 2.5**) were tested at the same minimum dilution of 1:10,000 as the minimum dilution used to evaluate rhEGF hydrogels. In addition, the minimal control of rhEGF used in the colorimetric assay, in which cells are incubated with culture medium only, was used as a comparison to assess the differences in the data. Then, when comparing the absorbance at 578 nm, no statistically significant differences were observed between the three different groups evaluated (N = 10 per group, ANOVA p-value = 0.740) (see **Section 6.4.2**), confirming that Methocel™ K4M does not affect the colorimetric assay.

Figure 3.20 shows the results of *in vitro* specific biological activity of all tested samples, free and integrated rhEGF in DELOS nanovesicles in both liquid dispersion and gellified. As shown, non-significant statistical differences were observed for the free rhEGF in dispersion medium and its hydrogel formulation, then the protein's biological activity was preserved when gellified. However, the specific bioactivity of the aqueous dispersion and hydrogel of rhEGF-DELOS nanovesicles increased compared to the aqueous solution of free rhEGF and its hydrogel formulation.

These results are consistent with previously reported rhEGF-DELOS nanovesicles in **Chapter 2**, in which higher cell proliferative activity than free rhEGF was obtained at the same bulk concentration[63]. On the other hand, the specific bioactivity of the hydrogel-based on rhEGF-DELOS nanovesicles increased statistically significantly compared to the aqueous solution of the same rhEGF-DELOS nanovesicles (**Figure 3.20**). Since there is no change in specific bioactivity for the free rhEGF in aqueous solution compared to the hydrogel formulation, a plausible reason for the increase in specific bioactivity of rhEGF-DELOS nanovesicles gellified as compared to the aqueous solution could be the stability of the binding of rhEGF to the nanovesicles surface area increased in the presence of Methocel™ K4M. It is likely that the nanoconjugate is more stable upon dilution in the presence of Methocel™ K4M at the large dilutions (>1:10,000 for 100 $\mu g \cdot mL^{-1}$ of rhEGF) used in the cell proliferation assay. Recently we have no experimental evidence for this finding and further studies will be necessary to elucidate the reasons for the increased specific biological activity of rhEGF-DELOS nanovesicles in the Methocel™ K4M hydrogel compared to the aqueous dispersion.

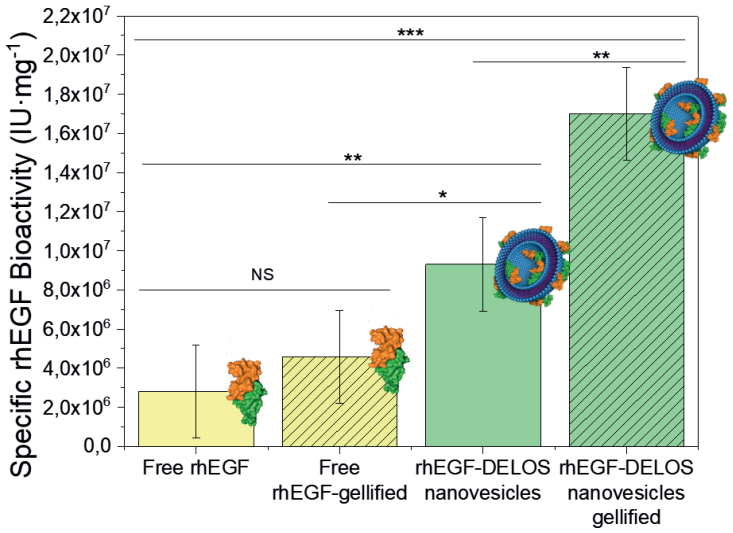

Figure 3.20: ***In vitro*** specific biological activity of free rhEGF and rhEGF-DELOS nanovesicles in a cell proliferation assay in 3T3 A43 murine fibroblast cell line. Free rhEGF and rhEGF-DELOS nanovesicles 100 µg·mL^{-1} were formulated in aqueous solution or in Methocel™ K4M hydrogel, performed by CIGB team from Cuba. Data plotted as mean (N = 3 per group) specific bioactivities are represented by the height of the bars with 95% confidence intervals represented by the error bars. Statistical analyzes were performed by one-way ANOVA followed by Tukey pairwise comparison. *p < 0.05, **p < 0.01, ***p < 0.001 and NS: non-significant differences.

Summarizing, the development of rhEGF-DELOS nanovesicle-based hydrogels using 2 wt% Methocel™ K4M has presented several and important advantages thereof, such as not only ensuring the integrity and stability of the nanoformulation, but also achieving adequate rheological properties for the intended use. It is worth noting here that the bioactivity of the rhEGF, when formulated as rhEGF-DELOS nanovesicle-based hydrogels, has shown a significant increase, probably due to the stabilization of the binding of rhEGF to the surface of the nanovesicles in the presence of Methocel™ K4M, confirming the therapeutic potential of rhEGF-DELOS nanovesicle-based hydrogels as a pharmaceutically significant drug product for complex wound treatments.

3.2.3 Summary of the section

The outcome of the development of a final dosage form of rhEGF-DELOS nanovesicles led to different conclusions. First, convenient dosage forms were developed to facilitate the topical administration of rhEGF-DELOS nanovesicles, consisting of the suspension administered by both a spray device and a 2 wt% Methocel™ K4M hydrogel containing rhEGF-DELOS nanovesicles. Consequently, gaseous and semi-solid dosage forms have been considered as future potential dosage forms for the topical treatment of complex wounds such as DFUs and VLUs.

Furthermore, it should be highlighted that FRET fluorescence measurements and cryo-TEM imaging verified the integrity of the nanoformulation upon gelation. In both cases, it was confirmed that DELOS nanovesicles maintain their stability in the semi-solid form, which is a relevant factor to consider for the effectiveness of the formulation and that is not widely considered in the literature.

3-3 Development of new DELOS nanovesicle formulations and pharmaceutical hydrogel dosage forms for topical administration

After observing the promising results in the development of a final drug product based on rhEGF-DELOS nanovesicles for topical administration, e.g., for the treatment complex wounds, this framework provided a platform for further research and application. Therefore, it was an inspiration and a starting point for the company and the research group to further improve the DELOS platform and have a wider range of potential DELOS nanovesicle formulations suitable for topical administration.

To this end, in the present study, we report the development of new and promising well-tolerated DELOS nanoformulations by first exploring the preparation and characterization of the nanoformulations using different surfactants and dispersant media for those that have fewer concerns about skin tolerance and thus a greater skin acceptance for topical delivery. Afterwards, we transformed these new liquid dispersions of DELOS nanovesicles into new semi-solid dosage forms for being used as more efficient carriers for topical drug delivery.

3.3.1 Development of DELOS nanovesicle suspensions with different surfactant counterions and dispersant media

3.3.1.1 CTAC: an interesting alternative to CTAB surfactant

There are several ways to improve the DELOS nanoformulations for topical applications. One of the easiest ways to do this is to study the potential impact of different compositions on the nanovesicles, for example, by changing the membrane components of the nanoformulation such as the quaternary ammonium surfactant. In the formulation based on rhEGF-DELOS nanovesicles, described in **Chapter 2**, the chosen surfactant was CTAB, which consists of a 16-carbon hydrophobic chain with a charged polar ammonium head and bromide as a counter ion (**Figure 3.21a**).

It is important to note that CTAB is a surfactant widely used in several cosmetic products and has demonstrated antibacterial properties that can play an important role in skin formulations to prevent wound infections[64–66]. However, the approach proposed here is based on the use of a similar surfactant with chloride as counter ion (the major ion in the human body) named

hexadecyltrimethylammonium chloride (CTAC) (**Figure 3.21b)**, which has also been demonstrated to possess an antimicrobial activity. The medical regulatory agency FDA has approved CTAC for topical[67], and reported that this ingredient is commonly found in lotions at 0.2 wt%, indicating its safety at this concentration[68–70]. Besides, it should be noted that previous work has shown that cationic surfactants nanostructured in nanovesicles broadly reduced their potential irritation effect[63].

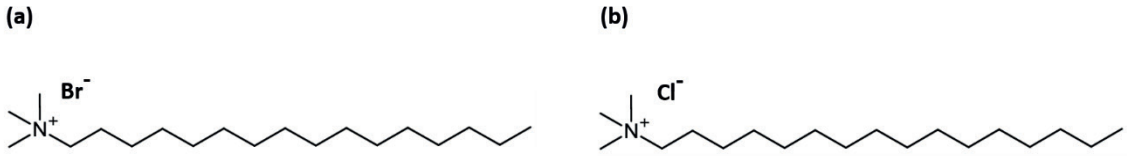

Figure 3.21: Chemical structure of (a) CTAB and (b) CTAC surfactant.

Therefore, assessing the effect of the chloride as the counter ion in DELOS nanovesicle production would allow the generation of a new DELOS nanovesicle formulation, as another possible optimum alternative for dermal drug delivery.

3.3.1.2 Screening of dispersant medium for DELOS nanovesicles production

On the other hand, it is important to emphasize that, in addition to the composition of the vesicle itself, dispersant medium is an important subject of study, since it is crucial to provide stability to the formulation, which must safeguard biocompatibility and be suitable for topical administration. Therefore, besides the surfactant nature, various dispersant media in the DELOS nanovesicle systems were evaluated according to the need to strive for better skin compatibility of the nanoformulations. Five dispersant media were selected: water; sodium citrate buffer (citrate buffer), pH = 5.0; sodium acetate buffer (acetate buffer), pH = 5.0; histidine buffer, pH = 7.0; and phosphate-buffered saline (PBS), pH = 7.4.

All buffers were prepared at a concentration of 5 mM to compare all of them to the buffer used in the previously reported rhEGF-DELOS nanovesicle nanoformulation in **Chapter 2**, which was histidine buffer (5 mM, pH = 7.0), for complex wound healing[63]. Then, to understand in better detail the dispersant media used, they are listed below.

1. **Water**: It was used as a reference medium and as a model to prepare DELOS nanovesicle formulations[71,72].
1. **Acetate buffer (5 mM, pH = 5.0):** It contains 1.63 mM of acetic acid and 3.36 mM of sodium acetate, an interesting molecule associated with esterase metabolites present in the skin and therefore widely used as a fragrance in cosmetics and as a buffering agent due to its skin tolerance[73].

1. **Citrate buffer (5 mM, pH = 5.0):** This buffer contains 2.91 mM of sodium citrate and 2.09 mM of citric acid, which is a metabolic substance found in animals and plants. Its pH is 5.0, which corresponds to healthy skin's pH[74–76]. It is used in cosmetics not only as a cheating agent but also as a pH adjuster, and as a fragrance. Sodium citrate buffer up to 5% $w \cdot v^{-1}$ in aqueous solution is reported to be non-irritating to skin and suitable for skin diseases and wound healing treatment[76–80].

1. **Histidine buffer (5 mM, pH = 7.0):** It is an essential and neutral amino acid that exhibits anti-inflammatory and antioxidant properties. It has been used as a therapy to treat some skin diseases like atopic dermatitis and can easily be combined with proteins or other amino acids and treated as a supplement for a variety of disorders[81,82]. Furthermore, recent results suggest that L-histidine has the potential to facilitate wound healing in both *in vitro* and *in vivo* models of aging skin[83]. Simultaneously, this medium was used in rhEGF-DELOS nanovesicle conjugates for the treatment of complex wounds[63,84], as previously described in **Chapter 2**.

At the same time, histidine buffer has also been described as the most common buffer of commercially available protein therapeutics, such as antibody formulations, with histidine concentrations ranging from 3 mM to 50 mM and pH = 5.5-6.5[85–87]. Consequently, this buffer is convenient when a pH close to 7.0 is required for the treatment of a skin disorder.

1. **Phosphate Buffered Saline (5 mM, pH = 7.4):** This is a commonly used buffer in biological research based on a saline solution containing sodium chloride (NaCl), sodium hydrogen phosphate (Na_2HPO_4) and sodium phosphate monobasic (NaH_2PO_4) which balances the salt concentration around the cells, prevents osmosis and is therefore suitable for skin applications[88]. Among all PBS recipes, in this Thesis we used PBS consisting of 4.80 mM of NaCl, 0.15 of Na_2HPO_4 and 0.05 mM NaH_2PO_4.

3.3.1.3 Preparation of new DELOS nanovesicles formulations for topical administration

To assess all parameters previously described, DELOS nanovesicles were prepared using the eco-efficient DELOS methodology (see **Section 6.2.1**). With this in mind, in this investigation we attempted to evaluate a wide range of possible nanoformulations for being used in topical drug delivery as summarized in **Table 3.6**.

Table 3.6: Overview of the membrane components and dispersant media tested in the DELOS nanovesicles formulations under study.

Vesicle membrane components	Dispersant medium[1]
Cholesterol:CTAB (CTAB-DELOS nanovesicles)	Water pH *ca.* 7.0 Sodium citrate buffer (5 mM, pH = 5.0) Sodium acetate buffer (5 mM, pH = 5.0) Histidine buffer (5 mM, pH = 7.0) PBS buffer (5 mM, pH = 7.4)
Cholesterol:CTAC (CTAC-DELOS nanovesicles)	Water pH *ca.* 7.0 Sodium citrate buffer (5 mM, pH = 5.0) Sodium acetate buffer (5 mM, pH = 5.0) Histidine buffer (5 mM, pH = 7.0) PBS buffer (5 mM, pH = 7.4)

[1] All the samples contain 10% v·v^{-1} of EtOH.

As shown in **Table 3.6**, 10 different nanoformulations were prepared in this work, performing replicates of each of them. In all cases, the final concentration of the membrane components was the same as the optimal intermediate product obtained for rhEGF-DELOS nanovesicles, which was 7.3 mM of each compound (cholesterol and surfactant) with a theoretical equimolar ratio between cholesterol and surfactant (**Table 2.5**). It should be noted that all DELOS nanoformulations contain 10% v·v^{-1} of ethanol from the DELOS-susp process. The presence of this amount of EtOH can be beneficial since it is known for its positive value as an enhancer for skin treatments[89].

Particle size and PDI of the nanoformulations were evaluated using DLS over time. From **Figure 3.22**, it can be observed that planned comparisons of the use of CTAB and CTAC surfactant in the DELOS nanovesicle formulations revealed that both surfactants lead to similar mean nanovesicle size in the different evaluated dispersant media. Additionally, proper colloidal stability of the nanovesicles was observed regarding the screening of dispersant media based on water; acetate buffer (5 mM, pH 5.0); histidine buffer (5 mM, pH = 7.0); and PBS buffer (5 mM, pH = 7.4).

As can be seen in **Figure 3.22**, for all nanoformulations there was a tendency for the mean particle size to decrease during the first week and to stabilize over at least one month, the period studied. This size trend and the great stability of this type of vesicular system have already been shown in **Chapter 2** and described in detail in our Nanomol Group. It could be hypothesized that this tendency to decrease in particle size over time correlates with the thermodynamic aspects of the vesicles. DELOS nanovesicles have been shown to be dynamic systems that evolve to an equilibrium state over time by minimizing the free energy of the system through the formation of small and energetically stabilized vesicles[90]. For instance, an extreme long-term stability of at least 1000 days at 4 °C for CTAB-DELOS nanovesicles in water with 10% v·v^{-1} of EtOH has already been demonstrated[91].

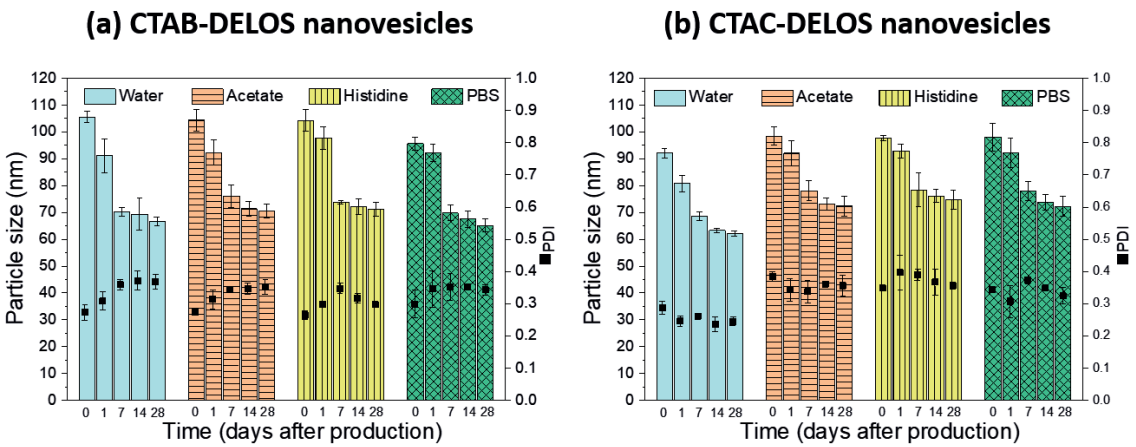

Figure 3.22: (a) Evolution of CTAB-DELOS nanovesicles and (b) CTAC-DELOS nanovesicles over time on particle size and polydispersity index (PDI) with the effect of different dispersant media: water (blue); acetate buffer (5 mM, pH = 5.0) (orange, horizontal line); histidine buffer (5 mM, pH = 7.0) (yellow, vertical line); and PBS buffer (5 mM, pH = 7.4) (green, square).

Conversely, the use of citrate buffer (5 mM, pH = 5.0) was the only notable exception in this study, as it showed immediate sedimentation of vesicle membrane components in all formulations after one day of production (**Figure 3.23**).

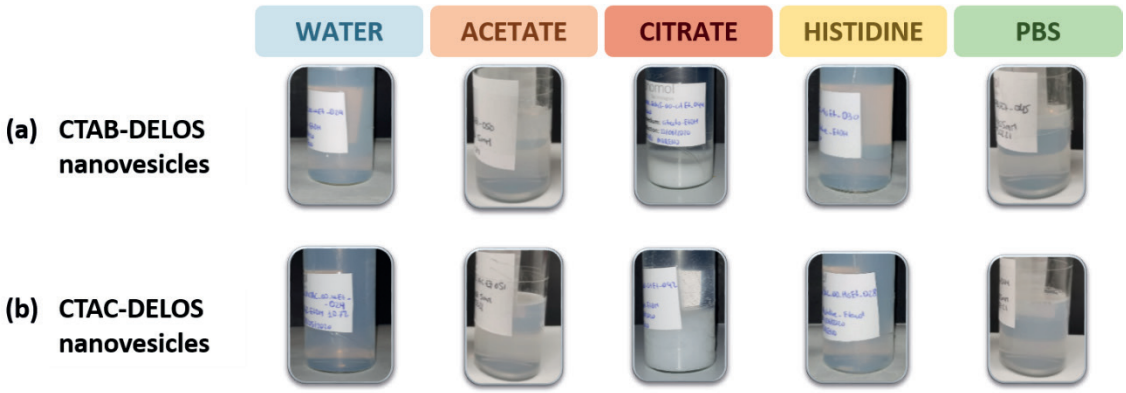

Figure 3.23: Macroscopic appearance of (a) CTAB-DELOS nanovesicles and (b) CTAC-DELOS nanovesicles in water (blue); acetate buffer (5 mM, pH = 5.0) (orange); citrate buffer (5 mM, pH = 5.0) (red); histidine buffer (5 mM, pH = 7.0) (yellow); and PBS buffer (5 mM, pH = 7.4) (green).

This phenomenon was also detected by the zeta potential measurement, which indicates the degree of repulsion between the charged particles in the dispersion, as explained in **Chapter 2**. It is important to know that high positive and negative zeta potential values, i.e., > +30 mV or < –30 mV, indicate highly charged particles, avoiding particle aggregation due to electrical repulsion. However, at a small zeta potential value between +30 mV and –30 mV, attraction overcomes repulsion and the sample is expected to first aggregate and then evolve to sedimentation[92]. Zeta

potential measurements of all obtained nanoformulations are displayed in **Figure 3.24**. As shown, all nanoformulations prepared with water, acetate, histidine, and PBS buffers present a zeta potential value above +100 mV, although in acetate and PBS, a quite lower zeta potential value compared to histidine and water was observed for both CTAB- and CTAC-DELOS nanovesicles (**Figure 3.24**). However, when these vesicles were prepared in citrate buffer, they showed a zeta potential value below +30 mV. This interesting finding may indicate that there was a strong electrostatic interaction between the positive charge of the quaternary ammonium surfactant and the negative charge of the citrate molecule, which hindered vesicle formation and caused aggregation and sedimentation of the system. Therefore, in this work, the formation of CTAB- and CTAC-DELOS nanovesicles using citrate buffer (5 mM, pH = 5.0) as the medium was discarded.

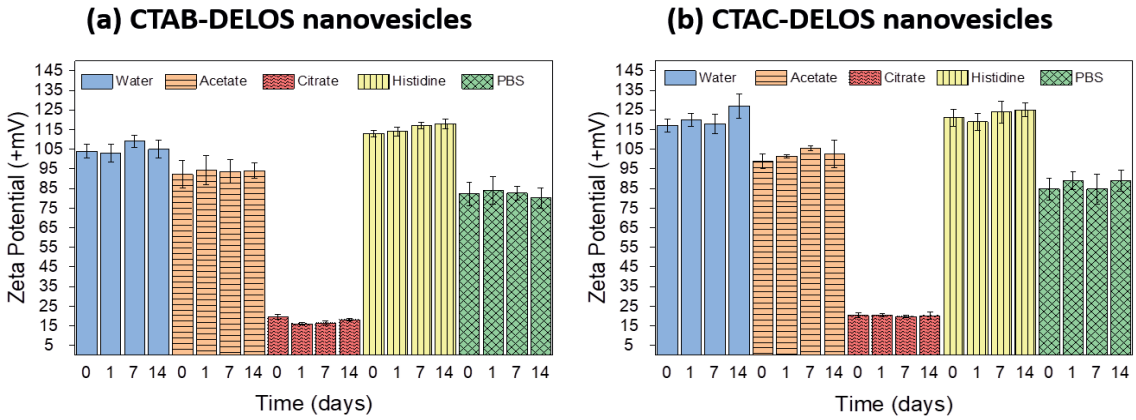

Figure 3.24: Evolution of (a) CTAB-DELOS nanovesicles and (b) CTAC-DELOS nanovesicles over time on the zeta potential values with the effect of different dispersant media: water (blue); acetate buffer (5 mM, pH = 5.0) (orange, horizontal line); citrate buffer (5 mM, pH = 5.0) (red, waves); histidine buffer (5 mM, pH = 7.0) (yellow, vertical line); and PBS buffer (5 mM, pH = 7.4) (green, square).

Regarding the size and morphology of the obtained nanovesicles, they were also examined using cryo-TEM. Similarly shaped nanovesicles were observed as seen in **Figure 3.25** in the prepared CTAB- and CTAC-DELOS nanovesicle formulations in water, acetate, histidine, and PBS buffers. It is remarkable to appreciate that there are almost no variation differences in the morphology of the vesicles when neither the surfactant, CTAB or CTAC, nor the dispersant medium are changed. In fact, most of the vesicles are homogeneous unilamellar nanovesicles with spherical morphology, ranging in size between 50 and 100 nm in diameter, consistent with the results reported in the literature by our Nanomol Group and Nanomol Technologies SL[63,93–95].

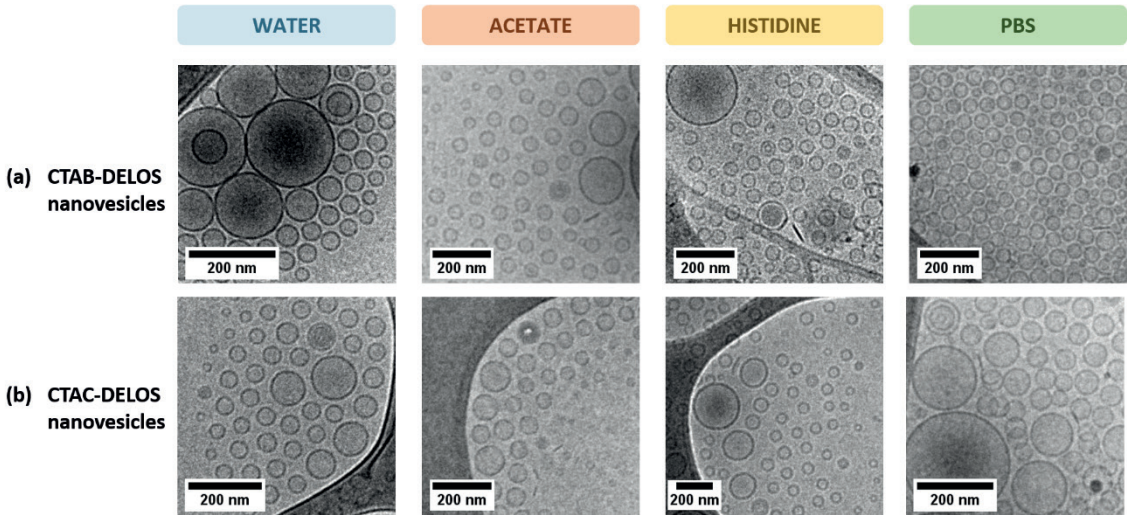

Figure 3.25: Cryo-TEM images of (a) CTAB-DELOS nanovesicles and (b) CTAC-DELOS nanovesicles in different dispersant media: water (blue); acetate buffer (5 mM, pH = 5.0) (orange); histidine buffer (5 mM, pH = 7.0) (yellow); and PBS buffer (5 mM, pH = 7.4) (green).

Thanks to these favorable physicochemical properties of DELOS nanovesicles, we can propose that either the use of CTAB or CTAC surfactant with bromide or chloride counterion respectively, and the presence of water; or acetate; histidine; or PBS buffers in the nanoformulation are promising components to formulate DELOS nanovesicle liquid dispersions that are more tolerable for skin application. It should be emphasized that these nanoformulations have the potential to be translated into other types of treatments that require these formulation properties in terms of pH or composition.

3.3.2 Designing novel DELOS nanovesicles hydrogels dosage forms

As already explained, the formulation of a drug product includes due consideration of each component used in the final product, such as the physicochemical and biological properties to achieve proper patient compliance[96]. In this case, considering that CTAB-DELOS nanovesicles with and without integrating rhEGF in histidine buffer (5 mM, pH = 7.0) are compatible with hydrogelling agents such as Methocel™ K4M, it is also relevant to determine if and into what extent the presence of the new prepared formulations of DELOS nanovesicles can be gelled. Then, CTAB- and CTAC- DELOS nanovesicles in the different dispersing media tested: water, histidine buffer (5 mM, pH = 7.0), acetate buffer (5 mM, pH = 5.0) and PBS buffer (5 mM, pH = 7.4) were evaluated when gelled with Methocel™ K4M polymer.

Furthermore, this study led to the introduction of other innovative hydrogelling agents besides the Methocel™ K4M to expand the possibilities to generate new DELOS nanovesicle-based hydrogels for many other routes of administration. Therefore, an alternative polymer called Poloxamer 407 was also explored.

3.3.2.1 Methocel™ K4M-based hydrogels

Preparation and physicochemical characterization of DELOS nanovesicles-based Methocel™ K4M hydrogels

Following the same methodology as described in **Section 3.2.2.3**, the most promising formulations mentioned above-CTAB- and CTAC-DELOS nanovesicles dispersed in water, acetate, histidine, and PBS- were gelled and evaluated using 2 wt% Methocel™ K4M (see details in **Section 6.2.4**). Note that the use of 2 wt% hydrogelling agent was a predefined value as previous results described in this Chapter indicated that this was the most promising in terms of physicochemical properties for rhEGF-DELOS nanovesicles final drug product and also a concentration commonly used for topical formulations[37].

As previously described, in order to assess the response to translation of the liquid DELOS nanovesicles dispersion into a semi-solid hydrogel dosage form, there were several important considerations. First, Methocel™ K4M-based hydrogels were examined macroscopically. Colorless and homogeneous semi-solid formulations with appropriate consistency were obtained, thus showing excellent organoleptic properties.

To further evaluate the formulated hydrogels, they were then examined by optical microscopy (**Section 6.3.9**). **Figure 3.26** illustrates the microscopic appearance of the hydrogels using the different quaternary ammonium surfactants and dispersant media. Hydrogels enriched with DELOS nanovesicles dispersed in water or histidine medium showed no change in microscopic appearance. However, micron-sized particles were observed in the semi-solid formulations enriched with DELOS-nanovesicles containing sodium acetate and PBS. This is probably related to the negative charge of acetate and phosphate anions of these buffers and their electrostatic interactions with the cationic surface charge of the DELOS nanovesicles, as evidenced by the small decrease in zeta potential of both CTAB- and CTAC-DELOS nanovesicles in acetate and PBS dispersant media (**Figure 3.24**).

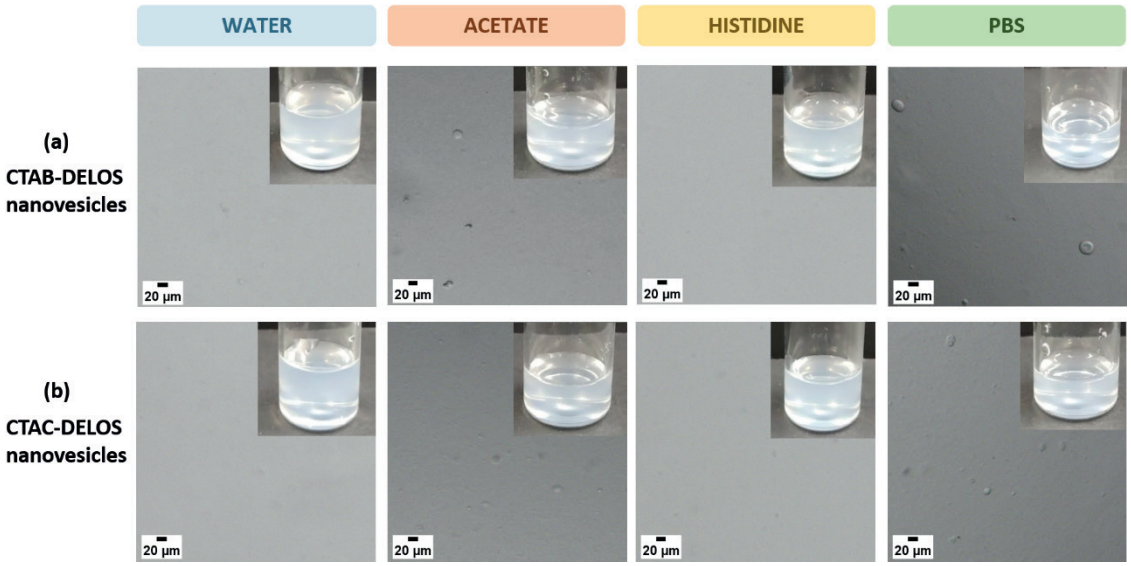

Figure 3.26*:* Optical microscopy and macroscopic images of Methocel™ K4M hydrogels of (a) CTAB-DELOS nanovesicles and (b) CTAC-DELOS nanovesicles in different dispersant media: water (blue); acetate buffer (5 mM, pH = 5.0) (orange); histidine buffer (5 mM, pH = 7.0) (yellow); and PBS buffer (5 mM, pH = 7.4) (green).

Moving to a deeper evaluation of hydrogels, the viscosity profile of the hydrogels is a key feature related to the polymeric network and the strength of the interactions of the components, as stated before. Then, the viscosity and rheological measurements performed on the formulated hydrogels based on DELOS nanovesicles provided important information about the three-dimensional network properties, which were influenced by the presence of different surfactant counterions and dispersant media (see **Section 6.3.10**). The viscosity of the control hydrogels (without DELOS nanovesicles) showed no statistically significant differences between the different dispersant media evaluated (ANOVA p-value = 0.300) (**Figure 3.27**).

Viscosity measurements helped to understand the behavior of the hydrogels when containing DELOS nanovesicles. As can be seen in **Figure 3.27**, changes in the dispersant medium of the CTAB- and CTAC-DELOS nanovesicles led to different viscosity values of the obtained hydrogels. The use of water and histidine buffer (5 mM, pH = 7.0) in the hydrogels showed similar results with the presence and absence of DELOS nanovesicles with statistically insignificant differences.

However, it was also apparent that the addition of salts such as acetate buffer (5 mM, pH = 5.0), and PBS buffer (5 mM, pH = 7.4) provided a statistically significant increase in viscosity compared to the control. This increase could be related to the ability of these salts (probably the presence of acetate and phosphate anions) to induce the presence of micrometric particles in the original formulation of DELOS nanovesicles, as already observed microscopically (**Figure 3.26**).

It is reported that semi-solid dispersions with a constant solids volume fraction can differ in viscosity due to differences in particle size and PDI[97]. Changes in viscosity can also provide information about intermolecular interactions[98]. Regarding the use of the two different quaternary ammonium surfactants, CTAB or CTAC, in the nanovesicle formulation when being gellified, no differences in viscosity were found.

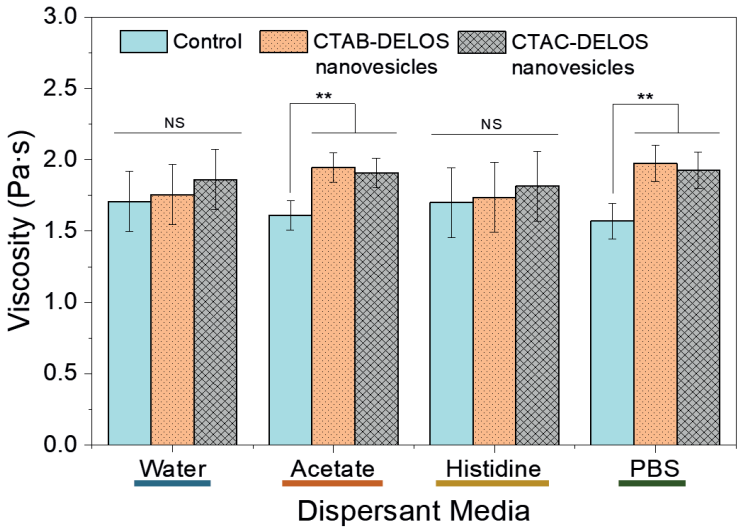

Figure 3.27: Viscosity measurements of the evaluated Methocel™ K4M hydrogels, controls (samples without the nanovesicles, blue), and DELOS nanovesicle-based hydrogels using CTAB- (orange, dots) or CTAC-DELOS (grey, squares) nanovesicles in water, acetate, histidine, and PBS (N = 3). Data plotted as mean viscosity is represented by the heights of the bars with 95% confidence intervals represented by the error bars. Statistical analyzes were performed by one-way ANOVA followed by Tukey pairwise comparison. **$p < 0.01$ and NS: non-significant differences.

Focusing on the viscosity value of the hydrogels, we can observe that all the hydrogels present a value consistent with the value obtained with Methocel™-based hydrogels containing rhEGF-DELOS nanovesicles (**Table 3.5**), which are values similar to those reported in the literature for topical formulation products[43].

On the other hand, the rheological characterization of the developed DELOS nanovesicle-based hydrogel formulations was also assessed. The flow curves of the Methocel™ K4M hydrogels based on DELOS nanovesicles revealed a non-Newtonian pseudoplastic flow behavior. **Figure 3.28** displays the shear stress versus shear rate for all the prepared DELOS nanovesicle-based Methocel™ K4M hydrogels. In all cases, non-Newtonian model of pseudoplastic flow behavior was observed, as shown similarly in **Section 3.2.2.5** with Methocel™ K4M-based hydrogels containing rhEGF-DELOS nanovesicles. As previously explained, this is due to the reversible deformation of the hydrogel together with increasing force velocity in terms of shear rate[48]. It is important to mention again that

this is a desirable property for topical products as it indicates that the product can be spread easily under mild forces, allowing film formation on the skin's surface.

In addition, little or no thixotropy was observed in all samples, which presented a small or null hysteresis loop area. Furthermore, no effect on rheological behavior was found when hydrogels contained CTAB or CTAC, or the different dispersant media.

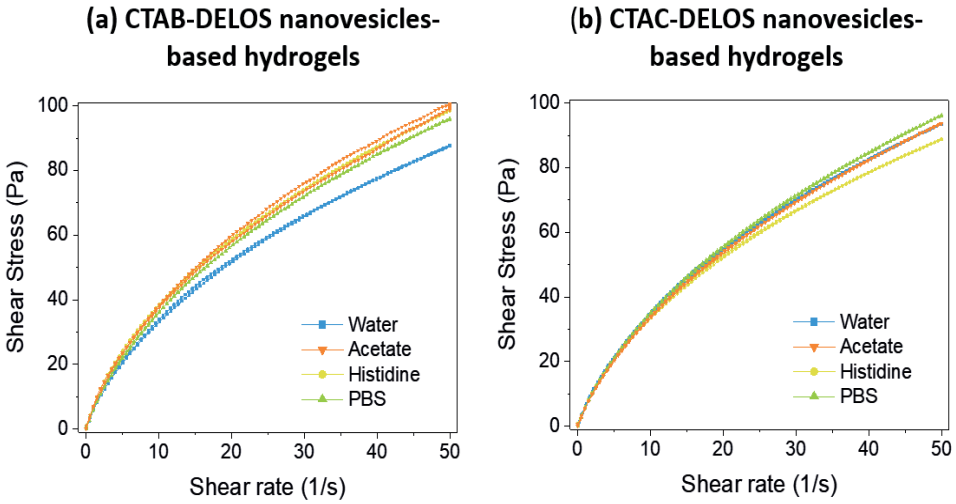

Figure 3.28: Shear rate as a function of shear stress of hydrogels enriched with (a) CTAB-DELOS nanovesicles and (b) CTAC-DELOS nanovesicles in different dispersant media: water (blue ■); **acetate buffer (5 mM, pH = 5.0) (orange ▼); histidine buffer (5 mM, pH = 7.0) (yellow ●); and PBS buffer (5 mM, pH = 7.4) (green ▲).**

The results of this study allow concluding that there exists a complete suitability and feasibility of novel DELOS nanovesicles as a semi-solid dosage form for topical administration. Then, these liquid dispersions were gellified for the first time by adding 2 wt% Methocel™ K4M obtaining DELOS nanovesicles-based hydrogels with good macroscopic appearance and appropriate rheological properties for the intended use. However, the presence of particles in the micrometric range was observed under optical microscopy in those semi-solid formulations that contained sodium acetate and PBS buffers, probably related to the presence of acetate and phosphate anions and its potential electrostatic interaction with the cationic surface charge of the nanovesicles. This change of particle size distribution was correlated with a significant viscosity increase of these formulations.

Therefore, Methocel™ K4M hydrogels containing CTAB- and CTAC- DELOS nanovesicles formulated in water and histidine buffer (5 mM, pH = 7.0) will be selected as the optimal ones in future studies. They have been demonstrated to be the most promising systems as they show advances in stability over the other studied DELOS nanovesicles-based hydrogels containing acetate (5 mM, pH 5.0) and PBS buffer (5 mM, pH 7.4).

3.3.2.2 Poloxamer as new polymer for converting DELOS nanovesicles suspension to hydrogels semi-solid form

As already mentioned in the previous section, the findings on the preparation of Methocel™ K4M hydrogels containing DELOS nanovesicles have made an important contribution to the field of converting DELOS nanovesicles into a new suitable semi-solid dosage form for topical administration. Since most of the current evidence for the preparation of DELOS nanovesicle hydrogels supports the use of non-ionic hydrogelling agents, this study also provided some important insights into another approach to expand the possibility of converting DELOS nanovesicle suspensions into a semi-solid dosage form and so, expand the company's product portfolio of DELOS nanovesicle final dosage forms.

Among the non-ionic hydrogelling agents found in the market, Poloxamer is an interesting polymer that has been proposed for various pharmaceutical applications such as parenteral, oral, subcutaneous, ophthalmic, rectal and topical administration[99–101]. This polymer is based on block polymers of ethylene oxide and propylene oxide conforming to the general formula shown in **Figure 3.29** and to date it is considered to be biodegradable, non-toxic and a stable material accepted and listed in the US and European Pharmacopeia. In addition, the registered trademarks of these copolymers may be Pluronic and Synperonic, among other names[99,101,102].

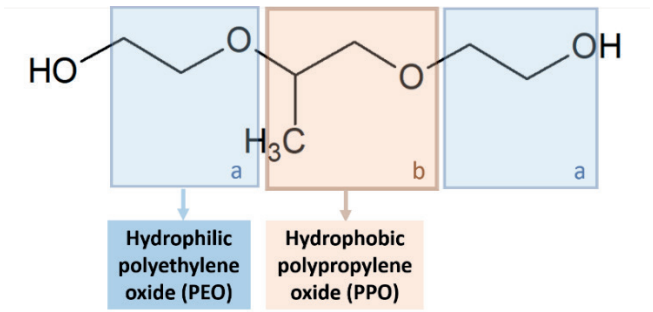

Figure 3.29: General chemical structure of Poloxamer, where "a" and "b" are the repeating units of polyethylenoxide (in blue) and polypropylene oxide (in brown), respectively.

This type of polymer has been widely reported in the literature due to its thermoreversibility behavior. This property involves the transition from a solution to a gel state upon raising the temperature above a critical point defined as the gelation temperature ($T_{sol\text{-}gel}$). Then, on cooling, the reverse transition takes place[103].

Understanding the molecular mechanism of thermogelation is important not only for gel preparation but also for the possible behavior it can exhibit in the presence of other particles such as vesicles. Basically, gel formation occurs due to hydrophobic interactions between the Poloxamer copolymer chains. As reported in the literature, by increasing the temperature, Poloxamer copolymer

chains begin to aggregate into a micellar structure as a result of dehydration of the hydrophobic polyethylene oxide repeat units and define the first step of gelation, as seen in **Figure 3.30**[99,104].

In addition, it is also well-documented that the solution-to-gel transition is concentration-dependent and increases while decreasing concentration of the Poloxamer 407 in an aqueous solution. Thus, the aqueous Poloxamer solution remains in the liquid state below the $T_{sol\text{-}gel}$ value and when the temperature rises above this value, it adopts a semi-solid state[104].

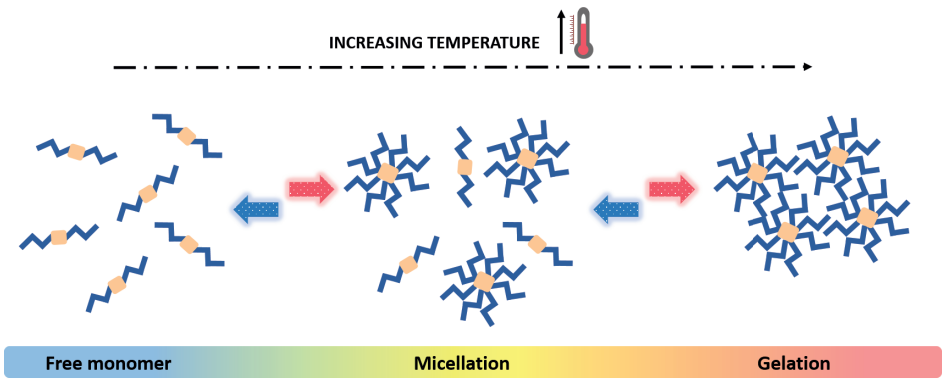

Figure 3.30: Schematic representation of the association mechanism of Poloxamer polymer with increasing temperature.

To ensure that the polymer association mechanism occurs, Poloxamer must be concentrated in an aqueous solution to undergo thermoreversible gelation. It is clear that considerable attention has been paid to this phenomenon as it represents an interesting option for optimizing drug formulations and drug delivery applications[104]. For example, several advantages of the thermoreversibility property have been considered in the literature, such as:

1. When used for wound treatment applications, $T_{sol\text{-}gel}$ is known to be one of the key points for *in situ* gelling systems. Not only can it be sprayed in liquid form onto the injured tissue, but gels form *in situ* with skin temperature. This property is required to avoid the friction of the product with the injured tissue, which means a reduction of the patient's suffering[101].

2. Due to its amphiphilic structure, the hydrophobic core of the micelle that can be formed serves as a compartment for the incorporation of hydrophobic compounds which can sometimes be challenging[105,106].

3. It is considered a viable approach for transdermal and injectable drug delivery systems[107]. The thermoreversible capacity of Poloxamer allows for the formation of drug depots in the skin when administered intradermal. Therefore, the transition of the polymer from liquid to gel state at skin temperature causes the skin to act as *in situ* skin patch. This issue has been widely addressed in the research community as Poloxamer may have the potential to both increase skin permeation and induce sustained transdermal drug delivery[108].

Then, among all the large volume of different Poloxamer types that exist in the market, in this Thesis we examined the effect of using Poloxamer 407 as a possible hydrogelling agent for the conversion of the liquid DELOS nanovesicles suspension into a semi-solid final dosage form. This polymer was selected as a proof-of-concept compound due to the significant number of patents associated with it and the great interest in optimizing drug formulation[99]. However, it should be noted that numerous researchers have reported its use as a potential biomaterial in wound healing, which fits very well with this chapter as this work focuses specifically on topical administration such as the treatment of complex wounds, among other applications[109,110].

Thus, this study provides an exciting opportunity to advance our knowledge of converting DELOS nanovesicle liquid suspension into novel hydrogels options as a new semi-solid final dosage form.

Poloxamer 407, also called Pluronic F-127/Kolliphor P 407 or Synperonic PE/F-127, consists of polyethylene oxide with 101 repeating units and propylene oxide with 56 repeating units arranged in a triblock structure that exhibits amphiphilic properties[99] as shown in **Figure 3.29**.

Literature data indicates that liquid aqueous solutions containing from 20 to 40 wt% of Poloxamer 407 convert to a highly gel-like state at human body temperature, which corresponds to the desired quality since it is fundamental for preventing its removal from the application site, prolonging the retention of the hydrogel *in situ*[111].

Then, considering this information, in this section, we analyzed the impact of using Poloxamer 407 as a hydrogelling agent to convert the liquid DELOS nanovesicle suspension into a semi-solid dosage form, using the same strategy as the one used with Methocel™ K4M polymer. So, to evaluate the Poloxamer 407 potentiality, the main issues addressed in this work is devoted to the gelation of the nanoformulations previously prepared in **Section 3.3.1.3** using this polymer and then the resulting hydrogels were studied them by visual analysis, micro- and nanoscopic observation and the rheological response.

Preparation and physicochemical characterization of Poloxamer 407 DELOS nanovesicles-based hydrogels

Poloxamer 407-based hydrogels were prepared using a 25 wt% of polymer with CTAB- and CTAC-DELOS nanovesicles obtained in **Section 3.3.1.3** containing water, histidine buffer (5 mM, pH 7.0), acetate buffer (5 mM, pH 5.0) and PBS buffer (5 mM, pH 7.4) as dispersant medium according to the methodology described **in Section 6.2.5**. In addition, control Poloxamer 407-based hydrogels were also prepared by only using the dispersant media and the Poloxamer 407 polymer. To do it, Poloxamer 407 was mixed until dissolved and kept at between 5-10 °C under magnetic stirring. This temperature range is necessary to ensure that the polymer is in monomeric form and so the

aqueous solution of this compound is a liquid, as the sol-gel transition for 25 wt% of polymer is around 23 °C[112].

It should be highlighted that 25 wt% of Poloxamer 407 polymer is one of the concentrations found in the literature that has shown satisfactory results for its galenic use as a thermoreversible drug carrier[99,113], for this reason was used in our proof-of-concept study.

Hydrogel homogeneity was inspected by visual observations once Poloxamer 407 was dissolved in either CTAB- and CTAC-DELOS nanovesicles or their respective dispersant media: water, acetate buffer (5 mM, pH = 5.0), histidine buffer (5 mM, pH = 7.0), and PBS buffer (5 mM, pH = 7.4) in 10% EtOH ($v \cdot v^{-1}$). The macroscopic appearance of the controls, which were the Poloxamer hydrogels only in the dispersant media of the nanoformulations, presented homogeneity and colorless transparent hydrogels in all cases (**Figure 3.31 – top right for each medium**).

For further characterization, optical microscopy was used to check the homogeneity of the hydrogels (see **Section 6.3.9**). As shown in **Figure 3.31**, this technique allowed verification that the control groups, Poloxamer 407-based hydrogels without the DELOS nanovesicles, exhibited sample homogeneity without the presence of aggregates.

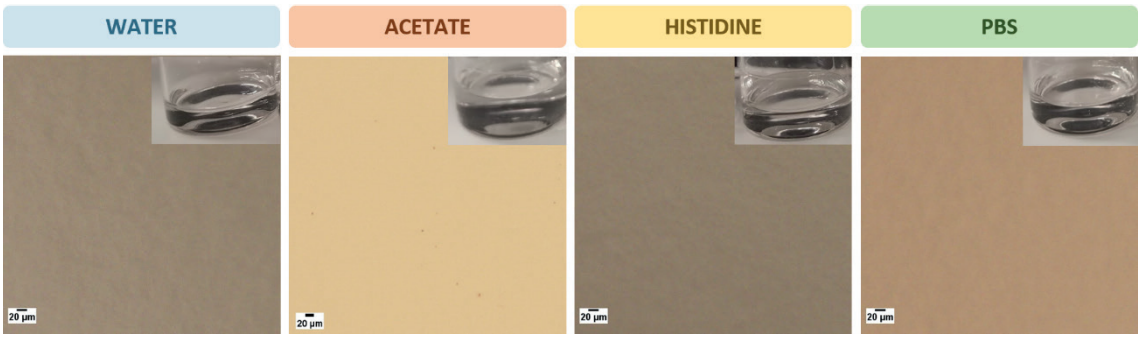

Figure 3.31: Macro- and microscopic appearance Poloxamer 407-based hydrogel controls: in water (blue); acetate buffer (5 mM, pH = 5.0) (orange); histidine buffer (5 mM, pH = 7.0) (yellow); and PBS buffer (5 mM, pH = 7.4) (green).

Regarding Poloxamer 407-based hydrogels containing DELOS nanovesicles, all CTAB- and CTAC-DELOS nanovesicles with different dispersant media showed proper homogeneity and colorless transparent hydrogels except those placed in acetate buffer (5 mM, pH = 5.0) (**Figure 3.32 – top right for each medium**). Furthermore, optical microscopy imaging of hydrogels enriched with CTAB- or CTAC-DELOS nanovesicles dispersed in water, histidine buffer (5 mM, pH 7.0), and PBS buffer (5 mM, pH 7.4) showed significant differences compared to the control groups, which were hydrogels without DELOS nanovesicles. From **Figure 3.32**, it can be seen micron-sized structures are present, which get more abundant and bigger in the presence of buffer such as histidine and PBS

compared to water. Overall, these results indicate clearly, the presence of vesicles and salts impact in the Poloxamer behavior, which tends to induce aggregation at the microscopic level, as it was not observed macroscopically. Little is known about these micrometric particles, and it is not clear what factors can influence them. Although micrometric particles are not a disadvantage in our samples so far for topical administration, the associated stability over time is a requirement that needs to be evaluated in the future to ensure the suitability of the hydrogels for correct administration.

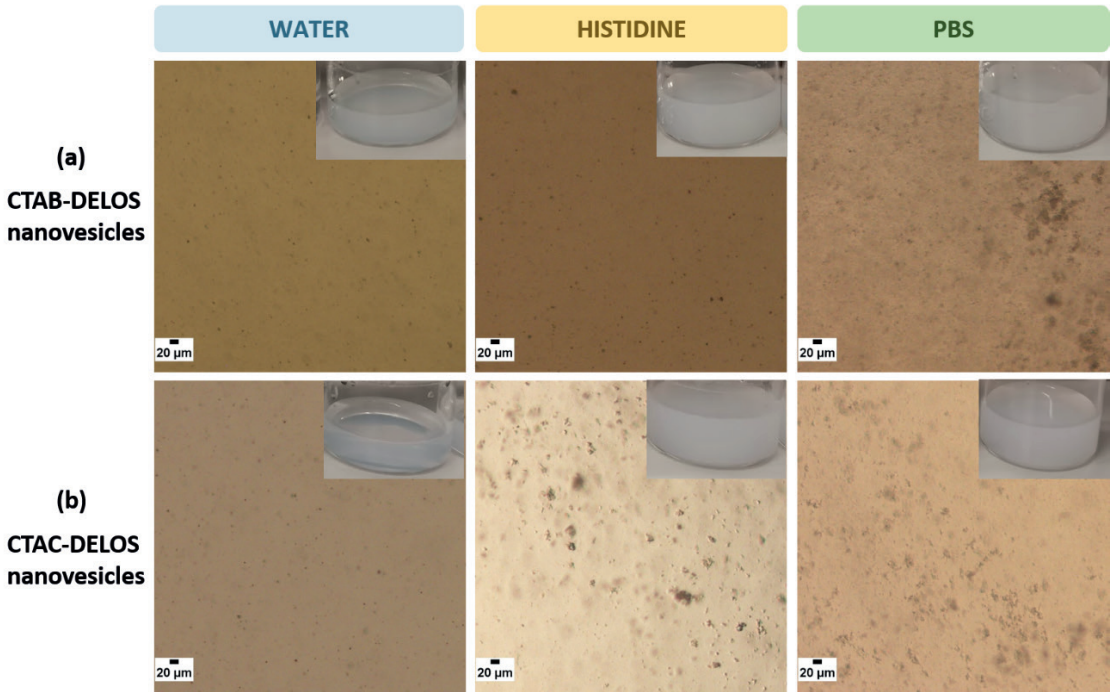

Figure 3.32: Microscopic appearance of Poloxamer 407-based hydrogels of (a) CTAB and (b) CTAC-DELOS nanovesicles in water (blue); histidine buffer (5 mM, pH = 7.0) (yellow); and PBS buffer (5 mM, pH = 7.4) (green).

Regarding CTAB- and CTAC-DELOS nanovesicles in acetate buffer (5 mM, pH = 5.0), their macroscopic appearance showed a variety of instability patterns (**Figure 3.33)**, such as hydrogel inhomogeneity. While CTAB-DELOS formulation clearly presented white lumps at the top of the vial (**Figure 3.33a)**, CTAC-DELOS formulation showed small white features (**Figure 3.33b**). Then, this suggests that the presence of acetate buffer in both CTAB- and CTAC-DELOS nanovesicles have an impact on Poloxamer 407 and limit gelation. Importantly, it has been reported that the gelation process of Poloxamer can be affected by the presence of other substances or additives, which could be the situation of our study case[114].

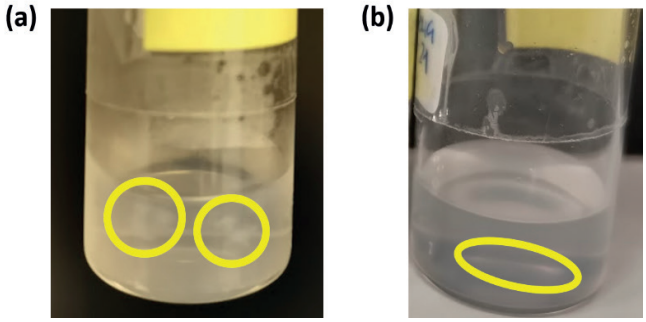

Figure 3.32: Macroscopic appearance of Poloxamer 407 (a) CTAB- and (b) CTAC-DELOS nanovesicle-based hydrogel in acetate buffer (5 mM, pH 5.0). Yellow circles represent the observed lumps and some small features, indicating the instability of the hydrogel in this formulation.

For overpassing the resolution limit in optical microscopy and directly observe whether DELOS nanovesicles maintain their structure upon gellification, cryo-TEM microscope was used (see **Section 6.3.3**). First, Poloxamer 407-based hydrogels of CTAB- and CTAC-DELOS nanovesicles in water were observed. For this purpose, Poloxamer 407-based hydrogels were taken from the fridge, so in liquid form, and diluted 1:10 in water at room temperature for an adequate fixation and preservation of the hydrogel sample in the grid.

It should be highlighted that the sample dilutions were frozen at by liquid nitrogen approximately at-150 °C from Poloxamer 407-based hydrogels at room temperature (around 25 °C), which means that Poloxamer should be in its micellar/gellified form. Considering that Poloxamer 407 has a critical micellar concentration (CMC) of 2.8 μM at 37 °C[115], and that we are working at a concentration of 25 wt% (19.84 mM), upon 10-fold dilution (1.98 mM), we are still working above the CMC, thereby ensuring the presence of Poloxamer micelles[116].

As seen in **Figure 3.34**, it was quite surprising that both CTAB- and CTAC-DELOS nanovesicles exhibited a dense layer completely covering the vesicle and thus a considerable increase in DELOS nanovesicle membrane, acting as a coating agent. Furthermore, the morphology of the vesicles, not only their spherical shape but also their unilamellarity, is preserved, although there is an increase in particle size attributed to the polymeric coating of the vesicles.

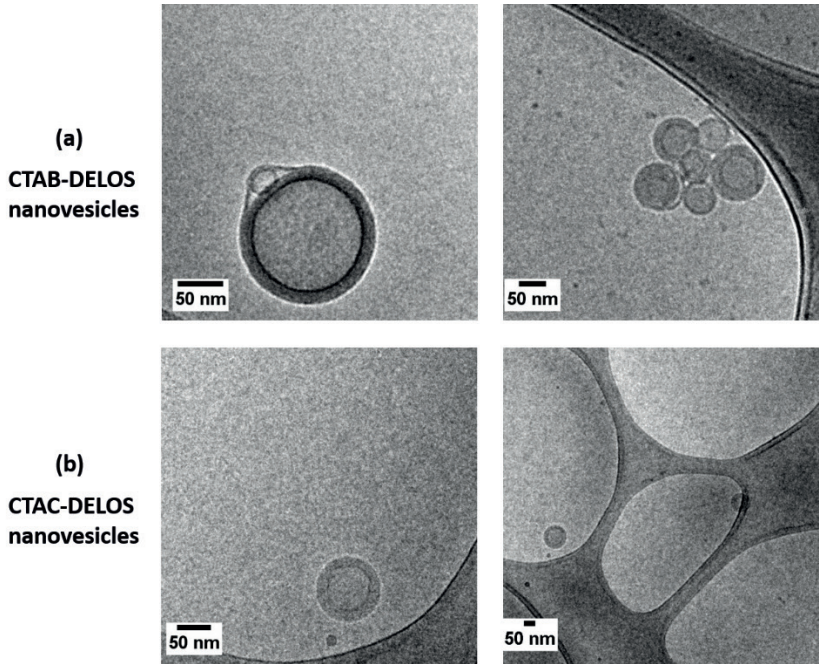

Figure 3.34: Cryo-TEM image of Poloxamer 407-based hydrogels containing (a) CTAB- and (b) CTAC-DELOS nanovesicles in water. Gellified nanovesicles were previously diluted 1:10 in water at room temperature for an adequate fixation and preservation of the hydrogel sample in the grid.

According to the literature, this effect could be explained by the amphiphilic character of Poloxamer, as the copolymers exhibit surface-active properties that allow interaction with hydrophobic surfaces and biological membranes[117]. Furthermore, it has been reported that Poloxamer has been used in nanomedical applications to modify the surface of polymeric nanoparticles and complex phospholipid nanovesicles[118]. Most of the work in the literature has studied the interaction of phospholipid vesicles with Poloxamer at low concentration and found that this polymer improves the stabilization and the micromechanical properties of the bilayers, which is related to the stability and strength of the bilayer[119].

In principle, when Poloxamer is in monomeric form, the hydrophobic blocks can be incorporated inside the bilayer, sandwiched between lipid molecules, leading to bilayer expansion, as observed from atomic force microscopic characterization in the literature[106,119]. The polymer is thus absorbed onto particle surfaces from an aqueous solution by hydrophobic interaction of the hydrophobic moiety acting as an anchor block with the particle surface. Then, the hydrophilic block extends into the aqueous medium to form a hydrophilic layer[120], as represented in **Figure 3.35**. Then, it was suggested that this could be a new relevant strategy to protect and improve the performance of DELOS nanovesicles, if necessary and depending on the desired application.

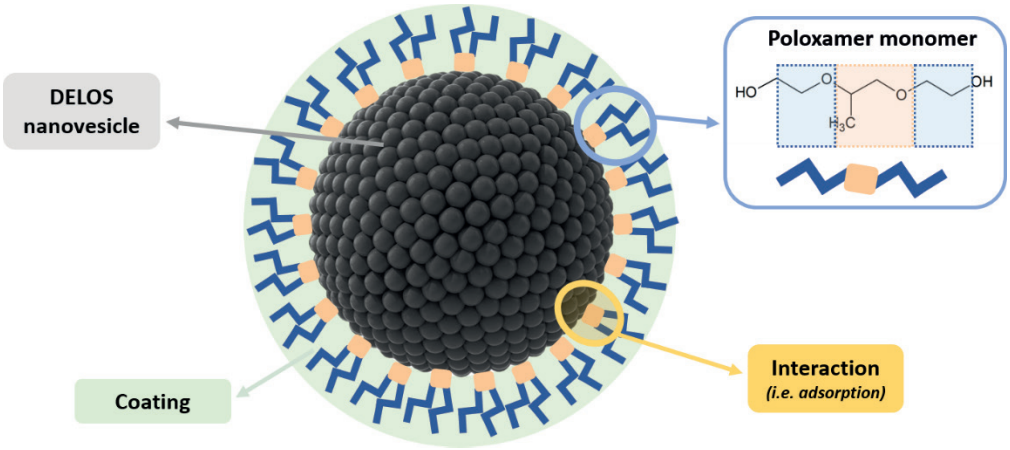

Figure 3.35: Schematic representation of the Poloxamer-coated DELOS nanovesicles. The interaction between these two compounds is based on the interaction of the hydrophobic block of the Poloxamer with the vesicle surface, while the hydrophilic part extends to the aqueous medium.

Then, to check whether the presence of buffers such as histidine (5 mM, pH 7.0) and PBS (5 mM, pH 7.4) in the DELOS nanovesicle formulation affect the presence of the vesicle's surface modification through the absorptions of a Poloxamer 407 overcoating layer, the hydrogels prepared with these dispersant media were also observed by cryo-TEM microscopy.

As expected and shown in **Figure 3.36**, the presence of the absorbed coating layer of Poloxamer 407 was observed on both CTAB- and CTAC-DELOS nanovesicles in histidine buffer (5 mM, pH 7.0) and in PBS buffer (5 mM, pH 7.4). Then, these results suggest that the presence of salts in histidine and PBS buffers do not interfere in the interaction between the Poloxamer 407 polymer and the DELOS nanovesicles.

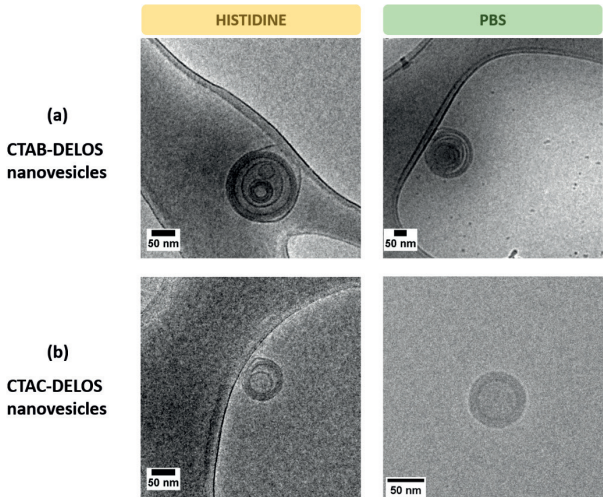

Figure 3.36: Cryo-TEM image of Poloxamer 407-based hydrogels containing (a) CTAB- and (b) CTAC-DELOS nanovesicles in histidine buffer (5 mM, pH 7.0) and PBS buffer (5 mM, pH 7.4) respectively. Gellified nanovesicles were previously diluted 1:10 in water at room temperature for an adequate fixation and preservation of the hydrogel sample in the grid.

Reversibility of the Poloxamer 407 coating in DELOS nanovesicles

In order to gain fundamental knowledge about Poloxamer 407-based hydrogels containing DELOS nanovesicles and thus lay the basis for improved and novel applications, it was of interest to assess the reversibility of the coating. It is known that Poloxamer exhibits reversible thermal gelation and so it is temperature-dependent and the self-assembly behavior is driven by the interactions between the hydrophobic part of the polymer and water with increasing temperature[121]. So, at low temperatures, Poloxamer 407 should be expected to be in a monomeric form and thus not adhered to any surface. However, when increasing the temperature around the room temperature and so close to the $T_{sol\text{-}gel}$ (23 °C) for 25 wt% of polymer, it may form micelles. In this case, DELOS nanovesicles have already shown to be coated with Poloxamer 407 (**Figure 3.34**).

Then, to assess the reversibility of this polymer, Poloxamer 407-based hydrogels containing CTAB-DELOS nanovesicles in water were taken directly from the fridge (4 °C) and rapidly diluted 1:10 in water and placed back in the fridge. Afterwards, the samples coming out of the fridge then frozen in the similar manner to the other previously evaluated samples and placed directly on the cryo-TEM grid to for observation.

As shown in **Figure 3.34a and Figure 3.37**, the images from direct observation of the hydrogels at approx. 4 and 25 °C match each other perfectly.

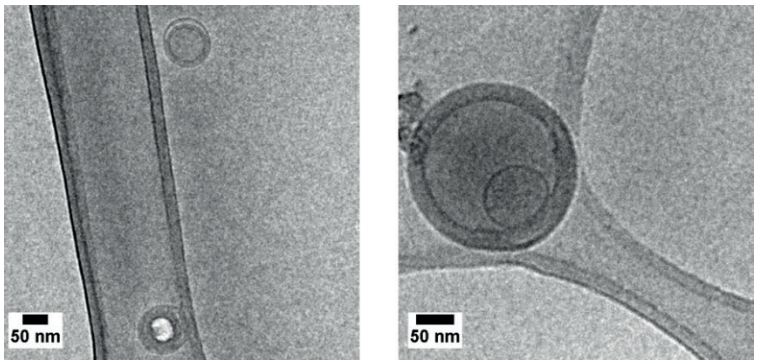

Figure 3.37: Cryo-TEM image of Poloxamer 407-based hydrogels containing CTAB-DELOS nanovesicles in water. Gellified nanovesicles were previously diluted 1:10 in water and placed at the fridge at 4 °C before the fixation and preservation of the hydrogel sample in the grid.

In summary, these results are intriguing and help justify the Poloxamer 407 behavior in presence of DELOS nanovesicles as they illustrate two things:

1. A portion of the polymer in monomeric form can evolve into micelles upon temperature since increase in the viscosity can be observed by visual inspection.
2. The polymer in monomeric form can interact with DELOS nanovesicles, causing an irreversible coating of the vesicles independent the temperature. A possible explanation for this

phenomenon is that the interaction between the Poloxamer 407 polymers and the DELOS nanovesicle membrane is more favorable, stronger, and preserved than the transition of the polymer to a monomeric form by changing the temperature alone.

As a result, this may allow new properties of the formulation such as more stability and protection, among other characteristics that need to be examined more closely. Then, although the hydrogels exhibit an interesting reversible thermal property macroscopically, irreversible interaction of Poloxamer with DELOS nanovesicles occurs at the nanoscopic level.

Rheological characterization of Poloxamer 407-based hydrogels

Viscosity measurements contributed to comprehending the behavior of the Poloxamer 407 hydrogels when containing DELOS nanovesicles. The rheological properties like the viscosity and the rheological behavior of Poloxamer 407-based hydrogels were examined in the gel state at room temperature (25 °C), using the same methodology used for the Methocel™ K4M-based hydrogels and described in the **Section 6.3.10**.

The viscosity results obtained from the rheological analysis are presented in **Figure 3.38**. From this data, it is clear that good reproducibility of the results between replicates is achieved of each studied group: control, CTAB- and CTAC-DELOS nanovesicles-based hydrogels. Additionally, it is clear that no differences were observed in the control groups of Poloxamer 407 hydrogels, which were the ones prepared using the Poloxamer 407 polymer with the dispersant media used in the nanoformulations (water, histidine buffer (5 mM, pH 7.0) and PBS buffer (5 mM, pH 7.4)). Thus, the presence of different dispersant media, such as the use of salts, did not alter the viscosity values obtained.

However, the most striking result to emerge from the data is that the Poloxamer-based hydrogels in presence of CTAB- and CTAC-DELOS nanovesicles presented higher values of viscosity compared to the controls. Therefore, these results indicate that there is an effect of the presence of both CTAB- and CTAC-DELOS nanovesicles in gelation properties, making the Poloxamer-based hydrogel with the presence of DELOS nanovesicles more viscous than the gel in absence of them. The considerable difference observed between these groups could be attributable to the interaction between the Poloxamer 407 and the DELOS nanovesicles, as observed previously by the cryo-TEM images (**Figure 3.34 and Figure 3.36**).

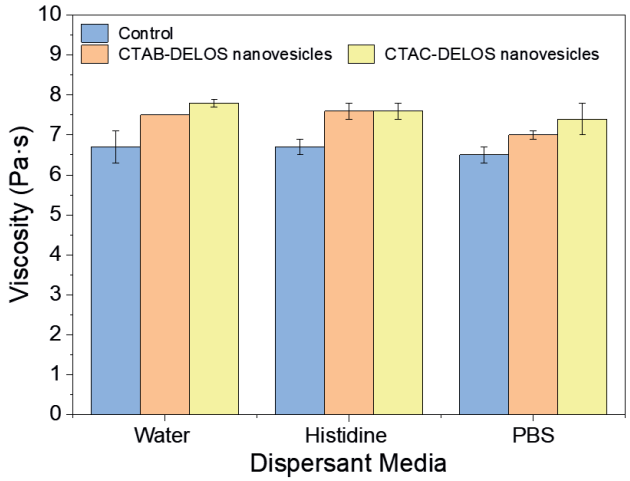

Figure 3.38: Viscosity measurements of the evaluated Poloxamer 407-based hydrogels, controls (samples without the nanovesicles, in blue) and with DELOS nanovesicles-based hydrogels using CTAB- (orange) or CTAC-DELOS (yellow) nanovesicles in water, histidine buffer (5 mM, pH 7.0), and PBS (5 mM, pH 7.4) (N = 2).

Regarding the study of the flow properties of Poloxamer 407-based hydrogels and their deformation, shear stress changes upon shear rates were evaluated to determine the rheological behavior of the formulations. As seen in **Figure 3.39**, all Poloxamer 407-based hydrogels, both the controls and the CTAB- and CTAC-DELOS nanovesicles in all the dispersant media evaluated, water, histidine and PBS are classified as non-Newtonian pseudoplastic fluids since they present almost constant shear stress while the shear rate is increasing. Consequently, it reveals a decrease of the apparent viscosity, which is the correlation between the shear stress to shear rate, with increasing shear rate, indicating some intramolecular interactions were present and responsible for shear thinning. Interestingly, if hydrogels become less viscous as the shear rate increases, it means that it facilitates the flow of the formulation when applied which is a proper characteristic for the topical practical use of this type of hydrogels.

Moreover, it is noteworthy to mention that in **Figure 3.39** all the hydrogels present a flow curve with pronounced thixotropy. This is represented as a hysteresis loop visually observed by the area that encloses the process of shear rate increasing with time until it reaches a maximum shear value and thereafter, the process is reversed by decreasing the shear rate, leading the formation of up and down curves[50]. Specifically, thixotropy is related to viscosity-induced structural changes that are time-dependent since it needs time for regrouping the structure.

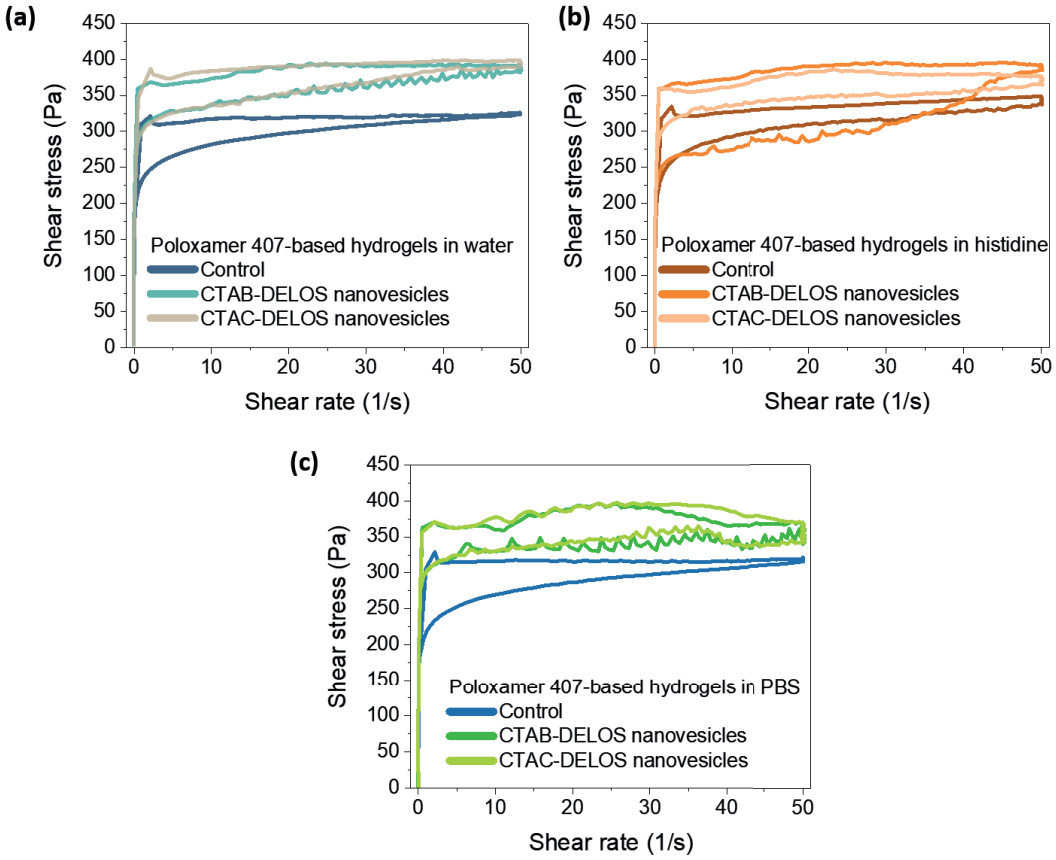

Figure 3.39: Rheological characterization of Poloxamer 407-based hydrogels in the presence and absence of CTAB- and CTAC-DELOS nanovesicles in (a) water, (b) histidine buffer (5 mM, pH 7.0) and (c) PBS buffer (5 mM, pH 7.4).

This behavior is in accordance with the experiments reported in the literature describing the Poloxamer 407 properties when in gel state at high concentrations[122,123]. Together these results provide important insights into major applications in pharmaceutical formulations including hydrogels, since thixotropic property plays an integral role in defining therapeutic efficacy of the pharmaceutical formulations by mainly influencing on the controlled release of loaded drugs and the bioavailability[50].

As summary, Poloxamer 407 as a hydrogelling agent has offered new and promising perspectives in the development of novel DELOS nanovesicles semi-solid formulations for topical drug delivery, among other administration routes. Clearly, the most optimal and promising developed semi-solid formulations are the ones containing CTAB- and CTAC-DELOS nanovesicles in water, histidine buffer (5 mM, pH 7.0) and PBS (5 mM, pH 7.4), mainly due to their stability over time when gellified with 25 wt% of Poloxamer 407. Furthermore, it should be highlighted that future studies on the current topic are therefore recommended to investigate in more detail the coating and so interaction and the respective effect of Poloxamer 407 in DELOS nanovesicles.

3.3.3 Summary of the section and perspectives

In conclusion, this chapter has approached DELOS nanovesicles to topical drug delivery by converting them into suitable final dosage forms.

New DELOS nanovesicles formulations were screened by DELOS-susp methodology by using CTAB or CTAC surfactants and different dispersant media to achieve better skin compatibility of these DELOS nanovesicle systems. Among these systems, when they were gellified with 2 wt% of Methocel™ K4M-based hydrogels only CTAB- and CTAC-DELOS nanovesicles formulated in water and histidine buffer (5 mM, pH 7.0) were chosen as the optimal ones.

Moreover, Poloxamer 407-based hydrogels containing DELOS nanovesicles have presented interesting results mostly when using CTAB- and CTAC-DELOS nanovesicles in water, histidine buffer (5 mM, pH 7.0) and PBS buffer (5 mM, pH 7.4) with 25 wt% of Poloxamer 407. Overall, a part from observing that these hydrogels exhibit proper properties in terms of rheological behavior for topical use, a complete coating of the DELOS nanovesicles is produced by the polymer independently of the temperature. Then, the use of Poloxamer 407 in the development of new DELOS nanovesicle-based hydrogels is a promising agent to confer potential new properties on the DELOS nanovesicle drug delivery system.

Finally, after observing all the possibilities of converting DELOS nanovesicles into a semi-solid dosage form by either Methocel™ K4M or Poloxamer 407, some recommendations for their improvement were made. There is evidence of the possibility of using Hydroxypropyl Methyl Cellulose derivatives such as Methocel™ K4M with Poloxamer 407, which has been used in the literature to modulate the viscoelastic and adhesive properties or even prolong drug release of Poloxamer 407 hydrogels[100,124]. Then, there is much room for further progress in the field of hydrogels of DELOS nanovesicles.

In this context, this study has contributed to the internal know-how of the Nanomol Group and Nanomol Technologies, while expanding the use of the DELOS platform which is owned by the company. Moreover, all the learned knowledge is relevant for the development of a final pharmaceutical product related to hydrogels. For instance, it can be applied to other projects of the company that require a final formulation in semi-solid dosage form such as oral and subcutaneous applications, and thus expanding the company's product portfolio.

1. Part of the above reported results have been published in "Ballell-Hosa, L., González-Mira, E., Santana, H., Morla-Folch, J., Moreno-Masip, M., Martínez-Prieto, Y.,... & Ventosa, N. (2022). DELOS Nanovesicles-Based Hydrogels: An Advanced Formulation for Topical Use. *Pharmaceutics*, *14*(1), 199"[125].

3.4 References

1. N. Rathore, R.S. Rajan. Current perspectives on stability of protein drug products during formulation, fill and finish operations. *Biotechnol. Prog.* **2008**, 24 (3), 504–514.
2. M.A.. Fakhree, S. Ahmadian. Pharmaceutical dosage forms: Past, present, future; Nova Science Publishers, Inc: Hauppauge, NY, USA, **2011**.
3. Y.H. Almoshari. Novel Hydrogels for Topical Applications: An Updated Comprehensive Review Based on Source. *Gels* **2022**, 8 (3), 174.
4. M.I. Noordin. Advance Delivery System Dosage Form for Analgesic, Their Rationale, and Specialty; IntechOpen, London, UK, **2017**.
5. E.M. Agency. ICH Topic Q 5 E Comparability of Biotechnological/Biological Products- Step 5; **2005**.
6. E.M.A. Committee for Human Medicinal Products. ICH guideline Q8 (R2) on pharmaceutical development; **2017**.
7. T.N. Demidova-Rice, M.R. Hamblin, I.M. Herman. Acute and Impaired Wound Healing: Pathophysiology and Current Methods for Drug Delivery, Part 1: Normal and Chronic Wounds: Biology, Causes, and Approaches to Care. *Adv. Skin Wound Care* **2012**, 25 (7), 304.
8. G. Dabiri, E. Damstetter, T. Phillips. Choosing a Wound Dressing Based on Common Wound Characteristics. *Adv. Wound Care* **2016**, 5 (1), 32.
9. T.F. O'Donell Jr, M.A. Passman, W.A. Marston, et al. Management of venous leg ulcers: Clinical practice guidelines of the Society for Vascular Surgery® and the American Venous Forum. *J. Vasc. Surg.* **2014**, 60 (2), 3S-59S.
10. A. Mitra, S.A. Ibrahim. Development of Topical and Transdermal Dosage Forms : Regulatory Perspective. In *Dermal Drug Delivery*; CRC Press, **2020**; pp 391–414.
11. C. Ghobril, M.W. Grinstaff. The chemistry and engineering of polymeric hydrogel adhesives for wound closure: a tutorial. *Chem. Soc. Rev.* **2015**, 44 (7), 1820–1835.
12. J. Menon. Managing exudate associated with venous leg ulceration. *Br. J. Community Nurs.* **2012**, 17 (Sup6), S6–S16.
13. P. Pleguezuelos-Beltrán, P. Gálvez-Martín, D. Nieto-García, J.A. Marchal, E. López-Ruiz. Advances in spray products for skin regeneration. *Bioact. Mater.* **2022**, 16, 187–203.
14. N. Pawar, P. Jalwal. Non-Pressurized Topical Spray Pharmaceutical-Methodology of Formulation Development and Quality Control Management. *Int. J. Pharm. Investig.* **2021**, 11 (3), 260–268.
15. R. Sritharadol, T. Nakpheng, P. Wan Sia Heng, T. Srichana. Development of a topical mupirocin spray for antibacterial and wound-healing applications. *Drug Dev. Ind. Pharm.* **2017**, 43 (10), 1715–1728.

16. S. Thomas, D. Durand, C. Chassenieux, P. Jyotishkumar. Handbook of Biopolymer-Based Materials From Blends and Composites to Gels and Complex Networks; Wiley-VCH, **2013**.

17. M. Bahram, N. Mohseni, M. Moghtader. An Introduction to Hydrogels and Some Recent Applications. In *Emerging Concepts in Analysis and Applications of Hydrogels*; IntechOpen, **2016**; pp 9–38.

18. K. Varaprasad, G.M. Raghavendra, T. Jayaramudu, M.M. Yallapu, R. Sadiku. A mini review on hydrogels classification and recent developments in miscellaneous applications. *Mater. Sci. Eng. C* **2017**, 79, 958–971.

19. M.M. Elsayed. Hydrogel Preparation Technologies: Relevance Kinetics, Thermodynamics and Scaling up Aspects. *J. Polym. Environ.* **2019**, 27 (4), 871–891.

20. T. Ur-Rehman. Controlled Release Gel Formulations and Preclinical Screening of Drug Candidates. "Doctoral dissertation," Umea University, **2011**.

21. S. Thakur, V.K. Thakur, O.A. Arotiba. History, Classification, Properties and Application of Hydrogels: An Overview. In *Gel Horizons: From Science to Smart Materials*; Springer, Singapore, **2018**; pp 29–50.

22. G. Calixto, A.C. Yoshii, H.R. e Silva, B.S.F. Cury, M. Chorilli. Polyacrylic acid polymers hydrogels intended to topical drug delivery: preparation and characterization. *Pharm. Dev. Technol.* **2015**, 20 (4), 490–496.

23. W.H. Organization. Topical semi-solid dosage forms. In *The International Pharmacopoeia*; **2020**; pp 1–3.

24. I. Harrison, F. Spada. Hydrogels for Atopic Dermatitis and Wound Management: A Superior Drug Delivery Vehicle. *Pharmaceutics* **2018**, 10 (2), 71.

25. R. Song, J. Zheng, Y. Liu, et al. A natural cordycepin/chitosan complex hydrogel with outstanding self-healable and wound healing properties. *Int. J. Biol. Macromol.* **2019**, 134, 91–99.

26. G. Bonacucina, M. Cespi, G.F. Palmieri. Characterization and Stability of Emulsion Gels Based on Acrylamide/Sodium Acryloyldimethyl Taurate Copolymer. *AAPS PharmSciTech 2009 102* **2009**, 10 (2), 368–375.

27. S. Baghel, V.S. Nair, A. Pirani, et al. Luliconazole-loaded nanostructured lipid carriers for topical treatment of superficial Tinea infections. *Dermatol. Ther.* **2020**, 33 (6), e13959.

28. N.S.V. Capanema, A.A.P. Mansur, S.M. Carvalho, et al. Bioengineered carboxymethyl cellulose-doxorubicin prodrug hydrogels for topical chemotherapy of melanoma skin cancer. *Carbohydr. Polym.* **2018**, 195, 401–412.

29. Colorcon. Using METHOCEL Cellulose Ethers for Controlled Release of Drugs in Hydrophilic Matrix Systems; **2000**.

30. S. Ponsubha, A.K. Jaiswal. Effect of interpolymer complex formation between chondroitin sulfate and chitosan-gelatin hydrogel on physico-chemical and rheological properties. *Carbohydr. Polym.* **2020**, 238, 116179.

31. Otto Chemie Pvt Ltd. HPMC, K4M (9004-65-3) https://www.ottokemi.com/carbohydrates-a-to-z/hydroxy-propyl-methyl-cellulose-hpmc-k4m.aspx (accessed Jan 10, 2022).

32. Dow Chemical Company. Methocel Cellulose Ethers. In *Technical Handbook*; Midland, MI, USA, **1997**; pp 1–32.

33. Chemistry of METHOCEL™ Cellulose Ethers-A Technical Review Pharma & Food Solutions.

34. S. Pramanick, D. Singodia, V. Chandel. Excipient Selection In Parenteral Formulation Development. *Pharma Times* **2013**, 45 (3), 65–77.

35. N.A. Patel, N.J. Patel, R.P. Patel. Design and evaluation of transdermal drug delivery system for curcumin as an anti-inflammatory drug. *Drug Dev. Ind. Pharm.* **2009**, 35 (2), 234–242.

36. L. Vlaia, G. Coneac, I. Olariu, V. Vlaia, D. Lupuleasa. Cellulose-Derivatives-Based Hydrogels as Vehicles for Dermal and Transdermal Drug Delivery. In *Emerging Concepts in Analysis and Applications of Hydrogels*; IntechOpen, **2016**; pp 159–200.

37. F. Laffleur, B. Strasdat. Gelatin-based formulations for dermal application. *Eur. Polym. J.* **2019**, 118, 542–550.

38. L. Binder, J. Mazál, R. Petz, V. Klang, C. Valenta. The role of viscosity on skin penetration from cellulose ether-based hydrogels. *Ski. Res. Technol.* **2019**, 25 (5), 725–734.

39. W. Zhang, J. Chen, H. Zeng. Polymer processing and rheology. In *Polymer Science and Nanotechnology*; Elsevier, **2020**; pp 149–178.

40. Rheology & rheological properties of non Newtonian fluids and soft solids https://www.malvernpanalytical.com/en/products/measurement-type/rheology-viscoelasticity (accessed Jul 3, 2018).

41. A. Katoch, A. Roy Choudhury. Understanding the rheology of novel guar-gellan gum composite hydrogels. *Mater. Lett.* **2020**, 263, 127234.

42. Lubrizol. Pharmaceutical Bulletin 7: Flow and Suspension Properties; **2008**.

43. T. Garg, G. Rath, A.K. Goyal. Comprehensive review on additives of topical dosage forms for drug delivery. *Drug Deliv.* **2015**, 22 (8), 969–987.

44. R.P. Chhabra. Non-Newtonian Fluids: An Introduction. In *Rheology of complex fluids*; Springer, New York, **2010**; pp 3–34.

45. H.. George, F. Qureshi. Newton's Law of Viscosity, Newtonian and Non-Newtonian Fluids; Wang, Q. J., Chung, Y., Eds.; Springer, Boston, MA, **2013**.

46. M.V. Ghica, M. Hîrjău, D. Lupuleasa, C.E. Dinu-Pîrvu. Flow and Thixotropic Parameters for Rheological Characterization of Hydrogels. *Molecules* **2016**, 21 (6), 786.

47. Y. Singh. Rheology. In *Martin's physical pharmacy and pharmaceutical sciences*; Patrick, J. S., Ed.; New Jersey: Department of Pharmaceutics Ernest Mario School of Pharmacy Rutgers, The State University of New Jersey, **2006**; pp 469–490.

48. L.A. Shah, T.U. Rehman, M. Khan. Synthesis of graphene oxide doped poly(2-acrylamido-2-methyl propane sulfonic acid) [GO@p(AMPS)] composite hydrogel with pseudo-plastic thixotropic behavior. *Polym. Bull.* **2020**, 77 (8), 3921–3935.

49. G. Calixto, A.C. Yoshii, H. Rocha E Silva, B. Stringhetti Ferreira Cury, M. Chorilli. Polyacrylic acid polymers hydrogels intended to topical drug delivery: preparation and characterization. *Pharm. Dev. Technol.* **2015**, 20 (4), 490–496.

50. C.H. Lee, V. Moturi, Y. Lee. Thixotropic property in pharmaceutical formulations. *J. Control. Release* **2009**, 136 (2), 88–98.

51. J. Morla-Folch, G. Vargas-Nadal, T. Zhao, et al. Dye-Loaded Quatsomes Exhibiting FRET as Nanoprobes for Bioimaging. *ACS Appl. Mater. Interfaces* **2020**, 12 (18), 20253–20262.

52. A. Ardizzone, S. Kurhuzenkau, S. Illa-Tuset, et al. Nanostructuring Lipophilic Dyes in Water Using Stable Vesicles, Quatsomes, as Scaffolds and Their Use as Probes for Bioimaging. *Small* **2018**, 14 (16), 1703851.

53. Xiaoting Zhang, Renfa Liu, Zhifei Dai. Multicolor nanobubbles for FRET/ultrasound dual-modal contrast imaging. *Nanoscale* **2018**, 10 (43), 20347–20353.

54. K.T. Kim, Y. Moon, Y. Jang, et al. Molecular mechanisms of atlastin-mediated ER membrane fusion revealed by a FRET-based single-vesicle fusion assay. *Sci. Rep.* **2017**, 7 (1), 1–8.

55. J. Gravier, L. Sancey, E. Rustique, et al. FRET imaging approaches for in vitro and in vivo characterization of synthetic lipid nanoparticles. *Mol. Pharm.* **2014**, 11 (9), 3133–3144.

56. T. Chen, B. He, J. Tao, et al. Application of Förster Resonance Energy Transfer (FRET) technique to elucidate intracellular and In Vivo biofate of nanomedicines. *Adv. Drug Deliv. Rev.* **2019**, 143, 177–205.

57. D.M. Charron, G. Zheng. Nanomedicine development guided by FRET imaging. *Nano Today* **2018**, 18, 124–136.

58. G. Vargas-Nadal. Novel Quatsome nanovesicles, prepared using compressed CO2, for the development of advanced nanomedicines "Doctoral dissertation," Universitat de Barcelona, **2020**.

59. X. Sun, G. Wang, H. Zhang, et al. The blood clearance kinetics and pathway of polymeric micelles in cancer drug delivery. *ACS Nano* **2018**, 12 (6), 6179–6192.

60. S. Illa-Tuset. Molecular Modelling of Quatsome nanovesicles "Doctoral dissertation," Universitat Autònoma de Barcelona, **2019**.

61. A. Delledonne, J. Morla-Folch, M. Anzola, et al. Increasing resonance energy transfer upon dilution: a counterintuitive observation in CTAB micelles. *J. Mater. Chem. C* **2021**, 9 (33), 10952–10964.

62. J.R. Lakowicz. Principles of Fluorescence Spectroscopy, 2nd ed.; Springer Science & Business Media, New York, USA, **2006**.

63. L. Ferrer-Tasies, H. Santana, I. Cabrera-Puig, et al. Recombinant Human Epidermal Growth Factor/Quatsome Nanoconjugates: A Robust Topical Delivery System for Complex Wound Healing. *Adv. Ther.* **2021**, 4 (6), 2000260.

64. K. Nakata, T. Tsuchido, Y. Matsumura. Antimicrobial cationic surfactant, cetyltrimethylammonium bromide, induces superoxide stress in Escherichia coli cells. *J. Appl. Microbiol.* **2011**, 110 (2), 568–579.

65. H. Jang, S.H. Lim, J.S. Choi, Y. Park. Antibacterial properties of cetyltrimethylammonium bromide-stabilized green silver nanoparticles against methicillin-resistant Staphylococcus aureus. *Arch. Pharm. Res.* **2015**, 38 (10), 1906–1912.

66. S. Pang, L. Willis, F.A. Andersen. Final report on the safety assessment of Cetrimonium Chloride, Cetrimonium Bromide and Steartrimonium Chloride. *Int. J. Toxicol.* **1997**, 16 (3), 195–220.

67. Michael Ash. Handbook of Preservatives; Synapse Info Resources, **2004**.

68. B. Findlay, P. Szelemej, G.G. Zhanel, F. Schweizer. Guanidylation and Tail Effects in Cationic Antimicrobial Lipopeptoids. *PLoS One* **2012**, 7 (7), e41141.

69. R.R. Kashapov, Y.S. Razuvayeva, A.Y. Ziganshina, et al. Self-assembling and biological properties of single-chain dicationic pyridinium-based surfactants. *Colloids Surfaces B Biointerfaces* **2019**, 175, 351–357.

70. F. and D. Administration, FDA. Cetrimonium Chloride UNII UC9PE95IBP; **2021**.

71. I. Cabrera, E. Elizondo, O. Esteban, et al. Multifunctional Nanovesicle-Bioactive Conjugates Prepared by a One-Step Scalable Method Using CO2-Expanded Solvents. *Nano Lett.* **2013**, 13 (8), 3766–3774.

72. E. Elizondo, E. Moreno, I. Cabrera, et al. Liposomes and Other Vesicular Systems: Structural Characteristics, Methods of Preparation, and Use in Nanomedicine. *Prog. Mol. Biol. Transl. Sci.* **2011**, 104, 1–52.

73. B. Heldreth, W.F. Bergfeld, D. V Belsito, et al. Final Report of the Cosmetic Ingredient Review Expert Panel on the Safety Assessment of Methyl Acetate. *Int. J. Toxicol.* **2012**, 31 (4_suppl), 112S-136S.

74. M.H. Schmid-Wendtner, H.C. Korting. The pH of the Skin Surface and Its Impact on the Barrier Function. *Skin Pharmacol. Physiol.* **2006**, 19 (6), 296–302.

75. P.L. Bigliardi. Role of Skin pH in Psoriasis. *Curr. Probl. Dermatology* **2018**, 54, 108–114.

76. E. Proksch. Buffering Capacity. *Curr. Probl. Dermatology* **2018**, 54, 11–18.

77. M.M. Fiume, B.A. Heldreth, W.F. Bergfeld, et al. Safety Assessment of Citric Acid, Inorganic Citrate Salts, and Alkyl Citrate Esters as Used in Cosmetics: *Int. J. Toxicol.* **2014**, 33 (2_suppl), 16S-46S.

78. E. Proksch, M. Soeberdt, C. Neumann, et al. Influence of Buffers of Different pH and Composition on the Murine Skin Barrier, Epidermal Proliferation, Differentiation, and Inflammation. *Skin Pharmacol. Physiol.* **2019**, 32 (6), 328–336.

79. E. Bernstein. Use of citric acid and low concentrations of alpha-hydroxy acids for superficial skin treatment. U.S. Patent Application No. 10/689,002, 2005.

80. I. Weil. Skin treatment composition containing monoester of citric acid. U.S. Patent No. 5,047,166, 1991.

81. M. Holeček. Histidine in Health and Disease: Metabolism, Physiological Importance, and Use as a Supplement. *Nutrients* **2020**, 12 (3), 848.

82. S.P. Tan, S.B. Brown, C.E. Griffiths, R.B. Weller, N.K. Gibbs. Feeding filaggrin: effects of l-histidine supplementation in atopic dermatitis. *Clin. Cosmet. Investig. Dermatol.* **2017**, 10, 403.

83. Y. Kim, E. Kim, Y. Kim. l-histidine and l-carnosine accelerate wound healing via regulation of corticosterone and PI3K/Akt phosphorylation in d-galactose-induced aging models in vitro and in vivo. *J. Funct. Foods* **2019**, 58, 227–237.

84. H. Santana, Y. González, P.T. Campana, et al. Screening for stability and compatibility conditions of recombinant human epidermal growth factor for parenteral formulation: Effect of pH, buffers, and excipients. *Int. J. Pharm.* **2013**, 452 (1–2), 52–62.

85. H. Holmegaard Sorensen, L. Skriver, A. Rassing Hoelgaard. A stabilized pharmaceutical formulation comprising growth hormone and histidine. DK Patent EP1197222A2, 2002.

86. D. Sek. Breaking old habits: Moving away from commonly used buffers in pharmaceuticals https://www.europeanpharmaceuticalreview.com/article/13699/breaking-old-habits-moving-away-from-commonly-used-buffers-in-pharmaceuticals/ (accessed Nov 15, 2021).

87. R.G. Strickley, W.J. Lambert. A review of Formulations of Commercially Available Antibodies. *J. Pharm. Sci.* **2021**, 110 (7), 2590–2608.

88. N.C. Martin, A.A. Pirie, L. V. Ford, et al. The use of phosphate buffered saline for the recovery of cells and spermatozoa from swabs. *Sci. Justice - J. Forensic Sci. Soc.* **2006**, 46 (3), 179–184.

89. D.W. Lachenmeier. Safety evaluation of topical applications of ethanol on the skin and inside the oral cavity. *J. Occup. Med. Toxicol.* **2008**, 3 (1), 1–16.

90. P.K. Yuet, D. Blankschtein. Molecular-Thermodynamic Modeling of Mixed Cationic/Anionic Vesicles. *Langmuir* **1996**, 12 (16), 3802–3818.

91. L. Ferrer-Tasies, E. Moreno-Calvo, M. Cano-Sarabia, et al. Quatsomes: Vesicles Formed by Self-Assembly of Sterols and Quaternary Ammonium Surfactants. *Langmuir* **2013**, 29 (22), 6519–6528.

92. S. Samimi, N. Maghsoudnia, R.B. Eftekhari, F. Dorkoosh. Lipid-based nanoparticles for drug delivery systems; Elsevier Inc., **2019**.

93. M. Rossetti, L. Stella, J. Morlà-Folch, et al. Engineering DNA-Grafted Quatsomes as Stable Nucleic Acid-Responsive Fluorescent Nanovesicles. *Adv. Funct. Mater.* **2021**, 31 (46), 2103511.

94. G. Vargas-Nadal, M. Muñoz-Ubeda, P. Alamo, et al. MKC-Quatsomes: a stable nanovesicle platform for bio-imaging and drug-delivery applications. *Nanomedicine Nanotechnology, Biol. Med.* **2020**, 24, 102136.

95. A. Boloix, N. Feiner-Gracia, M. Köber, et al. Engineering pH-Sensitive Stable Nanovesicles for Delivery of MicroRNA Therapeutics. *Small* **2021**, 18 (3), 2101959.

96. L. V. Allen. Dosage form design and development. *Clin. Ther.* **2008**, 30 (11), 2102–2111.

97. E. Gonzalez-Mira, S. Nikolić, A.C. Calpena, et al. Improved and Safe Transcorneal Delivery of Flurbiprofen by NLC and NLC-Based Hydrogels. *J. Pharm. Sci.* **2012**, 101 (2), 707–725.

98. O. Eskens, G. Villani, S. Amin. Rheological investigation of thermoresponsive alginate-methylcellulose gels for epidermal growth factor formulation. *Cosmetics* **2021**, 8 (1), 3.

99. G. Dumortier, J.L. Grossiord, F. Agnely, J.C. Chaumeil. A Review of Poloxamer 407 Pharmaceutical and Pharmacological Characteristics. *Pharm. Res.* **2006**, 23 (12), 2709–2728.

100. A.A. Koffi, F. Agnely, G. Ponchel, J.L. Grossiord. Modulation of the rheological and mucoadhesive properties of thermosensitive poloxamer-based hydrogels intended for the rectal administration of quinine. *Eur. J. Pharm. Sci.* **2006**, 27 (4), 328–335.

101. G.G. Pereira, F.A. Dimer, S.S. Guterres, et al. Formulation and characterization of poloxamer 407®: thermoreversible gel containing polymeric microparticles and hyaluronic acid. *Quim. Nova* **2013**, 36 (8), 1121–1125.

102. R.C. Rowe, P. Sheskey, M. Quinn. Handbook of Pharmaceutical Excipients, Sixth.; Libros Digitales-Pharmaceutical Press, **2009**.

103. M.T. Cook, P. Haddow, S.B. Kirton, W.J. McAuley. Polymers Exhibiting Lower Critical Solution Temperatures as a Route to Thermoreversible Gelators for Healthcare. *Adv. Funct. Mater.* **2021**, 31 (8), 2008123.

104. A. Fakhari, M. Corcoran, A. Schwarz. Thermogelling properties of purified poloxamer 407. *Heliyon* **2017**, 3 (8), e00390.

105. K. Vehanen, M. Hornof, A. Urtti, H. Uusitalo. Peribulbar poloxamer for ocular drug delivery. *Acta Ophthalmol.* **2008**, 86 (1), 91–96.

106. Y.Y. Chieng, S.B. Chen. Interaction and complexation of phospholipid vesicles and triblock copolymers. *J. Phys. Chem. B* **2009**, 113 (45), 14934–14942.

107. E.J. Ricci, M.V.L.B. Bentley, M. Farah, R.E.S. Bretas, J.M. Marchetti. Rheological characterization of Poloxamer 407 lidocaine hydrochloride gels. *Eur. J. Pharm. Sci.* **2002**, 17 (3), 161–167.

108. S. Khan, M.U. Minhas, I.A. Tekko, R.F. Donnelly, R.R.S. Thakur. Evaluation of microneedles-assisted in situ depot forming poloxamer gels for sustained transdermal drug delivery. *Drug Deliv. Transl. Res.* **2019**, 9 (4), 764–782.

109. X. Yang, R. Yang, M. Chen, et al. KGF-2 and FGF-21 poloxamer 407 hydrogel coordinates inflammation and proliferation homeostasis to enhance wound repair of scalded skin in diabetic rats. *BMJ Open Diabetes Res. Care* **2020**, 8 (1), e001009.

110. J. Russo, J. Fiegel, N.K. Brogden. Rheological and Drug Delivery Characteristics of Poloxamer-Based Diclofenac Sodium Formulations for Chronic Wound Site Analgesia. *Pharmaceutics* **2020**, 12 (12), 1214.

111. E. Giuliano, D. Paolino, M. Fresta, D. Cosco. Mucosal Applications of Poloxamer 407-Based Hydrogels: An Overview. *Pharmaceutics* **2018**, 10 (3), 159.

112. A.C.S. Akkari, J.Z. Boava, G.K. Garcia, et al. Poloxamer 407/188 binary thermosensitive hydrogels as delivery systems for in fi ltrative local anesthesia : Physico-chemical characterization and pharmacological evaluation. *Mater. Sci. Eng. C* **2016**, 68, 299–307.

113. U.C. Galgatte, P.D. Chaudhari. Preformulation study of poloxamer 407 gels: effect of additives. *Int. J. Pharm. Sci. Res.* **2014**, 6 (1), 130–133.

114. P. Alexandridis, T. Alan Hatton. Poly(ethylene oxide)poly(propylene oxide)poly(ethylene oxide) block copolymer surfactants in aqueous solutions and at interfaces: thermodynamics, structure, dynamics, and modeling. *Colloids Surfaces A Physicochem. Eng. Asp.* **1995**, 96 (1–2), 1–46.

115. P. Kolliphor. Kolliphor ® P 407 Poloxamer Ph. Eur., Poloxamer USP/NF Poloxamer for Pharmaceutical Use; **2019**.

116. J. Suksiriworapong, T. Rungvimolsin, A. A-Gomol, V.B. Junyaprasert, D. Chantasart. Development and characterization of lyophilized diazepam-loaded polymeric micelles. *AAPS PharmSciTech* **2014**, 15 (1), 52–64.

117. E. V. Batrakova, A. V. Kabanov. Pluronic block copolymers: Evolution of drug delivery concept from inert nanocarriers to biological response modifiers. *J. Control. Release* **2008**, 130 (2), 98–106.

118. C. Caddeo, M.L. Manca, M. Matos, et al. Functional response of novel bioprotective poloxamer-structured vesicles on inflamed skin. *Nanomedicine Nanotechnology, Biol. Med.* **2017**, 13 (3), 1127–1136.

119. X. Liang, G. Mao, K.Y.S. Ng. Effect of chain lengths of PEO–PPO–PEO on small unilamellar liposome morphology and stability: an AFM investigation. *J. Colloid Interface Sci.* **2005**, 285 (1), 360–372.

120. H.M. Redhead, S.S. Davis, L. Illum. Drug delivery in poly(lactide-co-glycolide) nanoparticles surface modified with poloxamer 407 and poloxamine 908: In vitro characterisation and in vivo evaluation. *J. Control. Release* **2001**, 70 (3), 353–363.

121. J.M. White, M.A. Calabrese. Impact of small molecule and reverse poloxamer addition on the micellization and gelation mechanisms of poloxamer hydrogels. *Colloids Surfaces A Physicochem. Eng. Asp.* **2022**, 638, 128246.

122. J.Y. Chang, Y.K. Oh, H. gon Choi, Y.B. Kim, C.K. Kim. Rheological evaluation of thermosensitive and mucoadhesive vaginal gels in physiological conditions. *Int. J. Pharm.* **2002**, 241 (1), 155–163.

123. M.V.L.B. Bentley, J.M. Marchetti, N. Ricardo, Z. Ali-Abi, J.H. Collett. Influence of lecithin on some physical chemical properties of poloxamer gels: rheological, microscopic and in vitro permeation studies. *Int. J. Pharm.* **1999**, 193 (1), 49–55.

124. K.A. Soliman, K. Ullah, A. Shah, D.S. Jones, T.R.R. Singh. Poloxamer-based in situ gelling thermoresponsive systems for ocular drug delivery applications. *Drug Discov. Today* **2019**, 24 (8), 1575–1586.

125. L. Ballell-Hosa, E. González-Mira, H. Santana, et al. DELOS Nanovesicles-Based Hydrogels: An Advanced Formulation for Topical Use. *Pharmaceutics* **2022**, 14 (1), 199.

"Try again, fail again, fail better"

– Samuel Beckett

4 Opening the frontiers of DELOS nanovesicles for advances in emerging new delivery systems

4.1 Introduction

In the previous **Chapters**, DELOS nanovesicles have been described as an emerging strategy platform for the diagnosis and therapy of different health-related problems within the company's research and development arm. However, Nanomol Technologies SL is also interested in being involved in fundamental research to enrich internal know-how. Therefore, the purpose of this **Chapter** is to present new research lines in which new and valuable proof-of-concepts are evaluated. Then, since we will concentrate on basic research and thus on initial product development approaches, we will focus on TRL such as TRLs like TRL1 and TRL2.

With this aim in mind, our company, together with Nanomol Group, the two institutions involved in this thesis, have participated in many collaborative projects around the world. In this Chapter, part of the research leading to these results was funded by a European project called MSCA-RISE-2017 Research and Innovation Staff Exchange Nano-OligoMed Project, which is financed by the European Union's Horizon 2020 research and innovation program under Marie Skłodowska-Curie grant agreement number 778133.

Considering that this is a Research and Innovation Staff Exchange (RISE) project, it stimulates international and cross-sector collaboration through exchanging research and innovation staff, and sharing knowledge and ideas from research to market (and vice-versa).

Then, this project aims to develop a framework to investigate the development and optimization of novel hybrid bio-responsible nano/microstructured materials for system delivery of oligonucleotide-based therapeutic agents. In particular, the scientific aim of this project is the creation of degradable hybrid structures with the delicate programmable oligonucleotides or artificial oligonucleotide-mimics that will enable:

1. The degradation of the drug carrier at the presence of a specific input as a function of the intrinsic bio-responsive feature of oligonucleotides.
2. The activation of a therapeutic function because of the biomolecular interaction between the oligonucleotide-based material and the molecular target.
3. The delivery of the chemical payload (DNA and/or artificial mimics, even in combination with cancer drugs) upon cell internalization.

As part of this thesis, this project was supported by two internships by collaborating with the laboratory of Prof. Luisa de Cola at the University of Strasbourg in France and with the group of Prof. Maria E. Lanio at the University of Havana in Cuba. Considering that DELOS nanovesicles have demonstrated to be excellent candidates to be used as nanocarriers for the protection and delivery of active ingredients[1], in both stays, the aim was the development of hybrid structures using DELOS nanovesicles. (**Figure 4.1**). This approach is a good strategy to provide not only versatility but also an opportunity for enhancement of colloidal properties of the nanoformulations and result in additional advantages over conventional drug delivery systems (DDSs).

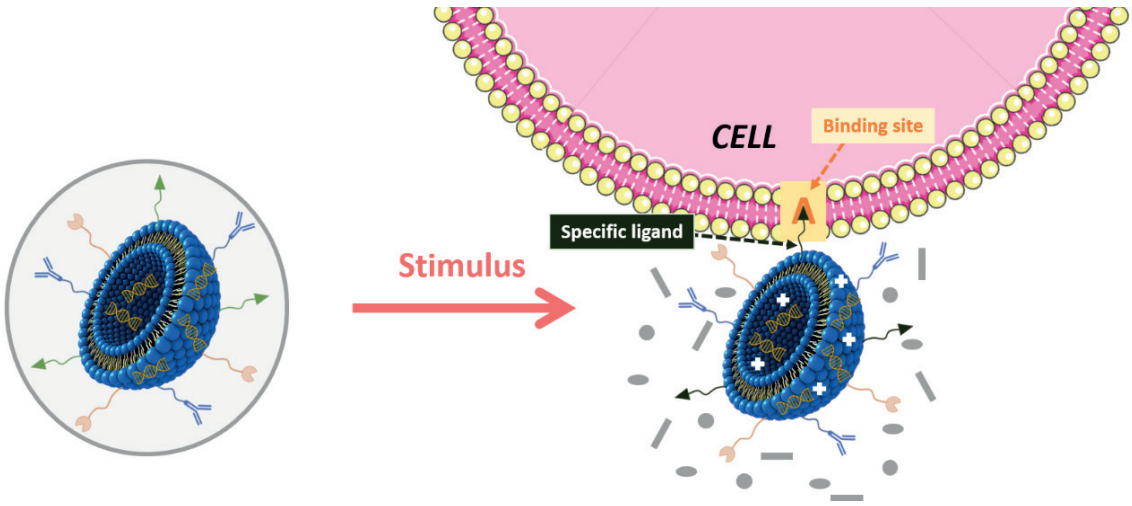

Figure 4.1: Schematic illustration of a hybrid DELOS nanovesicle-based system.

Motivated by the above considerations, in this work we aimed to investigate the possibility of developing new hybrid DELOS nanovesicles-based systems by combining them with two current attractive tools for biotechnological and pharmaceutical applications. Bionanotechnology is an area of science that has transformed the field of drug delivery by integrating biological molecules into nanomaterials, which can lead to improved therapeutic outcomes, not only by making treatments more effective and valuable, but also by reducing their adverse side effects[2,3]. Among all the different existing approaches, and as demonstrated in **Chapter 2** in rhEGF-DELOS nanovesicles formulation

development, the interaction of a protein with some nanomaterials can be a suitable strategy for their functionalization. Therefore, it can enhance the behaviour of the material such a nanocarrier.

In this study, we seek to examine one type of proteins that represents an attractive target for the development of new hybrid biologic-organic nanoparticles based on DELOS nanovesicles and pore-forming proteins (PFPs) like actinoporins. In particular, the use of pore-forming proteins such as sticholysins[4], largely characterized by the Center of Protein Studies at the University of Havana, will be of interest to be integrated into DELOS nanovesicles in order to develop these new hybrid systems. One of the most significant characteristic that this type of protein presents is their capacity to bind specifically to sphingomyelin-containing membranes and suffer a conformational change that drives them to make pores[5,6] (**Figure 4.2**).

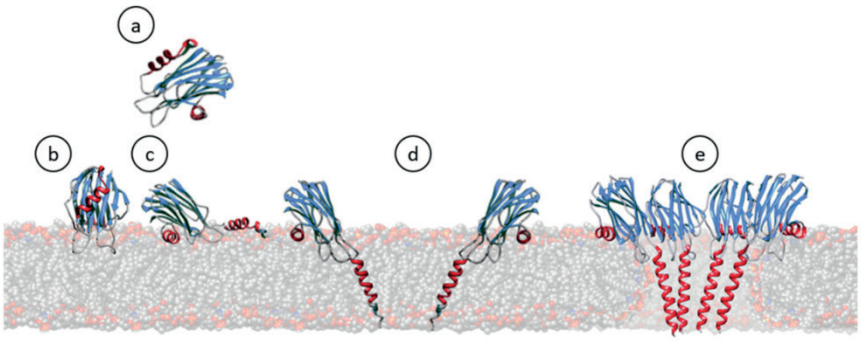

Figure 4.2: Schematic representation showing most of the steps generally accepted for the pore formation mechanism of actinoporins. (a) In solution, they remain soluble and stably folded. However, (b,c,d) upon interaction with a lipid membrane containing sphingomyelin, the protein is extended and inserted in the membrane. (e) Finally, a pore is established. Adapted from[5].

The pore-forming ability of these proteins is a valuable characteristic from a biochemical point of view as they represent a potential use in facilitating drug cell penetration, e.g. oligonucleotides, which are of great interest within the Nano-OligoMed project[5]. Understanding the cellular uptake and intracellular transport of oligonucleotides provides an important basic underpinning for the emerging field of oligonucleotide-based therapeutics[7].

Nonetheless, all forms of oligonucleotides, whether “free” or linked to a drug delivery system, can enter the interior of the cell by endocytic uptake. Endocytosis includes several stages. First, the drug is surrounded by membrane cell invaginations that pinch off to form membrane-bound vesicles, also known as early endosomes. Afterwards, these endosomes traffic downstream endomembrane compartments, initially maturing into late endosomes where drugs can be delivered to various destinations. However, a substantial fraction of the internalized molecules will be transported to lysosomes for degradations. The late endosome fuse with lysosomes where degradation of the endocyted molecules takes place due to the presence of hydrolases[8–10].

Although it appears to be a very idyllic process, a key hindrance to the therapeutic use of oligonucleotides concerns their inability to escape endosomal compartments to reach the cytosol or nucleus of their target cells in sufficient concentrations[11]. Therefore, recent attention has focused on the late endosomal body as a key site for the release of oligonucleotides from this compartment to the cytosol or nucleus of cells[12].

In view of this problematic, in this project we aim to encapsulate oligonucleotides in DELOS nanovesicles that contain sticholysins in their surface. Consequently, using our approach, it is expected that once the hybrid formulation has been entrapped in endosomes, these pore-forming proteins will disrupt these membranes and allow the oligonucleotide delivery to the cytosol[13,14] (**Figure 4.3**).

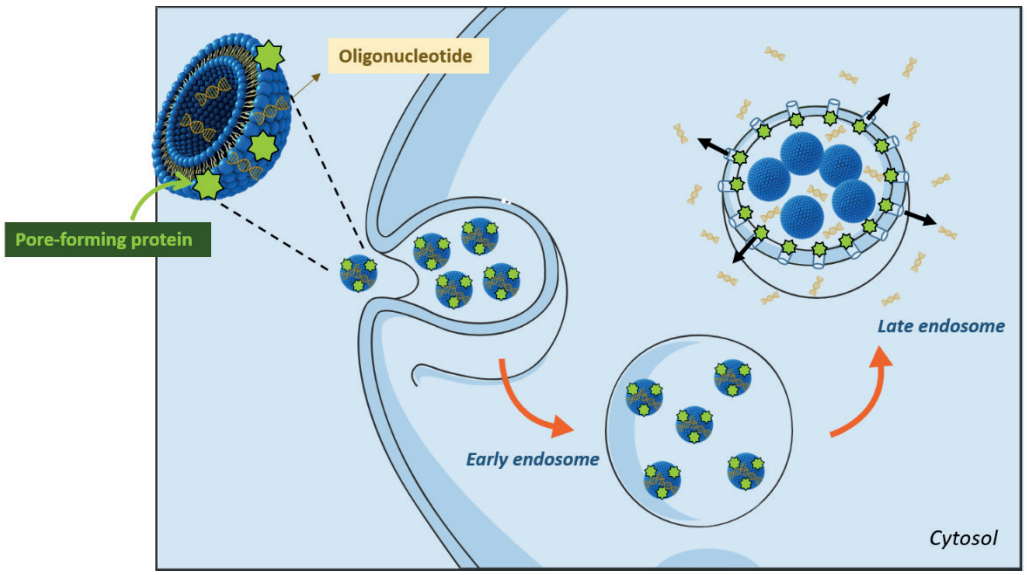

Figure 4.3: Schematic illustration of the endocytosis pathways of the hybrid DELOS nanovesicles containing pore-forming proteins with the objective to deliver oligonucleotides to the cytosol.

In addition, despite the exploratory nature of this study, it offers some insight into new DELOS nanovesicles biomedical applications taking advantage of the functional activity of sticholysins. Interestingly, as these proteins present immunomodulatory properties, the most impactful results reported in the literature were the production of a vaccine platform containing sticholysins. Therefore, as these experimental results encouraged to approach cancer in both preventive and therapeutic scenarios, this proof-of-concept study will serve as a base for future studies in vaccine development using this new hybrid DELOS nanovesicles[15] (**Figure 4.4a**).

On the other hand, thanks to the collaboration with the laboratory of Prof. Luisa de Cola, another approach to be explored was the creation of hybrid organic/inorganic nanostructures based on silica-coated DELOS nanovesicles (**Figure 4.4b**). Undoubtedly, the creation of such a hybrid material is expected

to be a promising class of materials due to the different but complementary nature of the properties intrinsic in these diverse classes of materials. Consequently, complementarity leads to a perfect synergy of properties of the desired material and therefore to a very wide field of applications[16], not only the oligonucleotide delivery as expected in the frame of this project but also many other applications. For instance, the use of a silica coating in DELOS nanovesicles can enhance its stability and improve the encapsulation efficiency of some molecules by inhibiting the leakage from the nanoformulation.

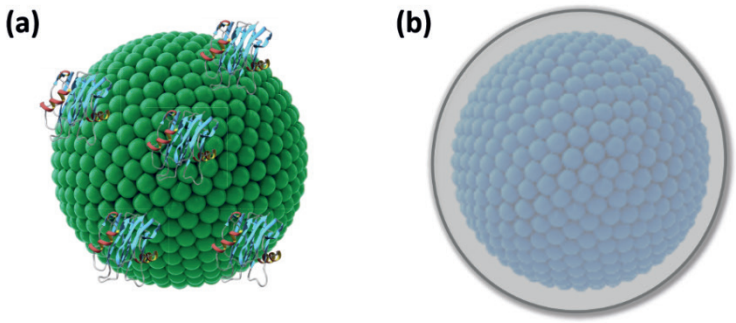

Figure 4.4: Schematic representation of the two evaluated hybrid DELOS nanovesicles systems (a) hybrid system based on sticholysins and DELOS nanovesicles and (b) hybrid system based on silica-coating DELOS nanovesicles.

Finally, outside of this Nano-OligoMed European project, but in the scope of this Ph.D. thesis, different DELOS nanovesicle formulations have been extensively characterized to explore new research lines for the topical drug delivery, a part of complex wounds as defined in the previous **Chapters**. In particular, this study has helped to improve our understanding of the antimicrobial activity of different formulations of DELOS nanovesicles not only in bacteria but also as an antifungal agent. Moreover, it helped to evaluate a broad spectrum of options basically focused on skin diseases in which antimicrobial treatments are needed.

4.2 Hybrid biologic-organic structures based on pore-forming proteins and DELOS nanovesicles

4.2.1 Characteristics of Sticholysins, pore-forming toxins produced by the Caribbean Sea anemone *Stichodactyla helianthus*

Sea anemones are sedentary soft-bodied animals that rely on their venomous secretions to not only paralyze and prepare prey for digestion, but also to defend themselves against predators by secreting large numbers of peptide and protein toxins, enzymes and cytolysins. Regarding cytolysins, they are pore-

forming toxins that exert their activity by creating pores in selected membranes, specifically the ones containing sphingomyelin[17–20]. It should be pointed out that up to now, several families of cytolysins have been identified from diversity wide variety of sources. Particularly, those produced by sea anemones have been named actinoporins, given their functional activity and the order they belong to.

Actinoporins have been found to possess important physicochemical properties for the design of molecular tools with potential medical and biotechnological applications[21]. A part from being pore-forming proteins, they constitute an attractive target in the construction of membrane-acting immunotoxins directed against tumour cells[21–23] and also as an agent with immunomodulatory properties[13,24]. Consequently, integrating them into DELOS nanovesicles, forming a new hybrid system, might give new functions to the nanoformulation. It would not only endow immunostimulatory properties to the system but also it might facilitate drugs to enter into the cytosol by the formed pores and so increase the efficacy of conventional cytosolic anticancer agents[25].

It is worth remarking that most of the actinoporins isolated from sea anemones are small proteins with molecular weight around 20 kDa and with an isoelectric point generally basic, usually above nine. Moreover, most of them are cysteine-less proteins and consequently lack intramolecular or intermolecular disulphide bonds[26].

If we focus on *Stichodactyla helianthus*, a sea anemone from the Caribbean Sea, it produces three isoforms of actinoporin: sticholysins I, II, and III, denoted as StI, StII, and StIII respectively, with the former two being fairly abundant and easily purified in large quantities, while StIII is expressed at much lower levels[5].

Regarding StI and StII, they are the most studied sticholysins at the Faculty of Biology of the University of Havana, our collaborators of Nano-OligoMed project. Both StI and StII show a high amino acid sequence identity between them (93%)[27,28], with the main differences being found in their N-terminus, which is more hydrophobic in StII than in StI (**Figure 4.5**). Then, considering that this region is involved in pore formation, different pore-forming activities are found between both proteins, partly due to their different membrane-binding affinities[4,5].

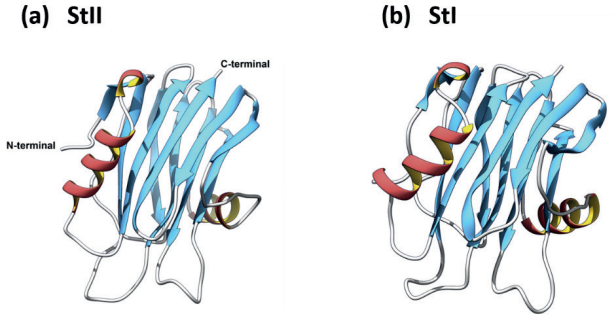

Figure 4.5: Three-dimensional structures of (a) StII and (b) StI showing their similarity. α helices are depicted in red and yellow. β-strands are in light blue. Regions with non-periodic secondary structures are in light grey. Adapted from[29].

In terms of three-dimensional (3D) structure, both StI and StII consist of a tightly folded β-sandwich flanked by two α-helices, one of them located at the N-terminus and directly involved in transmembrane pore formation[30,31]. Moreover, another well-studied protein domain involved in the initial membrane binding step is the exposed aromatic amino acid cluster situated on the broad loop at the bottom of the molecule and the helix α2 as illustrated in **Figure 4.6**. Although this part of the protein is known to have affinity for the membrane interface[31,32], their tryptophan residues have also been shown to be essential for the process of membrane binding. For instance, tryptophan 111 (indicated as W111) present in StI has demonstrated to be key for sphingomyelin recognition[32]. It should be mentioned that in the case of StII, this tryptophan is located in the position 110 instead of 111.

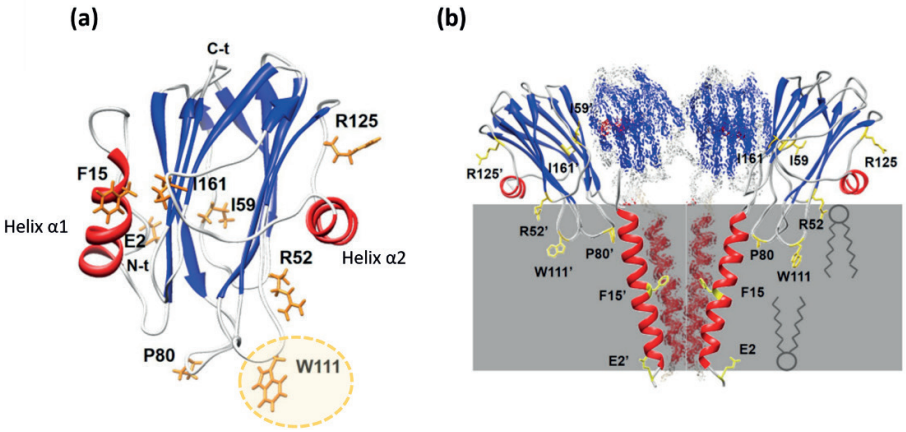

Figure 4.6: (a) Three-dimensional structure of StI, in which the Trp residue (W) W111 is highlighted in yellow round, which is an important amino acid for the interaction of sticholysins with cell membranes. It is important to highlight that StII present similar structure, but the Trp residue is placed in position 110 instead of 111. (b) StI topology in membrane, showing that the W111 residue is placed in the lipid membrane. Adapted from[33].

In this regard, it is hypothesized that sticholysin bind the membrane first via the aromatic cluster and then, N-terminal helix translocates from the surface of the β-sandwich to the membrane and, finally crosses the lipid bilayer, forming the cation-selective pore[34], as previously observed in **Figure 4.2**.

Knowing that the targeting and attachment of proteins to membranes is one of the key steps in many cellular processes, two forms of sticholysins were specifically studied during this Ph.D. thesis, namely StII and a mutant of recombinant StI. It is important to emphasize that although it seems logical to evaluate the StI instead of the StII, due to availability factors, the StI could not be examined. Then, while StI will be considered in further studies, StII was used as a first approach in this study due to the high similarity between StII and StI.

As previously mentioned, most sea anemone actinoporins are cysteine-less proteins. Therefore, the introduction of cysteine (Cys) residues by site-directed mutagenesis has been a useful strategy for understanding the structure-function relationship of actinoporins. In our case, a single mutant of StI named StIW111C was used, in which the Trp 111 residue located at the membrane binding region (**Figure 4.6**) was changed for a cysteine.

What is interesting about this mutant is that it can spontaneously dimerize through disulphide bridging. Then, thanks to this dimerization, the lytic activity of the protein can be inactivated but recovered under a reducing environment[23,31,35]. For instance, it has been demonstrated that it exhibited eight-fold lower pore formation activity than the StI due to its lower affinity for the membrane[36]. Therefore, this behaviour confirmed the importance of residue 111 in binding of the protein to the lipid bilayer[31] and so in its pore-forming ability. Therefore, using this mutant, designated StIW111C, could be possible to design constructions with low unspecific cytotoxicity activity for delivering molecules to the cytosol of target cells.

Knowing all these characteristics and that the interest in these toxins lays in its pore-forming capacity, forming pores with a diameter of around 2 nm in cell membranes[37] and helping in the delivery in the cytosol or nucleus of cells, the aim of this work is to develop a new hybrid system based on DELOS nanovesicles that contains sticholysins in their structure as an approach to optimize the drug delivery of oligonucleotides.

Therefore, the aim of this research project has therefore been to study for the first time the interaction of DELOS nanovesicles and sticholysins as a proof-of-concept for the development of thesenew hybrid systems for oligonucleotide delivery purposes. In particular, the objective of this research was to study whether or not sticholysins and DELOS nanovesicles could interact and the effects of the interactions.

4.2.2 DELOS nanovesicles as approach to create new hybrid system containing sticholysins

With this idea in mind, DELOS nanovesicles will be considered as the nanocarrier responsible for integrating oligonucleotides and also the sticholysins, which will be the factor that would enhance the delivery of nucleic acids to the cytosol thanks to their pore-forming capacity.

When considering DELOS nanovesicles, it is important to know that they are based on the mixture of sterols and ionic surfactants, such as cationic quaternary ammonium surfactants. Then, due to the negatively charged nature of oligonucleotides, the use of cationic formulations has been described as an intriguing strategy for the development of new nucleic acid drug delivery systems[38,39]. For instance, it has been reported that nucleic acid-based cationic liposomes are potential bionanomaterial in the application of therapeutic nucleic acid delivery[40].

Then, considering this information and the possible surfactants used for the preparation of DELOS nanovesicles, CTAB surfactant was considered. As seen in **Figure 4.7a** and described previously, CTAB consists of a 16-carbon hydrophobic chain and a charged polar ammonium head with bromide as a counter ion. Interestingly, this surfactant exhibits many properties such as its potentiality for being used in DNA extraction and also in nanoparticle synthesis[41].

Furthermore, previous studies reported that this cationic surfactant can induce conformational changes in sticholysin proteins during surfactant–protein interaction[42]. Then, studying the interaction of these pore-forming proteins with CTAB-DELOS nanovesicles seems to be a reliable and useful approach.

In addition, for this proof-of-concept study, we also tried Myristalkonium chloride (MKC) surfactant, which is widely used in Nanomol Group for parenteral applications[43]. As shown in **Figure 4.7b**, MKC is a fourteen-carbon homolog of benzalkonium chloride (BAK). BAK is a mixture of different homologs with alkyl chain lengths ranging from 8 to 18 carbon atoms[44], which has already been used as an antimicrobial preservative in 74% of ophthalmic preparations (EMA/352187/2012)[45] and parenteral formulations on the EU and USA market, thus backing up the safety of its use[46]. Up to now, MKC-DELOS nanovesicle formulation based on cholesterol and MKC has proven to be a stable lipid-based nanovesicle platform for *in vivo* injections as it is not destroyed in the presence of human serum, its structure seems to be preserved even after intravenous injection in mice. More importantly, no toxicity was found[47].

It should be mentioned that both types of used surfactants, MKC and CTAB, although they are cationic quaternary ammonium surfactants, they present different polar heads. While CTAB has three methyl group in the ammonium polar head, MKC contains besides a benzene ring on it (**Figure 4.7b**). So, it could be interesting to evaluate if there is any effect of the surfactant polar head on the interaction with sticholysins.

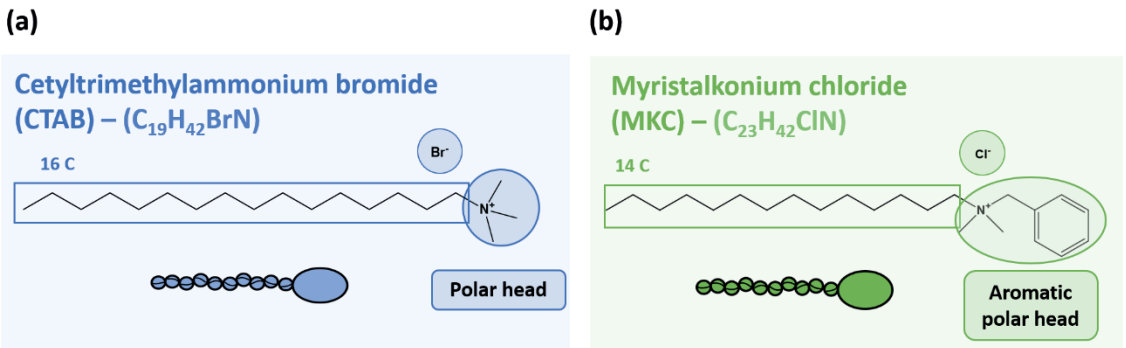

Figure 4.7: Molecular structures of quaternary ammonium surfactants (a) CTAB and (b) MKC in which polar head differences can be observed.

Therefore, having all this information in mind and with the objective to create hybrid structures based on sticholysins and DELOS nanovesicles for the delivery of oligonucleotides, this work specifically concentrates on studying if there exists any evidence of interaction between both systems. Specifically, the interaction between the pore-forming proteins described above, StII and StIW111C, and DELOS nanovesicle formulations prepared using surfactants of different nature (CTAB and MKC) were investigated by using different characterization techniques such as fluorescence spectroscopy and acrylamide quenching to provide useful information about it.

4.2.3 Fluorescence spectroscopy to study the interaction between sticholysins and DELOS nanovesicles

4.2.3.1 Intrinsic fluorescence of sticholysins

In order to address the questions outlined above, the intrinsic fluorescence of sticholysin proteins has been considered as one of the key characteristics to be assessed, as it has been extensively investigated in the literature as an attempt to evaluate lipid-protein interactions[48,49].

Towards this aim, the use of fluorescence spectroscopy to study proteins is focused on evaluating their intrinsic fluorescence originated from the aromatic amino acids (tryptophan (Trp), tyrosine (Tyr), and phenylalanine (Phe)) that absorb UV light for excitation[50–52]. Among these three amino acids, tryptophan is usually the one to be studied since its emission is highly sensitive to its local environment, and hence it is often used as a reporter group for protein conformational changes[53]. For instance, changes in the fluorescence emission spectrum of a protein observed upon addition of lipid vesicles can be a useful tool for studying protein structure and dynamics[54].

As stated above, it is remarkable to mention that the presence of tryptophan in sticholysins is conserved in most other known actinoporins and are located in strategic positions, including the cluster of amino acids involved in the first steps of membrane-protein interaction[55]. StII contains five tryptophans residues while StIW111C has four. So, by using the mutant StIW111C, it was interesting to examine the relevance of this residue located in the cluster of aromatic amino acids that plays a role in membrane recognition and binding but have only a minor influence on the following diffusion and oligomerization steps needed to finally assemble a functional pore[55]. Then, by comparing the changes in fluorescence intensity related tryptophan residues when the protein is free or interacting with the nanovesicles, it would be possible to estimate whether any interaction is happening in these moieties.

Therefore, the question of how sticholysins can interact with DELOS nanovesicles is the area to which this thesis now turns. In this context, to get a concise understanding of this concept, firstly we have been prompted to study and compare the behaviour of StII with the surfactants used in

the preparation of the DELOS nanovesicles to be tested. Specifically, CTAB and MKC in monomeric form were evaluated (**Figure 4.7**).

4.2.3.2 Interaction of StII with free CTAB and MKC surfactants

The effect of CTAB surfactant on the conformation and function of StII has already been studied by fluorescence spectroscopy by Prof. Lanio and coworkers (2007). In this case, it was conclusively shown that the interaction of this surfactant with StII induces subtle conformational changes in the protein that favour the formation of lytic competent structures[42]. Then, knowing that an interaction could occur between CTAB and StII, we first tried to reproduce the same previously reported process.

First, surfactant-induced StII conformational changes were assessed by measuring the protein's intrinsic fluorescence intensity by exciting its Trp residues. To do it, StII was placed in PBS (100 mM, pH 7.4) in a total concentration of 1 µM at room temperature (25 °C). Afterwards, the Trp residues of StII were excited at 295 nm, and fluorescence spectra were recorded in the range of 315-375 nm. Then, the free surfactants were titrated by stepwise addition and after each added volume, fluorescence spectrum was recorded (see **Section 6.7.1**).

As indicated in **Figure 4.8**, and based on previous information[42], it was confirmed that the fluorescence intensity of StII increased with increasing CTAB concentration and reached a constant value at surfactant concentrations above 100 µM. Therefore, these data suggest that CTAB provokes significant changes in the environment of Trp residues of the protein and so changes in the protein conformation. As a result, these residues increase their exposure to solvent and thus their fluorescence intensity increases[42].

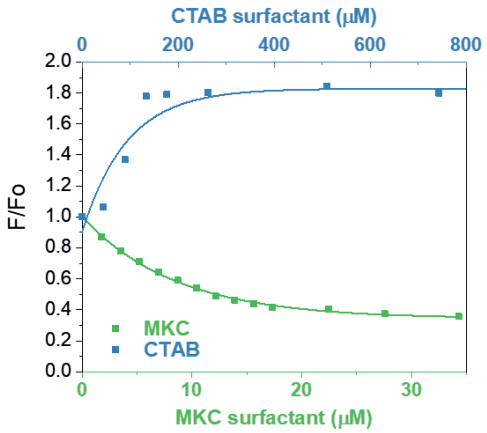

Figure 4.8: Effect of surfactant concentration on the fluorescence intensity of StII (excitation = 295 nm). CTAB:StII (■), MKC:StII (■). StII concentration 1 µM. F/F_0 is the ratio of fluorescence intensities in the presence and absence of surfactant.

Contrary to expectations, the addition of MKC surfactant was first evaluated in this work showing the opposite effect than CTAB, and so suggesting a different kind of interaction with StII. In this case, MKC induced a decrease in the protein's intrinsic fluorescence intensity with increasing concentration of surfactant. Apparently, the MKC surfactant acts as a quencher causing a reduction in fluorescence intensity, what could be related to the differences in the polar heads of the two surfactants (**Figure 4.7**).

As an explanation, we hypothesize that, considering that the MKC surfactant contains a benzene group in its polar head (**Figure 4.7b**), a Π-Π stacking interaction could occur between this aromatic ring and the StII tryptophan residues (**Figure 4.9**). Then, this could explain the quenching effect of this surfactant on the intrinsic StII fluorescence. Moreover, as reported, it can be hypothesized that the quenching effect can also result from tryptophan exposure upon protein unfolding due to the interaction of the surfactant. As a result, it will lead to an overall decrease in the intensity of emission[52].

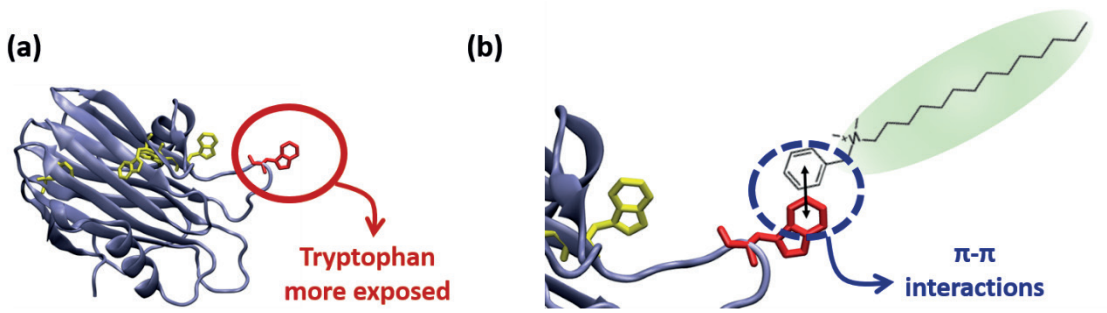

Figure 4.9: Image of (a) StII protein and its tryptophan more exposed (Trp110) and (b) hypothesis of π-π interactions coming from the benzene ring of the MKC surfactant polar head and the most exposed aromatic tryptophan ring of the StII.

In addition, the data shown in **Figure 4.8** indicate that significant changes in the environment of tryptophan residues occur at concentrations below the critical micellar concentration (CMC) of the surfactant (CMC_{CTAB}= 0.9 mM, and CMC_{MKC}= 2.18 mM) and thus occur in surfactant monomer form. Furthermore, as is evident from the data, the addition of both surfactants in monomer form causes saturation of the StII fluorescence intensity. Interestingly, the signal saturates at lower MKC surfactant concentration (15 µM) compared to CTAB (around 200 µM).

In conclusion, StII was shown to interact oppositely with the two evaluated cationic surfactants, CTAB and MKC, which was not expected since both are quaternary ammonium surfactants. However, the chemistry of the surfactant head group has a determining role in protein–surfactant interactions, and so it could be the reason for their opposite behaviour upon interaction with sticholysins measured by fluorescence spectroscopy. Interestingly, as MKC surfactant has shown to produce a quenching effect on the Trp of StII, it will be further studied in next steps.

4.2.3.3 Comparison of the interaction of StII and StIW111C with MKC-systems

Once observed that MKC surfactant in monomer form can interact with StII, we were also interested going to a step forward by examining the interaction of MKC-DELOS nanovesicles with sticholysins.

In the present work, we extend our previous work by incorporating the two sticholysins of interest, StII and StIW111C, and using three different MKC-based systems: MKC-monomers, MKC-micelles and MKC-DELOS nanovesicles, as shown in **Figure 4.10.** MKC-DELOS nanovesicles were prepared using a protocol based on DELOS-susp technology (described in detail in **Section 6.2.1**) and using an equimolar ratio between cholesterol and MKC and a concentration of 7.3 mM of each component. In this protocol, the cholesterol is dissolved in ethanol, and the ethanolic solution is introduced inside a high-pressure vessel and pressurized with CO_2. Finally, the CO_2-expanded solution is then depressurized over an aqueous solution of MKC in PBS (100 mM, pH 7.4).

It has to be mentioned that as stated in the Doctoral Thesis of Dr. Guillem Vargas, the use of a saline medium such as PBS (100 mM, pH 7.4) for the preparation of MKC-DELOS nanovesicles is required to achieve a nanoformulation with appropriate physicochemical properties[43].

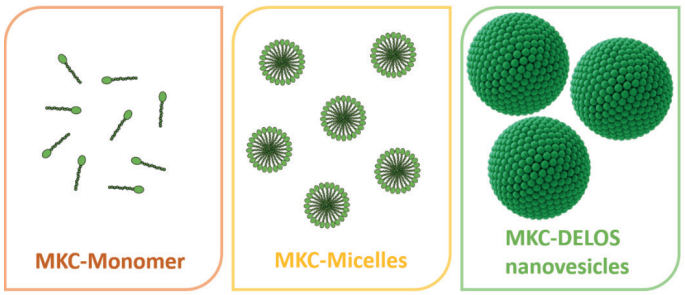

Figure 4.10: Schematic representation of MKC-monomer, MKC-micelles and MKC-DELOS nanovesicles.

Then, to explore how these MKC-based systems interact with sticholysins (StII and StIW111C), titration of the different sticholysins with increasing amounts of MKC-based systems was performed (see **Section 6.7.1**). The methodology used was the same as previously described. First, StII or StIW111C at a protein concentration of 1 µM were placed in PBS (100 mM, pH 7.4) in a total constant concentration of 1 µM at room temperature (25 °C). Afterwards, the Trp residues of StII and StIW111C were excited at 295 nm, and fluorescence spectra were recorded in the range of 315-375 nm. Finally, the MKC-based systems, also placed in PBS (100 mM, pH 7.4) were titrated by stepwise addition from 0 to 34.16 µM of surfactant concentration for MKC-monomer and to 60.55 µM for MKC-DELOS nanovesicles, while for MKC-micelles the evaluated concentration was up to 11.33 mM. Then, after each addition, fluorescence spectrum was recorded.

Figure 4.11 shows a representative series of intrinsic Trp fluorescence emission spectra recorded after the titration of increasing amounts of MKC-based systems over StII or StIW111C. The fluorescence emission spectra in absence of MKC-based systems in StII and StIW111C showed a λ_{max} of 334 nm and 350 nm, respectively. However, when the proteins were titrated with increasing amounts of MKC-based systems, their fluorescent intensities were found to be significantly decreased.

From **Figure 4.11a**, it can be observed that as the ratio of MKC-based systems/StII protein starts to grow, a dramatic decrease of the fluorescence intensity of the protein is induced, indicating the quenching between the surfactant-based system and the protein. In addition, a slight blue-shift can be observed, what could indicate that the tryptophans of the protein enter in a more hydrophobic environment such as the DELOS nanovesicles membrane[56,57].

Conversely, as plotted in **Figure 4.11b**, because of the lower Trp content of StIW111C, the fluorescence spectra exhibit considerable lower reduction of the intrinsic fluorescence intensity of the protein compared to the spectra of StII when interacting with the MKC-based systems. In addition, this reduction involves a slight red-shift in the wavelength of maximum emission, suggesting that StIW111C seems to have less interaction with DELOS nanovesicles membrane compared to StII. This effect could be due to the absence of Trp 111, which is an important residue for the membrane union (**Figure 4.11b**). Moreover, the reason of this minimum red-shift effect would be that the StIW111C protein's buried tryptophan residues are subjected to a more polar environment. Therefore, Trp residues have a greater solvent exposure due to an interaction with the surfactant-based systems[58].

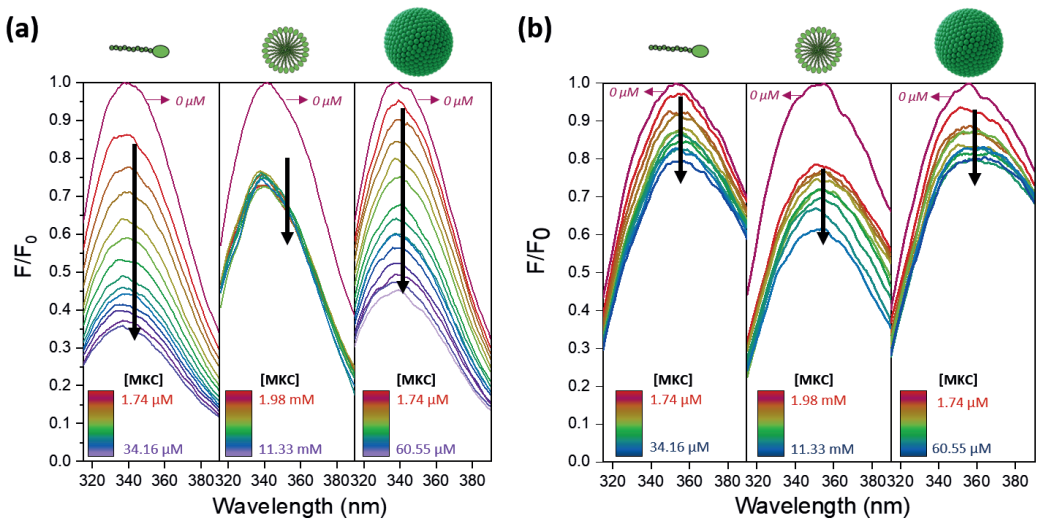

Figure 4.11: Normalized intrinsic Trp fluorescence emission spectra (excitation 295 nm) recorded after the titration of (a) StII (1 µM) and (b) StIW111C (1 µM) with increasing amounts of MKC surfactant (vertical black arrows) by adding MKC-monomers, MKC-micelles and MKC-DELOS nanovesicles respectively. The top curve is a spectrum of the sticholysin fluorescence without the addition of any MKC-based system and decreasing curves are the fluorescence of sticholysin + MKC-based system interaction upon addition of increasing concentration of MKC-based system.

Taken together, the present findings confirm that, in general, all three MKC-based systems evaluated in the titration experiment provoke a decrease in the intrinsic fluorescence intensity of both sticholysins as the MKC surfactant concentration is increased. Focusing on StII, it shows a larger decrease in fluorescence intensity than StIW111C when working with MKC-monomers and MKC-DELOS nanovesicles (**Figure 4.12 a,c**). This phenomenon could be related to the absence of tryptophan 111 in the StIW111C structure, the most exposed tryptophan residue in the Sts structure and the one associated with membrane binding[31]. Consequently, this tryptophan appears to have a relevant role in detecting the interaction between the protein and the MKC surfactant.

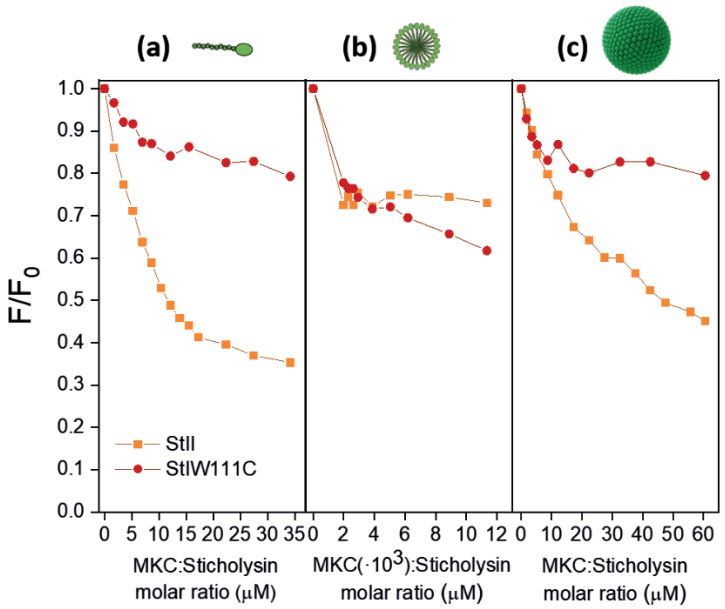

Figure 4.12: Plot of the ratio of total fluorescence intensity (excitation = 295 nm) of 1 μM of StII at 334 nm (orange) and 1 μM of StIW111C at 350 nm (red) in the presence (F) and in the absence (F_o) of (a) MKC-monomers, (b) MKC-micelles and (c) MKC-DELOS nanovesicles versus their concentration.

Interestingly, as shown in **Figure 4.12b,** the titration of MKC-micelles over both sticholysins, a similar decrease in fluorescence intensity was also detected. However, in this case, signal saturation was rapidly reached with increasing MKC concentration. This could be related to the presence of higher concentrations of MKC compared to the other groups, since we are working above the CMC value to have the surfactant in its micellar form. Then, above CMC, the high amount of surfactant molecules can bind to the most accessible tryptophans of the protein and rapidly saturate their fluorescence emission signal.

Finally, increasing concentrations of MKC-DELOS nanovesicles also caused a decrease in intrinsic fluorescence intensity for StII and StIW111C. In this case, although it bears a resemblance to the interaction profile of MKC-monomers, MKC-monomers achieve a greater reduction in StII tryptophan fluorescence intensity with almost half the MKC concentration. As shown in **Figure 4.12**,

while MKC-monomers achieve 65% of fluorescence reduction with 35 µM of MKC surfactant, MKC-DELOS nanovesicles achieve 55% with nearly 60 µM of MKC surfactant. This phenomenon could be attributed to how is the surfactant nanostructured. Therefore, the different arrangement of the surfactant can impact on the accessibility of the MKC benzene ring for the StII tryptophan residues. As discussed in the literature, a possible explanation could be that the nature of a surfactant-protein interaction depends on the geometric properties of the surfactant. The presence of monomeric surfactant is of potential concern as it can interact with regions of the protein that would not be accessible to a surfactant integrated into a bilayer such as in DELOS nanovesicles or micelles[59].

At the same time, it is also reported that the factors responsible for protein properties may depend on the physicochemical properties of the microenvironment in which the protein works[60,61]. Therefore, variations in the structure of the MKC surfactant could alter the protein microenvironment and thus be determinative of the protein-surfactant interaction[62].

In summary, fluorescence interaction analysis provides a useful approach to detect differences in the interaction between sticholysins and surfactant-based systems, demonstrating that depending on the quaternary ammonium surfactant disposition, the interaction can change.

In the light of the reported results evaluating the interaction of surfactant-based systems with sticholysins, StII demonstrate more changes in fluorescence emission in the presence of DELOS nanovesicles and so, there could be more interaction compared to StIW111C. However, more studies should be carried out to determine the potentiality of the new hybrid system. For instance, not only should structural studies be carried out to understand the structure of the proteins when interacting with DELOS nanovesicles but also the reversibility of the interaction should be considered. Furthermore, the cytotoxicity of the protein is a key parameter to consider when it is interacting with DELOS nanovesicles compared when it is in free form.

4.2.3.4 Comparison of the interaction of StII and StIW111C with CTAB- and MKC-DELOS nanovesicles

Considering previous measurements, CTAB-DELOS nanovesicle formulation was also analysed to expand the use of DELOS nanovesicles to interact with sticholysins as a strategy to create a new drug delivery platform.

For this purpose and as explained previously, CTAB-DELOS nanovesicle system was chosen as a well-established reference DELOS nanovesicle system. In this case, this system was also prepared by DELOS-sup procedure, following the same steps and concentrations as mentioned in previous **Section 4.2.3.3** but CTAB surfactant was used instead of MKC (see **Section 6.2.1**). Then, the same titration experiment of this DELOS nanovesicle system over sticholysins was performed as previously described (**see Section 6.7.1**).

As shown in **Figure 4.13**, the result of this analysis is then compared with the one obtained with MKC-DELOS nanovesicles. From these results, it is clear that CTAB-DELOS nanovesicles had a similar tendency of fluorescence intensity reduction of the protein tryptophans as observed previously for MKC-DELOS nanovesicles (**Figure 4.12**). Moreover, the reduction of tryptophan fluorescence of the sticholysins was more abrupt in StII compared to StIW111C. These findings indicated again that such reduction was significantly associated with the interaction of the most exposed tryptophan of sticholysins, which is absent in the mutant StIW111C, with DELOS nanovesicle membrane.

Furthermore, by comparing MKC- versus CTAB-DELOS nanovesicles, it can be observed that the reduction in fluorescence intensity using CTAB-DELOS nanovesicles was not as severe as in MKC-DELOS nanovesicles. Up to now, it was hypothesized that the benzene ring of the MKC surfactant of MKC-DELOS nanovesicles was one of the responsible factors for the interaction of DELOS nanovesicles and sticholysins interaction. However, thanks to the use of CTAB-DELOS nanovesicles, it is also suggested that the protein-DELOS nanovesicle interaction might also involve other parameters such as electrostatic affinity, adsorption, among other types of interactions[63,64].

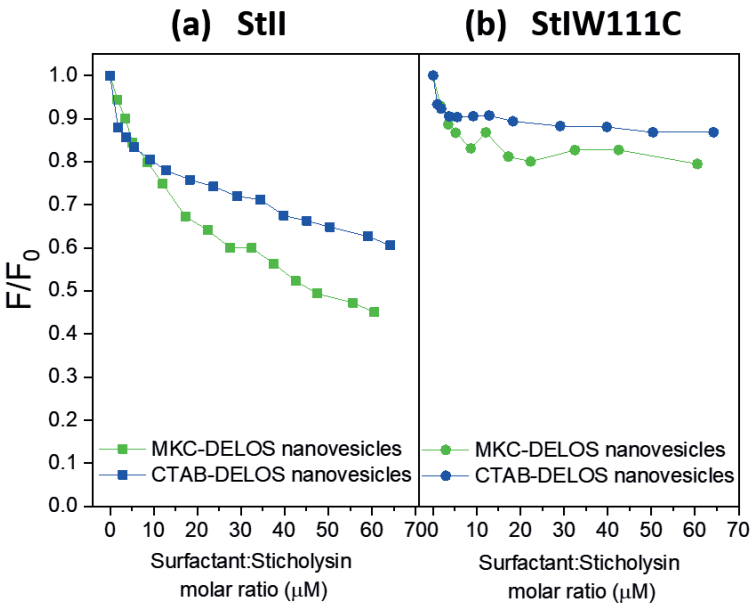

Figure 4.13: Plot of the ratio of total fluorescence intensity (excitation = 295 nm) of (a) 1 μM of StII at 334 nm and (b) 1 μM of StIW111C at 350 nm in the presence (F) and in the absence (F_0) of increasing concentrations of MKC- and CTAB-DELOS nanovesicle (green and blue, respectively).

Interestingly, it should be pointed out that marked differences in the titration of CTAB surfactant assembled into DELOS nanovesicles or as a free monomer over sticholysins were obtained, which to the best of our knowledge is unprecedented in the literature. Intrinsic sticholysin fluorescence profiles reveal that when the CTAB surfactant is assembled into DELOS nanovesicles, the Sts fluorescence decreases, while in monomeric form, it acts as a fluorescence intensity enhancer of

these proteins (ref), as shown in **Figure 4.8**. These observations, in turn, indicate that sticholysin proteins can exhibit different fluorescence properties depending on both the type and assembly approach of the quaternary ammonium surfactant form. Furthermore, these differences may be due to different surfactant recognition sites in sticholysins, which could be close to the tryptophan residues. Consequently, different conformational changes can occur, causing differences in fluorescence emission.

It should be highlighted that this new hybrid system will be studied in more detail outside the scope of this Thesis. Not only circular dichroism will be performed to understand the conformational change of proteins upon interaction with DELOS nanovesicles but also the reversibility of the interaction will be considered.

To further study the interaction of sticholysins and the surfactant-based systems, we next explored a fluorescence quenching method. Indeed, fluorescence quenching is a powerful method to study the solvent accessibility and localization of fluorescent molecules within assemblies such as lipid bilayers. Therefore, it allows determining the depth of penetration of tryptophan residues into membranes, which helps to interpret the nature of interaction of the proteins with different systems, such as vesicles[65]. In this regard, the level of exposure of tryptophan residues in proteins could be estimated by the efficiency of tryptophan fluorescence quenching.

4.2.3.5 Acrylamide quenching of sticholysin tryptophan fluorescence

In the present study, acrylamide (2-propenamide) was used as a model quencher molecule as it is widely used as a quencher of tryptophan fluorescence in studies designed to elucidate the structure and function of proteins[66]. This substance can diffuse into the interior of the protein and then induce a quenching reaction by physical contact with the excited indole ring of tryptophan or proteins located on the surface of the protein, or by the presence of channels leading to the interior of the protein[67].

Quenching intrinsic protein fluorescence by acrylamide is a proper method to monitor protein conformational changes associated with an interaction. In our case, an attempt was made to correlate the accessibility of surfactant-based systems with the tryptophan regions of the proteins by quenching fluorescence with acrylamide. Therefore, when the proteins interacts or binds with the surfactant-based systems close to the protein's tryptophan, the acrylamide's accessibility for the tryptophan can change and so the quenching capacity[66].

Thus, to investigate the tryptophan exposure of the two types of sticholysins in the presence of surfactant-based systems, we recorded the fluorescence emission spectra of each protein, StII and StIIW111C, containing the mixture of 1 μM of protein and the maximum concentration of

the surfactant-based system evaluated in previous section and then, progressive additions of acrylamide were used. Afterwards, changes in the fluorescence intensity of the proteins were monitored in the presence and absence of all evaluated surfactant-based systems **(see Section 6.7.1 for details)**.

To confirm the quenching mechanism, the spectral data was evaluated by Stern-Vomer equation **(Equation 4.1)**, where F_0 and F are fluorescent intensities of protein in absence and presence of the quencher respectively, Ksv is the Stern-Volmer quenching constant, which denotes the accessibility of tryptophan to the quencher and the quenching efficacy, and Q is the concentration of the quencher.

$$\frac{F_0}{F} = 1 + K_{SV}(Q)$$

Equation 4.1: Stern-Volmer relationship, where F_o and F are the fluorescence intensities in the absence and presence of quencher, respectively, K_{SV} is the Stern-Volmer quenching constant and Q is the quencher concentration.

By plotting F_0/F vs Q, the slope obtained is equal to the Stern-Volmer constant, as shown in **Figure 4.14**. In all the cases studied, a positive and linear deviation from the Stern-Volmer behaviour was observed, indicating that an homogeneous population of Trp is equally accessible to quencher, and therefore, most likely, also in terms of protein conformation in the Trp microenvironment[65,67,68].

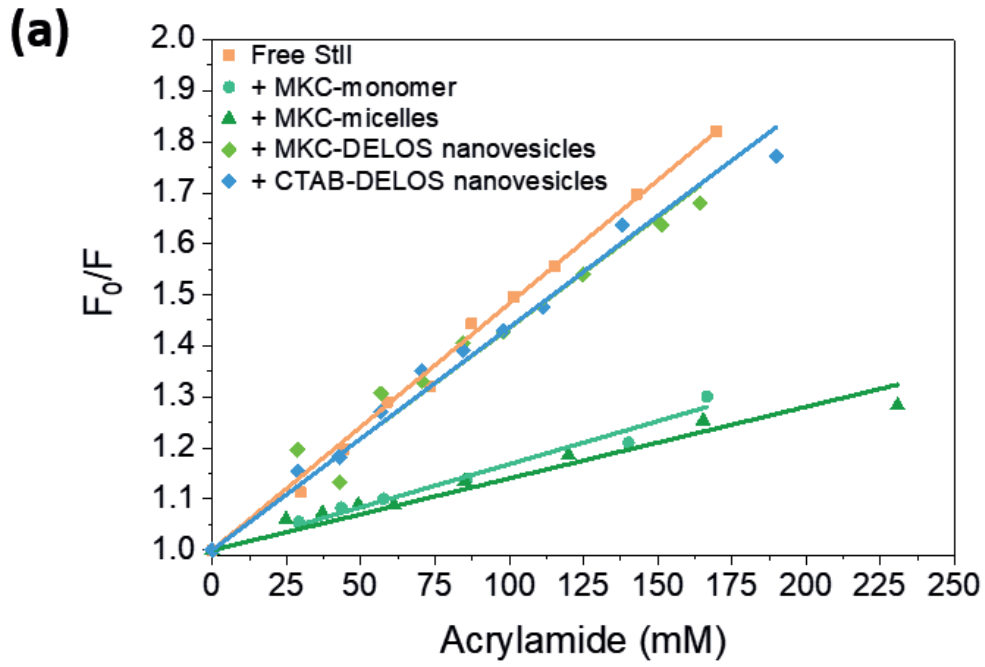

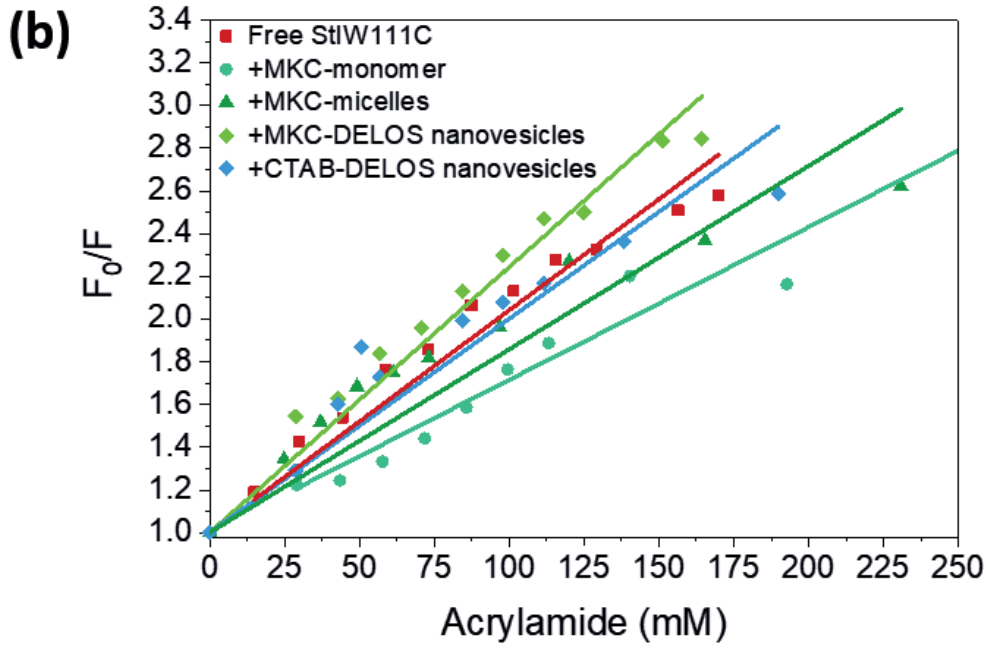

Figure 4.14: Stern-Volmer plots of (a) StII and (b) StIW111C Trp quenching by acrylamide in the absence and presence of MKC-monomer, MKC-micelles, MKC- and CTAB-DELOS nanovesicles. F is the measured fluorescence intensity and F_o is the initial fluorescence intensity in the absence of acrylamide but in the maximum concentration of the surfactant-based system.

Key results then emerge from the extracted Stern-Volmer constant given in **Table 4.1**. On the one hand, free StII and StIW111C showed different Stern-Volmer constants, 4.83 ± 0.06 $\cdot 10^{-3}$ and 10.40 ± 0.35$\cdot 10^{-3}$ M^{-1}, respectively. These values agree with the difference of number of tryptophans present in both proteins and so the difference of accessibility of tryptophan to quencher.

On the other hand, similar conclusions were reached by the comparison of both proteins, StII and StIW111C in the presence of all surfactant-based systems. First, when evaluating the presence of MKC-monomer and MKC-micelles in sticholysins, differences in the quenching curves, and so the Stern-Volmer constant (**Figure 4.14** and **Table 4.1**), were observed compared to the free protein. These differences in quenching might be related to the capacity of MKC-monomers and MKC-micelles to quench Trp residues and so, acrylamide do not have access to that tryptophans.

Contrary to expectations, this study did not find a significant difference in the Stern-Volmer constants of both proteins in the presence of both MKC- and CTAB-DELOS nanovesicles compared to the free protein. This phenomenon indicates that the protein tryptophans, with and without the presence of DELOS nanovesicles, are almost equally accessible to quenchers. Then, the results obtained here suggest that DELOS nanovesicles do not promote a change in protein structure. However, it is crucial at this stage to mention that acrylamide might compete with DELOS nanovesicles to quench the protein tryptophans, indicating a transient and weak binding affinity between sticholysins and DELOS nanovesicles.

Table 4.1: Stern-Volmer constants of sticholysins in solution and the presence of surfactant-based systems.

System*	StII ($\cdot 10^{-3}$ M^{-1})	StIW111C ($\cdot 10^{-3}$ M^{-1})
Free protein	4.83 ± 0.06	10.40 ± 0.35
MKC-monomer	1.68 ± 0.06	7.10 ± 0.27
MKC-micelles	1.40 ± 0.07	8.60 ± 0.63
MKC-DELOS nanovesicles	4.30 ± 0.14	12.40 ± 0.37
CTAB-DELOS nanovesicles	4.36 ± 0.10	10.02 ± 0.66

*All systems were evaluated in PBS (100 mM, pH 7.4).

In this context, it is useful to note that although fluorescence spectroscopy has not provided detailed information about the structure of protein folding, acrylamide suggests that the interaction between the components of this new hybrid system is dynamic. Then, although many other studies are suggested to be carried out to understand this new hybrid system, different strategies can be applied to improve the interaction. On the one hand, one approach to enhance the strength of the interaction would be anchoring a moiety in the protein that would help the membrane protein integration. However, another strategy could be to favor the electrostatic interaction between DELOS nanovesicles and sticholysins with tunable pH sensitivity. It would be then interesting that sticholysins are released from DELOS nanovesicles upon cell internalization, specifically at late endosome pH (**Figure 4.3**). Then, sticholysins would favor the pore-forming capacity in these membranes and help deliver the desired active components such as oligonucleotides.

4.2.4 Summary of the section

In summary, this study has shown that different interactions can emerge from the development of a new hybrid biologic-organic system composed of DELOS nanovesicles and sticholysins for the oligonucleotide delivery.

On the one hand, the results indicate that the structural arrangement of the surfactant molecules has an impact on the way sticholysins, StII and StIW111C, and MKC-based system interact, as the effects are completely different using MKC-monomers, MKC-micelles or MKC-DELOS nanovesicles. Fortunately, we have provided experimental evidence supporting that DELOS nanovesicles could interact with sticholysins mostly through π-π interactions when there is the presence of MKC surfactant. However, acrylamide quenching studies suggest that the interaction of StII and StIW111C with CTAB- and MKC-DELOS nanovesicles might be transient.

Taken together, this study has demonstrated, for the first time, that MKC- and CTAB DELOS nanovesicles are feasible formulations to interact with sticholysins and so create a new hybrid formulation for the delivery of oligonucleotides, among other applications. Consequently, this study opened up new challenges in this field and so open a new area of possibilities for being used in future delivery systems.

However, little is known about how the formation of this new hybrid system can influence the physical, chemical, and biological properties of sticholysins when interacting with DELOS nanovesicles. For this reason, more research is required to understand in detail the interaction between DELOS nanovesicles and sticholysins. Experiments using circular dichroism to understand how the secondary structure of the protein changes when interacting with DELOS nanovesicles, or the use of DLS and cryo-TEM to observe other important physicochemical characteristics of the hybrid system are needed. Moreover, studying the reversibility of the interaction would be also a key factor to consider. Depending on the interaction strength, changes in the protein would be considered to favour stronger interactions with DELOS nanovesicles.

Finally, it should be mentioned that the present study makes several noteworthy contributions to the development of a methodology for studying proteins and DELOS nanovesicles by fluorescence spectroscopy. Then, this research extends the current know-how of the Nanomol Group and Nanomol Technologies for studying protein-vesicle interactions and for sure, it would be very useful for studying other types of proteins in the future.

4.3 Hybrid inorganic-organic structures based on silica and DELOS nanovesicles

4.3.1 Strategy for developing a hybrid DELOS nanovesicle system and silica

As already explained in the Introduction of this **Chapter**, one of the main scientific goals of the Nano-OligoMed project is the creation of new degradable hybrid structures that integrate sensitive programmable oligonucleotides or artificial oligonucleotide-mimics.

In this regard, the design and preparation of nanostructured materials with one or more predetermined functions, i.e., the development of so-called functional or multifunctional materials, represents an extraordinary challenge for the science and technology of materials. Examples include hybrid materials that are provided with specific function in response to different stimuli. Therefore, they can act on their environment through predictable activity, either spontaneously or by stimulating physical and chemical processes[69].

The development of hybrid DELOS nanovesicles with the capacity to respond to a given stimulus has attracted extensive interest owing to their dramatically enhanced selectivity and specificity. To date, current efforts to create hybrid systems in the world of nanoparticles have revolved around the modification of the surface such as the use of polymers or coatings to enhance their properties and so the applicability[70,71]

For instance, nanoparticle surface coatings are often required to increase their stability, to reduce immune clearance and thereby increase circulation times allowing the carriers to reach their target site, which is usually solved by using synthetic polymers, most commonly polyethylene glycol (PEG)[72]. However, other alternative bioinspired or synthetic strategies exist for nanoparticle shielding strategies. For instance, some ways in which polymers can become part of the architecture of the nanoparticle are by physical or chemical absorption or by electrostatic interaction, among others[73,74]. However, the appropriate coating will need to be chosen based on the requirements of the nanoparticle application (**Figure 4.15**).

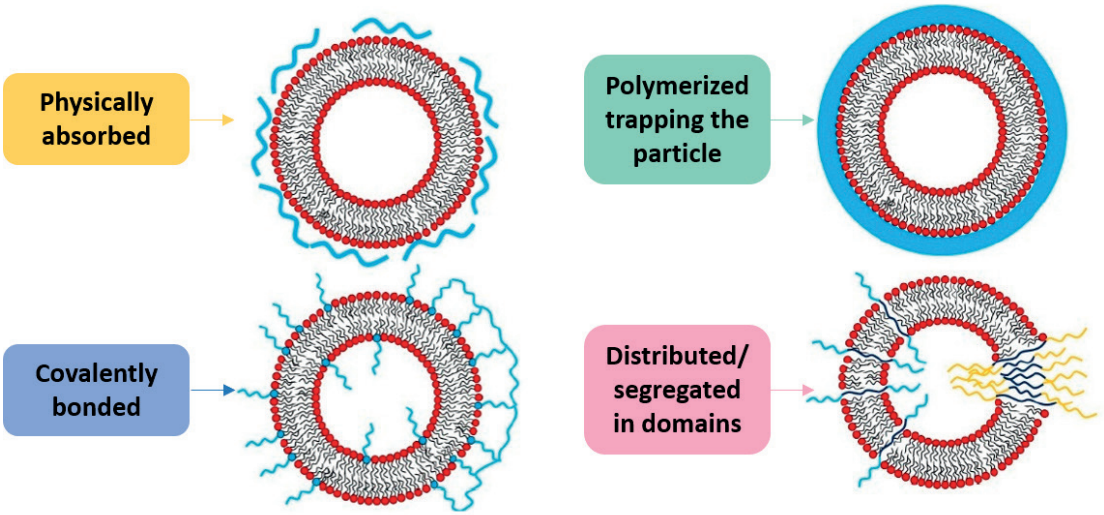

Figure 4.15: Representative image of some of the nanoparticle surface coating approaches used. Adapted from[74].

With this objective in mind, in collaboration with the laboratory of Prof. Luisa de Cola (Laboratory of Supramolecular Biomaterials and Chemistry) in the Supramolecular Science and Engineering Institute (ISIS) from the University of Strasbourg in France, we explored the creation of hybrid organic/inorganic nanostructures based on DELOS nanovesicles and inert silica. Among all the possible coatings, in this Thesis we will focus on silica-based coatings due to our collaborators' expertise in nano and porous silica structures, such as silica mesoporous nanoparticles (MSNPs) for biomedical applications (**Figure 4.16a**). Up to now, there are growing appeals for silica due to its promising characteristics like chemical inertness, its biocompatibility and also it is inexpensive, hydrophilic and

low-priced[75,76] (**Figure 4.16b**). Additionally, not only does the FDA approve silica a material for oral use, but it has also been reported to be stable at around pH 1-2 when it forms a coating. Then, silica may be an appropriate strategy to protect nanovesicles from the harsh environment of the gastrointestinal tract, making it an attractive material to enhance oral delivery[77,78].

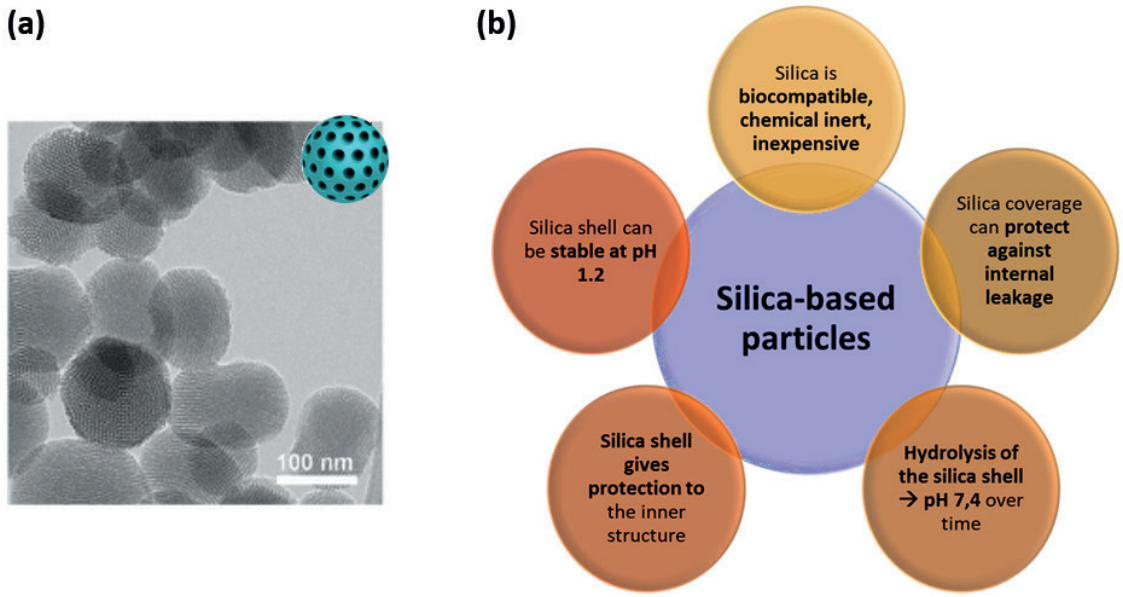

Figure 4.16: (a) TEM image of MSNPs, showing the nanochannel pattern and dimensions, adapted from[79] and (b) Scheme of the principle characteristics of silica-based particles.

In terms of silica functionalities, a large number of silica-coated nanoparticles models have demonstrated that its use can be a proper strategy to overcome some problems associated with current technologies, such as the stability of the liposome bilayers[80,81]. Additionally, when used as a coating agent in nanoparticles, it can offer several remarkable properties such as protection the inner structure, protection against internal leakage and also the ability to control the release of the integrated drug[82,83].

Then, of particular interest is the combination of silica and DELOS nanovesicles, what may lead to new hybrid materials with new characteristics. For instance, the use of silica might endow protection to DELOS nanovesicles in front of aggressive dispersant media such as the gastric one and at the same time, converting them into a system with a favourable on-demand site-specific controlled drug release. Herein, we present a simple and highly efficient method to prepare silica-coated DELOS nanovesicles, which was successfully achieved for the first time during the thesis of Dr. Kubli from ISIS in the frame of the same Nano-OligoMed project. In this regard, this Chapter is devoted to exploring and discussing the physicochemical properties of this organic-inorganic hybrid nanomaterial, and its stimuli-responsive capacity has been evaluated by using different approaches.

4.3.2 Fundamentals of the silica-coated DELOS nanovesicles (SCDN)

The preparation of SCDN was based on the optimized methodology previously studied by Dr. Mariel Kubli. This methodology was developed during her stay in Nanomol Group in the frame of Nano-OligoMed project, obtaining promising results in covering DELOS nanovesicles with silica (**Figure 4.17**).

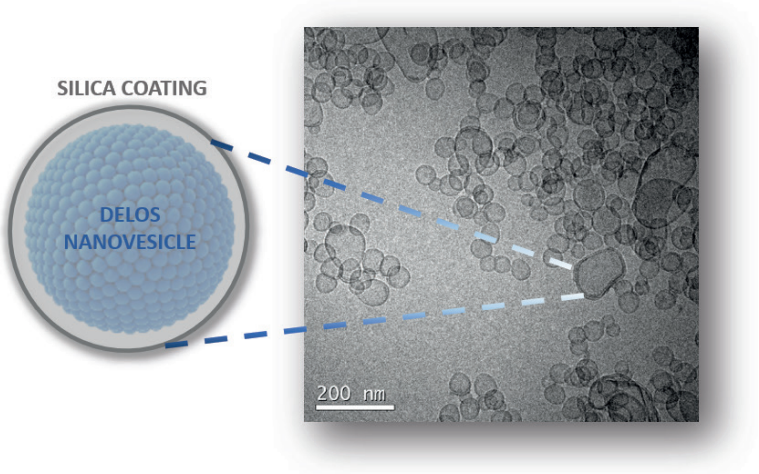

Figure 4.17: Schematic representation of a SCDN and its morphology observed a by cryo-TEM and using the optimized formulation obtained by Dr. Mariel Kubli, in which a thicker layer of the vesicle is observed indicating the presence of the silica coating around DELOS nanovesicles.

This methodology, described in **Section 6.7.2**, basically involves coupling a precursor inorganic silica framework material with DELOS nanovesicles by template synthesis. A fundamental condition for this method is that an attractive interaction between the template and the silica precursor is produced to ensure inclusion of the structure director without phase separation taking place[84]. So, in case of using positively charged DELOS nanovesicles, an interaction of the silica precursor (negatively charged above its isoelectric point around pH = 2[85]) and the cationic surfactant will be produced.

Then, the synthesis of the silica coating typically involves the hydrolysis and condensation of silanes, in aqueous solution under basic or acidic catalysis, as observed in **Figure 4.18a**, producing silica silica frameworks over time[86–88]. For instance, the silica precursor used in this work is the an alkoxysilane such as tetramethyl orthosilicate (TEMOS), as shown in **Figure 4.18b.**

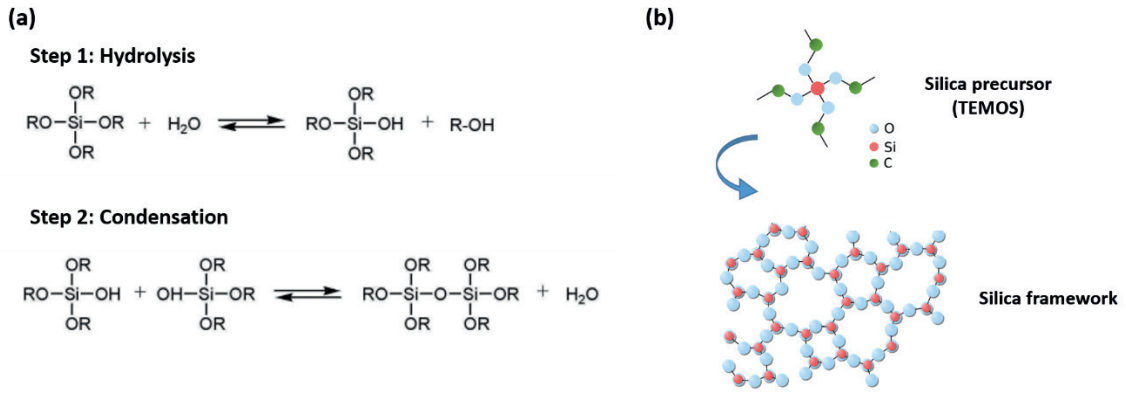

Figure 4.18: (a) Reaction scheme of the hydrolysis and condensation of silica precursors, (b) TEMOS chemical structure and a representation of a silica framework representative of the coating in DELOS nanovesicles.

It should be noted that the presence of surfactants such as CTAB micelles during these reactions is known to acts as a structure-directing agent[84]. Then, in our case, DELOS nanovesicles are used as templates for the deposition of silica from aqueous solution leading to silica-coated vehicles[84,88,89] (**Figure 4.17**).

Knowing that SCDN can be produced, the present Chapter concentrates on their preparation and characterization to demonstrate its potentiality. In particular, this work will focus on evaluating the silica coating behaviour, such as its stability and so it integrity in different dispersant media.

4.3.3 Preparation and physicochemical characterization of SCDN for evaluating silica coating behaviour

In an attempt to understand the behaviour of SCDN, the stability and so the integrity of the coating was evaluated in presence of different dispersant media. To do it, FRET phenomenon was considered as a proper strategy as explained in **Section 3.2.2.6** from **Chapter 3**.

However, in this case, the experimental set up was based on using DELOS nanovesicles integrating DiI dye (donor) in the membrane of the vesicles and Alexa Fluor 647 dye (acceptor) in the silica coating (**Figure 4.19**). In particular, Alexa Fluor 647 is also a synthetic cyanine dye that has demonstrated to be more resistant to photobleaching and brighter than cyanine dies[90].

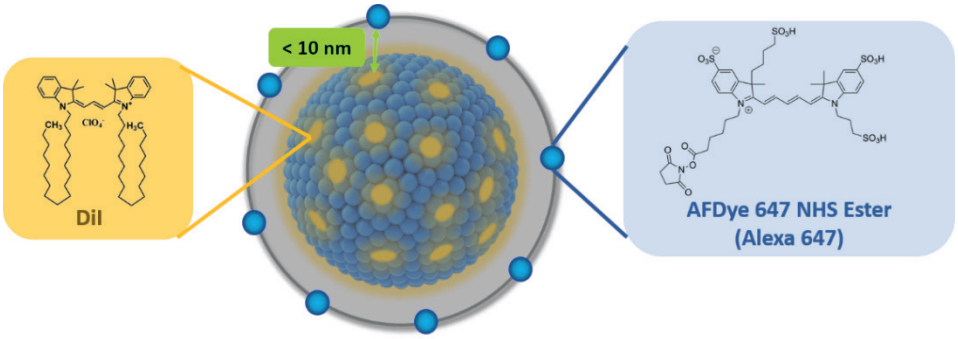

Figure 4.19: Schematic representation of the DiI-SCDN integrating Alexa Fluor 647 dye in the silica coating.

It is important to highlight that both dyes are considered a FRET dye pair as one essential requirement for FRET phenomena is accomplished, which is that the emission spectra of the donor fluorophore and the absorption spectra of the acceptor molecule overlap, as observed in **Figure 4.20**.

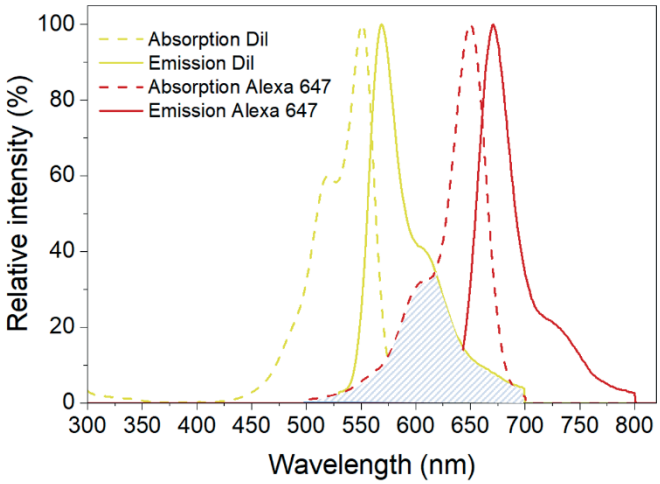

Figure 4.20: Absorption and emission spectra of DiI (yellow) and Alexa Fluor 647 dye (red), used as a FRET pair. The blue hatched area shows the overlap between the donor emission and acceptor absorption spectra, which is a necessary requirement for FRET. Adapted from[91].

Then, as stated in **Chapter 3**, FRET establishes the possibility of studying on a localized spatial scale the interactions between two dyes. Specifically, if the intermolecular distance between these two dyes is close enough (less than 10 nm), energy transfer can take place between the donor and the acceptor, and the FRET effect can be detected. Therefore, it can be understood that upon modification of the silica coating, such as destabilization and hence a breaking, a reduction in the FRET effect is expected to be observed by increasing the distance between the donor and acceptor dyes[92–94].

4.3.3.1 Suitability of the SCDN methodology as a confirmation before FRET evaluation

Before starting all the preparation of samples for FRET study, we first confirmed that the preparation of SCDN could be perfectly achieved. To do it, DiI-SCDN sample was prepared using DiI-DELOS nanovesicles and TEMOS as silica precursor for the silica coating (Figure 4.21) (see Section 6.7.2).

Briefly, DiI-DELOS nanovesicles were prepared by DELOS-susp using 1:1 molar ratio of cholesterol:CTAB with 7.3 mM of each component, 100 µM of DiI, and water/10% EtOH ($v \cdot v^{-1}$) as dispersant medium (**see Section 6.2.1**). Then, in order to prepare DiI-SCDN, TEMOS (DELOS nanovesicle:TEMOS molar ratio of 1:108) was dissolved in ethanol and added to a syringe.

Afterwards, it was added in 1 $\mu L \cdot min^{-1}$ in a balloon where DiI-DELOS nanovesicles in water were found around pH 3.0 under stirring. Once finished the addition of TEMOS, the solution was left stirring for 5 days to ensure a proper coating. Finally, the reaction was stopped by changing the dispersant medium of the sample to water around pH 6.0-7.0. Then, samples were left in the fridge for better conservation.

It should be mentioned that DiI-DELOS nanovesicles without any coating, now called uncoated DiI-DELOS nanovesicles (**Figure 4.21**) were evaluated as a control sample, as they follow the same methodology described for the preparation of DiI-SCDN but without any silica precursor involved.

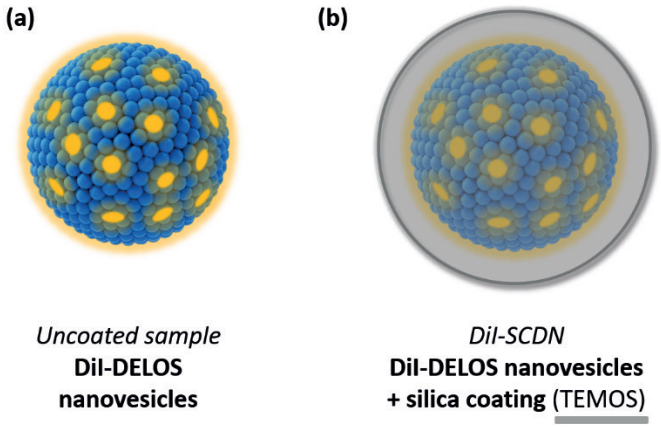

Figure 4.21: Representative image of the uncoated DiI-DELOS nanovesicles and the DiI-SCDN.

Then, once samples were prepared, they were characterized by DLS (**see Section 6.3.1**). First, it was proven that the procedure used for preparing SCDN did not provoke any alteration of the nanovesicles. As observed for the control sample, it presents proper particle size distribution, PDI and zeta potential values, compared to the non-processed sample. Moreover, as shown in **Table 4.2**, both uncoated DiI-DELOS nanovesicles and DiI-SCDN systems presented a similar particle size distribution suggesting that the presence of TEMOS silica around the DELOS nanovesicles do not destabilize the particle size of the system.

In terms of zeta potential values, a difference between them was observed. As shown in **Table 4.2**, a reduction of the zeta potential was observed comparing the uncoated DiI-DELOS nanovesicles and the DiI-SCDN. Therefore, it indicates the strong electrostatic interaction between the negatively charged silica and the positively charged DELOS nanovesicles and so the presence of silica coating around the DELOS nanovesicles.

Table 4.2: Physicochemical characterization of the hydrophobic drug model (DiI) systems used for the release study.

	Size (nm)	PDI	Zeta Potential (mV)
Non-processed DELOS nanovesicles	133 ± 1	0.3 ± 0.0	95 ± 1
Uncoated DiI-DELOS nanovesicles	120 ± 0	0.2 ± 0.1	94 ± 1
DiI-SCDN	119 ± 3	0.2 ± 0.0	10 ± 1

4.3.3.2 Preparation and characterization of SCDN for FRET evaluation

To prepare proper samples for evaluating the evolution of the stability the silica coating, two groups of samples were synthetized following the procedure explained in **Section 6.7.2**, which were (**Figure 4.22**):

1. **Control system**: the uncoated DiI-DELOS nanovesicles were prepared as explained in previous section.
1. **Alexa-SCDN:** This system was synthesized at room temperature by acid catalyzed polymerization of silica precursors, which were all the components forming the silica coating. In this case, the silica precursors were based on TEMOS mixed with Alexa Fluor 647 dye, which was incorporated in the coating thanks to the presence of aminopropylthriethoxysilane (APTES). This molecule was used to covalent link the Alexa Fluor 647 dye by the primary amine of the APTES with the ester group of the Alexa Fluor 647 dye (see **Table 4.3 for quantitates**).

Then, to prepare Alexa-SCDN, the methodology of preparation was the same as used in DiI-SCDN.

Table 4.3: Composition of the silica coating components in Alexa-SCDN.

Molar ratio membrane components:coating component			
System	**TEMOS**	**APTES**	**Alexa Fluor 647 dye**
Alexa-SCDN	108	0.04	0.03

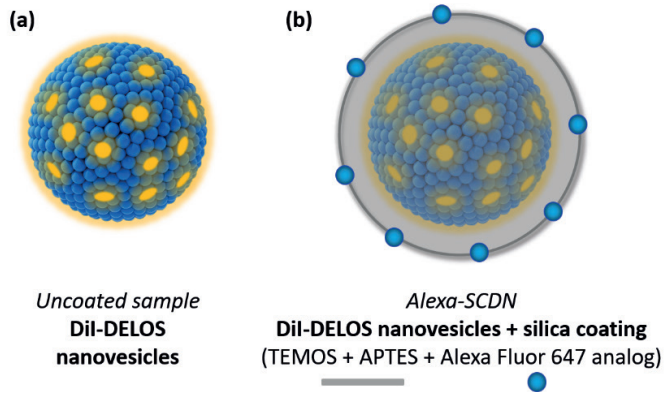

Figure 4.22: Schematic description of all the evaluated samples for the stability studies, (a) uncoated sample (control) and (b) Alexa-SCDN.

Once the samples were produced, in order to check its physicochemical properties, DLS and zeta potential measurements were carried out. The results of zeta potential are presented in **Table 4.4**. However, the evaluation of the particle size for Alexa-SCDN could not be possible since Alexa Fluor 647 is a blue dye that absorbs at 647 nm, a similar operative wavelength of the Zetasizer equipment which is 655 nm.

Regarding the zeta potential values, some differences can be observed (**Table 4.4**). Again, a decrease in zeta potential of Alexa-SCDN compared to the uncoated DiI-DELOS nanovesicles was observed indicating the presence of the negatively charged silica coating around the DELOS nanovesicles, and so confirming the presence of a silica coating.

Table 4.4: Zeta potential values the studied systems before the breakability study.

	Zeta Potential (mV)
Uncoated DiI-DELOS nanovesicles under procedure	+ 95 ± 1
Alexa-SCDN	- 20 ± 2

Following the characterization of the samples, the presence of silica in the samples was also confirmed by attenuated total reflectance Fourier transform infrared spectroscopy (ATR-FTIR). This technique is based on evaluating the interaction of infrared light (IR) with mater. So, when the IR beam is directed onto a sample, the absorbed wavelengths depend on the molecular vibrations of the substance. As a result, this is an effective technique for determining chemical bonding structures such as Si-O bond[95,96], whose IR band for its stretching vibration mode is reported to be in the range of 1000-1200 cm^{-1} [97,98].

Samples were analysed using the methodology described in **Section 6.7.3**. As can be seen in **Figure 4.23a**, the spectrum of the uncoated DiI-DELOS nanovesicles, used as a control, did not show silica-related peak due to its absence, confirming the proper use of this technique. Then, as expected and

indicated in **Figure 4.23b,** the ATR-FTRIR spectra of Alexa-SDCN reveal the presence of the typical peaks for silica vibrational modes between 1000 and 1100 cm^{-1}, attributed to the stretching of Si-O bonds. Therefore, the presence of the silica content in the Alexa-SCDN indicated that the silica coating was successfully formed around DELOS nanovesicles.

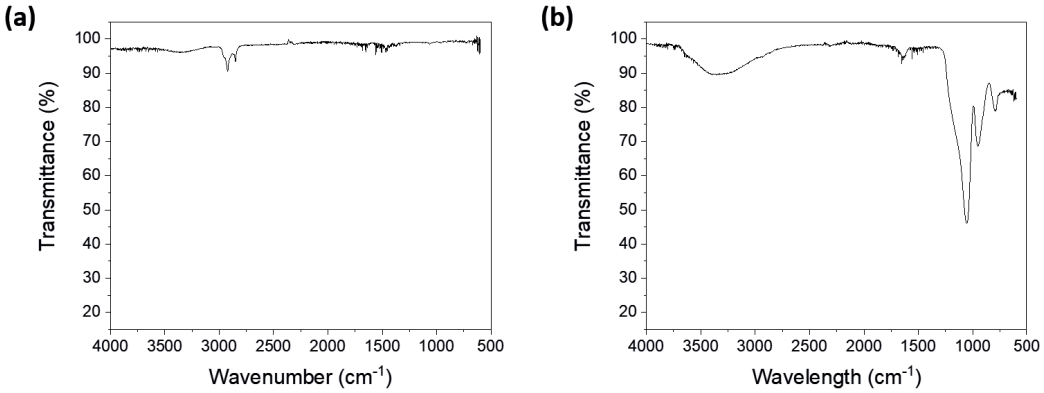

Figure 4.23: ATR-FTIR spectra of (a) uncoated DiI-DELOS nanovesicles, (b) Alexa-SCDN.

Alternatively, another approach was used to gain insight into the properties and performance of the systems of interest. In this case, a scanning transmission electron microscope (STEM) was employed, which helped us to identify the coating of DELOS nanovesicles (see **Section 6.7.4**).

STEM was a perfect tool to visualize the structure of the silica coating in DELOS nanovesicles directly from the original batch as the sample did not undergo any modification. This microscope uses a focused beam of electrons that scans across the sample in a raster pattern. What is interesting about it is that STEM beam is focused on a large angle and converges to a focal point giving more contrast in the samples compared to TEM[99]. It is important to highlight that Dr. Mariel Kubli previously tried using TEM, but the contrast of the silica coating versus the inner part, where DELOS nanovesicles are supposed to be placed could not be observed. For this reason, cryo-TEM has been commonly used to observe these kinds of samples. However, cryo-TEM was not available while conducting these experiments in Luisa de Cola's laboratory, and therefore STEM proved to be a suitable and inexpensive technique that can be used to characterize SCDN samples from now on.

One thing to consider is that STEM works at high vacuum, so if no treatment is applied to the nanovesicular system, such as a proper coating, they are supposed to break under. So, in our case, this was confirmed by evaluating the uncoated-DELOS nanovesicles. As can be observed in **Figure 4.24a**, any uncoated-DELOS nanovesicles was detected since DELOS nanovesicles lose their structure when in vacuum. Consequently, what was only observed was a layer that was being burnt as the electron beam was irradiating the sample, which could be associated to the aggregates of the membrane components of the sample on their own.

Remarkably, as shown in **Figure 4.24b**, Alexa-SCDN presented round-shape and homogeneous SCDN, indicating the presence of silica coating distributed across the DELOS nanovesicle surface and what is more, silica protects DELOS nanovesicles to get broken in vacuum.

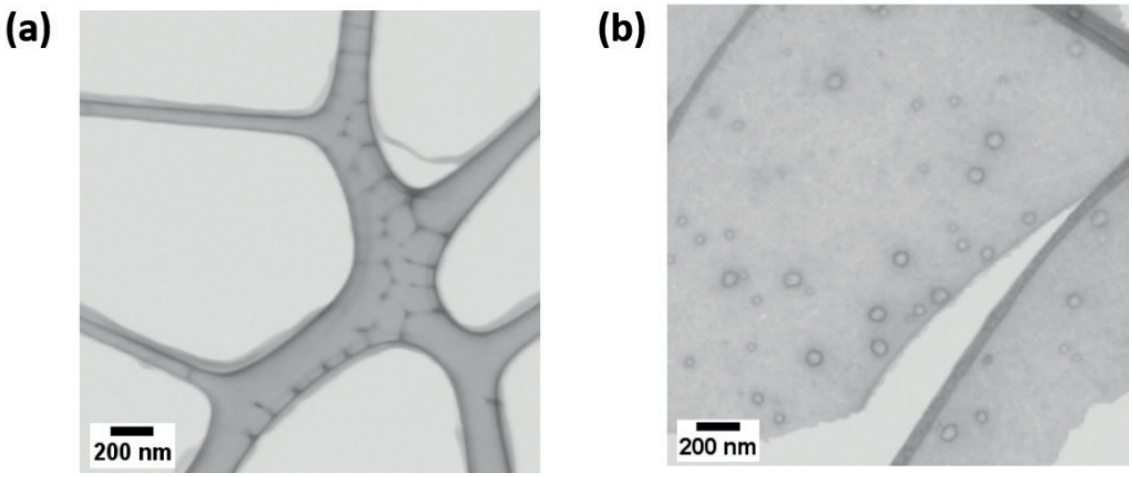

Figure 4.24: STEM images of (a) uncoated DiI-DELOS nanovesicles, (b) Alexa-SCDN.

4.3.4 Stability of the silica coating in SCDN by fluorescence

The medical potential of silica-based nanomaterials has been extensively demonstrated in simple fluids, such as water and buffers. However, their physicochemical properties and biological activity can significantly change when exposed to complex media[100]. For this reason, the main purpose of the present investigation is to characterize our new hybrid systems based on SCDN by evaluating the stability and integrity of the silica coating.

To this end, the integrity of the silica coating in Alexa-SCDN was evaluated in different media such as water and PBS with and without the presence of glutathione (GSH). Glutathione is a water-soluble tripeptide composed of the amino acids glutamine, cysteine, and glycine (**Figure 4.25**), being the most important low molecular weight antioxidant synthesized in cells. Due to the presence of a thiol group as part of the cysteine residue and which is a potent reducing agent, GSH plays a role in protecting the cells from oxidative damage by neutralizing many reactive oxygen species (ROS)[101,102]. In addition, although it is present in in the cytosol of cells in the range 1-10 mM, it is not surprising that an imbalance of GSH is observed in a wide range of pathologies[103,104]. Therefore, evaluating the impact of GSH in the integrity of the silica coating would be of great interest, as it is a relevant molecule present in our body.

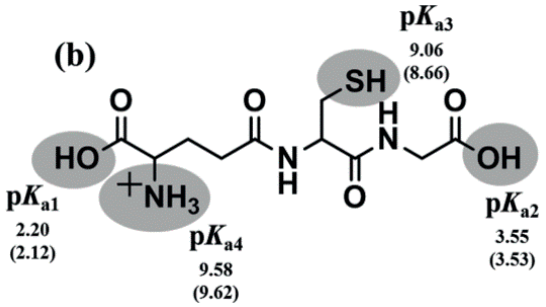

Figure 4.25: Chemical structure of GSH and its corresponding pKa. Adapted from[105].

Then, this study was conducted as described in **Section 6.7.5**. First, samples were dispersed in a cuvette by diluting them 1:4 in different dispersant media such as water, and PBS at pH 7.4 (0.01 M phosphate buffer, 0.0027 M of potassium chloride and 0.137 M of sodium chloride), to check if the presence of salts could influence the integrity of the silica coating. In addition, the presence of GSH (10 mM) was also evaluated in the stability of the silica coating. It should be highlighted that GSH presents a pI of 5.93, and so it is negatively charged at water and PBS working pH (**Figure 4.25**).

Finally, all the samples were placed at 37 °C and stirred up to 4 days (96 h) to evaluate long-term conditions. So, to evaluate the integrity of the silica coating, samples were excited at 500 nm and observing the emission in the range of 525-800 nm over time.

4.3.4.1 Stability of the uncoated DiI-DELOS nanovesicles as control

Figure 4.26a,b presents the macroscopic appearance evolution over time of the uncoated DiI-DELOS nanovesicles in the presence of water and water with the presence of GSH respectively. From visual inspection, negligible effects of the samples could be observed. Regarding the fluorescence spectra (recorded at donor (DiI) excitation wavelength) of uncoated DiI-DELOS nanovesicles in water and water with GSH are represented in **Figure 4.26c,b** respectively.

From these graphs, it was discovered that the fluorescence emission from DiI integrated into uncoated DiI-DELOS nanovesicles is stable when diluted in water up to 50 h after their dilution. However, after 96 h its intensity is reduced by half (**Figure 4.26c**). In contrast, when evaluating the presence of GSH in the sample, it can be observed that although the DiI fluorescence emission is conserved up to 50 h, DiI fluorescence emission slightly increases after 96 h. Then, it could be assumed that GSH enhanced the photostability with the DiI dye, stabilizing it. A similar interaction was previously reported, which provided information on cyanine-based fluorescent probes for the detection of glutathione. In this case, near-infrared fluorescent cyanines presented a reactivity profile with thiols by promoting sulfonamide cleavage, making it a good strategy for the design of thiol-selective probes[106].

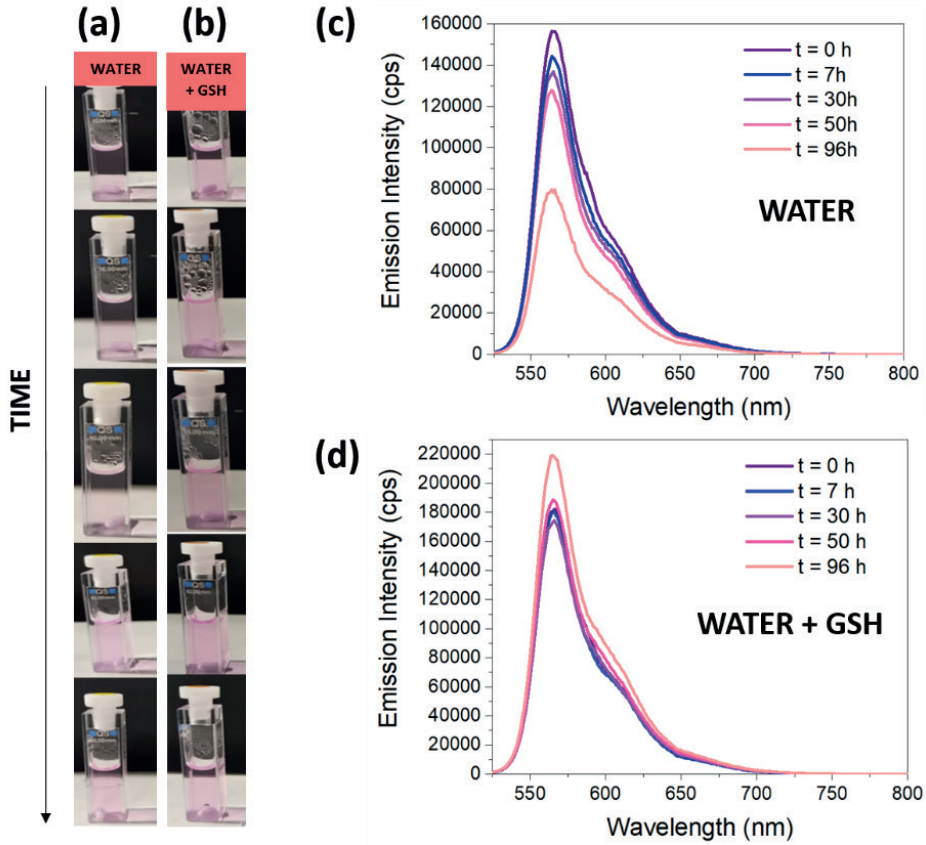

Figure 4.26: Macroscopic appearance evolution of uncoated DiI-DELOS nanovesicles in (a) water and (b) water + GSH. Time-dependent spectral evolution of DiI fluorescence emission in uncoated DiI-DELOS nanovesicles in (c) water and (d) water + GSH.

Next, the macroscopic appearance and spectral properties of uncoated DiI-DELOS nanovesicles after PBS dilution in the absence and presence of GSH were investigated. On the one hand, as observed macroscopically (**Figure 4.27a**), the presence of PBS salts in the sample provokes a constant decrease in the fluorescence emission of DiI over time (**Figure 4.27c**). Therefore, it seems that PBS salts can be interacting with the DELOS nanovesicle bilayer provoking its destabilization. Surprisingly, opposed results were obtained in the presence of GSH. As shown in **Figure 4.27b,d,** one can clearly see that the DiI fluorescence emission is kept almost constant with a slight increase. Then, these observations highlighted that the stability of DiI fluorescence emission over time is mainly GSH responsible.

This finding was unexpected and suggests that probably, GSH is negatively charged at water and PBS pH, and so it can be located around the DELOS nanovesicles by electrostatic interaction and so stabilizing the system, which is a very relevant factor. Surprisingly, this interaction may help phosphate salts from PBS to not interact directly with the DELOS nanovesicle membrane and so stabilize the formulation.

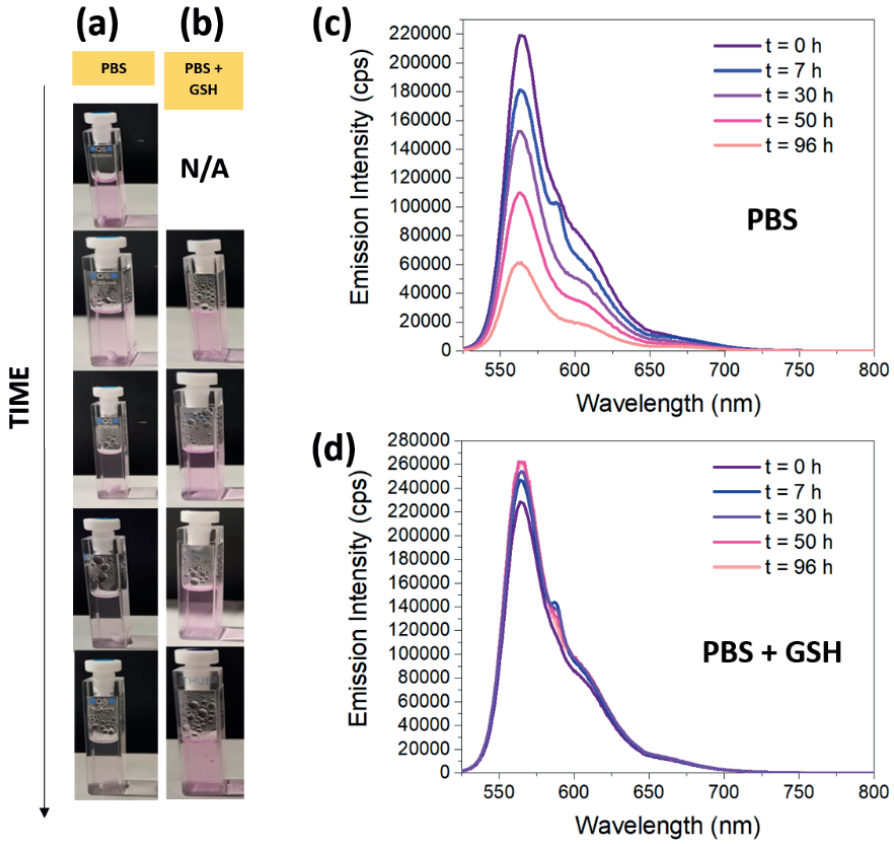

Figure 4.27: Macroscopic appearance evolution of uncoated DiI-DELOS nanovesicles in (a) PBS and (b) PBS + GSH. Time-dependent spectral evolution of DiI fluorescence emission in uncoated DiI-DELOS nanovesicles in (c) PBS and (d) PBS + GSH.

4.3.4.2 Stability of the Alexa-SCDN

The stability of the silica coating in Alexa-SCDN after its transfer to different aqueous media was also studied. First, if we focus on using water as dispersant medium with the absence and presence of GSH (**Figure 4.28a,b**), no macroscopic changes were observed. Then, the time-dependent emission fluorescence was monitored under the DiI excitation (500 nm), from which different results emerged. First, the results demonstrate the adequacy of the FRET method, as the functionalization of the DELOS nanovesicles with DiI dye and the silica coating with Alexa 647 analog demonstrates that this phenomenon can be generated (**Figure 4.28c,d**).

As can be seen from these plots, the fluorescence emission of the Alexa Fluor 647 (maximum emission around 690 nm) shows similar emission profiles over time for the absence and presence of GSH in water. In the presence of water **(Figure 4.28c),** FRET was characterized by a decrease

in the donor (DiI) emission and an increase in acceptor (Alexa Fluor 647) emission. As a result, enhancement of FRET phenomenon was observed over time, which has been reported to be due to continuous thermodynamic dye distribution between the system[107]. Then, these results suggest that the Alexa Fluor 647 integrated into the silica coating was not static and therefore a dynamic process was likely involved, such e.g., its exchange or penetration into the membrane of DELOS nanovesicles.

In the case of the dispersant based on water in the presence of GSH, as observed in **Figure 4.28d**, the fluorescence emission of the Alexa Fluor 647 dye over time shows emission profiles similar to those in **Figure 4.28c**, again indicating that FRET phenomena can occur dynamically. However, in this case, the DiI fluorescence emission (emission peak around 564 nm) increases after 7 h of incubation and is maintained over time, so it is not reduced as expected suggesting that GSH plays a role in stabilizing DiI. However, it can also be observed that the presence of a DiI fluorescence emission shoulder close to 600 nm was reduced over time, indicating that GSH is responsible for the alteration of DiI molecule.

It is important to highlight that all these results are interesting findings for understanding the behaviour of the silica coating, and it could be hypothesized that silica coating is stable in water at least after 96 h in the presence and absence of GSH.

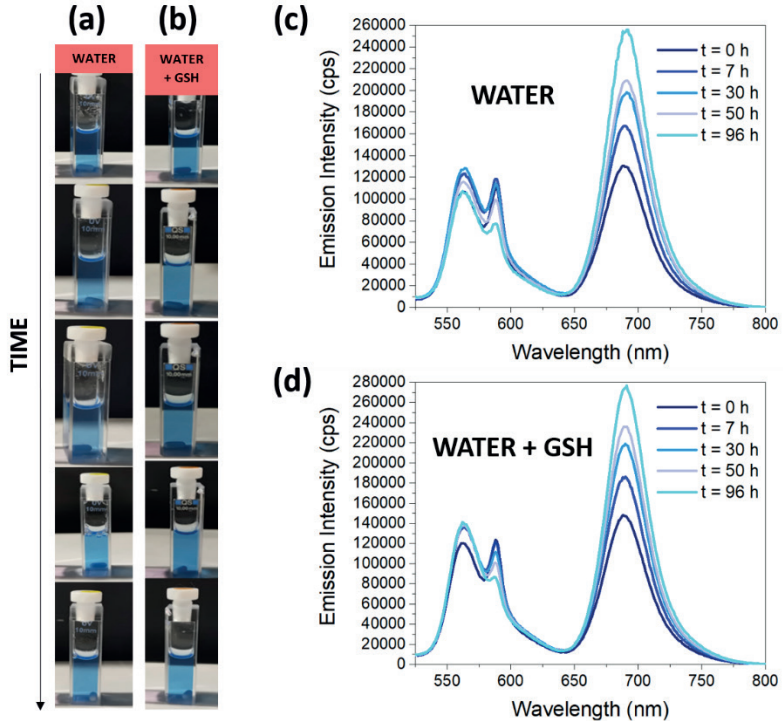

Figure 4.28: Macroscopic appearance evolution of Alexa-SCDN in (a) water and (b) water + GSH. Time-dependent spectral evolution of the FRET between DiI and Alexa 647 analog in Alexa-SCDN in (c) water and (d) water + GSH.

Despite the excellent FRET phenomenon of the Alexa-SCDN in water with and without GSH, its stability is significantly different when they are transferred into PBS. In this case, macroscopic aggregation can be observed for this system in PBS but not with the presence of GSH (**Figure 4.29a,b**). This phenomenon is accompanied by a reduction of the FRET phenomena over time for the presence of PBS. Then, the stability of the silica coating in Alexa-SCDN seems to be PBS dependent.

As discussed in the literature, the high ionic strength of dispersant media such as PBS is associated with the induction of aggregation of silica nanoparticles, thereby modifying and even losing their functionality. Therefore, the stability of SCDN appears to be questioned when exposed to biological media such as PBS. To understand this phenomenon, it is important to know that the colloidal stability of such systems is determined by the balance of different interaction forces, which can be modified by parameters such as pH and electrolyte concentration (ionic strength)[100,108].

Since the isoelectric point of silica close to pH = 2[85], when working with PBS at pH 7.4, a negative surface charge of the particles is observed coming from the proton dissociation of surface acidic silanol groups (≡Si-OH → ≡ SI-O^-). However, the presence of electrolytes in solution, such as PBS salts, can create a shielding effect on the electrostatic forces and promote a reduction of repulsion between particles and lead to loss of colloidal stability. It should be noted that in our case, silica coating is functionalized with APTES which brings to positive surface charges (-$NH3^+$) that counterbalance the negative charges of acidic silanol groups (≡Si-O^-), and so it reduces the absolute value zeta potential and electrostatic repulsion compared to the absence of it[100,109].

Regardless of the previous results and hypotheses, when GSH is present, the FRET phenomenon stabilizes and even shows an increase in donor and acceptor fluorescence emission. In addition, the presence of GSH causes the second peak of DiI related to aggregation to disappear. Consequently, the presence of GSH peptide could favourably affect the stability of all systems evaluated over time. It should be emphasized that incubation with GSH, which has a pI of 5.93, and is therefore negatively charged at physiological pH like PBS, avoiding SCDN to aggregate. Following the previous assumption, the absence of aggregation could be attributed to the presence of peptide absorption in the surface of SCDN, thus providing negative charge on the silica surface, as a source of colloidal stability[100].

Again, contrary to expectations, GSH provides stability not only in Alexa-SCDN, but also in uncoated DiI-DELOS nanovesicles. Then, this suggests that the stabilization mechanism might depend not only on the electrostatic interactions as it stabilizes negatively charged silica and positively charged DELOS nanovesicles, but other interactions such hydrogen bonding can also take place. Therefore, the strategy of using this molecule in the dispersant medium might be used in the future as an approach to stabilize both systems, uncoated DELOS nanovesicles and SCDN in general.

Moreover, for future studies, it will be recommended to study the colloidal stability in detail by dynamic light scattering and zeta potential measurements.

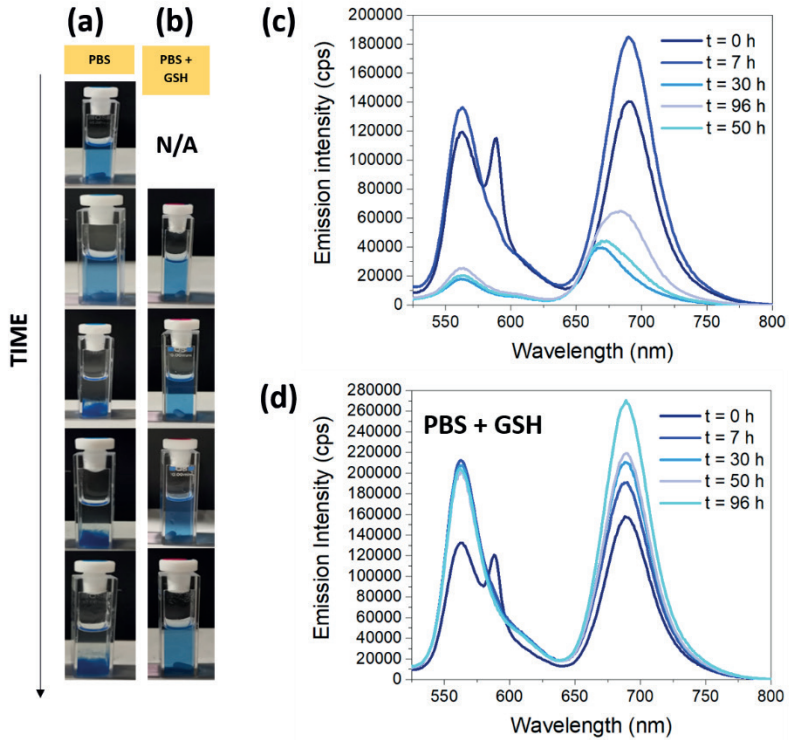

Figure 4.29: Macroscopic appearance evolution of Alexa-SCDN in (a) PBS and (b) PBS + GSH. Time-dependent spectral evolution of the FRET between DiI and Alexa Fluor 647 in Alexa-SCDN in (c) PBS and (d) PBS + GSH.

Taken together, these results suggest that could be possible that the GSH is diffused inside of the silica coating or maybe the silica coating is porous enough to help GSH to reach DiI dye. In addition, we also wonder if Alexa Fluor 647 dye is properly incorporated into the silica coating or if it diffuses into the DELOS nanovesicles membrane. Then, all of these cast doubts whether FRET phenomenon is the right mechanism to understand the breakability of the system.

In summary, we have built up evidence for the role of dispersant media on the stability and integrity of the silica coating, which can be affected by pH and ionic strength. Moreover, GSH seems to play an important role in stabilizing the system, which is an important parameter that could occur due to electrostatic forces or hydrogen bonding. However, additional tests should be considered to gain a better understanding.

4.3.5 Stability test of the SCDN in simulated gastric fluid by microscopical techniques

To further characterize the integrity of the silica coating, a possible hypothesis came out wondering if silica coating could protect DELOS nanovesicles under simulated gastrointestinal

conditions compared to uncoated DELOS nanovesicles. As previously mentioned, silica is a good tool for oral delivery due to its resistance to acidic pH and enzymatic degradation[110] (**Figure 4.16**). Then, it was hypothesized that using a silica coating in DELOS nanovesicles could be a new strategy to expand the use of DELOS nanovesicles for oral delivery.

Furthermore, in this work, two dispersant media were evaluated. Not only was simulated gastric fluid (SGF at pH 1.2, composed of 34 mM of NaCl and 0.07 mM HCl) evaluated but also PBS pH 7.4, to confirm the results previously observed and try to characterize them more precisely.

In this study, standard-SCDN was prepared using CTAB-DELOS nanovesicles without any dye and with TEMOS as silica precursor. To prepare it, DELOS nanovesicles were prepared by DELOS-susp using 1:1 molar ratio of cholesterol:CTAB with 7.3 mM of each component, and water/10% EtOH ($v \cdot v^{-1}$) as dispersant medium (see **Section 6.2.1**). Then, standard-SCDN were prepared following the same procedure described in **Section 6.7.2**. In this case, as the obtained samples were evaluated by non-fluorescence techniques, they did not contain any fluorophore in the silica coating. As a result, standard-SCDN were prepared by just using TEMOS as a silica precursor, considering the same relationship used before, molar ratio membrane components:silica precursor 1:108.

Once the standard-SCDN was prepared, to analyse the stability of the samples, they were diluted 1:4 in PBS and in SGF (34 mM NaCl and 0.07 mM HCl, pH 1.2) and then, they were for 24 h at 37 °C with continuous stirring. After that time, in order to assess the morphology of the systems, cryo-TEM and scanning electron microscopy (SEM) was used. It must be clarified that these experiments were done at ICMAB-CSIC facilities and so all the microscopic characterization was carried out in collaboration with the Microscopy service of Autonomous University of Barcelona.

In line with the results previously observed, standard-SCDN presented a proper morphology as observed by SEM (**Figure 4.30b**), indicating that proper silica coating was achieved around DELOS nanovesicles. In addition, in this case element mapping by scanning electron microscopy with energy dispersive x-ray analysis (SEM-EDX) was used to generate more information about the sample. As observed in **Figure 30c**, EDX detector revealed that the silica element was present in the sample and concentrated in the surface of the DELOS nanovesicles, which correspond to the contrast in the bright-field of SEM images.

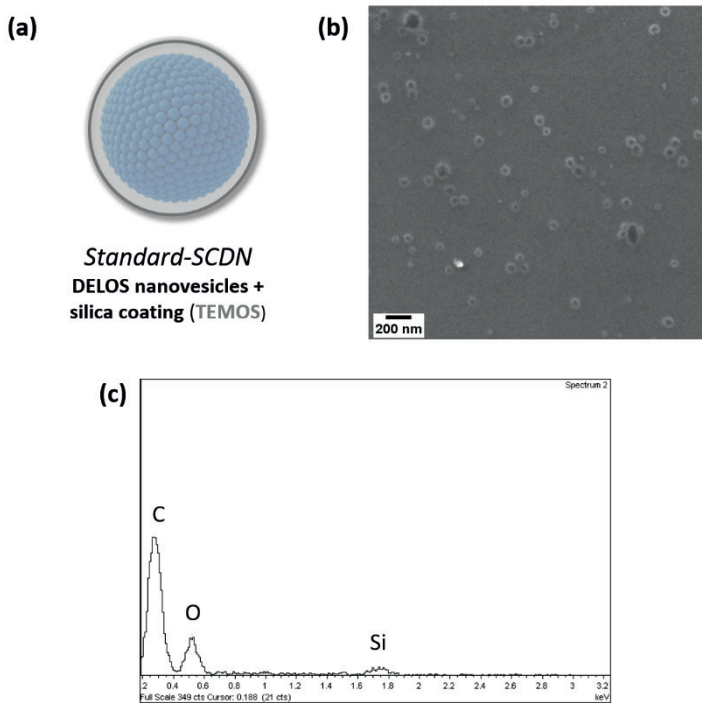

Figure 4.30: (a) Schematic representation, (b) SEM image of standard-SCDN and (c) EDX graph showing the presence of silicon in the sample.

4.3.5.1 Characterization of standard-SCDN in PBS after 24 h of incubation

Once the SCDN system has been incubated in PBS after 24 h, precipitation of the system was macroscopically observed suggesting its instability with this dispersant medium (**Figure 4.31a**), as previously observed in **Section 4.3.4.2**. To investigate the influence of PBS on the stability and so the degradability of the silica coating, different microscopic techniques were used. As observed in **Figure 4.31b**, SEM images show the presence of big aggregates of SCDN. However, the round shape SCDN can be individually observed, suggesting that silica coating is not fully degraded after 24 h of incubation in PBS.

Moreover, regarding cryo-TEM microscopy (**Figure 4.31c**), it can be observed how the SCDN are still spherical and although aggregated, they silica coating can be found using this approach since the membrane of the vesicles seem to be thicker and darker. Then, it can be suggested that the presence of PBS in standard-SCDN does not fully degrade silica coating but aggregate SCDN, as expected from the results observed in section 4.X. Again, this might be due to the presence of high concentration of salts in PBS, reducing the electrostatic charge of silica and so, promoting a reduction of the particle repulsion and leading to the loss of colloidal stability and aggregation.

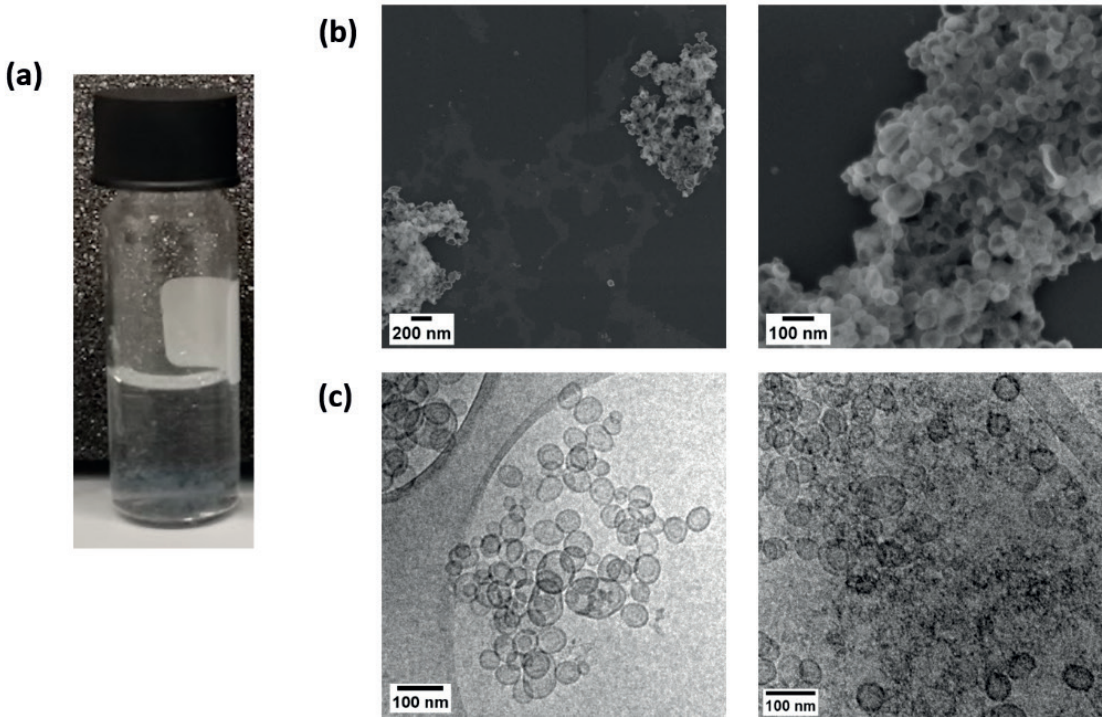

Figure 4.31: (a) Macroscopic appearance, (b) SEM image of the aggregates in presence of PBS and (c) cryo-TEM image showing of frozen standard-SCDN after 24 h of incubation in PBS.

4.3.5.2 Characterization of standard-SCDN in SGF after 24 h of incubation

Finally, the influence of SGF on standard-SCDN on the silica coating behaviour was examined. The results, shown in **Figure 4.32a**, indicates some condensation of the particles since two phases can be observed in the vial. When observing this system by SEM, different key points emerge. On the one hand, as observing **Figure 4.32b**, a big layer can be observed which could be related to the high presence of salts and free silica. However, despite this layer, during this gastric environment, standard-SCDN can be perfectly observed and distributed without aggregation (**Figure 4.32c**). Then, it suggests that silica coating persisted after 24 h demonstrating stability what could be related to a more protection of DELOS nanovesicles compared to uncoated samples.

Interestingly, this phenomenon could be again related to the electrostatic interactions. In this case, instead of having negatively charged SCDN, the simulated gastric fluid with pH values as low as pH 2.0, will result in the net particle charge of SCDN being positive[111].

As reported, SGF produces low silica dissolution as the silica solubility is strongly pH dependent and is the highest under alkaline pH conditions. This finding has important implications for developing a new hybrid system based on DELOS nanovesicles for oral drug delivery.

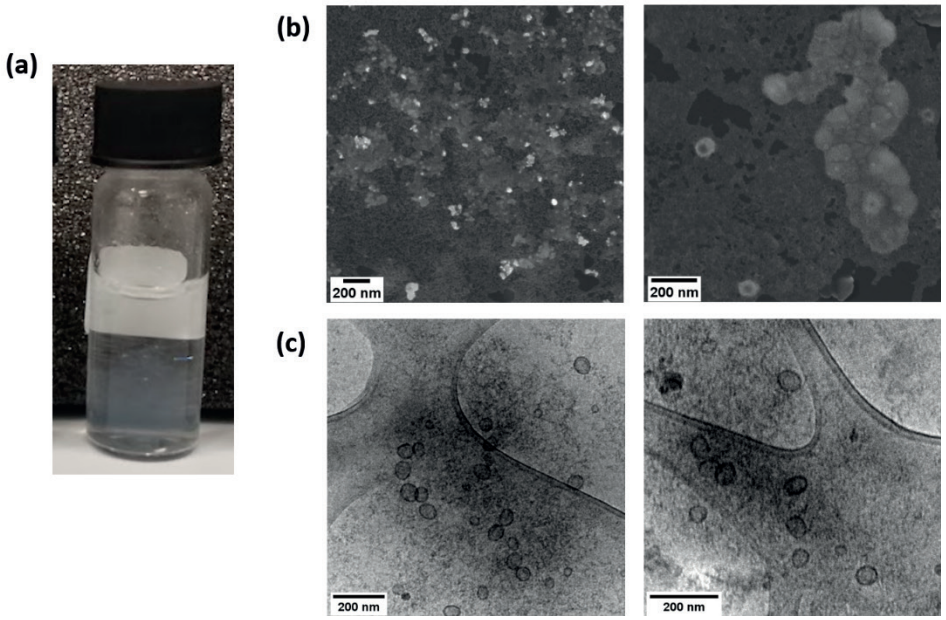

Figure 4.32: (a) Macroscopic appearance, (b) SEM image of the aggregates in presence of PBS and (c) cryo-TEM image showing of frozen standard-SCDN after 24 h of incubation in SGF.

In summary, it seems that silica coating stability can be modulated under a given use of dispersant media. Depending the type of buffer pH and composition different behaviour depending on desired administration route.

It should be highlighted that this new hybrid system has provided promising results in presence of SGF and so, opening new strategies for using DELOS nanovesicles for oral route. In addition, although this studies have been focused on characterizing some of the physicochemical characteristics of the hybrid system, future studies will be focused on the oligonucleotide integration, as desired in the frame of Nano-OligoMed project.

4.3.6 Conclusions of the section and future steps

On this basis, we conclude that a new hybrid system based on SCDN have been deeply produced and characterized to construct a new hybrid DELOS nanoformulation for delivery of oligonucleotides, following the methodology studied by Dr. Mariel Kubli.

The stability of SCDN has demonstrated to be strongly dependent on the dispersant medium in which the system is found. The presence of ionic salts such as PBS buffer on SCDN provokes destabilization of the formulation compared to water and SGF. Moreover, future research should focus on the interaction of GSH and SCDN as it has been shown to be an important parameter to stabilize the systems, contrary the expected behaviour.

Up to now, it has been indicated that SCDN have potential applications to be further explored, such as oral delivery. However, looking forward, new approaches of the characterization with a broader perspective will be carried out to fully understand the behavior and the advantages of these new hybrid formulations. Further attempts could also be related to investigating the formation of SCDN using other DELOS nanovesicle formulations such as MKC-DELOS nanovesicles, what would be of great interest since it has been deeply studied in the frame of Nano-OligoMed project. Finally, the integration of oligonucleotides into this hybrid system will be also considered to be studied.

4.4 Topical DELOS nanovesicles for antimicrobial treatments in skin diseases

As already mentioned in the Introduction of this Chapter, another area that required further exploration for DELOS nanovesicles is defining their potentiality as antimicrobial agents in skin diseases. This represents an important topic to study as people worldwide remain at risk of infectious diseases and current treatments are being depleted due to antibiotic resistance. Therefore, the synthesis and formulation of novel materials to combat antimicrobial resistance is crucial[112].

4.4.1 Biofilms definition and current treatments

In order to fully understand this section, it is necessary to first clarify the reason why antimicrobial resistance exists. Numerous reports have highlighted that the resistance of microorganisms to disinfection is often associated with the presence of biofilms on surfaces[113]. A biofilm forms when microorganisms grow adhered to almost any surface and form architecturally complex communities. These communities are enclosed in an extracellular polymeric matrix produced by the bacteria themselves and composed of proteins, lipids and polysaccharides[114], that provides structural stability and protection to the biofilms[115] (**Figure 4.33**).

After the biofilm has matured into three-dimensional structures where the biofilm exhibits maximum resistance to antibiotics, the biofilm community undergoes a disassembly process that causes to focal areas of the biofilm to disintegrate, releasing bacterial cells that can spread to other sites where new biofilms can be formed[115]. Since biofilms are dynamic and complex systems, bacteria have evolved a vast network of tools to modify and tune biofilm progress with changing environmental conditions. Therefore, biofilm formation is used as a strategy for survival and persistence in the human host and can serve as a reservoir for spread to new sites of infection[116,117].

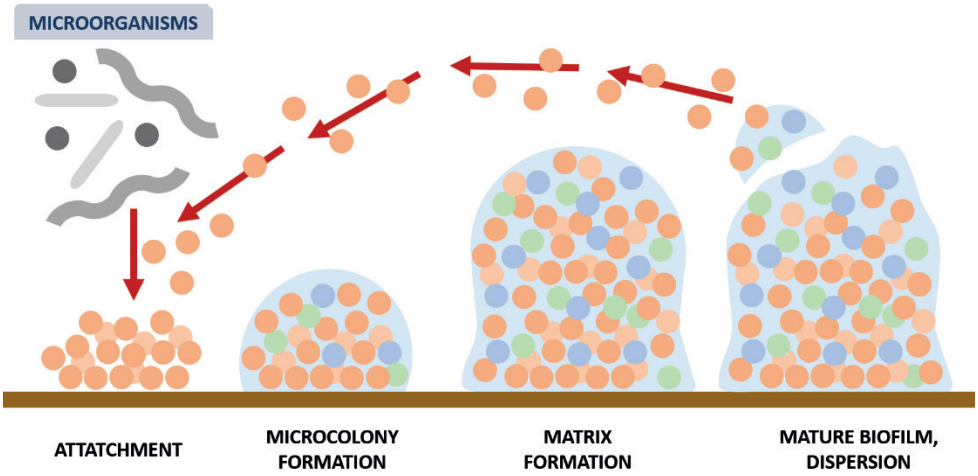

Figure 4.33: Schematic representation of the stages of biofilm development and dispersion.

One of the common characteristics of biofilms is that they show increased resistance to antimicrobial, immunological, predatory, and chemical attack compared to bacteria as "free entities" in liquid environment. Therefore, biofilms are extremely tolerant of removal and eradication[118]. Then, biofilms can influence humans in many ways as they can form in natural, medical and industrial environments. For example, biofilms are a well-recognized problem observed in prolonged infections due to colonization of medical devices such as implants or prostheses, and so it is an important consideration as a risk factor for complications postoperatively[119]. Furthermore, infections have been linked to the formation of biofilms on human surfaces such as teeth, skin and the urinary tract or even in different types of wounds, such as chronic infections, causing their failure to heal[114,115,118].

Given that biofilm infections contribute significantly to patient morbidity and healthcare costs, new strategies to treat these infections are urgently required. Of note, biofilm infections are usually formed by more than one bacterial species simultaneously interacting between them and so increasing persistence. As a result, personalized antimicrobial treatment approaches are expected to emerge[117,120].

So far, there have been various approaches preventing biofilm formation, which can be divided into two groups. The first group focuses on targeting the biofilm by using some strategies such as the dissolution of the already established biofilm by physical or photodynamic treatment. In addition, targeting the biofilm matrix for degradation and disruption of biofilm regulation are also being considered, among other strategies. Then, another group of anti-biofilm technologies is considering modifying the biomaterial surfaces with changed physical and chemical properties that prevent adhesion and thus biofilm formation[121,122].

However, the available evidence shows that although for device-associated biofilms removal of the implant (if possible) is the best therapeutic option, for tissue-related biofilms the only therapy available today is antibiotic treatment. Then, despite long-term antibiotic therapy, to which bacteria show *in vitro* susceptibility, biofilm-growing bacteria persist and destroy infected tissues due to a long-term inflammatory response, resulting in chronic infection[123]. Therefore, it is now generally agreed that effective treatment of biofilms requires combination therapy of an antibiofilm compound with an effective antibiotic, but no antibiofilm therapies are currently used clinically[120].

4.4.2 DELOS nanovesicles as a platform to treat resistant biofilms and skin infection disorders

Considering that biofilms can be very challenging in biomedical contexts due to the exponential rise in antibiotic resistant bacteria, a promising strategy may be the use of DELOS nanovesicles as an alternative platform to treat antibiotic resistant biofilms.

The interesting characteristic about DELOS nanovesicles is that the membranes themselves can harbour antimicrobial compounds such as QAC, which show an inherent antibiofilm effect as they target the bacterial cell membrane. The mechanism of action is based on electrostatic interactions between the positively charged QAC head and the negatively charged bacterial cell membrane. Then, permeation of the QAC side chains into the intramembrane region occurs, resulting in leakage of cytoplasmic material and cell lysis. Consequently, the use of QAC prevent deposition and growth of bacterial biofilms[124,125]. In addition, QACs have shown to be present antifungal effect. In this case, it is reported that QAC does not provoke fungus cell lysis but rather change of cell surface charge from negative to positive[125].

Then, since a large body of evidence suggests that QAC are one of the most effective class of disinfectants for nearly a century[124], in the frame of this thesis, there was the desire to characterize in detail DELOS nanovesicles of different nature as strategy to develop a product to treat resistance biofilms and other microbial diseases.

Up to now, as experimentally demonstrated in **Chapter 2**, DELOS nanovesicles themselves (devoid of any active principle) presented antiseptic activity being, in this case, attractive for topical treatments[126].

In addition, in view of all that has been mentioned so far about the potentiality of DELOS nanovesicles, it can be also suggested to integrate antibiotics in this nanovesicular system. This strategy would not only make the antibiotic formulation more active thanks to the synergy with the nanovesicle antimicrobial activity but also wound open new perspectives in the treatment of antibiotics.

Then, here we report on the preparation of DELOS nanovesicles by DELOS-susp containing equimolar amounts of cholesterol and one of the quaternary ammonium surfactants reported in

Table 4.5, which were CTAB and CTAC (as described in **Chapter 3**), MKC (as described previously in this **Chapter**) and Cetylpyridinium chloride (CPC) and Stearalkonium chloride (ST).

It has already been seen in the previous section that CTAB, CTAC and MKC are promising QACs that a part from presenting proper physicochemical properties when used for DELOS nanovesicles production, they are known to have antimicrobial properties. However, in this study there was the aim to obtain a wide screening of DELOS nanovesicles as antimicrobial agents as a proof-of-concept. Therefore, CPC- and ST-DELOS nanovesicles were also considered as they have been studied in Nanomol Group and Nanomol Technologies SL while presenting promising physicochemical properties.

CPC is a cationic quaternary pyridinium surfactant compound (**Figure 4.34c**) used as antimicrobial in various oral care, cosmetics, pharmaceutical and home care products. What is more, it is considered as safe and efficacious by US FDA for use in oral care, commonly found in mouthwashes, toothpastes[127]. On the other hand, ST is also a cationic quaternary ammonium salt (**Figure 4.34d**) that is broadly used in cosmetic products for its surfactant and antimicrobial properties[128]. Then, on the basis of the evidence at hand, we aim to investigate the antimicrobial effect of these surfactant when being part of DELOS nanovesicles as new antimicrobial product approach.

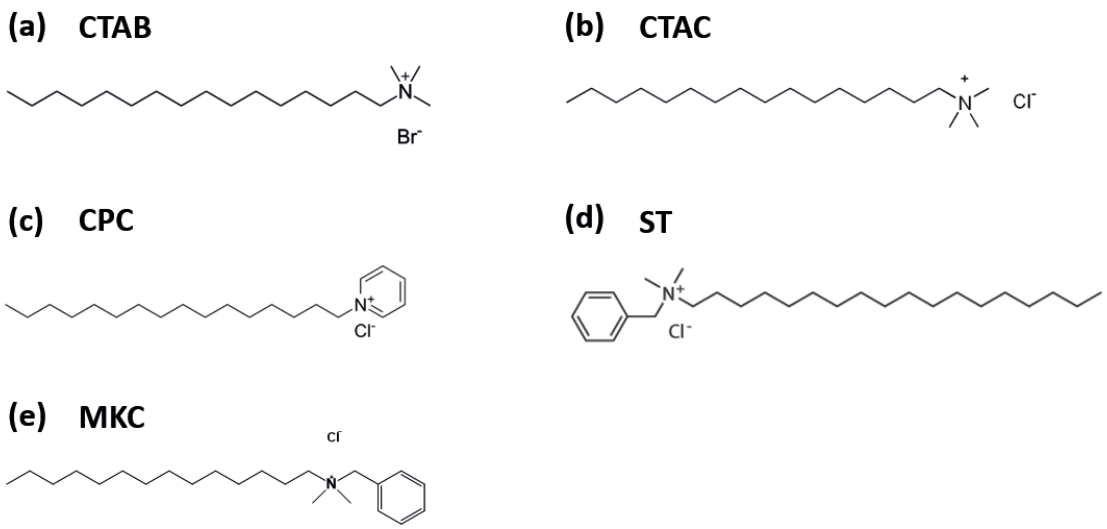

Figure 4.34: Chemical structure of the quaternary ammonium surfactants used in the DELOS nanovesicle production: (a) CTAB, (b) CTAC, (c) CPC, (d) ST, (e) MKC.

DELOS nanovesicles using different surfactant nature (**Figure 4.34**) were prepared and characterized in our facilities and then, they were sent to the Eurofins Scientific company to study their antimicrobial effects. In particular, as a first study to assess the DELOS nanovesicles antimicrobial potentiality, their Minimum Inhibitory Concentration (MIC) was determined in presence of microbial strains linked to skin infection disorders.

4.4.3 Preparation and characterization of the DELOS nanovesicles

DELOS nanovesicles were prepared by DELOS-susp using the composition described in **Table 4.5** (see **Section 6.2.1**). It should be mentioned that the dispersant medium used for each formulation is the one that has presented more stability. In all the cases water/10% EtOH ($v \cdot v^{-1}$) was used as dispersant media, except for the DELOS nanovesicles composed on cholesterol and MKC. In this case, MKC-DELOS nanovesicles were produces using PBS (100 mM, pH 7.4)/10% EtOH ($v \cdot v^{-1}$) as dispersant medium, which reported suitable and promising results in the Doctoral Thesis of Dr. Guillem Vargas[43].

Table 4.5: Sample composition of all the DELOS nanovesicles prepared for the MIC evaluation.

DELOS nanovesicles					
Sample	**Surfactant component**		**Sterol component**		**Dispersant medium**
Chol:CPC	CPC	7.3 mM, 2.48 $mg \cdot mL^{-1}$	Chol	7.3 mM, 2.82 $mg \cdot mL^{-1}$	Water/10% EtOH ($v \cdot v^{-1}$)
Chol:CTAB	CTAB	7.3 mM, 2.66 $mg \cdot mL^{-1}$	Chol	7.3 mM, 2.82 $mg \cdot mL^{-1}$	Water/10% EtOH ($v \cdot v^{-1}$)
Chol:CTAC	CTAC	7.3 mM, 2.34 $mg \cdot mL^{-1}$	Chol	7.3 mM, 2.82 $mg \cdot mL^{-1}$	Water/10% EtOH ($v \cdot v^{-1}$)
Chol:ST	ST	7.3 mM, 3.10 $mg \cdot mL^{-1}$	Chol	7.3 mM, 2.82 $mg \cdot mL^{-1}$	Water/10% EtOH ($v \cdot v^{-1}$)
Chol:MKC	MKC	7.3 mM, 2.69 $mg \cdot mL^{-1}$	Chol	7.3 mM, 2.82 $mg \cdot mL^{-1}$	PBS (100 mM, pH 7.4)/10% EtOH ($v \cdot v^{-1}$)

Physicochemical properties such as size, PDI and zeta potential were measured after 2 weeks after their preparation, as they are deeply studied systems in our group and defined to present proper characteristics. As can be observed in **Table 4.6**, all the samples yielded to an average size distribution of 70-110 nm and low PDI for CPC-, CTAC- and MKC-DELOS nanovesicles around 0.2, and slightly higher PDI values around 0.4 for CTAB and ST-DELOS nanovesicles. Furthermore, all the formulations exhibited positive zeta potential values after 2 weeks of production and higher than +30 mV, considered optimum for good stabilization of the nanoformulations[129].

Table 4.6: Physicochemical characterization of the different formulations of DELOS nanovesicles after 2 weeks of production.

DELOS nanovesicles				
Sample	**Surfactant component**	**Size (nm)**	**PDI**	**Zeta Potential (mV)**
Chol:CPC	CPC	76 ± 1	0.25 ± 0.01	111 ± 4
Chol:CTAB	CTAB	70 ± 4	0.41 ± 0.02	84 ± 4
Chol:CTAC	CTAC	72 ± 1	0.28 ± 0.01	104 ± 2
Chol:ST	ST	86 ± 0	0.36 ± 0.01	89 ± 6
Chol:MKC	MKC	107 ± 2	0.23 ± 0.01	59 ± 5

In addition, samples were also characterized by cryo-TEM after 1 month of production. As shown in **Figure 4.35**, the analysis of the CPC-, CTAB-, CTAC- and ST-DELOS nanovesicles revealed the presence of spherical, homogeneous, and unilamellar vesicles, as expected. In contrast, MKC-DELOS nanovesicles presented oval or peanut shaped instead of being spherical due to the presence of PBS salts, causing this non-spherical shape, as reported in the Doctoral Thesis of Dr. Guillem Vargas[43].

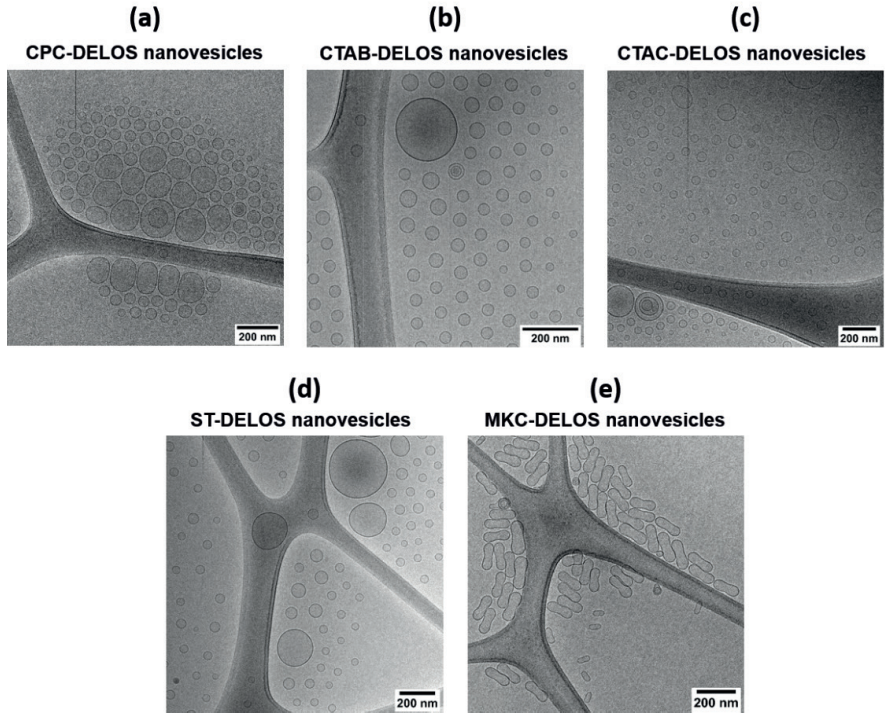

Figure 4.35: Cryo-TEM images of (a) CPC-, (b) CTAB-, (c) CTAC-, (d) ST-DELOS nanovesicles in water/10% EtOH ($v \cdot v^{-1}$) and (e) MKC-DELOS nanovesicles in PBS 100 mM/10% EtOH ($v \cdot v^{-1}$) after 1 months of production.

4.4.4 Determination of the Minimum Inhibitory Concentration (MIC)

One way to validate the effectiveness of the decontamination and disinfection of DELOS nanovesicles is to compare the behaviour of selected microorganisms when treated with the nanoformulation. The "gold standard" for determining the susceptibility of organisms to antimicrobial agents is the minimum inhibitory concentration (MIC). MIC is thus defined as the lowest concentration of an antimicrobial agent that inhibits the visible growth of a microorganism after incubation[130,131]. To quantify it, serial dilutions of the antimicrobial agent are made in the culture media and then, the microorganism is added at a constant concentration. After that, the dilutions are incubated at the temperature and time depending on the microorganism and finally a spectrophotometric and visual inspection is performed. It should be emphasized that the presence of turbidity in the sample corresponds to microbial growth (**Figure 4.36**).

Then, knowing MIC value can have a significant influence on the choice of a therapeutic strategy, which affects the efficiency of infection therapy.

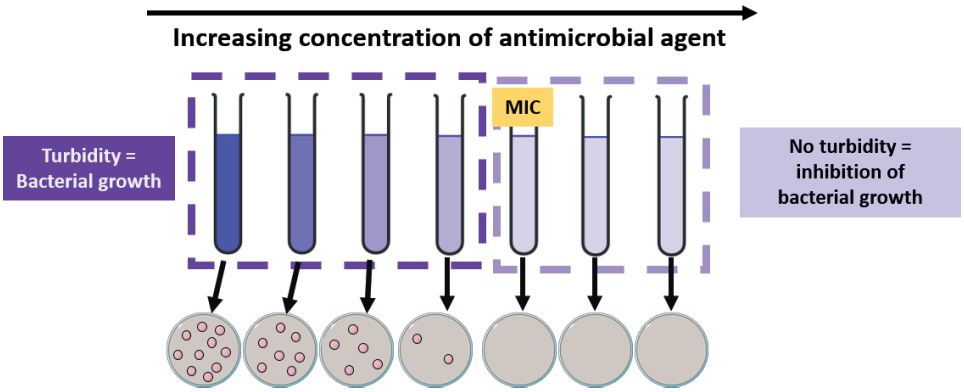

Figure 4.36: Schematic representation of the preparation of antimicrobial agent in increasing concentration and inoculated with microorganisms from tubes. The MIC value is determined when no turbidity or growth is observed.

In this regard, in the present study carried out in Eurofins Scientific company, it was evaluated the MIC value of the DELOS nanovesicle formulations described in **Table 4.5** against different microbial strains involved in skin disorders described in **Table 4.7**.

It should be mentioned that on the skin surface, mainly bacteria of the genera of *Propionibacteria and Staphylococci* constitute the microbial community. The interaction between members of this cutaneous microbiota is essential for maintaining healthy skin. However, they can also act as opportunistic pathogens and when perturbed may lead to various skin diseases[132,133], producing different effects. For instance, *Staphylococcus aureus* skin infections represent a major threat to public health given the massive numbers of infections as well as the widespread emergence of antibiotic resistant strains[134].

In addition, it has long been known that a part from bacteria, fungi can also colonize the skin and nails, affecting more than 20-25% of the world's population[135,136]. For this reason, fungi, such as relevant yeasts and molds, were also considered for this study. Therefore, in this study, we aim to compare the susceptibility of different bacterial and fungal strains typically found in the skin when DELOS nanovesicles are present acting as an antimicrobial agent.

Table 4.7 Summary of the different types of microorganisms studied and their characteristics.

Type of microorganism	***Strain***	**Characteristics**
Bacteria	*Acinetobacter baumannii* ATCC 15149 (Gram-negative bacteria)	Standard strain clinically relevant for skin infections[137]
	Propionibacterium acnes (Gram-positive bacteria)	Common skin organism, notably recognized for its role in acne[138]
	Staphylococcus aureus ATCC 29213 (Gram-positive bacteria)	Found in the vast majority of bacterial skin infections[139], relevant for atopic dermatitis and psoriasis
Fungi	*Malassezia furfur* ATCC 14251 (Lipophilic yeast)	Typically in atopic dermatitis and psoriasis[140]
	Candida albicans ATCC 10231 (Hydrophilic yeast)	It colonizes skin, mucosa and reproductive tract[141]
	Trichonphyton mentagrophytes ATCC 9533 (mold)	Prevalent in skin foot diseases[142]
	Tricophyton rubrum CECT2794 (mold)	Most common fungus causing infections that remain to the surface of skin, hair or nails of in human[143]

The antimicrobial activity is tested by following the methodology developed in Eurofins Scientific company and described in **Section 6.4.8**.

4.4.4.1 MIC determination for bacteria

Based on the results of the screening of the different types of bacteria and DELOS nanovesicles presented, the detailed MIC values of all bacteria evaluated are shown in **Table 4.8**. From this table, we make the following observations. On the one hand, proper and very promising MIC results were obtained with *Propionibacterium acnes* and *Staphylococcus aureus* ATCC 29213, both gram-positive bacteria. These two bacteria have interesting MIC values in the presence of DELOS nanovesicles as antimicrobial agent, close to the range of commercial antibacterial agents (**Table 4.9**). Then, these antimicrobial activities make DELOS nanovesicles suitable candidates to kill these two types of gram-positive bacteria.

However, *Acinetobacter baumannii* ATCC 15149 presented a high MIC value in comparison to the other two bacteria. This suggests that a higher concentration of DELOS nanovesicles is required to completely kill this gram-negative bacterium.

Table 4.8: MIC values of the different DELOS nanovesicles against three different bacteria.

	MIC (μg·mL^{-1}) Bacteria		
DELOS nanovesicles	*Acinetobacter baumannii* ATCC 15149	*Propionibacterium acnes*	*Staphylococcus aureus* ATCC 29213
Chol:CPC	80	5	5
Chol:CTAB	80	5	5
Chol:CTAC	70	9	9
Chol:ST	464	6	12
Chol:MKC	80	5	5

Table 4.9: MIC quality control ranges for Staphylococcus aureus ATCC 29213.

Controls	**MIC Range (μg·mL^{-1})**
Clindamycin (topic)	0.06-0.25
Fusidic acid (topic)	0.06-0.25
Tobramycin (ocular)	0.12-1

It is important to highlight here that, as seen in the literature, the MIC values for QACs such as MKC and CTAB are in the range of 5–10 μg·mL^{-1} and 0.75–3 μg·mL^{-1} across different strains[112], respectively. Hence, one of the issues that emerges from these findings is that when nanostructuring these QACs in DELOS nanovesicles, the antimicrobial effect of the surfactant is not affected. Consequently, we

can consider DELOS nanovesicles as a proper approach for the treatment of bacterial infection of *Propionibacterium acnes* and *Staphylococcus aureus* ATCC 29213, avoiding the antibiotic resistance and so being a useful alternative to target not only acne therapy but also some other skin-related infections, such as atopic dermatitis and psoriasis.

In addition, it is important to highlight that the use DELOS nanovesicles as antibacterial agents present additional benefits. As already mentioned in **Chapter 1**, DELOS-susp is an eco-efficient platform that allows scalable production of the nanovesicular systems, and so the capacity of producing high quantities in an easy way[144,145].

Moreover, as shown in **Section 2.3.1.5** from **Chapter 2**, CTAB-DELOS nanovesicles demonstrated proper skin tolerance in the Episkin™ skin irritation test. It should be emphasized that in this case, the evaluated membrane concentration was around 1000 times higher compared to the obtained MICs values. Therefore, DELOS nanovesicles can be classified not only as antibacterial substances but also as non-irritating and thus well-tolerated when administered topically, which are important requirements for appropriate topical administration[146].

4.4.4.2 MIC determination for yeast and mold

The antifungal, also known as antimycotic, effect of DELOS nanovesicles with strains of *Malassezia furfur* (yeast) and *Candida albicans* (yeast) and *Trichophyton mentagrophytes* (mold) and *Tricophyton rubrum* (mold) was determined using the same procedure as previously described in **Section 6.4.8**.

As can be seen in **Table 4.10**, we did not observe any effect for any of the studied DELOS nanovesicles formulations in the *Malassezia furfur* as all MIC values are very high, while anti-yeast activity was observed for *Candida albicans*. In this case, a similar MIC range for antibacterial activity was obtained for all DELOS nanovesicle formulations. It should be noted that the presence of surfactants such as CPC, MKC and ST, which have an aromatic ring in their polar head present slightly lower MIC values. Recently, the importance of aromatic rings has been reported in the literature, suggesting that aromatic rings may have an impact on the interaction with some yeasts and fungi[124,147,148].

Regarding the mold (**Table 4.10**), all DELOS nanovesicles were effective for *Trichophyton mentagrophytes* as they exhibited a low MIC value close to the range of standard controls (**Table 4.11**) and also as previously observed for the acceptable antibacterial activity of DELOS nanovesicles (**Table 4.8**). However, DELOS nanovesicles showed almost no antimicrobial activity against *Tricophyton rubrum.* Therefore, it can be assumed that DELOS nanovesicles are a promising treatment for dermatomycosis caused by *Trichophyton mentagrophytes*, mainly present in skin foot such as nail infection[149].

Table 4.10: MIC values of the different DELOS nanovesicles against yeast and mold (fungi).

	MIC (μg·mL^{-1}) Fungi			
	Yeast	Yeast	Mold	Mold
DELOS nanovesicles	*Malassezia furfur* ATCC 14251	*Candida albicans* ATCC 10231	*Trichophyton mentagrophytes* ATCC 9533	*Tricophyton rubrum* CECT2794
Chol:CPC	>1240	2	5	>1240
Chol:CTAB	>1330	10	5	>1330
Chol:CTAC	>1170	9	5	>1170
Chol:ST	>1550	6	12	116
Chol:MKC	>1345	5	5	>1345

Table 4.11: MIC quality control ranges for antifungal products to treat skin infections.

	MIC Range (μg·mL^{-1})	
Controls	*Trichophyton mentagrophytes*	*Tricophyton rubrum*
Ciclopirox	0.5-2	0.5-2
Terbinafine	0.002-0.008	-

4.4.5 Summary of the section and perspectives

This study showed the potent and antimicrobial activity of DELOS nanovesicles. The outcome of the different MIC determinations confirmed the antimicrobial effect of CPC-, CTAB-, CTAC-, ST- and MKC-DELOS nanovesicles in different strains such as gram-positive bacteria like *Propionibacterium acnes* and *Staphylococcus aureus* ATCC 29213, yeast such as *Candida albicans* ATCC 10231 and fungi like *Trichophyton mentagrophytes* ATCC 9533. In all the cases, the MIC value obtained was acceptable in the range of 2-10 μg·mL^{-1}, as expected.

From these results, we can confirm that the antimicrobial activity of DELOS nanovesicles targeting various bacteria and fungi offers a great advantage over the antibiotics, since they can act simultaneously with different microorganisms. Then, DELOS nanovesicles appear to be promising candidates to overcome some of the disadvantages of current treatments. Importantly, compared to antibiotics, they can increase antimicrobial efficacy while reducing the resistance usually induced. At the same time, it is important to consider that CTAB-DELOS nanovesicles are non-irritant in high concentrations as previously shown by the Episkin™ test, further demonstrating the potentiality of their use for topical applications. Furthermore, since DELOS nanovesicles are nanocarriers, they can incorporate antibiotics onto them and act synergistically while reducing the cytotoxicity of antibiotics and also lowering the MIC value.

What is more, DELOS nanovesicles produced by the DELOS-susp platform have enormous potential not only because of their ease of preparation but also using surfactants in their formulation, which are cheaper and more stable alternatives compared to antibiotic production.

As there is abundant room for further progress in understanding of the behaviour of the antimicrobial effect of DELOS nanovesicles, also new strains of the microorganisms that has shown to be susceptible to them will be considered.

So, the use of DELOS nanovesicles are a possible strategy for addressing and overcoming bacteria-resistance and so to combat persistent infections such as the ones presents in complex wounds, deeply studied in this thesis. Then, observing that DELOS nanovesicles present antimicrobial activity, next steps will focus on evaluating the antibiofilm activity in *in vitro* and *in vivo* models. Furthermore, in future investigations, the treatment of atopic dermatitis, psoriasis, acne and some other skin-related infections, such as nail and foot inflections will be considered as they are the ones that have shown to be the most promising to treat their related-antimicrobials by DELOS nanovesicles.

4.5 Bibliography

1. I. Cabrera, E. Elizondo, O. Esteban, et al. Multifunctional Nanovesicle-Bioactive Conjugates Prepared by a One-Step Scalable Method Using CO_2 -Expanded Solvents. *Nano Lett.* **2013**, 13 (8), 3766–3774.
2. G. Orive, R.M. Hernández, A.R. Gascón, A. Domínguez-Gil, J.L. Pedraz. Drug delivery in biotechnology: Present and future. *Current Opinion in Biotechnology*. Elsevier Ltd December 1, 2003, pp 659–664.
3. J.K. Patra, G. Das, L. Fernandes Fraceto, et al. Nano based drug delivery systems: recent developments and future prospects. *J Nanobiotechnol* **2018**, 16, 71.
4. C. Alvarez, U. Ros, A. Valle, et al. Biophysical and biochemical strategies to understand membrane binding and pore formation by sticholysins, pore-forming proteins from a sea anemone. *Biophys. Rev.* **2017**, 9 (5), 529–544.
5. E. Rivera-De-torre, J. Palacios-Ortega, J. Peter Slotte, et al. Functional and structural variation among sticholysins, pore-forming proteins from the sea anemone stichodactyla helianthus. *Int. J. Mol. Sci.* **2020**, 21 (23), 8915.
6. I. Alm, S. García-Linares, J.G. Gavilanes, Á. Martínez-Del-Pozo, J.P. Slotte. Cholesterol stimulates and ceramide inhibits Sticholysin II-induced pore formation in complex bilayer membranes. *Biochim. Biophys. Acta - Biomembr.* **2015**, 1848 (4), 925–931.
7. R.L. Juliano. Intracellular Trafficking and Endosomal Release of Oligonucleotides: What We Know and What We Don't. *Nucleic Acid Ther.* **2018**, 28 (3), 166–177.
8. G. Sahay, D.Y. Alakhova, A. V Kabanov. Endocytosis of nanomedicines. *J. Control. Release* **2010**, 145 (3), 182–195.
9. Y. Hu, E.B. Dammer, R. Ren, G. Wang. The endosomal-lysosomal system : from acidification and cargo sorting to neurodegeneration. *Transl. Neurodegener.* **2015**, 4 (1), 1–10.
10. J.L. Jeger. Endosomes , lysosomes , and the role of endosomal and lysosomal biogenesis in cancer development. *Mol. Biol. Rep.* **2020**, 47 (12), 9801–9810.
11. J.P. Bost, M. Ojansivu, M.J. Munson, et al. Novel endosomolytic compounds enable highly potent delivery of antisense oligonucleotides. *Commun. Biol.* **2022**, 5 (1), 1–14.
12. R.L. Juliano. Chemical Manipulation of the Endosome Trafficking Machinery: Implications for Oligonucleotide Delivery. *Biomedicines* **2021**, 9 (5), 512.
13. R.J. Laborde, O. Sanchez-Ferras, M.C. Luzardo, et al. Novel Adjuvant Based on the Pore-Forming Protein Sticholysin II Encapsulated into Liposomes Effectively Enhances the Antigen-

Specific CTL-Mediated Immune Response. *J. Immunol.* **2017**, 198 (7), 2772–2784.

14. R.L. Juliano. The delivery of therapeutic oligonucleotides. *Nucleic Acids Res.* **2016**, 44 (14), 6518–6548.
15. C. Alvarez, F. Pazos, C. Soto, R. Laborde, M.E. Lanio. Pore-forming toxins from sea anemones : from protein- membrane interaction to its implications for developing biomedical applications. In *Advances in Biomembranes and Lipid Self-Assembly*; Academic Press, **2020**; Vol. 31, pp 129–183.
16. M.S. Saveleva, K. Eftekhari, A. Abalymov, et al. Hierarchy of hybrid materials-the place of inorganics-in-organics in it, their composition and applications. *Front. Chem.* **2019**, 7, 179.
17. K.Č. Kristan, G. Viero, M. Dalla Serra, P. Maček, G. Anderluh. Molecular mechanism of pore formation by actinoporins. *Toxicon* **2009**, 54 (8), 1125–1134.
18. J. Palacios-Ortega, E. Rivera-de-Torre, J.G. Gavilanes, J.P. Slotte, Á. Martínez-del-Pozo. Evaluation of different approaches used to study membrane permeabilization by actinoporins on model lipid vesicles. *Biochim. Biophys. Acta - Biomembr.* **2020**, 1862 (9), 183311.
19. J. Palacios-Ortega, S. García-Linares, E. Rivera-de-Torre, et al. Sticholysin, Sphingomyelin, and Cholesterol: A Closer Look at a Tripartite Interaction. *Biophys. J.* **2019**, 116 (12), 2253–2265.
20. J. Palacios-Ortega, E. Rivera-De-Torre, S. Garciá-Linares, et al. Oligomerization of Sticholysins from Förster Resonance Energy Transfer. *Biochemistry* **2021**, 60 (4), 314–323.
21. S. Ramírez-Carreto, B. Miranda-Zaragoza, C. Rodríguez-Almazán. Actinoporins: From the Structure and Function to the Generation of Biotechnological and Therapeutic Tools. *Biomolecules* **2020**, 10 (4), 539.
22. M. Tejuca, I. Díaz, R. Figueredo, et al. Construction of an immunotoxin with the pore forming protein StI and ior C5, a monoclonal antibody against a colon cancer cell line. *Int. Immunopharmacol.* **2004**, 4 (6), 731–744.
23. D. Pentón, V. Pérez-Barzaga, I. Díaz, et al. Validation of a mutant of the pore-forming toxin sticholysin-I for the construction of proteinase-activated immunotoxins. *Protein Eng. Des. Sel.* **2011**, 24 (6), 485–493.
24. A. del Valle, N. Acosta-Rivero, R.J. Laborde, et al. Sticholysin II shows similar immunostimulatory properties to LLO stimulating dendritic cells and MHC-I restricted T cell responses of heterologous antigen. *Toxicon* **2021**, 200, 38–47.
25. R.C. Soletti, G. Pinto, D. Faria, et al. Potentiation of anticancer-drug cytotoxicity by sea anemone pore-forming proteins in human glioblastoma cells. *Anticancer. Drugs* **2008**, 19 (5), 517–525.
26. A. Valle, J. Alvarado-Mesén, M.E. Lanio, et al. The multigene families of actinoporins (part I):

Isoforms and genetic structure. *Toxicon* **2015**, 103, 176–187.

27. M.E. Lanio, V. Morera, C. Alvarez, et al. Purification and characterization of two hemolysins from Stichodactyla helianthus. *Toxicon* **2001**, 39 (2–3), 187–194.
28. V. Huerta, V. Morera, Y. Guanche, et al. Primary structure of two cytolysin isoforms from Stichodactyla helianthus differing in their hemolytic activity. *Toxicon* **2001**, 39 (8), 1253–1256.
29. J. Palacios-Ortega, S. García-Linares, E. Rivera-de-Torre, et al. Structural foundations of sticholysin functionality. *Biochim. Biophys. Acta - Proteins Proteomics* **2021**, 1869 (10), 140696.
30. U. Ros, M.A. Edwards, R.F. Epand, et al. The sticholysin family of pore-forming toxins induces the mixing of lipids in membrane domains. *Biochim. Biophys. Acta - Biomembr.* **2013**, 1828 (11), 2757–2762.
31. V. Antonini, V. Pé Rez-Barzaga, S. Bampi, et al. Functional Characterization of Sticholysin I and W111C Mutant Reveals the Sequence of the Actinoporin's Pore Assembly. *PLoS One* **2014**, 9 (10), e110824.
32. J.M. Mancheño, J. Martín-Benito, M. Martínez-Ripoll, J.G. Gavilanes, J.A. Hermoso. Crystal and electron microscopy structures of sticholysin II actinoporin reveal insights into the mechanism of membrane pore formation. *Structure* **2003**, 11 (11), 1319–1328.
33. Y.P. Hervis, A. Valle, S. Dunkel, et al. Architecture of the pore forming toxin sticholysin I in membranes. *J. Struct. Biol.* **2019**, 208 (1), 30–42.
34. Q. Hong, I. Gutiérrez-Aguirre, A. Barli, et al. Two-step membrane binding by equinatoxin II, a pore-forming toxin from the sea anemone, involves an exposed aromatic cluster and a flexible helix. *J. Biol. Chem.* **2002**, 277 (44), 41916–41924.
35. A. Valle, L.B. Pérez-Socas, L. Canet, et al. Self-homodimerization of an actinoporin by disulfide bridging reveals implications for their structure and pore formation. *Sci. Reports 2018 81* **2018**, 8 (1), 1–18.
36. C. Alvarez Valcarcel, M. Dalla Serra, C. Potrich, et al. Effects of Lipid Composition on Membrane Permeabilization by Sticholysin I and II, Two Cytolysins of the Sea Anemone Stichodactyla helianthus. *Biophys. J.* **2001**, 80 (6), 2761–2774.
37. C. Álvarez, J.M. Mancheño, D. Martínez, et al. Sticholysins, two pore-forming toxins produced by the Caribbean Sea anemone Stichodactyla helianthus: Their interaction with membranes. *Toxicon* **2009**, 54 (8), 1135–1147.
38. R. Ni, R. Feng, Y. Chau. Synthetic Approaches for Nucleic Acid Delivery: Choosing the Right Carriers. *Life* **2019**, 9 (3), 59.
39. R. Tenchov, R. Bird, A.E. Curtze, Q. Zhou. Lipid Nanoparticles from Liposomes to mRNA Vaccine Delivery, a Landscape of Research Diversity and Advancement. *ACS Nano* **2021**, 15

(11), 16982–17015.

40. P.N. Vigneshkumar, E. George, J. Joseph, F. John, J. George. Liposomal bionanomaterials for nucleic acid delivery. In *Fundamentals of Bionanomaterials*; Barhoum, A., Jeevanandam, J., Danquah, M. K., Eds.; Elsevier, Amsterdam, Netherlands, **2022**; pp 327–362.
41. J.A. Da Silva, R.P. Dias, G.C.A. Da Hora, T.A. Soares, M.R. Meneghetti. Molecular dynamics simulations of cetyltrimethylammonium bromide (CTAB) micelles and their interactions with a gold surface in aqueous solution. *J. Braz. Chem. Soc.* **2018**, 29 (1), 191–199.
42. M.E. Lanio, C. Alvarez, C. Ochoa, et al. Sticholysins I and II interaction with cationic micelles promotes toxins' conformational changes and enhanced hemolytic activity. *Toxicon* **2007**, 50 (6), 731–739.
43. G. Vargas-Nadal. Novel Quatsome nanovesicles, prepared using compressed CO2, for the development of advanced nanomedicines "Doctoral dissertation," Universitat de Barcelona, **2020**.
44. P. J. Sheskey, W.G. Cook, C.G. Cable. Handbook of Pharmaceutical Excipients, Eight edit.; **2017**.
45. E.M.A. Committee for Human Medicinal Products. Benzalkonium chloride used as an excipient (EMA/CHMP/352187/2012); **2017**.
46. A. Okahara, H. Tanioka, K. Takada, K. Kawazu. Ocular Toxicity of Benzalkonium Chloride Homologs Compared with Their Mixtures. *J. Toxicol. Pathol.* **2013**, 26 (4), 343–349.
47. G. Vargas-Nadal, M. Muñoz-Ubeda, P. Alamo, et al. MKC-Quatsomes: a stable nanovesicle platform for bio-imaging and drug-delivery applications. *Nanomedicine Nanotechnology, Biol. Med.* **2020**, 24, 102136.
48. J. Dufourcq, J.F. Faucon. Intrinsic fluorescence study of lipid-protein interactions in membrane models. Binding of melittin, an amphipathic peptide, to phospholipid vesicles. *Biochim. Biophys. Acta - Biomembr.* **1977**, 467 (1), 1–11.
49. B. Christiaens, S. Symoens, S. Vanderheyden, et al. Tryptophan fluorescence study of the interaction of penetratin peptides with model membranes. *Eur. J. Biochem.* **2002**, 269 (12), 2918–2926.
50. J.M. Beechem, L. Brand. Time-resolved fluorescence of proteins. *Annu. Rev. Biochem.* **1985**, 54 (1), 43–71.
51. P. Fluorescence. Topics in Fluorescence Spectroscopy; Lakowicz, J. R., Ed.; Kluwer Academic Publishers, New York, **2000**.
52. C.A. Royer. Probing protein folding and conformational transitions with fluorescence. *Chem. Rev.* **2006**, 106 (5), 1769–1784.

53. J.R. Lakowicz. Principles of Fluorescence Spectroscopy, 2nd ed.; Springer Science & Business Media, New York, USA, **2006**.

54. J. Chen, E.J. LeBoeuf, S. Dai, B. Gu. Fluorescence spectroscopic studies of natural organic matter fractions. *Chemosphere* **2003**, 50 (5), 639–647.

55. S. García-Linares, T. Maula, E. Rivera-De-Torre, et al. Role of the tryptophan residues in the specific interaction of the sea anemone stichodactyla helianthus's actinoporin sticholysin II with biological membranes. *Biochemistry* **2016**, 55 (46), 6406–6420.

56. J.A. Killian, R. Keller. Tryptophan fluorescence study on the interaction of the signal peptide of the Escherichia coli outer membrane protein PhoE with model membranes. *Biochemistry* **1990**, 29 (35), 8131–8137.

57. S.R. Hsieh, P.M. Reddy, C.J. Chang, et al. Exploring the behavior of bovine serum albumin in response to changes in the chemical composition of responsive polymers: Experimental and simulation studies. *Polymers (Basel).* **2016**, 8 (6), 238.

58. J.R. Lakowicz, S. Keating-Nakamoto. Red-Edge Excitation of Fluorescence and Dynamic Properties of Proteins and Membranes. *Biochemistry* **1984**, 23 (13), 3013–3021.

59. S.L. Rouse, M.S.P. Sansom. Interactions of lipids and detergents with a viral ion channel protein: Molecular dynamics simulation studies. *J. Phys. Chem. B* **2015**, 119 (3), 764–772.

60. D. Otzen. Protein-surfactant interactions: A tale of many states. *Biochim. Biophys. Acta - Proteins Proteomics* **2011**, 1814 (5), 562–591.

61. D.E. Otzen. Protein unfolding in detergents: Effect of micelle structure, ionic strength, pH, and temperature. *Biophys. J.* **2002**, 83 (4), 2219–2230.

62. G. Savelli, N. Spreti, P. Di Profio. Enzyme activity and stability control by amphiphilic self-organizing systems in aqueous solutions. *Curr. Opin. Colloid Interface Sci.* **2000**, 5 (1–2), 111–117.

63. H.K. Kimelberg. Protein-liposome interactions and their relevance to the structure and function of cell membranes. *Mol. Cell. Biochem.* **1976**, 10 (3), 171–190.

64. Y. Liu, Z. Cao, J. Wang, W. Zong, R. Liu. The interaction mechanism between anionic or cationic surfactant with HSA by using spectroscopy, calorimetry and molecular docking methods. *J. Mol. Liq.* **2016**, 224, 1008–1015.

65. L. Ronda, B. Pioselli, S. Catinella, et al. Quenching of tryptophan fluorescence in a highly scattering solution: Insights on protein localization in a lung surfactant formulation. *PLoS One* **2018**, 13 (8), e0201926.

66. M. Friedman. Chemistry, Biochemistry, and Safety of Acrylamide. A Review. *J. Agric. Food Chem.* **2003**, 51 (16), 4504–4526.

67. M.A. Kowalska, W. Leyko. Acrylamide Quenching Study of Gamma-irradiated Human Haemoglobin. *Int. J. Radiat. Biol. Relat. Stud. Physics, Chem. Med.* **1981**, 39 (4), 431–435.

68. O. Azimi, Z. Emami, H. Salari, J. Chamani. Probing the interaction of human serum albumin with norfloxacin in the presence of high-frequency electromagnetic fields: Fluorescence spectroscopy and circular dichroism investigations. *Molecules* **2011**, 16 (12), 9792–9818.

69. E. Ruiz-Hitzky. Functionalizing inorganic solids: Towards organic-inorganic nanostructured materials for intelligent and bioinspired systems. *Chem. Rec.* **2003**, 3 (2), 88–100.

70. S.J.H. Soenen, U. Himmelreich, N. Nuytten, et al. Intracellular Nanoparticle Coating Stability Determines Nanoparticle Diagnostics Efficacy and Cell Functionality. *Small* **2010**, 6 (19), 2136–2145.

71. T.U. Wani, S.N. Raza, N.A. Khan. Nanoparticle opsonization: forces involved and protection by long chain polymers. *Polym. Bull.* **2020**, 77 (7), 3865–3889.

72. N.M. Gulati, P.L. Stewart, N.F. Steinmetz. Bioinspired Shielding Strategies for Nanoparticle Drug Delivery Applications. *Mol. Pharm.* **2018**, 15 (8), 2900–2909.

73. M. Barrow, A. Taylor, P. Murray, M.J. Rosseinsky, D.J. Adams. Design considerations for the synthesis of polymer coated iron oxide nanoparticles for stem cell labelling and tracking using MRI. *Chem. Soc. Rev.* **2015**, 44 (19), 6733–6748.

74. V. De Leo, F. Milano, A. Agostiano, L. Catucci. Recent advancements in polymer/liposome assembly for drug delivery: From surface modifications to hybrid vesicles. *Polymers (Basel).* **2021**, 13 (7), 1027.

75. L. Tang, J. Cheng. Nonporous silica nanoparticles for nanomedicine application. *Nano Today* **2013**, 8 (3), 290–312.

76. A.M. Mebert, C.J. Baglole, M.F. Desimone, D. Maysinger. Nanoengineered silica: Properties, applications and toxicity. *Food Chem. Toxicol.* **2017**, 109, 753–770.

77. C. Li, Y. Zhang, T. Su, et al. Silica-coated flexible liposomes as a nanohybrid delivery system for enhanced oral bioavailability of curcumin. *Int. J. Nanomedicine* **2012**, 7, 5995.

78. U.S Food & Drug Administration. CFR - Code of Federal Regulations Title 21; **2020**.

79. A. Bertucci, E.A. Prasetyanto, D. Septiadi, et al. Combined Delivery of Temozolomide and Anti-miR221 PNA Using Mesoporous Silica Nanoparticles Induces Apoptosis in Resistant Glioma Cells. *Small* **2015**, 11 (42), 5687–5695.

80. Z. Cao, Y. Ma, X. Yue, et al. Stabilized liposomal nanohybrid cerasomes for drug delivery applications. *Chem. Commun.* **2010**, 46 (29), 5265–5267.

81. N. V. Beloglazova, O.A. Goryacheva, E.S. Speranskaya, et al. Silica-coated liposomes loaded

with quantum dots as labels for multiplex fluorescent immunoassay. *Talanta* **2015**, 134, 120–125.

82. L. Maggini, I. Cabrera, A. Ruiz-Carretero, et al. Breakable mesoporous silica nanoparticles for targeted drug delivery. *Nanoscale* **2016**, 8 (13), 7240–7247.
83. J. Bellare, N. Dwivedi, M.A. Arunagirinathan, S. Sharma. Silica-coated liposomes for insulin delivery. *J. Nanomater.* **2010**, 2010.
84. F. Hoffmann, M. Cornelius, J. Morell, M. Fröba. Silica-Based Mesoporous Organic□Inorganic Hybrid Materials. *Angew. Chemie Int. Ed.* **2006**, 45 (20), 3216–3251.
85. A. Lazaro, N. Vilanova, L.D.B. Torres, et al. Synthesis, Polymerization, and Assembly of Nanosilica Particles below the Isoelectric Point. *Langmuir* **2017**, 33 (51), 14618–14626.
86. C. Colleoni, S. Esposito, R. Grasso, et al. Delayed luminescence induced by complex domains in water and in TEOS aqueous solutions. *Phys. Chem. Chem. Phys.* **2016**, 18 (2), 772–780.
87. R.J.P. Corriu, D. Leclercq. Recent developments of molecular chemistry for sol-gel processes. *Angew. Chemie Int. Ed. English* **1996**, 35 (13–14), 1420–1436.
88. J.G. Croissant, Y. Fatieiev, A. Almalik, N.M. Khashab. Mesoporous Silica and Organosilica Nanoparticles: Physical Chemistry, Biosafety, Delivery Strategies, and Biomedical Applications. *Adv. Healthc. Mater.* **2018**, 7 (4), 1700831.
89. A.L. Hubert, D. H., Jung, M., Frederik, P. M., Bomans, P. H. H., Meuldijk, J., & German. Vesicle-Directed Growth of Silica. *Adv. Mater.* **2000**, 12 (17), 1286–1290.
90. J.E. Berlier, A. Rothe, G. Buller, et al. Quantitative Comparison of Long-wavelength Alexa Fluor Dyes to Cy Dyes: Fluorescence of the Dyes and Their Bioconjugates. *J. Histochem. Cytochem.* **2003**, 51 (12), 1699–1712.
91. T.F. Scientific. Fluorescence SpectraViewer https://www.thermofisher.com/order/fluorescence-spectraviewer?SID=srch-svtool&UID=282lip#!/?SID=srch-svtool&UID=282lip (accessed Jun 7, 2022).
92. R.B. Sekar, A. Periasamy. Fluorescence resonance energy transfer (FRET) microscopy imaging of live cell protein localizations. *J. Cell Biol.* **2003**, 160 (5), 629.
93. C. Berney, G. Danuser. FRET or no FRET: A quantitative comparison. *Biophys. J.* **2003**, 84 (6), 3992–4010.
94. A. West. Experimental Methods to Investigate Self-Assembly at Interfaces. In *Interface Science and Technology*; Ball, V., Ed.; Elsevier, **2018**; Vol. 21, pp 131–241.

95. S.E. Glassford, B. Byrne, S.G. Kazarian. Recent applications of ATR FTIR spectroscopy and imaging to proteins. *Biochim. Biophys. Acta - Proteins Proteomics* **2013**, 1834 (12), 2849–2858.

96. N. Nagai, H. Hashimoto. FT-IR-ATR study of depth profile of SiO2 ultra-thin films. *Appl. Surf. Sci.* **2001**, 172 (3–4), 307–311.

97. L. Travaglini, L. De Cola. Morphology control of mesoporous silica particles using bile acids as cosurfactants. *Chem. Mater.* **2018**, 30 (12), 4168–4175.

98. J.P. Borrajo, S. Liste, J. Serra, et al. Influence of the Network Modifier Content on the Bioactivity of Silicate Glasses. *Key Eng. Mater.* **2004**, 254–256, 23–26.

99. C. LibreTexts. Transmission electron microscopy (TEM): TEM versus STEM and HAADF https://chem.libretexts.org/Courses/Franklin_and_Marshall_College/Introduction_to_Materials_Characterization__CHM_412_Collaborative_Text/Electron_and_Probe_Microscopy/Transmission_electron_microscopy_(TEM)%3A_TEM_versus_STEM_and_HAADF (accessed Jun 12, 2022).

100. A. Da Cruz Schneid, L.J.C. Albuquerque, G.B. Mondo, et al. Colloidal stability and degradability of silica nanoparticles in biological fluids: a review. *J. Sol-Gel Sci. Technol.* **2022**, 102, 41–62.

101. H.J. Forman, H. Zhang, A. Rinna. Glutathione: Overview of its protective roles, measurement, and biosynthesis. *Mol. Aspects Med.* **2009**, 30 (1–2), 1–12.

102. D.M. Townsend, K.D. Tew, H. Tapiero. The importance of glutathione in human disease. *Biomed. Pharmacother.* **2003**, 57 (3–4), 145–155.

103. I. Imosemi. A review of the importance of glutathione in neurodegenerative diseases. *Eur. J. Pharm. Med. Res.* **2021**, 8 (6), 61–71.

104. G. Teskey, R. Abrahem, R. Cao, et al. Glutathione as a Marker for Human Disease. In *Advances in Clinical Chemistry*; Makowski, G. S., Ed.; Elsevier Ltd, **2018**; Vol. 87, pp 141–159.

105. A.K. Tummanapelli, S. Vasudevan. Ab Initio MD Simulations of the Brønsted Acidity of Glutathione in Aqueous Solutions: Predicting pKa Shifts of the Cysteine Residue. *J. Phys. Chem. B* **2015**, 119 (49), 15353–15358.

106. J. Yin, Y. Kwon, D. Kim, et al. Cyanine-based fluorescent probe for highly selective detection of glutathione in cell cultures and live mouse tissues. *J. Am. Chem. Soc.* **2014**, 136 (14), 5351–5358.

107. Z. Guan, L. Yang, W. Wang, et al. Thermosensitive micellar hydrogel for enhanced anticancer therapy through redox modulation mediated combinational effects. *RSC Adv.* **2017**, 7 (55), 34755–34762.

108. T. Tadros. General principles of colloid stability and the role of surface forces. In *Colloid Stability: The Role of Surface Forces – Part I*; Tadros, T. F., Ed.; WileyVCH Verlag GmbH & Co. KGaA, Weinheim, Germany, **2006**; Vol. 1, pp 1–22.

109. C. Graf, Q. Gao, I. Schütz, et al. Surface functionalization of silica nanoparticles supports colloidal stability in physiological media and facilitates internalization in cells. *Langmuir* **2012**, 28 (20), 7598–7613.

110. V.J. Mohanraj, T.J. Barnes, C.A. Prestidge. Silica nanoparticle coated liposomes: A new type of hybrid nanocapsule for proteins. *Int. J. Pharm.* **2010**, 392 (1–2), 285–293.

111. K. Giri, I. Kuschnerus, J. Ruan, A.E. Garcia-Bennett. Influence of a Protein Corona on the Oral Pharmacokinetics of Testosterone Released from Mesoporous Silica. *Adv. Ther.* **2020**, 3 (5), 1900110.

112. D. Hassan, C.A. Omolo, V.O. Fasiku, et al. Formulation of pH-Responsive Quatsomes from Quaternary Bicephalic Surfactants and Cholesterol for Enhanced Delivery of Vancomycin against Methicillin Resistant Staphylococcus aureus. *Pharmaceutics* **2020**, 12 (11), 1093.

113. A. Bridier, R. Briandet, V. Thomas, F. Dubois-Brissonnet. Resistance of bacterial biofilms to disinfectants: a review. *J. Bioadhesion Biofilm Res.* **2011**, 27 (9), 1017–1032.

114. D. López, H. Vlamakis, R. Kolter. Biofilms. *Cold Spring Harb. Perspect. Biol.* **2010**, 2 (7), a000398.

115. N. Høiby, T. Bjarnsholt, M. Givskov, S. Molin, O. Ciofu. Antibiotic resistance of bacterial biofilms. *Int. J. Antimicrob. Agents* **2010**, 35 (4), 322–332.

116. K. Schilcher, A.R. Horswill. Staphylococcal Biofilm Development: Structure, Regulation, and Treatment Strategies. *Microbiol. Mol. Biol. Rev.* **2020**, 84 (3), e00026-19.

117. G. Gebreyohannes, A. Nyerere, C. Bii, D.B. Sbhatu. Challenges of intervention, treatment, and antibiotic resistance of biofilm-forming microorganisms. *Heliyon* **2019**, 5 (8), e02192.

118. S.L. Percival, K.E. Hill, D.W. Williams, et al. A review of the scientific evidence for biofilms in wounds. *Wound Repair Regen.* **2012**, 20 (5), 647–657.

119. J. Jass, S. Surman, J. Walker, Eds. Microbial biofilms in medicine. In *Medical Biofilms: Detection, Prevention and Control*; John Wiley & Sons, **2003**; pp 1–27.

120. U. Römling, C. Balsalobre. Biofilm infections, their resilience to therapy and innovative treatment strategies. *J. Intern. Med.* **2012**, 272 (6), 541–561.

121. M. Chen, Q. Yu, H. Sun. Novel Strategies for the Prevention and Treatment of Biofilm Related Infections. *Int. J. Mol. Sci.* **2013**, 14 (9), 18488–18501.

122. S. Hogan, N.T. Stevens, H. Humphreys, J.P. O'Gara, E. O'Neill. Current and Future Approaches to the Prevention and Treatment of Staphylococcal Medical Device-Related Infections. *Curr. Pharm. Des.* **2015**, 21 (1), 100–113.

123. O. Ciofu, E. Rojo-Molinero, M.D. Macià, A. Oliver. Antibiotic treatment of biofilm infections. *Apmis* **2017**, 125 (4), 304–319.

124. M.C. Jennings, K.P.C. Minbiole, W.M. Wuest. Quaternary Ammonium Compounds: An Antimicrobial Mainstay and Platform for Innovation to Address Bacterial Resistance. *ACS Infect. Dis.* **2015**, 1 (7), 288–303.

125. D.B. Vieira, A.M. Carmona-Ribeiro. Cationic lipids and surfactants as antifungal agents: mode of action. *J. Antimicrob. Chemother.* **2006**, 58 (4), 760–767.

126. L. Ferrer-Tasies, H. Santana, I. Cabrera-Puig, et al. Recombinant Human Epidermal Growth Factor/Quatsome Nanoconjugates: A Robust Topical Delivery System for Complex Wound Healing. *Adv. Ther.* **2021**, 4 (6), 2000260.

127. K. Beers, J. Rheingans, K. Chinault, P. Cook, A. Waldroup. Microbial efficacy of commercial application of Cecure® CPC antimicrobial to ingesta-contaminated pre-chill Broiler Carcasses. *Int. J. Poult. Sci.* **2006**, 5 (8), 698–703.

128. Stearalkonium. Final Report on the Safety Assessment of Stearalkonium Chloride. *J. Am. Coll. Toxicol.* **1990**, 1 (2), 57–69.

129. S. Samimi, N. Maghsoudnia, R.B. Eftekhari, F. Dorkoosh. Lipid-Based Nanoparticles for Drug Delivery Systems. In *Characterization and Biology of Nanomaterials for Drug Delivery*; Mohapatra, S. S., Ranjan, S., Dasgupta, N., Mishra, R. K., Thomas, S., Eds.; Elsevier Inc., **2019**; pp 47–76.

130. B. Kowalska-Krochmal, R. Dudek-Wicher. The Minimum Inhibitory Concentration of Antibiotics: Methods, Interpretation, Clinical Relevance. *Pathogens* **2021**, 10 (2), 165.

131. J.M. Andrews. Determination of minimum inhibitory concentrations. *J. Antimicrob. Chemother.* **2001**, 48 (Suppl_1), 5–16.

132. B. Dréno, S. Pécastaings, S. Corvec, et al. Cutibacterium acnes (Propionibacterium acnes) and acne vulgaris: a brief look at the latest updates. *J. Eur. Acad. Dermatology Venereol.* **2018**, 32, 5–14.

133. E. Platsidaki, C. Dessinioti. Recent advances in understanding Propionibacterium acnes (Cutibacterium acnes) in acne. *F1000Research* **2018**, 7.

134. S. Krishna, L.S. Miller. Host–pathogen interactions between the skin and Staphylococcus aureus. *Curr. Opin. Microbiol.* **2012**, 15 (1), 28–35.

135. N.N. Schommer, R.L. Gallo. Structure and function of the human skin microbiome. *Trends Microbiol.* **2013**, 21 (12), 660–668.

136. B. Havlickova, V.A. Czaika, M. Friedrich. Epidemiological trends in skin mycoses worldwide. *Mycoses* **2008**, 51 (Suppl.4), 2–15.

137. A.Y. Peleg, H. Seifert, D.L. Paterson. Acinetobacter baumannii: Emergence of a successful pathogen. *Clin. Microbiol. Rev.* **2008**, 21 (3), 538–582.

138. A.L. Perry, P.A. Lambert. Propionibacterium acnes. *Lett. Appl. Microbiol.* **2006**, 42 (3), 185–188.

139. S. Krishna, L.S. Miller. Host–pathogen interactions between the skin and Staphylococcus aureus. *Curr. Opin. Microbiol.* **2012**, 15 (1), 28–35.

140. A. Prohic, T. Jovovic Sadikovic, M. Krupalija-Fazlic, S. Kuskunovic-Vlahovljak. Malassezia species in healthy skin and in dermatological conditions. *Int. J. Dermatol.* **2016**, 55 (5), 494–504.

141. S.W. Kashem, D.H. Kaplan. Skin Immunity to Candida albicans. *Trends Immunol.* **2016**, 37 (7), 440–450.

142. N. Zaias, G. Rebell. Clinical and mycological status of the Trichophyton mentagrophytes (interdigitale) syndrome of chronic dermatophytosis of the skin and nails. *Int. J. Dermatol.* **2003**, 42 (10), 779–788.

143. J. Chen, J. Yi, L. Liu, et al. Substrate adaptation of Trichophyton rubrum secreted endoproteases. *Microb. Pathog.* **2010**, 48 (2), 57–61.

144. M. Cano-Sarabia, N. Ventosa, S. Sala, et al. Preparation of uniform rich cholesterol unilamellar nanovesicles using CO2-expanded solvents. *Langmuir* **2008**, 24 (6), 2433–2437.

145. J. Merlo-Mas, J. Tomsen-Melero, J.L. Corchero, et al. Application of Quality by Design to the robust preparation of a liposomal GLA formulation by DELOS-susp method. *J. Supercrit. Fluids* **2021**, 173, 105204.

146. O. Uchechi, J.D.N. Ogbonna, A.A. Attama. Nanoparticles for Dermal and Transdermal Drug Delivery. In *Application of Nanotechnology in Drug Delivery*; IntechOpen, **2014**; pp 193–227.

147. C. Bortolus, M. Billamboz, R. Charlet, et al. A Small Aromatic Compound Has Antifungal Properties and Potential Anti-Inflammatory Effects against Intestinal Inflammation. *Int. J. Mol. Sci.* **2019**, 20 (2), 321.

148. P.B. Miniyar, A.A. Mahajan, S.N. Mokale, et al. Triazole hybrids as new type of anti-fungal agents. *Arab. J. Chem.* **2017**, 10 (3), 295–299.

149. R. Patiño-Herrera, R. Catarino-Centeno, M. Robles-Martínez, et al. Antimycotic activity of zinc oxide decorated with silver nanoparticles against Trichophyton mentagrophytes. *Powder Technol.* **2018**, 327, 381–391.

"Luck is what happens when preparation meets opportunity"

- Seneca

5 General Conclusions

From the work carried out in this Ph.D. Thesis on the translation of new DELOS nanovesicles into new pharmaceutical products, the following conclusions can be withdrawn:

1. The intermediate formulation of rhEGF-DELOS nanovesicles was successfully developed using the compressed CO_2-based DELOS-susp platform for the topical treatment of complex wounds, such as Diabetic Foot Ulcers (DFUs) and Venous Leg Ulcers (VLUs). To do it, the critical parameters that can impact on the performance of the drug product were optimized to improve the quality and safety of the nanoformulations. Specifically, excellent physicochemical properties were obtained using histidine buffer (5 mM, pH 7.0) as dispersant medium and by loading the CTAB in the organic phase during the production of rhEGF-nanovesicles by DELOS-susp. Furthermore, a complete reproducibility of the physicochemical characteristics of the intermediate product from bench-scale to pilot-scale was achieved, which is a relevant factor for the production of a pharmaceutical product at an industrial scale.
2. Preclinical assessment of the rhEGF-DELOS nanovesicles was carried out, examining the efficacy and toxicology and obtaining promising results. The nanoformulation was considered non-skin irritant and presented enhanced wound healing capacity compared to the free protein, which are desired characteristics for the treatment of complex wounds. Moreover, a 1-week dose range study in rats demonstrated that rhEGF-DELOS nanovesicles are well tolerated at the tested dose. Undoubtedly, rhEGF-DELOS nanovesicle intermediate formulation can be considered as an innovative product with high added value, since it meets the basic requirements of production, storage stability, patient compliance and high efficacy with minimal side effects. Consequently, this new nanovesicular formulation is ready to enter clinical trials for the treatment of DFUs and VLUs.
3. The translation of the rhEGF-DELOS nanovesicle intermediate product into gaseous and hydrogel dosage forms was successfully achieved, as a spray device and a 2 wt% Methocel™

K4M hydrogel containing rhEGF-DELOS nanovesicles, respectively. In both cases, proper characteristics of the dosage forms were obtained for the intended uses. Furthermore, the integrity of the nanoformulation upon gelation was verified, which is a relevant factor to consider for the effectiveness of the formulation and that is not widely considered in the literature. Consequently, gaseous and semi-solid dosage forms of rhEGF-DELOS nanovesicles have been considered as future potential dosage forms for the topical treatment of complex wounds such as DFUs and VLUs.

New DELOS nanovesicle formulations were designed for topical administration. CTAB- and CTAC-DELOS nanovesicles in water; acetate buffer (5 mM, pH = 5.0); histidine buffer (5 mM, pH = 7.0); and PBS buffer (5 mM, pH = 7.4) were successfully prepared by DELOS-susp to pursue more skin-tolerability studies of DELOS nanovesicle systems.

4. In addition, they were efficiently gellified with 2 wt% Methocel™ K4M presenting appropriate physicochemical properties such as suitable rheological properties for the intended use. Methocel™ K4M hydrogels containing DELOS nanovesicles formulated in water and histidine buffer were selected as the optimal ones.

5. Proper formulatabilty was also observed on developing other innovative DELOS nanovesicles-based hydrogels. We have shown for the first time the feasibility of using 25wt% of Poloxamer 407 polymer for the preparation of promising hydrogels of CTAB- and CTAC-DELOS nanovesicles in water; histidine buffer (5 mM, pH = 7.0); and PBS buffer (5 mM, pH = 7.4). These hydrogels present thermoreversibility, being liquid-like at low temperatures and gel at body temperature, allowing the ease of preparation and manageability. In addition, the use of Poloxamer 407 produce an irreversible coating around the vesicles, what could give new properties to the formulation.

6. It was demonstrated for the first time, that MKC- and CTAB-DELOS nanovesicles are feasible formulations to interact with pore-forming proteins called sticholysins and so create a new biologic-organic hybrid formulation for the enhance of drug delivery using DELOS nanovesicles. These pore-forming proteins produced by the Caribbean Sea anemone *Stichodactyla helianthus* have proven to have a potential use in facilitating drug cell penetration, consequently, this study opened new challenges in this field and so open a new area of possibilities for being used in future delivery systems.

7. Hybrid inorganic-organic structures based on DELOS nanovesicles coated with a silica shell have been deeply characterized. It has demonstrated that the stability of such structures is strongly dependent on the dispersant medium in which the system is found. In this regard, promising results have been found in presence of simulated gastric fluid and so, opening new strategies for using DELOS nanovesicles as nanocarriers for oral administration route.

8. CPC-, CTAB-, CTAC-, ST- and MKC-DELOS nanovesicles showed significant antimicrobial activity against as gram-positive bacteria like *Propionibacterium acnes* and *Staphylococcus aureus* ATCC 29213, yeast such as *Candida albicans* ATCC 10231 and fungi like *Trichophyton mentagrophytes* ATCC 9533. Thus, DELOS nanovesicles might be an encouraging alternative to develop metal-free new antimicrobial treatments for skin diseases and offer new approaches in front of the current multidrug resistance problematic.

Based on these general conclusions, we can confirm that this Ph.D. Thesis has contributed to the translation of DELOS nanovesicles into new pharmaceutical products.

The most important thing is to try and inspire people so that they can be great in whatever they want to do.

– Kobe Bryant

6 Experimental part

6.1 Materials

Components used in DELOS nanovesicle formulations preparation

Cholesten-3β-ol (Chol, purity 95%) was purchased from PanReac AppliChem (Castellar del Vallès, Spain). Cetyltrimethylammonium bromide (CTAB BioUltra, purity ≥99.0%), Cetyltrimethylammonium chloride (CTAC, purity ≥ 98.0%) and Cetylpyridinium chloride (CPC, purity ≥ 98.0%) were purchased from Sigma-Aldrich (Madrid, Spain). Myristalkonium chloride (MKC, purity 99.2%) was acquired from US Biological Life Science (Salem, USA). Stearalkonium chloride (ST, purity ≥ 98.0%) was obtained from TCI America (Cambridge, MA).

Ethanol (EtOH, HPLC grade purity), was obtained from Teknokroma (Sant Cugat del Vallès, Spain) and CO_2 (purity 99.9%) was supplied by Carburos Metálicos S.A. (Barcelona, Spain). However, in **Section 4.3.3** and **Section 4.3.4**, the EtOH used was Ethanol absolute anhydrous Pure acquired from Carlo Erba Reagents (Val-de-Reuil, France).

The water used was pre-treated with the Milli-Q Advantage A10 water purification system (Millipore Ibérica, Madrid, Spain). Buffer histidine was prepared using l-Histidine (Sigma Aldrich, St. Louis, MO, USA). Buffer phosphate and buffer PBS were prepared by using sodium chloride (NaCl, purity ≥ 99.5%) acquired from Thermo Fisher Scientific (Waltham, MA, USA), sodium hydrogen phosphate (Na_2HPO_4, purity ≥99.0%) and sodium phosphate monobasic dihydrate ($NaH_2PO_4 \cdot 2H_2O$, purity ≥99.0%) acquired from Merck KgaA (Darmstadt, Germany). Hepes ($C_8H_{18}N_2O_4S$, purity ≥99.5%) was purchased from Sigma-Aldrich (St. Louis, MO, USA). Buffer citrate was prepared using sodium citrate dehydrate purchased in Sigma Aldrich (St. Louis, MO, USA) and citric acid from Thermo Fisher Scientific (Waltham, MA, USA). Acetate buffer was obtained using sodium acetate (Sigma Aldrich, St. Louis, MO, USA) and acetic acid glacial purchased in Thermo Fisher Scientific (Waltham, MA, USA).

All the chemicals were used without further purification.

Active molecules

The recombinant human epidermal growth factor (rhEGF) used in all the experiments was produced by recombinant DNA technology using *Saccharomyces cerevisiae* and provided by the Center of Genetic Engineering and Biotechnology (La Habana, Cuba). L-Glutathione reduced (GSH, purity 98%) was purchased from Sigma-Aldrich (Saint Louis, USA). Sticholysin I and II were produced and provided by the University of Havana-Center of Molecular Immunology. StI (Swiss Protein Data Bank P07845) was obtained from the sea anemone by the procedure described by Lanio et al. (2001) and StI W111C was expressed and purified following the methods described by Pentón et al. (2011). Acrylamide was obtained from Sigma-Aldrich (St Louis, MO, USA).

Fluorophores

1,1'-dioctadecyl-3,3,3',3'-tetramethylindocarbocyanine perchlorate (DiI), 1,1'-dioctadecyl-3,3,3',3'-tetramethylindodicarbocyanine perchlorate (DiD) were purchased from Life Technologies (Carlsbad, USA). AFDye 647 NHS Ester (Alexa Fluor 647 analog) was acquired from Fluoroprobes (Scottsdale, USA).

Hydrogelling agents

Methocel™ K4M was provided by Dow Chemical Co. (Midland, MI, USA). Poloxamer 407 was obtained from Sigma-Aldrich (St Louis, MO, USA).

Silica coating

Tetra methyl orthosilicate (TEMOS, purity 98%), 3-Aminopropyl)tiethoxysilane (APTES, purity 99%) were obtained from Sigma-Aldrich (Saint Louis, USA).

Dispersant media used for dilutions

Simulated gastric fluid (SGF) was prepared using sodium chloride (NaCl) obtained from Thermo Fisher Scientific (Waltham, MA, USA), and hydrochloric acid (HCl, 37% a.r) purchased from Chem-

Lab (Belgium). In **Section 4.3**, Phosphate Buffered Saline Tablets (PBS) were obtained from Sigma-Aldrich (Saint Louis, USA). Dissolving one tablet of PBS buffer in 1 liter of deionized water yields 140 mM NaCl, 10 mM phosphate buffer, and 3 mM KCl, pH 7.4 at 25°C.

6.2 Preparation and processes of DELOS nanovesicles formulations

6.2.1 Preparation of DELOS nanovesicles by DELOS-susp

6.2.1.1 Equipment and procedure for preparation at lab-scale

DELOS nanovesicles were prepared using DELOS-susp methodology, based on compressed CO_2 and developed by Nanomol group (ICMAB-CSIC) and Nanomol Technologies SL. Depending on the desired batch size, two different configurations were used: the small lab-scale equipment (7.5 mL high-pressure vessel, batch size 25 – 75 mL) or the intermediate lab-scale equipment (25 mL or 50 mL high-pressure vessel, batch size 150 – 900 mL).

Configuration of small lab-scale equipment (7.5 mL high-pressure vessel)

The small lab-scale equipment used for the preparation of nanoconjugates using DELOS-susp is schematized in **Figure 6.1.** Briefly, the configuration consists of a 7.5 mL high pressure vessel (R), for which the temperature is kept using an external fluid heating jacket. CO_2 is pumped into the reactor through a thermostatic syringe pump (model 260D, ISCO Inc., Lincoln, US) (P) to introduce CO_2 inside the vessel through valves V-001 and V-002 until reaching working pressure. Further, by using a manual depressurization valve (V-007), the expanded liquid solution contained in the vessel (T-101) is depressurized into an aqueous phase placed in a collector (T-102) at atmospheric pressure, while at the same time, pressure of nitrogen (N_2) is adjusted by a pressure regulator (V-003) and introduced through valves V-004 and V-005 directly from a pressurized reservoir to the vessel.

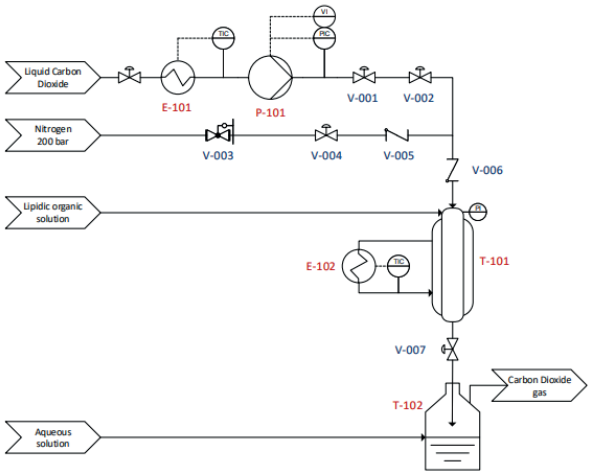

Figure 6.1: Process diagram of the small lab-scale equipment (7.5 mL high-pressure vessel) set-up used for the preparation of nanovesicles by DELOS-susp.

Configuration of intermediate lab-scale equipment (25/50 mL high-pressure vessel)

The intermediate lab-scale equipment used to prepare nanovesicles using DELOS-susp is schematized in **Figure 6.2**. In this case, the configuration consists of a 25 mL or a 50 mL (independent and interchangeable) high-pressure vessel (T-101), for which the temperature is maintained using an external fluid heating jacket. Temperature and pressure inside R are monitored by a temperature indicator (TIC) and a pressure indicator (PI). CO_2 is pumped into the reactor through a thermostatic syringe pump (model 260D, ISCO Inc., Lincoln, US) (P) to introduce CO_2 inside the vessel through valves V-001 and V-002 until reaching working pressure. A variable speed stirrer (S-101) inside T-101, ensures the homogeneity of the mixture in the volumetrically expanded phase. Further, by using a depressurization micrometric valve (V-007), the expanded liquid solution contained in the vessel is depressurized into an aqueous phase placed in a collector (T-102) under magnetic agitation (S-102) at atmospheric pressure, while at the same time, pressure of nitrogen (N_2) is adjusted by a pressure adjustment valve (V-003) and introduced through valves V-004 and V-005 directly from a pressurized reservoir to the vessel.

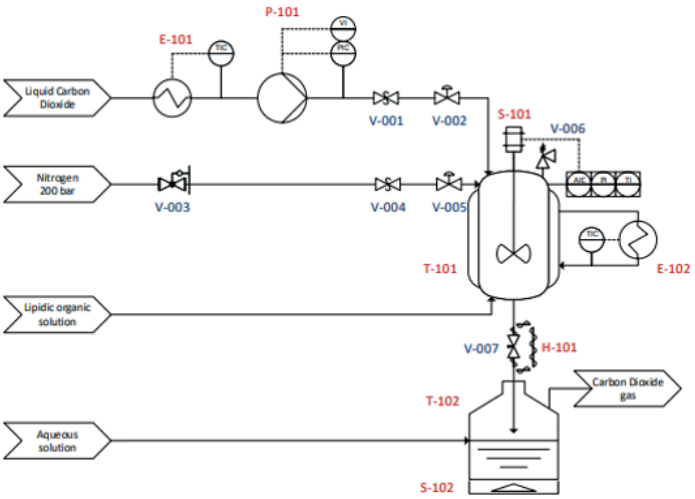

Figure 6.2: Process diagram of the intermediate lab-scale equipment (25/50 mL high pressure vessel) set up used for the preparation of nanovesicles by DELOS-susp.

6.2.1.2 Experimental procedure in the small and intermediate lab-scale equipment

The preparation of DELOS nanovesicles by DELOS-susp was performed according to the following procedure.

A desired mass of hydrophobic components (cholesterol and hydrophobic dyes) and hydrophilic components such as surfactants were solubilized in a known volume of ethanol at 38 °C, and introduced into the vessel, which was previously heated to the working temperature (Tw = 35 °C). After 20 minutes, once the solution has achieved Tw, the vessel is pressurized with compressed CO_2 through valve V-001 and V-002, producing a volumetric expansion of the liquid solution with the desired molar fraction of CO_2 (Xw = 0.64), at the working pressure (Pw = 10 MPa). The solution was left to equilibrate for 1h in the lab-scale equipment, or 15 min under stirring (500 rpm) in the intermediate lab-scale equipment, to achieve a complete homogenization and to attain thermal equilibration.

The CO_2-expanded solution was then depressurized from Pw to atmospheric pressure through the valve V-007 over an aqueous suspension. To do it, a flow of N_2, from valves V-003, V-004 and V-005, at Pw = 10- 11 MPa is used as a plunger to push down the expanded solution from the reactor, maintaining constant the pressure in the vessel during the depressurization. The aqueous solution contained the hydrophilic components (surfactants) if required or proteins such as rhEGF. In addition, the volumetric relation between the aqueous phase and the organic phase was 9:1 (V_{AP}:V_{OP}, aqueous phase:organic phase).

Then, the obtained dispersions were transferred to a container, hermetically sealed, and stored in the fridge until use at 5 ± 3 °C. In all the DELOS nanovesicle preparations, a theoretical concentration of 7.3 mM of each component (cholesterol and surfactant (CTAB, CTAC, MKC, CPC or ST)) was used in a dispersant medium containing 10% $v \cdot v^{-1}$ of ethanol.

Aqueous phase used:

1. Chapter 2: phosphate buffer (0.05, 5 mM and 10 mM, pH = 7.0), hepes buffer (5 mM, pH = 7) and histidine buffer (5 mM, pH = 7).
2. Chapter 3: water; sodium citrate buffer (5 mM, pH = 5.0); sodium acetate buffer, (5 mM, pH = 5.0); histidine buffer (5 mM, pH = 7); and phosphate-buffered saline (PBS) (5 mM, pH = 7.4).
3. Chapter 4: phosphate-buffered saline (100 mM, pH = 7.4).

In the case of the fluorescent-labeled DELOS nanovesicles, a carbocyanine dye such as 1,1′-dioctadecyl-3,3,3′,3′-tetramethyl-indocarbocyanine perchlorate (DiI) and 1,1′-dioctadecyl-3,3,3′,3′-tetramethyl-indodicarbocyanine perchlorate (DiD) were also dissolved with the membrane components in ethanol, achieving a total final concentration of 100 µM of dye in the final formulation. DiI/DiD-DELOS nanovesicles were prepared using CTAB as surfactant and water as media.

6.2.1.3 Integration of rhEGF into DELOS nanovesicles by DELOS-susp

The integration of the recombinant human epidermal growth factor (rhEGF) into DELOS nanovesicles by DELOS-susp, was performed following an identical experimental procedure as for the preparation of the DELOS nanovesicles. However, just before the depressurization of the CO_2-expanded solution, the rhEGF was diluted in the aqueous solution of histidine buffer (5 mM, pH = 7.0) to achieve a final bulk concentration of 25 or 100 $\mu g \cdot mL^{-1}$ of protein after depressurization. rhEGF-DELOS nanovesicles were prepared using cholesterol and CTAB as surfactant.

6.2.2 Tangential flow filtration for rhEGF-DELOS nanovesicles concentration

After DELOS-susp production, rhEGF-DELOS nanovesicles were submitted to a batch concentration step based on tangential flow filtration (TFF).

The concentration consists on passing the sample through a module or porous column, while no solvent is added. The setup for diafiltration, KrosFlo® Research IIi TFF System (KR2i) (Repligen,

Waltham USA), is schematized in **Figure 6.3a**. This equipment is based on the tangential flow filtration process and uses the transmembrane pressure (TMP) as a driving force. To separate the non-incorporated rhEGF and the dispersant medium from the DELOS nanovesicles, a 100 kDa cut-off modified polyether sulfone (mPES) hollow fiber column was used (reference C04-E100-05-N, Repligen, Waltham, USA). A known volume of sample was added to the feed reservoir, and submitted to the desired cycles of concentration, through the column while components with a size below pore size were removed (i.e. the solvent and the small molecules) (**Figure 6.3b**). In this Thesis, concentration factor ranged from 2 to 10-fold. A rotating pump recirculates the sample from the feed reservoir through the column and back to the original vessel with a TMP of 5 psi.

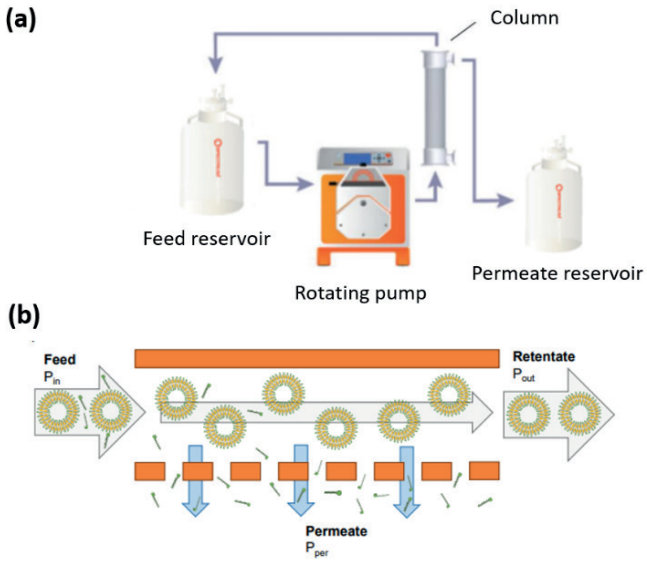

Figure 6.3: a) Scheme of the concentration and diafiltration setup, adapted from Repligen webpage[1] and b) scheme of the tangential flow process for the purification of DELOS nanovesicles.

6.2.3 Preparation and evaluation of DELOS nanovesicles in gaseous dosage form

To prepare Blank-DELOS nanovesicles and rhEGF-DELOS nanovesicles in gaseous dosage forms, samples were placed in the *Airless Dispensing Solution* device with an Advanced Preservative Free pump. Briefly, samples were manually poured into the flask device until it was completely full. Afterwards, the dispenser with the airless piston was introduced in the flask to close it.

On the other hand, the experimental set up and the method for the assessment of the dependence on the spray orientation and distance on its performance was as follows. The spray device was hold in clamp held in a metal stand support. Then, the orientations and distances were adjusted.

For each parameter to be studied, 10 replicates of spraying were performed with the two DELOS samples: Blank-DELOS and rhEGF-DELOS nanovesicles. Specifically, for spray orientation studies, the generated aerodispersion was placed in a vial in order to recover the sample and so be evaluated. Conversely, to evaluate the effect of the spray distance, each spayed was done in front of an absorbent paper. In this way, the sprayed surface area was calculated by measuring its diameter with a ruler.

6.2.4 Preparation of DELOS nanovesicles in hydrogel dosage form using Methocel™ K4M

To prepare the hydrogels enriched with DELOS nanovesicles, Methocel™ K4M was added to the dispersant media or DELOS nanovesicle formulation to have a final concentration of 2 wt% of hydrogelling agent. To ensure a proper polymer dissolution, after the addition of the full amount of Methocel™ K4M, the polymer was left hydrating at room temperature for a complete swelling for 2 h. After that, the dispersion was gently and continuously stirred with a glass rod until complete dissolution of the hydrogelling agent, and a semi-solid form was achieved (**Figure 6.4**). The same procedure was used for the preparation of control hydrogels (dispersant medium without nanovesicles), rhEGF-DELOS nanovesicles and DiI/DiD-DELOS nanovesicles-based hydrogels.

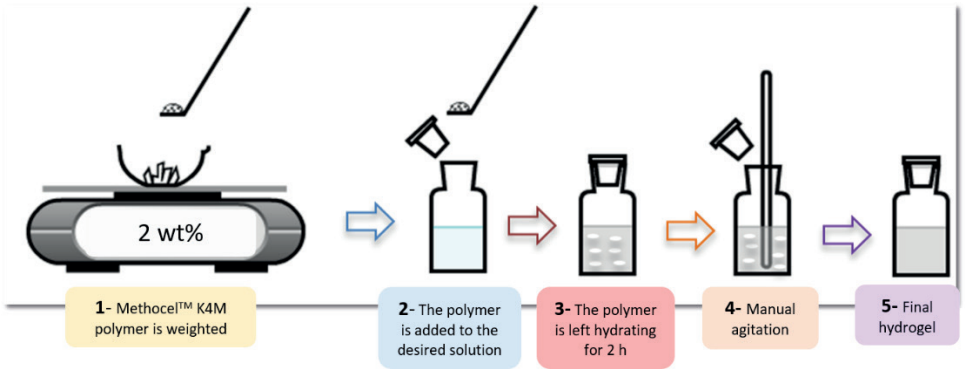

Figure 6.4: Schema of all the steps involved in the preparation of Methocel™ K4M-based hydrogels.

6.2.5 Preparation of DELOS nanovesicles in hydrogel dosage form using Poloxamer 407-based hydrogels

Poloxamer 407-based hydrogels were prepared using the "cold method". Briefly, Poloxamer 407 polymer was weighted and added to dispersant media or DELOS nanovesicles dispersion to have a final concentration of 25 wt% of hydrogelling agent. To properly dissolve it, it was slowly

dispersed in the desired dispersant media or DELOS nanovesicles formulation under constant stirring (200 rpm) at a controlled temperature around 5-10 °C until a clear solution was formed (around 3 h). The obtained hydrogels were stored in the fridge at 4 °C before the following analyses.

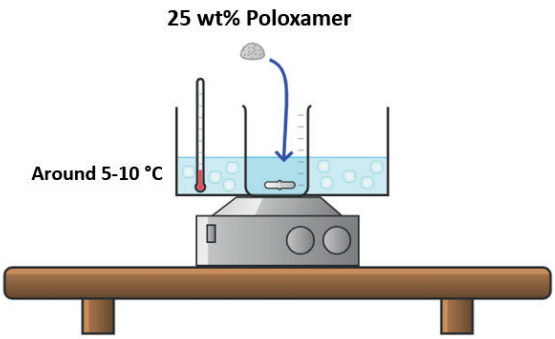

Figure 6.5: Schematic illustration of the formation of Poloxamer 407-based hydrogels.

6.3 Instruments, techniques and procedures used for the characterization of DELOS nanovesicle systems in liquid suspension and in gaseous and semi-solid dosage form.

6.3.1 Dynamic light scattering (DLS) and electrophoretic light scattering (ELS)

These measurements were performed in the Nanbiosis Soft Materials Service linked to Biomaterial Processing and Nanostructuring Unit (U6) at ICMAB-CSIC.

In all the **Chapters**, the hydrodynamic diameter and the polydispersity index (PDI) of all DELOS nanovesicles were determined with the Zetasizer Nano ZS (Malvern Instruments, UK) with non-invasive backscatter optics, equipped with He-Ne laser at 633 nm.

Particle size distribution, polydispersity index (PDI), and zeta potential of all the produced vesicles were measured using a dynamic light scattering (DLS) and electrophoretic light scattering (ELS) analyzer combined with non-invasive backscatter technology (NIBS) (Malvern Zetasizer Nano ZS, Malvern Instruments, U.K). The equipment was equipped with a 4 mW “red” He-Ne laser (λ = 632.8 nm), and with a thermostatic sample chamber. The detector was set at 173° for particle size distribution measurements, and 13° for zeta potential measurements.

Samples (1 mL) were placed in a disposable polystyrene cuvette (for DLS measurements) or in a disposable folded capillary cell (for zeta potential measurements, applied voltage 40 mV) and were analyzed without any previous modification or dilution.

All reported values correspond to the average result of three consecutive measurements at 20 °C on the same sample. Data was recorded using the Zetasizer Software 7.13 (Malvern Panalytical, UK). Size data was based on intensity size-distribution and corresponds to z-average ± SD between the three measurements. The use of scattered intensity is the most recommendable data when using DLS, since it comes from the original data provided by the analyzer, without further processing or involved assumptions for calculating particle size.

Apparent zeta potential of samples was also measured with the same instrument since it allows determining the electrophoretic mobility to assess the surface electrical charge of particles. All reported results are based on Smoluchowski model and corresponds to zeta potential average ± SD between the three measurements at 20 °C.

It should be mentioned that from **Section 4.3.3.1** to **Section 4.3.4.2**, particle size, PDI and zeta potential all types of uncoated DELOS nanovesicles and SCDN were determined by Delsa Nano C Particle Analyzer (Beckman Coulter, Brea, CA, USA; operative wavelength 655 nm) at room temperature (20 °C), respectively. To evaluate the zeta potential, samples were diluted 1:2 in water for appropriate measurement.

6.3.2 pH measurements

The determination of DELOS nanovesicles pH was measured using a HI5221-02 pH meter (Hanna Instruments, USA). Samples were left out from the fridge at least 30 minutes at room temperature before performing the measurement. The electrode was always cleaned between measurements. Stirring was used to ensure a proper equilibrium of the pH value.

In **Section 4.3**, pH was estimated by pH indicator strips (indicator strips pH 0 – 14, 1x4.8m, Filter-Lab), since not only was more comfortable but also it was not necessary a very accurate measurement.

6.3.3 Morphological analysis by cryo-TEM

The morphology of the systems was examined using cryogenic transmission electron microscopy (cryo-TEM), after sample plunge freezing. It allows direct assessment of colloidal systems, such as DELOS nanovesicles, in the vitrified, freeze-hydrated state, so their structure is fairly well preserved, and very close to their native state. Throughout procedure, it is necessary to work at cryogenic temperatures, which can be achieved with liquid nitrogen (N_2), in order to avoid damaging the sample due to the phase transition from the vitrified water to crystalline ice.

Cryo-TEM images were obtained using a JEOL JEM-2011 transmission electron microscope (Jeol Ltd, Tokyo, Japan) operating at 200 kV under low-dose conditions. 3.2 µL of the sample were deposited

onto the 400-mesh holey carbon grid and the excess of water was blotted with a filter paper. Immediately after film preparation, the grid was plunged into liquid ethane held at a temperature just above its freezing point (-179.15 °C) using a Leica EM GP cryoplunge (Leica, Wetzlar, Germany). Then, the vitrified sample was then transferred to the microscope for analysis and the specimens were kept cold (-96.15 °C) to prevent sample perturbation and the formation of ice crystals during both the transfer and viewing procedures. Images were recorded on a CCD Gatan 895 USC 4000 camera (Gatan, Pleasanton, USA) analyzed with the Digital Micrograph 1.8 software.

It should be mentioned that only in the case of Methocel™ K4M-based hydrogels, they were diluted 1:100 in water for an adequate fixation and preservation of the hydrogel sample in the grid. However, Poloxamer 407-based hydrogels were just diluted 1:10 in water.

6.3.4 Lamelarity determination by SAXS

SAXS is one characterization techniques used in colloidal science since it is non-invasive and non-destructive and can provide unique structural information with the advantage of measuring the average properties of the bulk samples, which can otherwise be obviated by using only microscopic techniques such as cryo-TEM or confocal microscopy.

From a fundamental point of view, the interaction of radiation with inhomogeneities in matter can cause a small deviation of the radiation from its incident direction, called small-angle scattering and can take place for a wide variety of radiation, such as X-rays (SAXS). This static light scattering technique is sensitive to the electron density contrast, so that the larger the difference in electron density, the larger the scattering contribution. So basically, SAXS measures the time-average intensity of the scattered X-rays as a function of the scattering angle and consequently, the measured intensity curve bears information on the radius of gyration, mean size, size distribution, shape, among other parameters[2] (**Figure 6.6**).

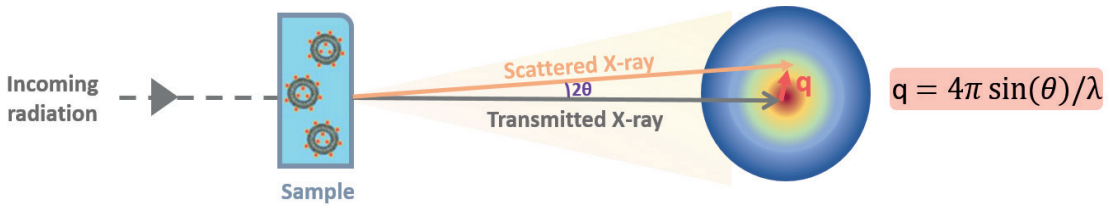

Figure 6.6: Representative image of the SAXS measurement. The modulus of the scattering vector is defined as q, the scattering angle as 2θ, and the X-ray wavelength as λ.

Small-Angle X-ray Scattering (SAXS) data from Blank-DELOS nanovesicles and rhEGF-DELOS nanovesicles with 100 $\mu g \cdot mL^{-1}$ rhEGF, were obtained on the NCD beamline at the ALBA Synchrotron (Catalonia, Spain). The radiation wavelength was set to λ = 0.148 nm and a MarCCD detector (two-dimensional position-sensitive detector) was used to record the scattering patterns. The sample-to-detector distance was set to ~1000 mm allowing a scattering vector modulus interval from 0.11 to 3.3 nm^{-1}, where q is the magnitude of the scattering vector defined by $q = (4\pi/\lambda) \sin\theta$ (2θ being the scattering angle). Samples were in a liquid sample holder between two mica windows with a 1 mm spacer, placed perpendicular to the incoming beam. The obtained curves (data collection of 5 minutes) were normalized by taking into account the X-ray beam intensity decrease during the experiment.

The scattering curve of the dispersant media was subtracted from the sample's SAXS signal, considering each sample's attenuation. All measurements were taken at room temperature of 22 °C. Additional measurements were done on an aged Blank-DELOS nanovesicles sample (20 months after preparation) at the in-house optimized Bruker AXS NanoSTAR instrument at Aarhus University, which uses an Excillum metal jet X-ray source. At this instrument, both the sample and background are measured in the same flow-through quartz capillary. The data were fitted with a model of spherical vesicles with a Gaussian number size distribution. The vesicles have a shell-core-shell cross-section structure, where the core has a negative scattering contrast due to the hydrocarbon parts of the surfactant and cholesterol, which have a lower electron density than the buffer, and the two shells have the same positive scattering length density, which is due to the higher electron density of the surfactant head group and the partly associated counterions. The interfaces between core and shells were graded. The model was fitted to the data using non-linear least-squares method[3], and the instrumental smearing was estimated and included[4].

6.3.5 Quantification of rhEGF-DELOS nanovesicles composition

For the quantification of cholesterol and CTAB self-assembled in the rhEGF-DELOS nanovesicles, HPLC technique (1100 series, Agilent Technologies (USA)) equipped with an Evaporative Light Scattering Detector, ELSD (1260 infinity ELSD, Agilent Technologies (USA)) was performed. For the quantification of CTAB and cholesterol, two different methods with two different columns were employed because of their distinct chemical nature. Cholesterol separation was carried out using a C18 Symmetry® (5 µm; 4.6 × 150 mm) column (Waters Cromatografía S.A.) with an ELSD nebulization temperature of 40 °C and evaporative temperature of 80 °C. The mobile phase for the cholesterol was a mixture of methanol with water (MeOH:H_2O) (95:5) (mobile phase A) and formic acid (0.1% HCOOH) in isopropanol (IPA) (mobile phase B) using gradient flow conditions. The separation of CTAB was carried out with an InfinityLab Poroshell 120 EC-C18 (4 µm; 4.6 x 100 mm) column (Agilent Technologies) with an ELSD nebulization temperature of 40 °C and evaporative

temperature of 90 °C. The mobile phase was a mixture of 50 mM CH_3COONH_4 and acetic acid (HAcO) pH = 3.6 (mobile phase A) and acetic acid (1% HAcO) in methanol (MeOH) (mobile phase B) using gradient flow conditions.

To determine the rhEGF molecular mass, High-Performance Liquid Chromatography-Electrospray Ionisation-Mass Spectrometry (HPLC-ESI-MS) system (Agilent Technologies) was used with the same column and gradient elution that was used for HPLC analysis. ESI mass spectrometry was performed in positive ionization mode at a drying gas temperature of 230°C. The dry gas flow rate was 10.0 $L \cdot min^{-1}$, and the capillary voltage was 5000 V. The pressure of the nebulizer was set at 68.00 psi, and the scan spectra range from m/z 100 to 3000 m/z.

6.3.6 UV-Vis spectroscopy

Absorption spectra were acquired using a Varian Cary 5000 UV-Vis-NIR spectrophotometer (Agilent Technologies, Santa Clara, USA). In particular, spectra were acquired by placing samples in a quartz SUPRASIL high precision cell (Hellma Analytics, Müllheim, Germany) with 1 cm pathlength at room temperature (25 °C).

6.3.7 Fluorescence spectroscopy

6.3.7.1 Intrinsic tryptophan fluorescence rhEGF

Fluorescence spectra were recorded on a Cary Eclipse fluorescence spectrophotometer (Varian Inc., USA) at 25 °C. The intrinsic fluorescence emission spectra of proteins were measured in the range of 305 – 450 nm after excitation at 295 nm, to obtain fluorescence spectra derived from the tryptophan (Trp) residues[5]. A bandwidth of 5 nm was used both for excitation and emission. A bulk-free rhEGF or rhEGF-DELOS nanovesicles concentration of 25 to 100 $\mu g \cdot mL^{-1}$ as well as quartz cuvettes of 1.0 cm optical path were used. The baseline was corrected using dispersant media solution for free rhEGF, and Blank-DELOS nanovesicles dispersion for rhEGF-DELOS nanovesicles.

Changes in the intrinsic fluorescence emission of Trp residues located in different microenvironments were measured after the addition of increasing amounts of acrylamide as a water-soluble attenuator[5,6]. The acrylamide concentration was manually titrated and ranged from 4 to 182 $mmol \cdot L^{-1}$. Three replicates of each sample were evaluated under agitation at 25 °C and 120 s response time. The ratio of acrylamide absence (F_O) and presence (F_{AA}) fluorescence intensities were determined for each acrylamide concentration ([AA]) and evaluated after excitation at 295 nm. The relative exposure of Trp residues in free rhEGF and rhEGF-DELOS nanovesicles structure

were estimated from the Stern-Volmer constant (K_{sv}). This constant is obtained from the linear regression of the experimental results according to the **Equation 6.1**[5]:

$$\frac{F_0}{F_{AA}} = 1 + K_{SV} \cdot [AA] \frac{F_0}{F_{AA}} = 1 + K_{SV} \cdot [AA] \qquad \textbf{(6.1)}$$

6.3.7.2 Fluorescence Spectroscopy Measurements of Dye-Labelled DELOS Nanovesicles

Fluorescence emission and excitation spectra were collected with a Varian Cary Eclipse (Agilent Technologies, Santa Clara, USA) in all **Chapters**, except for **Section 4.3**, in which Horiba Jobin–Yvon IBH FL-322 Fluorolog 3 spectrometer was used. The cuvette used was quartz SUPRASIL high precision cell (Hellma Analytics, Müllheim, Germany) with 1 cm pathlength.

1. In **Chapter 3**, fluorescence emission spectra were collected excitating at 490 nm and the emission were collected at 500–800 nm for non-gellified and gellified DiI/DiD-DELOS nanovesicles. In all the cases, samples were diluted 10 times in water.

The efficiency of energy transfer (E_{FRET}) which is the fraction of photons absorbed by the donor which are transferred to the acceptor was calculated by:

2. In **Chapter 4**, uncoated DiI-DELOS nanovesicles and Alexa-SCDN were excited at 500 nm and emission spectra were collected from 525-800 with an excitation and emission slit of 4 and 1 and 5 and 3, respectively.

6.3.8 Determination of rhEGF entrapment efficiency (EE%)

To determine the entrapment efficiency of rhEGF in the nanovesicles, an analytical methodology was defined. This method is useful to determine the rhEGF quantity integrated in the membrane of the DELOS nanovesicles and the free rhEGF in the dispersant medium.

This methodology consists on first ultracentrifugate the suspension of rhEGF-DELOS nanovesicles, by splitting the integrated rhEGF in the nanovesicles from the free rhEGF in the medium. To do it, a Sorvall Discovery M150 SE equipment and S150-AT rotor (Thermo Scientific, Massachusetts, USA) were used. In particular, 1 mL of sample was loaded in the sample tube. The ultracentrifugation tubes were placed in the 8-hole rotor and a constant force of 600.000 g at 4 °C for 6 h.

Afterwards, the supernatant was removed, and the pellet reconstituted with same dispersant media volume. The rhEGF content was analyzed by intrinsic Trp fluorescence spectra as previously described in **Section 6.3.7.1**. The EE% performed in triplicate was calculated using **Equation 6.2**, where [FI_{346nm}] is the fluorescence emission intensity at 346 nm.

$$EE(\%) = \frac{FI_{346\ nm\ of\ reconstituted\ pellet}}{FI_{346\ nm\ of\ starting\ sample}} \cdot 100 EE(\%) = \frac{FI_{346\ nm\ of\ reconstituted\ pellet}}{FI_{346\ nm\ of\ starting\ sample}} \cdot 100 \quad \textbf{(6.2)}$$

6.3.9 Optical microscopy of DELOS nanovesicle in liquid suspension and in hydrogel dosage form

Optical microscopy was used to control the homogeneity of the prepared DELOS nanovesicles in liquid suspension and in hydrogel dosage forms. To test them, a drop of the hydrogel samples was placed between a glass slide. Then, the microscopic examination was carried out at a temperature of 20.0 ± 0.1 °C by the Olympus DP20 Microscope Digital Camera, using a five times magnification to get a proper observation of the hydrogel.

6.3.10 Hydrogel rheological properties evaluation

The rheological characterization of hydrogels enriched with DELOS nanovesicles was determined by a HAAKE RheoStress 1 rheometer (Thermo Fisher Scientific™, Karlsruhe, Germany). Measurements were performed at 20.0 ± 0.1 °C using a configuration of a cone-and-plate geometry (plate diameter of 60 mm, and cone angle of 2° with a gap of 0.105 mm). Continuous shear investigations were performed to evaluate the shear stress (Pa) as a function of shear rate (s^{-1}). This study was carried out over a shear rate of 0–50 s^{-1} for 3 min, then measurement was maintained at a constant shear rate of 50 s^{-1} for 1 min, and back to 0 s^{-1} for 3 min, to mimic similar conditions to the real topic administration of a hydrogel. Viscosity was measured by evaluating the shear stress versus the shear rate in the phase of a constant shear rate of 50 s^{-1}.

In the case of Poloxamer 407-based hydrogels, samples were applied in the plate from the fridge and so in liquid state and then, left 1 minute at room temperature to gain the semisolid form.

6.3.11 Confocal Microscopic Characterization of Dye-Labelled DELOS Nanovesicles-Based Hydrogels

Gellified DiI/DiD-DELOS nanovesicles were imaged with a Leica TCS SP5 AOBS spectral confocal microscope (Leica Microsystems, Wetzlar, Germany) equipped with an HCX PL APO lambda blue 63.0 × 1.40 OIL UV objective (1.4 NA). To image the two dyes, present in the DELOS nanovesicles,

DiI and DiD, a drop of the hydrogel sample was placed on a MatTek 35 mm glass-bottom dish. The excitation wavelength was 488 and 633 nm for DiI and DiD, respectively. Detection was performed with photomultiplier tubes at specific ranges as follows: DiI was detected within the range of 540–610 nm and DiD within the 650–780 nm range. A z-stack of square images (512 × 512) at 8-bit depth were recorded at several positions for each sample using a z-step size of 0.17 µm. Finally, 3D reconstruction of the DiI/DiD-DELOS nanovesicles-based hydrogel images was generated from confocal z-stacks using the Imaris 9.2 Software (Oxford Instruments, Abingdon, UK).

6.4 *In vitro* preclinical assays

6.4.1 Quantification of rhEGF by ELISA

A sandwich-type ELISA was used to quantify the concentration of rhEGF. The rhEGF contained in the sample was captured in an initial step by a monoclonal antibody (mouse CB.EGF.1 clone, CIGB, Cuba) coupled to the solid phase, the second antibody bound to the enzyme (peroxidase-conjugated mouse CB.EGF.2 clone, CIGB, Cuba) recognizes rhEGF in a second step. The ELISA procedure was previously described>. For quantification in rhEGF-DELOS nanovesicles nanoconjugates, a first 1/10 dilution of samples in absolute ethanol was done to warranty the complete release of rhEGF protein. Then, further dilutions were done in assay buffer.

6.4.2 *In vitro* protein release

The protein release profile from the rhEGF-DELOS nanovesicles at 100 µg mL^{-1} rhEGF was monitored in 1 mL of dispersant media solution at pH 5.5 and 7.0 (histidine buffer (5 mM, pH 7.0/10% EtOH $v{\cdot}v^{-1}$), in a thermostatic bath (model SL-150/22, Solab) at 32 and 37 °C ± 2 °C. At the specific intervals (0, 0.5, 1, 2 and 3 days), the content of vials were centrifuged at 600.000 g at 4 °C for 6 h, the supernatant removed, and the protein concentration determined using the ELISA method, in triplicate. The cumulative percentage of released protein (CRP%) for each time point was calculated using **Equation 6.3**, where [rhEGF] is the rhEGF concentration by ELISA (see **Section 6.4.1**) . The CRP% was plotted versus time.

$$CRP(\%) = \left(\frac{[rhEGF]_{supernatant}}{[rhEGF]_{starting\ sample}}\right) \cdot 100 \qquad (6.3)$$

6.4.3 *In vitro* biological activity by cell proliferation assay.

The ability of free and rhEGF-DELOS nanovesicles to stimulate the proliferation of BALB/c 3T3 clone A31 murine fibroblast cells (ECACC, Wiltshire, UK) was measured by a colorimetric assay>. Cells were seeded at a density of $1.5 \cdot 10^5$ cells·mL^{-1} in 100 μL·well^{-1} of DMEM supplemented at 5% fetal bovine serum in 96-well plates. Then, cells were stressed until a quiescence state and incubated with different amounts of free rhEGF and rhEGF-DELOS nanovesicles (diluted in DMEM at dilutions > 1/1000). In the case of hydrogels, they were previously diluted 1:10 in water for adequate pipetting.

Afterward, the medium was removed, and the viable cells were determined by crystal violet staining. Finally, the plate was read at 578 nm using a Sensident Scan Microplate spectrophotometer (Merck, Germany). The results were expressed as international units (IU), compared to a working reference material that was calibrated against the 91/530 EGF standard (NIBSC, Hertfordshire, UK). The biological activity of free rhEGF and rhEGF-DELOS nanovesicles was assessed from the absorbance at 578 nm (A578 nm) using parallel line assay statistical software based on the previously described methodology>. Also by the same statistical software from dose-response curves were calculated the half-maximal effective dose (ED50). The specific activity of rhEGF in cell proliferation assay is defined by **Equation 6.4.**

$$\text{Specific rhEGF bioactivity } (IU \cdot mg^{-1}) = \left(\frac{\text{cell proliferation assay } (IU \cdot mL^{-1})}{\text{rhEGF nominal concentration } (mg \cdot mL^{-1})}\right) \quad (\mathbf{6.4})$$

The calculation of the percentage of maximum stimulation (MS%) of the free rhEGF and rhEGF-DELOS nanovesicles in the samples, at a preset concentration (Ci), was made from the absorbance readings at 578 nm (A), through **Equation 6.5**, where ACI is the absorbance of the sample with Ci concentration of rhEGF, A_{Blank} is the absorbance of the sample without free rhEGF and rhEGF-DELOS nanovesicles, and $A_{Maximum}$ is the absorbance of the sample with the highest concentration of free rhEGF and rhEGF-DELOS nanovesicles evaluated in the curve.

$$MS(\%) = \left(\frac{A_{Ci} - A_{Blank}}{A_{Maximum} - A_{Blank}}\right) \cdot 100 \quad (\mathbf{6.5})$$

6.4.4 Stability in the chymotrypsin protease model

The enzymatic reactions were prepared in the same dispersant media as rhEGF-DELOS nanovesicles (buffer histidine (5 mM, pH 7.0)/10% EtOH ($v \cdot v^{-1}$), and chymotrypsin was added to using an enzyme:substrate ratio of 1:20 ($w \cdot w^{-1}$). Then, 1.0 mL of free rhEGF and rhEGF-DELOS nanovesicles at 25 or 100 $\mu g \cdot mL^{-1}$ equivalent rhEGF solutions and chymotrypsin (Sigma, R9759) were mixed and incubated in a shaking incubator (120 rpm, 32 ± 2 °C) for 3, 6, 12 or 24 h. Reactions were terminated by the addition of 25 µL of formic acid (Sigma-Aldrich). Then, samples were diluted in the ELISA assay buffer and rhEGF quantitated as described below. At time 0 minutes, the same reaction was run and immediately stopped with formic acid. The percentages of remaining rhEGF against the data at 0 h' time point as 100% were plotted against time to show relative rates of EGF cleavage.

6.4.5 *In vitro* biocidal activity.

The effectiveness of the different nanoformulations was assayed against Gram-positive bacteria (*Staphylococcus aureus* ATCC 6538, *Bacillus subtilis* ATCC 6633), Gram-negative bacteria (*E. coli* ATCC 8739, *Pseudomonas aeruginosa* ATCC 9027), and fungi (*Candida albicans* ATCC 10231, *Aspergillus brasiliensis* ATCC 16404) using the technique of agar well diffusion method[1]>. These microorganisms were identified and provided by the Belgian Coordinated Collections of Microorganisms, BCCM/LMG (Belgium). Bacteria were grown overnight at 37 ± 2 °C in Tryptone Soy Broth (Oxoid), and fungi were incubated for 72 h at 28 ± 2 °C in Sabouraud Dextrose Broth (Oxoid). These suspensions were used as inocula. A final inoculum, using 100 µL of a suspension containing 106 colony-forming units mL^{-1} of bacteria, or 103 spores$\cdot mL^{-1}$ of fungus, was spread on Tryptone Soy Agar and Sabouraud Dextrose Agar (Oxoid) plates, respectively. Then, a hole with a diameter of 6 mm was punched aseptically with a sterile tip, and a volume of 100 µL of the Blank-DELOS nanovesicles or rhEGF-DELOS nanovesicles at rhEGF equivalent concentrations of 25 or 100 $\mu g \cdot mL^{-1}$ was introduced into the well. After that, agar assay plates were incubated at 37 ± 2 °C for 24 h for bacteria and at 28 ± 2 °C for 72 h for yeast and fungi, depending on the incubation time required for visible growth. The antimicrobial agent diffuses in the agar medium and inhibits the growth of the microbial strain tested, and then the diameters of inhibition growth zones are measured.

6.4.6 *Ex vivo* permeation experiments in damaged human skin.

Human skin from plastic surgery (Biopredic) was used to compare the permeation of free rhEGF and rhEGF-DELOS nanovesicles. The skin was obtained from the abdominal region of a healthy 40-year-old woman who voluntarily signed an IRB validated donor consent form

that specifically lists both the intended uses for the donation for non-clinical research and confirms the procedures for processing the samples are in compliance with all legal and ethical regulations. Skin was dermatomed to 400 µm thickness and shipped on dry ice. The absorption/permeation study was performed in Static Franz diffusion cells (GMBH – Analysesysteme), consisting of a receptor and a donor glass chamber fixed together with a clamp. The receptor chamber was filled with PBS (8 mL) and maintained constantly stirred and at 32 °C. Skin was removed from the freezer, cut in 4 cm^2 and left to thaw for 30 min at room temperature. Then, each piece was tape-stripped 10 times with Scotch Crystal Tape and placed on the Franz cells with the epidermal side facing up. Following 1 h, the Transepidermal water loss (TEWL) was measured with a specific probe (Dermalab series skinlab usb) to evaluate the integrity of the skin, showing similar values between 60 and 80 $g \cdot m^{-2} \cdot h$. Then, 100 µL of the test solutions were applied on the epidermal side of each skin and the opening of the donor compartment was sealed with parafilm, limiting product evaporation as with dressings. At different time points (0, 1, 2, 4, 6, 7, 8, 24 h), aliquots were collected from the receptor side and replaced with an equal volume of PBS immediately after each sample collection. After 24 h of product application, skin specimens were processed and 3 fractions were generated: The non-trespassed, the absorbed, and the permeated. rhEGF from these fractions as well as from the applied samples were quantified with the Human EGF DuoSet ELISA (R&D Systems) following manufacturer's instructions. In addition, CTAB from the applied and permeated samples was analyzed by UPLC-MS/MS.

6.4.7 *In vitro* skin irritation test using an *in vitro* reconstructed human epidermis.

To assess acute skin irritation of the nanocarriers Blank-DELOS nanovesicles and rhEGF-DELOS nanovesicles, the skin irritation test based on the OECD guideline 439 was carried out using the in vitro human epidermal model EpiSkin™. The method consists of the application of the test product and the subsequent determination of cell viability (assessed by MTT assay)[8] as well as the measurement of interleukin-1α (IL-1α) levels induced by the irritating processes (assessed by Diaclone *in vitro* test). Controls such as PBS and a solution of 5% SDS in PBS (negative and positive control, respectively), as well as CTAB surfactant solubilized in the dispersant medium and the dispersant medium alone, were used. To assess acute skin irritation, all the products were exposed to the epidermis for 24 and 48 h. According to this predictive model, a product is considered skin irritant when the cell viability is ≤ 50%, and the concentration of IL-1α release is ≥ 40 $pg \cdot mL^{-1}$.

6.4.8 MIC determinations

Antimicrobial activity of DELOS nanovesicles was assayed against *Acinetobacter baumannii* ATCC 15149, *Propionibacterium acnes*, *Staphylococcus aureus* ATCC 29213, *Malassezia furfur* ATCC 14251, *Candida albicans* ATCC 10231, *Trichonphyton mentagrophytes* ATCC 9533, *Tricophyton rubrum* CECT2794.

Sequential dilutions of DELOS nanovesicles were prepared in Mueller-Hinton broth supplemented with Ca and Mg for *Acinetobacter baumannii*, *Propionibacterium acnes* and *Staphylococcus aureus* strains. On the contrary, *Candida albicans*, *Trichonphyton mentagrophytes and Tricophyton rubrum* were diluted in RPMI media while *Malassezia furfur* was diluted with modified Dixon media.

After the preparation, 0.1 mL per well of each DELOS nanovesicles dilution, in replicate, were inoculated with the microorganism suspension, for a final microorganism count of $2\text{-}8\cdot10^5$ $CFU\cdot mL^{-1}$. In parallel, 0.1 mL per well of the media without DELOS nanovesicles were prepared in replicate as a growth control. Moreover, 0.1 mL per well of the media without microorganisms were also prepared as sterility control. The plates were incubated at the temperature and time required for each strain (see **Table 6.1**). Finally, visual and spectrophotometric lecture of the bacteria and Candida was carried out, while visual for fungi. Then, MIC was defined as the lowest concentration of DELOS nanovesicles at which no visible microbial growth was detected after the defined time.

Table 6.1: Media and incubation time recommended for each evaluated strain.

Strain	**Media**	**Incubation time (h)**
P. acnes	Broth Mueller-Hinton modified	72
S. aureus	Broth Mueller-Hinton modified	19
Baumanni	Broth Mueller-Hinton modified	19
M. furfur	Broth Dixon modified	72
Albicans	RPMI	24
T. rubrum	RPMI	96
T. mentagrophytes	RPMI	96

6.5 *In vivo* preclinical assays

6.5.1 Wound healing in a full-thickness skin defect db/db mouse model.

The preclinical studies of the nanoformulations are crucial to simulate the clinical environment. Experiments performed on animal models had to provide justifiable comparisons to human beings and were therefore made with db/db mice, which is the most widely used mouse model for Type 2 diabetes mellitus. The excisional wound in db/db mice has been validated as a relevant model for simulating the chronic wounds of type II diabetes[11]. The study was carried out in male db/db *Mus Musculus* mice (BKS(D)-Leprdb/JOrlRj), aged about 8 weeks, weighing 30 to 40 g (Janvier Laboratories, Le Genest-Saint-Isle, France). On the first day of the study, the animals were anesthetized (inhaled isoflurane) and the back of the animal was shaved and cleaned with disinfectant. Subsequently, a 1.2 mm thick silicone sheet was placed with a circular central opening of 12 mm internal diameter which was fixed with 4 stitches (Aragó silk 4/0) to minimize and avoid retraction of the skin. This rigid disk was sutured in the posterior part of the mouse, around the place where the wounds were made later to avoid contraction and that the healing occurs mainly by re-epithelialization. After this, the two wounds were made, with a total diameter of 0.8 cm and that extended to *Panniculus carnosus*. The wound was made using an 8 mm diameter circular biopsy punch, removing the skin from the mid-dorsal area. In the area of the wounds, the test product was administered with the help of a sterile drip micropipette on the peripheral edges and on the injury itself, which was subsequently covered with a sterile semi-permeable dressing Tegaderm™ (3M, St Paul, Minnesota). The monitoring and administration of the product was carried out three times a week for 14 days (d0, d2, d4, d7, d9, d11, d14). All treatments were administered locally (irrigating solution - 30 µL per wound) and then wounds were covered with Tegaderm™. One other daily dressing change consisted of sterile water for injection irrigation, treatment reapplication, and clean Tegaderm™ reapplication. The animals were randomly distributed into four treatments groups: rheGF-DELOS nanovesicles group containing 100 µg mL^{-1} rhEGF (N = 3), free rhEGF group containing 100 µg·mL^{-1} rhEGF (N=2), Blank-DELOS nanovesicles group (N = 3) and the dispersant medium control group (N = 3) (dispersant media served as the solvent in the other three groups). Wounds were photographed to evaluate the degree of wound closure. Subsequent image analysis was performed using ImageJ® software (Biophotonics Facility, University of McMaster, Canada). Wound closure was expressed as a percentage of original wound size, through **Equation 6.6**.

$$\text{Wound closure (\%)} = \left(\frac{\text{Wound area at day (0)} - \text{Wound area at day (x)}}{\text{Wound area at day (0)}}\right) \times 100 \qquad (\mathbf{6.6})$$

In addition, the health status of the animals was observed daily and signs of infection and inflammation in the wounds were assessed on each monitoring day. The body weights of the animals were also recorded at each follow-up. After the last measurement of the ulcerated area, and coinciding with the end of the study, blood was taken for general hematological and biochemical analysis.

All animal experiments were approved by the Committee on the Ethics of Animal Experiments of Minimally Invasive Surgery Centre Jesús Usón and by the Council of Agriculture and Rural Development of the Regional Government of Extremadura (APAFIS#4438-2015092514508030 v7), and in accordance with the INSERM guidelines and European Community directives for the care and use of laboratory animals (Cáceres, Spain).

6.5.2 *In vivo* toxicity study in rats by subcutaneous administration

Male and female Sprague-Dawley rats weighting approximately 250 g for females and 350 g for males were housed in suspended polypropylene/stainless steel grid cages and maintained with normal diet for the 1-week study. Three rats/sex/group were daily treated by the subcutaneous route with Group 1,2,3,4 and 5 samples (**Table 6.2**).

Criteria evaluated for treatment-related effects were body weight, clinical signs such signs of aggression, abnormal fur and behavior. One week before the endogenous levels of EGF in rat was quantified, using the Quantikine ELISA kit, to determine the Basal levels of protein at different points of the day (first thing in the morning, noon, late afternoon) and thus verify that the levels are minimal and not influenced by circadian cycles.

All animals were sacrificed at the same day of the dosing cycle (during the morning of the first day without compound), 4 h after las administration. Blood sampling (cholesterol and haematocrit) and macroscopic examination of post-mortem tissues and organs were performed. In addition, quantification of EGF and CTAB levels in brain, lung, heart, liver, spleen, pancreas and kidney were evaluated.

Table 6.2: Composition of the defined groups administered in the "1-week dose range study in rats" pilot assay.

	GROUP 1	GROUP 2	GROUP 3	GROUP 4	GROUP 5
Composition	Dispersant medium[1]	Blank-DELOS nanovesicles (Higher dose)	rhEGF-DELOS nanovesicles (Lower dose)	rhEGF-DELOS nanovesicles (original)	rhEGF-DELOS nanovesicles (Higher dose)
rh-EGF ($mg \cdot mL^{-1}$)	0,0	0,0	0,006	0,1	1,0
CTAB ($mg \cdot mL^{-1}$)	0,0	27,0	0,15	2,70	27,0
Cholesterol ($mg \cdot mL^{-1}$)	0,0	28,3	0,16	2,83	28,3
Histidine ($mg \cdot mL^{-1}$)	0,60	0,60	0,60	0,60	0,60
Ethanol ($mL \cdot mL^{-1}$)	0,107	0,107	0,107	0,107	0,107
Water for injection	c.s.	c.s.	c.s.	c.s.	c.s.

[1] The dispersant media is based on histidine buffer (5 mM, pH 7.0)/10% EtOH ($v \cdot v^{-1}$).

6.6 Statistical analysis

A four-parameter logistic transformation was used for the determination of the *in vitro* biological activity of EGF and the half-maximal effective dose (ED50). Results are expressed as a mean value with its standard deviation (mean ± SD) of each sample unless otherwise mentioned, and sample size (n) is reported in each figure legend with all experiments replicated at least 2-3 times.

Unless otherwise stated, the statistical significance among groups was analyzed by one-way analysis of variance (ANOVA) followed by Tukey's multiple comparison post-hoc test. For cytocompatibility, the statistical analysis was performed with the paired student's t-test. For *in vitro* skin irritation in the reconstructed human epidermal model Episkin™ and for ex vivo permeation through damaged skin, the statistical significance was determined via two-way ANOVA with Dunnett and Sidak post hoc test, respectively. In all cases, statistical differences were accepted as significant ($*p < 0.05$), very significant ($**p < 0.01$) or as highly significant ($***p < 0.001$) according to the obtained p-value. Statistical analysis was performed using Minitab-17 Statistical Software Package (Minitab Inc., State College, USA).

6.7 Preparation and characterization of new hybrid DELOS nanovesicle systems

6.7.1 Fluorescence titration of surfactant-based systems over sticholysins and quenching with acrylamide

Fluorescence measurements and titration experiments were performed at 25 °C using a Cary Eclipse fluorescence spectrophotometer (Varian Inc., USA)

Sticholysins (StII and StIW111C) were prepared in PBS 100 (Mm; pH 7.4) in a total concentration of 1 mM. An excitation wavelength of 295 nm was used, and both excitation and emission slits were set to 10 nm. Emission spectra were collected in the range of 310-450 nm.

Surfactant-based systems were titrated by stepwise addition of small aliquots into the cuvette containing the sticholysin solution. After each addition of surfactant-based systems, the fluorescence spectrum was recorded.

Fluorescence quenching by acrylamide was assessed using the same equipment as fluorescence measurements. In this case, acrylamide quenching was evaluated from the decrease in fluorescence intensity as a function of acrylamide concentration in the absence and presence of the maximum concentration of the surfactant-based systems. This concentration was the one assessed in the titration studies, in which the emission fluorescence of the stycholisins were already saturated.

The quenching constants, Ksv were obtained from the slopes of Stern-Volmer plots (**Equation 6.1**)

Data were analyzed with Origin (Pro), Version 2019b (OriginLab Corporation, Northampon, MA, USA). Recorded data were corrected subtracting background intensities measured in samples without protein and by its dilution factor.

6.7.2 Preparation of silica-coated DELOS nanovesicles (SCDN)

To prepare the SCDN in general, different steps were followed thanks to the described procedure obtained previously from the Thesis of Dr. Mariel Kubli. First, CTAB-DELOS nanovesicles or DiI-DELOS nanovesicles were prepared using DELOS-susp procedure (see **Section 6.2.1**). The DELOS nanovesicles suspension was then dialyzed to eliminate the free components and the EtOH of the formulation.

Afterwards, 1mL of DELOS nanovesicles suspension was further diluted with 6.5 mL of distilled water in a 25 mL round bottom flask. Once diluted, 50 mM of HCl were added to the solution until pH 3 was reached under stirring. In this case, pH indicator test strips non-bleeding, Dosatest from VWR Chemicals were used to determine the pH of the sample.

Then, silica precursors were prepared, using the following quantities:

Preparation of standard-SCDN

To prepare standard-SCDN, CTAB-DELOS nanovesicles membrane components:TEMOS molar ratio of 1:108 was used. The corresponding volume of TEMOS was mixed with pure EtOH reaching a total final volume of 1 mL. *To consider the mol of membrane components, first the concentration of membrane components in mg·mL^{-1} was calculated. Then, this value was converted to mol by just taking into consideration the molecular weight of the surfactant used. For example, if DELOS nanovesicles had a membrane concentration of 5.3 mg·mL^{-1} and the molecular weight of CTAB is 364.45, the total mol of membrane components would have been 1.45·10^{-5} mol*).

Preparation of Alexa-SCDN

The synthesis of Alexa-SCDN was similar to the one described for standard-SCDN. In this case DiI-DELOS nanovesicles were used and a similar molar ratio of DELOS nanovesicles membrane and TEMOS was used (1:108). In addition, TEMOS was combined with APTES and Alexa Fluor 647 dye and mixed with pure EtOH reaching a total final volume of 1 mL, using the following quantities (**Table 6.3**):

Table 6.3: Composition of the silica coating components in Alexa-SCDN

	Molar ratio membrane components:coating component		
System	**TEMOS**	**APTES**	**Alexa Fluor 647 dye**
Alexa-SCDN	108	0.04	0.03

It should be taken into account that all these values of equivalence were calculated previously from work of Dr. Mariel Kubli to have an excess of silica in the system that ensures the total coating of the DELOS nanovesicles.

At that point, the corresponding volume of the silica precursors was added to a syringe and placed in a syringe pump. Then, the syringe needle was placed inside the DELOS nanovescile solution balloon stirring at motion 9. A flux of 2 mL·min^{-1} was set and left pumping for 8 h. Once finished, the syringe and the needle were removed and the balloon was kept stirring at over 5 days at 1200 rpm for ensuring a correct coating of DELOS nanovesicles. Having completed this period, the reaction was stopped by sample dialysis over water (see **Section 6.7.2.1**) to remove unreacted and associated silica precursors and to eliminate the acidic environment to a more neutral one (**Figure 6.6**). All samples were stored at 4 °C for further studies.

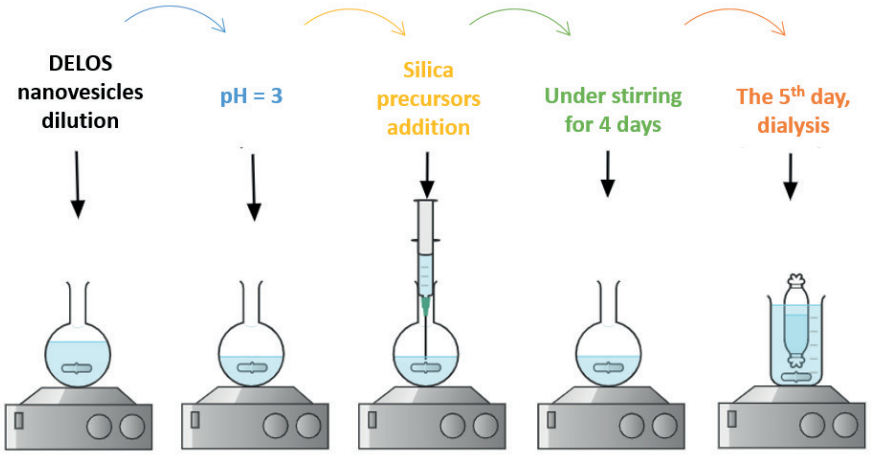

Figure 6.6: representative image of the steps involved in the preparation of the SCDN.

6.7.2.1 Purification of DELOS nanovesicles by dialysis

A volume of 5 mL of the DELOS nanovesicles formulation was put in a dialysis bag (around 15 cm in length) which was tied for both ends. Dialysis tubing consisted in cellulose membrane of average flat width of 25 mm (1.0 in.) and a typical molecular weight cut-off of 14 kDa. The dialysis bag was suspended in a 100 mL of water and maintained under stirring at 200 rpm. At intervals of 15 min, the dispersant medium was replaced with new one. This procedure is repeated 4 times. Then, samples were taken from the dialysis back with a Pasteur pipette and kept in vials at 4 °C.

6.7.3 Detection of Attenuated Total Reflectance (ATR-FTIR)

ATR measurements were performed on an ATR IRAffinity-1 instrument (Shimadzu Scientific Instruments). The analyzed samples were prepared by drop-casting 20 µL of the DELOS nanovesicles or the SCDN dispersion directly onto the sample plate surface. Since the sample was liquid, it was dried with air to measure it properly.

6.7.4 Morphology of SCDN by STEM and SEM

The morphology and structure of SCDN samples were characterized using a Scanning Transmission Electron Microscopy (STEM) (FEI Quanta FEG 250 instrument, FEI corporate, Hillsboro, Oregon, USA) with an acceleration voltage of 30 KV and a MERLIN FE-SEM scanning electron microscope (SEM). The energy-dispersive x-ray (EDX) was also performed during the scanning electron microscope measurements.

In all the cases, samples were prepared by drop-casting the formulations into a grid. The grid was left for being dried for 1 hour and then, images were taken.

6.7.5 Characterization of the stability of the silica coating

The stability of the silica coating of uncoated DiI-DELOS nanovesicles and Alexa-SCDN was monitored from 0 to 4 days using fluorescence spectroscopy as described in **Section 6.3.7.2**. Samples were diluted 1:4 in water or PBS in the presence and absence of 10 mM GSH (**Figure 6.7**) . The solution was kept in a quartz cuvette with mild stirring at 37 °C in a bath. For the stability of CTAB-DELOS nanovesicles and standard-SCDN, the same procedure was carried out and samples were diluted in SGF and PBS.

At different time points, samples were exited at 500 nm and the fluorescence emission spectra was recorded from 525-800 nm with Horiba Jobin–Yvon IBH FL-322 Fluorolog 3 spectrometer. In all the cases. For the control (uncoated DiI-DELOS nanovesicles), the excitation and emission slit of 4 and 1, respectively, while for Alexa-SCDN, the slits were 5 and 3, respectively.

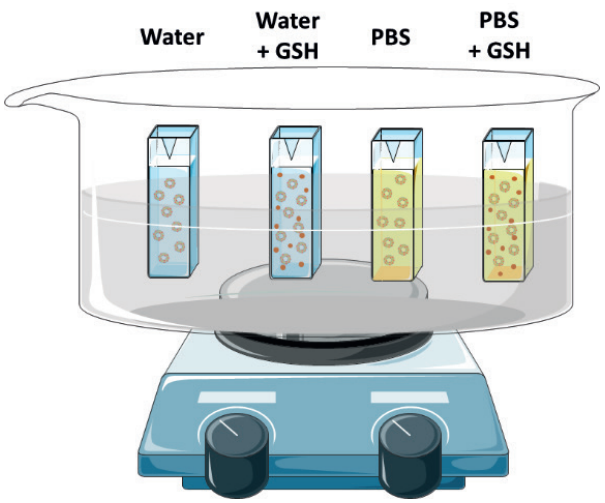

Figure 6.7: Design of the stability of the silica coating test set up.

6.8 References

1. Repligen. KrosFlo KR2i TFF system https://www.repligen.com/technologies/krosflo-tff/lab/kr2i (accessed Jun 14, 2022).
2. A. Schwamberger, B. De Roo, D. Jacob, et al. Combining SAXS and DLS for simultaneous measurements and time-resolved monitoring of nanoparticle synthesis. *Nucl. Instruments Methods Phys. Res. Sect. B Beam Interact. with Mater. Atoms* **2015**, 343, 116–122.
3. J.S. Pedersen. Analysis of small-angle scattering data from colloids and polymer solutions: modeling and least-squares fitting. *Adv. Colloid Interface Sci.* **1997**, 70 (1–3), 171–210.
4. J.S. Pedersen, D. Posselt, K. Mortensen, IUCr. Analytical treatment of the resolution function for small-angle scattering. *J. Appl. Crystallogr.* **1990**, 23 (4), 321–333.
5. J.R. Lakowicz. Principles of Fluorescence Spectroscopy, 2nd ed.; Springer Science & Business Media, New York, USA, **2006**.
6. H. Schägger, G. von Jagow. Tricine-sodium dodecyl sulfate-polyacrylamide gel electrophoresis for the separation of proteins in the range from 1 to 100 kDa. *Anal. Biochem.* **1987**, 166 (2), 368–379.
7. A. Leyva, H. Santana, M. Font, B. Pérez, R. Valdés. An ELISA for quantification of recombinant human EGF in production process samples, serum and urine. *Biologicals* **2018**, 51, 12–17.
8. T. Mosmann. Rapid colorimetric assay for cellular growth and survival: Application to proliferation and cytotoxicity assays. *J. Immunol. Methods* **1983**, 65 (1–2), 55–63.
9. D.J. Finney. Statistical Method in Biological Assay (Mathematics in Medicine Series), 3rd ed.; Griffin, C., Ed.; Arnold Hodder, London, UK, **1978**.
10. M. Balouiri, M. Sadiki, S.K. Ibnsouda. Methods for in vitro evaluating antimicrobial activity: A review. *J. Pharm. Anal.* **2016**, 6 (2), 71–79.
11. X.T. Wang, C.C. McKeever, P. Vonu, C. Patterson, P.Y. Liu. Dynamic Histological Events and Molecular Changes in Excisional Wound Healing of Diabetic DB/DB Mice. *J. Surg. Res.* **2019**, 238, 186–197.